

**Some pages of this thesis may have been removed for copyright restrictions.**

If you have discovered material in AURA which is unlawful e.g. breaches copyright, (either yours or that of a third party) or any other law, including but not limited to those relating to patent, trademark, confidentiality, data protection, obscenity, defamation, libel, then please read our [Takedown Policy](#) and [contact the service](#) immediately

FUNCTIONAL LOCALISATION OF HUMAN SENSORY-MOTOR CORTEX  
USING MAGNETOENCEPHALOGRAPHY

PAUL LAWRENCE FURLONG  
DOCTOR OF PHILOSOPHY

ASTON UNIVERSITY  
MARCH 1998

This copy of the thesis has been supplied on condition that anyone who consults it is understood to recognise that the copyright rests with its author and that no quotation from the thesis and no information derived from it may be published without the authors prior written consent.

Aston University

Functional Localisation of Human Sensory-Motor Cortex using  
Magnetoencephalography

Paul Lawrence Furlong  
Doctor of Philosophy  
1998

## Summary

The 19 channel Neuromagnetometer system in the Clinical Neurophysiology Unit at Aston University is a multi-channel system, unique in the United Kingdom.

A bite bar head localisation and MRI co-registration strategy which enabled accurate and reproducible localisation of MEG data into cortical space was developed. This afforded the opportunity to study magnetic fields of the human cortex generated by stimulation of peripheral nerve, by stimulation of visceral sensory receptors, and by those evoked through voluntary finger movement.

Initially, a study of sensory-motor evoked data was performed in a healthy control population. The techniques developed were then applied to patients who were to undergo neurosurgical intervention for the treatment of epilepsy and / or space occupying lesions. This enabled both validation of the effective accuracy of source localisation using MEG as well as to determine the clinical value of MEG in pre-surgical assessment of functional localisation in human cortex.

The studies in this thesis have demonstrated that MEG can repeatedly and reliably locate sources contained within a single gyrus and thus potentially differentiate between disparate gyral activation. This ability is critical in the clinical application of any functional imaging technique; which is yet to be fully validated by any other 'non-invasive' functional imaging methodology.

The technique was also applied to the study of visceral sensory representation in the cortex which yielded important data about the multiple cortical representation of visceral sensory function.

## Acknowledgements

I am greatly indebted to my supervisor, and friend, Professor Graham Harding. Thankyou for many years of support, advice and encouragement.

I have to acknowledge two other strong influences to my work. Thanks to Dr Ron Paul, the Neurophysiologist who first instilled in me a sense of interest and excitement to this speciality.

To my friend and colleague, the late Professor Peter Jeavons. His dedication, perseverance and diligence inspired all who knew him.

Sincere thanks to the Magnetometry team at Aston University, both past and present, for thier help and comradeship.

Special thanks are due to Dr Gareth Barnes and Dr Krish Singh who have written software, devised analysis strategies and provided countless hours of direct support throughout the course of these studies. Your support and friendship was vital to the success of this work. I hope we will continue to work together for many years to come. Thanks are also due to the support team in Clinical Neurophysiology Unit, especially Andrea Edson, Ian Fawcett and Vivica Tipper.

Qasim Aziz at Hope Hospital in Manchester deserves special mention. Thankyou for the years of support and friendship. Your insight, patience and perseverance opened up many new avenues in the study of visceral sensory perception. Our collaboration resulted in the data described in Chapter 6 in this thesis. Sincere thanks also to colleagues at Hope Hospital, Manchester, namely, Professor David Thompson, Anthony Hobson, Shaheen Hamdy and Josephine Barlow.

For their valuable input into the surgical studies and referral of the patients described in this thesis, particular thanks are due to Dr Nigel Walton at the Burden Hospital and Dr Shelley Renowden and Mr David Sandeman at Frenchay Hospital, Bristol. Thanks also to Mr Richard Walsh, Queen Elizabeth hospital, Birmingham.

Thanks to the Nuffield hospital in Birmingham for thier MRI support and to Mr Peter Weale, formerly Superintendent Radiographer at the Queen Elizabeth hospital, Birmingham, for all his support in the early days of MRI acquisition and fMRI studies.

Finally, to my wife Diane. Thankyou for supporting me with such understanding through all the years of study. Now that the thesis is written, I promise that we will rediscover what it means to have a social life.

Signed.....

**Dedication**

**With much love and thanks to my mother  
Sheila Furlong,  
and in loving memory of my father  
Harold Lawrence Furlong**

## INDEX

<b>Title Page</b>	<b>1</b>
<b>Thesis Summary</b>	<b>2</b>
<b>Acknowledgements</b>	<b>3</b>
<b>Dedication</b>	<b>4</b>
<b>Index</b>	<b>5</b>
<b>Index of Figures and Tables</b>	<b>12</b>

### **1. THE ANATOMY AND PHYSIOLOGY OF SENSORY-MOTOR PATHWAYS**

<b>1.1 The receptors</b>	<b>32</b>
1.1.1 Receptors of proprioception	32
<b>1.2 The Peripheral Nerve</b>	<b>37</b>
1.2.1 Somatosensory activity in peripheral nerve.	38
1.2.2 Proprioceptive activity in peripheral nerve	39
<b>1.3 Dorsal Nerve Roots</b>	<b>40</b>
<b>1.4 Pathways mediating sensation.</b>	<b>40</b>
1.4.1 Lemniscal System.	42
1.4.2 Anterolateral System	45
1.4.3 Lateral Cervical System	48
<b>1.5 Thalamic Nuclei</b>	<b>50</b>
<b>1.6 Thalamo - Cortical and Cortico - Cortical Projections</b>	<b>52</b>
<b>1.7 Sensory - Motor Cortex</b>	<b>53</b>
1.7.1 Somatosensory cortex	53
1.7.2 Motor cortex	57
<b>1.8 Motor control fibres from the cerebral cortex and brain stem</b>	<b>58</b>
1.8.1 Corticospinal Tract	60
1.8.2 Corticobulbar Tract	62
1.8.3 Corticorubral and Rubrospinal Tracts	62
1.8.4 Corticoreticular and Reticulospinal Tracts	62
<b>1.9 The Brain Gut Axis</b>	<b>63</b>
1.9.1 Gut sensation	64

<b>2. NEUROIMAGING TECHNIQUES</b>	<b>66</b>
<b>2.1 Introduction</b>	<b>66</b>
<b>2.2 Magnetic Resonance Imaging</b>	<b>66</b>
2.2.1 Signal origin	66
2.2.2 Image creation	69
2.2.3 Longitudinal (T1) and Transverse (T2) Relaxation	70
<b>2.3 Functional Magnetic Resonance Imaging</b>	<b>71</b>
2.3.1 Echo Planar Imaging	72
2.3.2 Artefacts	72
2.3.3 Clinical application	73
<b>2.4 Positron Emission Tomography</b>	<b>75</b>
2.4.1 Difficulties associated with PET	76
2.4.2 Clinical application	76
<b>2.5 Magnetoencephalography</b>	<b>77</b>
2.5.1 Direct and Inverse problem	78
2.5.2 MEG vs EEG	80
2.5.3 Measuring neuromagnetic fields	80
2.5.4 MEG-MRI co-registration	85
<b>2.6 Summary</b>	<b>86</b>
<b>3. MAGNETOENCEPHALOGRAPHIC LOCALISATION OF SOMATOSENSORY CORTEX IN HUMAN CONTROL SUBJECTS</b>	<b>88</b>
<b>3.1 Introduction</b>	<b>88</b>
<b>3.2 Aims</b>	<b>90</b>
3.2.1 Experimental design	90
<b>3.3 Method and Materials</b>	<b>92</b>
3.3.1 Magnetometer system	92
3.3.2 Recording protocol	92
3.3.3 Magnetic Resonance Images (MRI)	93
3.3.4 Functional Magnetic Resonance Imaging	93
3.3.5 Data analysis	94
3.3.6 Source localisation	95
3.3.7 Estimation of confidence for the localisation	95

3.3.8 Cortical localisation: Reference to co-ordinate systems	96
<b>3.4 Results</b>	<b>99</b>
3.4.1 Magnetic Field waveforms	99
3.4.1.1 Median nerve evoked components: reproducibility and morphology	99
3.4.1.2 Signal to noise ratio of median nerve data	103
3.4.1.3 Ulnar nerve evoked components: reproducibility and morphology	105
3.4.1.4 Signal-to-noise ratio of ulnar nerve data	107
3.4.1.5 Posterior Tibial nerve evoked components: reproducibility and morphology	109
3.4.1.6 Signal-to-noise ratio of posterior tibial nerve data	113
3.4.2 Dipole fitting	116
3.4.2.1 Median nerve dipole fits	116
3.4.2.2 Ulnar nerve dipole fits	119
3.4.2.3 Posterior Tibial dipole fits	119
3.4.3 MRI Co-registration and Talairach co-ordinates	120
3.4.4 Dipole localisations	122
3.4.4.1 Median nerve localisations	122
3.4.4.2 Ulnar nerve localisations	128
3.4.4.3 Posterior Tibial nerve localisations	131
3.4.5 Comparison of Talairach co-ordinates	133
3.4.6 Variation in the localisation of repeated trials.	139
3.4.7 Variation in localisation across the temporal window of acquisition.	141
3.4.7.1 Temporal localisations for right median nerve data	141
3.4.7.1.1 Cortical sources with temporal overlap	148
3.4.7.2 Temporal localisation for Posterior Tibial nerve data	149
3.4.8 Variation in hemisphere localisation (symmetry)	153
3.4.9 Functional MRI	154
3.4.10 Functional MRI and MEG co-registration.	157
<b>3.5 Summary and Conclusions</b>	<b>159</b>
3.5.1 Magnetic field waveforms	159
3.5.2 Dipole fitting	161
3.5.3 Repeatability of localisations	162
3.5.4 Localisation accuracy	163
3.5.5 Temporal sequence of activation	163
3.5.6 Comparison with stereotaxic atlas	164
3.5.7 Interhemispheric symmetry	167
3.5.8 Somatotopic organisation of the cortex	167
3.5.9 Ability to reliably identify the central sulcus	169
3.5.10 MEG-fMRI co-registration	170



<b>4. VOLUNTARY MOVEMENT RELATED EVOKED FIELDS</b>	<b>171</b>
<b>4.1 Introduction</b>	<b>171</b>
<b>4.2 Aims</b>	<b>172</b>
<b>4.3 Method</b>	<b>172</b>
<b>4.4 Results</b>	<b>174</b>
4.4.1 Waveform morphology	174
4.4.2 Dipole fitting	178
4.4.3 MRI Co-registration and Talairach co-ordinates	182
4.4.4 Index finger movement localisations	182
4.4.5 Localisations across the temporal window of acquisition	186
4.4.6 Comparison of Talairach co-ordinates	190
<b>4.5 Summary and Conclusion</b>	<b>191</b>
<b>5. PRESURGICAL LOCALISATION OF SENSORY-MOTOR CORTEX</b>	<b>194</b>
<b>5.1 Introduction</b>	<b>194</b>
<b>5.2 Aims</b>	
<b>5.3 Methods</b>	<b>197</b>
5.3.1.1 MEG acquisition	197
5.3.1.2 fMRI acquisition	197
5.3.1.3 Neuro-Radiographic localisation of the central sulcus	198
5.3.1.4 Surgical localisation of sensory-motor function	198
<b>5.4 Case Study Results</b>	<b>199</b>
5.4.1 Case study 1: Patient PR	199
5.4.1.1 Clinical History	199
5.4.1.2 MEG Results - Patient PR	199
5.4.1.3 MEG -MRI co-registration	202
5.4.1.4 Patient PR - Predicted location of the central sulcus	205
5.4.1.5 Functional Magnetic Resonance Imaging	206
5.4.1.6 Surgical validation	206
5.4.1.7 Patient PR - Summary.	208
5.4.2 Case Study 2: Patient DT	209
5.4.2.1 Clinical history	209
5.4.2.2 Investigations	209

5.4.2.3 MEG Results - Patient DT	209
5.4.2.4 MRI Co-Registration	211
5.4.2.5 Predicted location of the central sulcus	211
5.4.2.5.1 MEG Prediction	214
5.4.2.5.2 Neuro-Radiological prediction	214
5.4.2.6 Surgical validation	216
5.4.2.7 Summary - Patient DT	216
5.4.3 Case Study 3: Patient SM	216
5.4.3.1 Clinical History	216
5.4.3.2 Investigations	217
5.4.3.3 Magnetometry Results - Patient SM	217
5.4.3.4 MEG-MRI Co-Registration	218
5.4.3.5 Predicted line of the central sulcus	221
5.4.3.6 Surgical validation	221
5.4.4 Case study 4: Patient JC	222
5.4.4.1 Clinical History:	222
5.4.4.2 Investigations	222
5.4.4.3 Magnetometry Results - Patient JC	223
5.4.4.4 MEG-MRI Co-registration	224
5.4.4.5 Predicted line of the central sulcus	227
5.4.4.6 Surgical Validation	228
5.4.5 Case study 5: Patient TH	228
5.4.5.1 Clinical History	228
5.4.5.2 Investigations	228
5.4.5.3 Magnetometry Results - Patient TH	229
5.4.5.4 MEG-MRI Source localisations	231
5.4.5.5 Prediction of the central sulcus	232
5.4.5.6 Surgical Validation	233
5.4.6 Case Study 6: Patient AS	234
5.4.6.1 Clinical history	234
5.4.6.2 Investigations	234
5.4.6.3 Magnetometry Results - Patient AS	235
5.4.6.4 MEG - MRI Co-Registration	236
5.4.6.5 MEG-MRI Source localisation	237
5.4.6.6 Predicted location of the central sulcus	238
5.4.6.7 Surgical validation - Patient AS	240
5.4.7 Case study 7: Patient AD	240
5.4.7.1 Clinical History	240
5.4.7.2 Investigations	240
5.4.7.3 Magnetometry Results - Patient AD	241
5.4.7.4 MEG-MRI Co-registration	242
5.4.7.5 MEG-MRI Source localisations	243

5.4.7.6 Prediction of the central sulcus	245
5.4.7.7 Surgical validation in patient AD	246
5.4.8 Case study 8: Patient DB	246
5.4.8.1 Clinical history	246
5.4.8.2 Investigations	246
5.4.8.3 Magnetometry Results - Patient DB	246
5.4.8.4 MEG-MRI co-registration	248
5.4.8.5 MEG-MRI source localisation	248
5.4.8.6 Predicted location of the Central Sulcus	250
5.4.8.7 Surgical validation - Patient DB	251
5.4.9 Case study 9: Patient CJ	252
5.4.9.1 Clinical History:	252
5.4.9.2 Investigations	252
5.4.9.3 Magnetometry Results - Patient CJ	252
5.4.9.4 MEG-MRI co-registration	254
5.4.9.5 MEG-MRI source localisations	254
5.4.9.6 Patient CJ - Predicted location of the central sulcus	257
5.4.9.7 Surgical validation - Patient CJ	258
5.4.10 Case study 10: Patient PP	258
5.4.10.1 Clinical History:	258
5.4.10.2 Investigations	258
5.4.10.3 Magnetometry Results - Patient PP	258
5.4.10.4 MEG-MRI co-registration	259
5.4.10.5 MEG-MRI source localisation - Patient PP	260
5.4.10.6 Patient PP- Predicted location of the central sulcus	262
5.4.10.7 Surgical validation - Patient PP	263
5.4.11 Case study 11: Patient RL	263
5.4.11.1 Clinical History	263
5.4.11.2 Investigations	263
5.4.11.3 Magnetometry Results - Patient RL	263
5.4.11.4 MEG-MRI co-registration	265
5.4.11.5 MEG-MRI source localisation	266
5.4.11.6 Patient RL - Predicted location of the Central Sulcus	266
5.4.11.7 Surgical validation - Patient RL	270
5.4.12 Case Study 12: Patient JS	271
5.4.12.1 Investigations	271
5.4.12.2 Magnetometry Results - Patient JS	271
5.4.12.3 MEG-MRI co-registration	273
5.4.12.4 MEG-MRI source localisation	273
5.4.12.5 Patient JS - Predicted location of the Central Sulcus	277
5.4.12.6 Surgical validation - Patient JS.	278
5.4.13 Case study 13: Patient DO	279

5.4.13.1 Clinical History	279
5.4.13.2 Investigations	279
5.4.13.3 Magnetometry Results - Patient DO	279
5.4.13.4 MEG-MRI co-registration	281
5.4.13.5 MEG-MRI source localisation	282
5.4.13.6 Patient DO - Predicted location of the Central Sulcus	282
5.4.13.7 Surgical validation - patient DO	283
5.4.13.8 Summary - Patient DO	283
<b>5.5 Summary and discussion</b>	<b>285</b>
5.5.1 MEG, Neuro-Radiology and surgical validation	287
5.5.2 Median and Posterior Tibial nerve localisations	289
5.5.3 Self paced finger movement	289
5.5.4 fMRI	290
5.5.5 Conclusion	291
<b>6. CORTICAL LOCALISATION OF MAGNETIC FIELDS EVOKED BY OESOPHAGEAL DISTENSION.</b>	<b>294</b>
<b>6.1 Introduction</b>	<b>294</b>
<b>6.2 Aims</b>	<b>295</b>
<b>6.3 Method</b>	<b>295</b>
6.3.1 Subjects	295
6.3.2 Oesophageal Stimulation	295
6.3.3 Magnetometer system	296
6.3.4 Recording protocol	296
6.3.5 Magnetic Resonance Images (MRI)	297
6.3.6 Data analysis	298
6.3.7 Source localisation	298
6.3.8 Estimation of confidence for the localisation	299
6.3.9 Inter-subject comparisons	299
<b>6.4 Results</b>	<b>300</b>
6.4.1 Proximal Oesophageal Stimulation	300
6.4.2 Source locations for superior cortical aspects (proximal segment)	302
6.4.3 Source locations for lateral cortical aspects (proximal oesophagus)	306
6.4.4 Distal Oesophageal Stimulation	311
6.4.5 Source locations for superior cortical aspects (distal oesophagus)	311
6.4.6 Source locations for lateral cortical aspects (distal oesophagus)	312
6.4.7 Comparison of Proximal and Distal Oesophageal data	312

## 7. SUMMARY 319

## REFERENCES 322

APPENDIX I Evaluation of MRI-MEG/EEG co-registration strategies using Monte Carlo simulation 337

APPENDIX II Topographic mapping of cortical potentials evoked by distension of the human proximal and distal oesophagus. 343

## INDEX OF FIGURES AND TABLES

## CHAPTER 1 FIGURES

Figure 1.1 Cross section of the skin indicating the variety of sensory receptors. From McNaught and Callander (1983). 33

Figure 1.2 Cross section of spinal cord at approximately the C8/T1 segmental level. Tracts and nuclei of the cord are illustrated on the left; Rexed's laminar organisation of the grey matter are illustrated on the right. DSC= dorsal spinocerebellar tract; FC= fasciculus cuneatus; FG= fasciculus gracilis; IC=intermediolateral cell column; LCS= lateral corticospinal tract; LRS= lateral reticulospinal tract; LST= lateral spinothalamic tract; LT= Lissauer's tract; MRS= medial reticulospinal tract; ND= nucleus dorsalis; NP= nucleus proprius; PM= posteromarginal nucleus; RS= rubrospinal tract; SG= substantia gelatinosa; TS= tectospinal tract; VCS= ventral corticospinal tract; VHC= ventral horn cell columns; VS= vestibulospinal tract; VSC= ventral spinocerebellar tract. Adapted from Gilman and Newman (1987)

Figure 1.3 The central nervous system pathways mediating proprioception and stereognosis. NG= nucleus gracilis; NC= nucleus cuneatus; ACN= accessory cuneate nucleus; VPL= thalamic nucleus ventralis posterolateralis. Adapted from Gilman and Newman (1987). 41

Figure 1.4 The central nervous system pathways that mediate the sensations of pain and temperature. Adapted from Gilman and Newman (1987). 47

Figure 1.5 The central nervous system pathways mediating tactile sensation except for the lemniscal system. The lateral and ventral components of the lateral spinothalamic tract are shown. Adapted from Gilman and Newman (1987). 49

Figure 1.6 Thalamic nuclei. (A) A schematic dorsolateral view of the thalamus, which has been dissected from the left side of the brain, showing the boundaries of the thalamic nuclei. A= anterior nuclear group; CM= centromedian nucleus; DM= dorsomedial nucleus; LD= lateral dorsal nucleus; LP= lateral posterior nucleus; VA= ventral anterior nucleus; VLc= ventral lateral pars caudalis; VLo= ventral lateral pars oralis; VPL= ventral posterolateral nucleus; VPM= ventral posteromedial nucleus. Thalamic projections to the cortex are represented by the matching colours shown on the schematic brain C. Adapted from Gilman and Newman (1987).	51
Figure 1.7 Schematic transverse cross section of the central sulcus showing Brodman areas and thalamocortical projections in the human brain. VLc= ventral lateral pars caudalis; VLo= ventral lateral pars oralis; VPLc= ventral posterolateral pars caudalis; VPLo= ventral posterolateral pars oralis.	52
Figure 1.8 Brodmann cortical area classifications shown on a brain surface (from Talairach and Tournoux 1988).	54
Figure 1.9 Descending pathways. Adapted from Gilman and Newman (1987)	59

## CHAPTER 1 TABLES

Table 1-1 Receptors that transmit signals during movement (Matthews 1988)	36
---	----

## CHAPTER 2 FIGURES

Figure 2.1 Hardware components of a Magnetic Resonance Imaging system	68
Figure 2.2 Schematic showing the physiological mechanisms upon which fMRI and PET rely to detect cortical changes as a result of a correlated task. (Adapted from Raichle, Scientific American, 1994)	74
Figure 2.3 Types of Gradiometer array. Two alternatives to the simple flat coil (namely a magnetometer configuration, usable only with heavy shielding) are shown. These geometries are the most often used. The second-order gradiometer (b) permits successful operation even in unshielded environments.	82
Figure 2.4 The 19 channel Magnetometer system at Aston University is suspended in a wooden gantry in a magnetically shielded environment. The use of vacuum cushions and a bite bar ensure stability and accuracy of localisation.	84

## CHAPTER 3 FIGURES

- Figure 3.1 From Rademacher et al., 1993; the topography of lateral Brodmann area 4: Individual variations of the surface extent of area 4 (hatching) on the lateral cerebral surface in nine left (L) and nine right @ hemispheres (view from above, anterior is at the top). Sulci and gyri are labelled only for the first brain. Both the central and precentral sulci take a dorsoventral course from the superior hemispheric margin posteriorly toward the sylvian fissure anteriorly. This course of the precentral sulcus is generally discontinuous. Its intersection with the superior frontal sulcus provides a constant landmark. Abbreviations: F1= Superior Frontal Gyrus , PRG= Precentral Gyrus, POG= Post Central Gyrus, sf= superior frontal sulcus , prc= precentral sulcus, ce= central sulcus , poc= postcentral sulcus. 98
- Figure 3.2 Traces in each block show magnetic field waveforms for three separate trials superimposed following right median nerve (right traces) and left median nerve (left traces) stimulation. The vertical scale alongside the waveforms is expressed in femtoteslas (fT). 100
- Figure 3.3a&b Group mean waveforms for left median nerve stimulation (left upper traces) and right median nerve stimulation (right upper traces) with their respective integrated global field power plots shown below. The vertical scale alongside the waveforms is expressed in femtoteslas (fT). 102
- Figure 3.4 A plot of latency versus signal-to-noise ratio's for right median nerve stimulation in six control subjects (C1-C6). 103
- Figure 3.5 Magnetic field distribution between 20 and 55 milliseconds following electrical stimulation of the right median nerve at the wrist. Grid of maps represent the magnetic field distribution across the neuromagnetometer dewar surface with the orientation and location of the dewar depicted in the schematic on the far right. Red and yellow colours represent magnetic field from the head towards the magnetometer and blue/pink represents the return field moving away from the magnetometer. 104
- Figure 3.6 Traces show magnetic field waveforms for two separate trials following right ulnar nerve stimulation. The vertical scale alongside the waveforms is expressed in femtoteslas (fT). 105
- Figure 3.7 Group mean waveforms for right ulnar nerve stimulation (upper traces) with their respective global field power plots shown below. The vertical scale alongside the waveforms is expressed in femtoteslas (fT). 106
- Figure 3.8 A plot of latency versus signal-to-noise ratio's for right ulnar nerve stimulation in six control subjects (C1-C6). 107
- Figure 3.9 Magnetic field waveforms for two separate trials following left and right posterior tibial nerve stimulation (left and right sided traces respectively). The vertical scale alongside the waveforms is expressed in femtoteslas (fT). 109

- Figure 3.10 a-c. 19 channels of MEG data are superimposed following a single trial of right and/or left posterior tibial nerve stimulation. Lower traces in each example show the corresponding Global Field Power of the data. 112
- Figure 3.11 Magnetic field distribution between 35 and 70 milliseconds following electrical stimulation of the right posterior tibial nerve at the ankle. Grid of maps represent the magnetic field distribution across the neuromagnetometer dewar surface. Red and yellow colours represent magnetic field from the head towards the magnetometer and blue/pink represents the return field moving away from the magnetometer. Waveforms (right) show magnetic field plot from the 19 magnetometers (upper) with the corresponding Global Field Power plot (lower). 113
- Figure 3.12 A plot of latency versus signal-to-noise ratio's for right posterior tibial nerve stimulation in six control subjects (C1-C6). 115
- Figure 3.13 Graphs depicting the parameters for Equivalent Current Dipole source localisations across the acquisition epoch. Correlation co-efficients and GammaQ outputs are shown (top) with the Chi values shown below. A plot of signal-to noise ratio's against latency (bottom) also indicates the values for 95% confidence volumes achieved through MonteCarlo analysis (expressed in cubic millimetres). The vertical lines passing through all three graphs indicate the points from which the best confidence volumes were achieved. 116
- Figure 3.14 Plot of latency versus signal-to-noise ratio for right median nerve data with the sizes of scatter plot points representing the relative 95% confidence volumes (in cubic millimetres) following Monte Carlo analysis of dipole fits. Only confidence volumes of less than  $2 \text{ cm}^3$  were plotted. 117
- Figure 3.15 Chi values of 12 or less were plotted for each of the control group subjects. 118
- Figure 3.16 Plot of latency versus signal-to-noise ratio for right ulnar nerve data with the sizes of scatter plot points representing the relative 95% confidence volumes (in cubic millimetres) following Monte Carlo analysis of dipole fits. 119
- Figure 3.17 Plot of latency versus signal-to-noise ratio for posterior tibial nerve data with the sizes of scatter plot points representing the relative 95% confidence volumes (in cubic millimetres) following Monte Carlo analysis of dipole fits. 119
- Figure 3.18 Digitised headshape files achieved in the MEG laboratory were superimposed onto the co-registered MRI to monitor the success of the transform. Data on control subject 6 shown. 120
- Figure 3.19 Talairach co-ordinate templates were established for each control subject by identifying the midline position of the anterior and posterior commissures. 121



- Figure 3.20 a-f. Median nerve localisations for control subjects. Monte Carlo ellipses for three separate trials of right median nerve stimulation (top left) and the corresponding ellipses for left median nerve stimulation (top middle) are shown. The juxtaposition of right and left median nerve data are shown on a single axial slice for comparison (top right) with the central sulcus line indicated by arrows. Latencies selected for localisations were concomitant with the N20m component. White gridlines indicate the base-planes (AC-PC and VCa-VCp lines) for Talairach (1988) co-ordinates. MRI slices below (lower left and middle) indicate the relative positions of the Central Sulcus as predicted from Talairach atlas co-ordinates. 125
- Figure 3.21 Right ulnar (white) and Right median (black) Monte Carlo confidence ellipses are shown for control subject 2-5 for comparison of localisation. 129
- Figure 3.22 Right ulnar (white) and Right median (black) Monte Carlo confidence ellipses are shown for control subject 6 for comparison of localisation. 130
- Figure 3.23 Differences in Median and Ulnar nerve localisations are represented in the graph above. Data was provided by the subtraction of the Talairach co-ordinates for the mean point of the smallest confidence volume for ulnar nerve data from the median nerve counterpart in control subjects. Negative values in a given plane therefore indicate a larger Talairach co-ordinate for the ulnar nerve compared to the median nerve counterpart. 130
- Figure 3.24 a-d Monte Carlo ellipses for separate trials of Right and / or Left Posterior Tibial nerve localisations for each control subject are shown. 131
- Figure 3.25 Group mean Talairach co-ordinates for Median, Ulnar and Rt + Lt Posterior Tibial nerve data. Error bars show 1 standard deviation from the mean value. 133
- Figure 3.26 Mean localisations for right median (black circle) and left median (white circle with black cross) nerve trials are plotted onto the nearest matching sagittal slice from the Talairach and Tournoux atlas (1988). Error bars represent one standard deviation from the mean. Right hand plate is an enlargement from the full plate. 135
- Figure 3.27 Mean localisations for right median (right side of plate) and left median nerve trials are plotted onto the nearest matching coronal slice from the Talairach and Tournoux atlas (1988). Mean ulnar nerve data (white circle) is plotted for comparison. Error bars represent one standard deviation from the mean. Right hand plate is an enlargement from the full plate. 136
- Figure 3.28 Plate a) shows mean Talairach co-ordinate localisations for right and left median nerve data. Error bars indicate one standard deviation from the mean. Plate b) shows the mean Talairach co-ordinate localisation for right posterior tibial data with one standard deviation error bars. Plate c) is an enlargement from b). 137

- Figure 3.29 Mean Talairach co-ordinate for right posterior tibial nerve data plotted onto the nearest matching sagittal (a) and coronal (b) slices from the Talairach and Tournoux atlas (1988). 138
- Figure 3.30 A measure of the scatter of localisations obtained by repeated trials of nerve stimulation. Data was obtained by subtraction of the minimum x.y and z Talairach co-ordinates from the maximum values obtained following three successive trials of nerve stimulation. Right and Left Median nerve data is shown (upper) together with Right and Left Posterior Tibial nerve data (lower). 139
- Figure 3.31 Right median nerve stimulation in control subject 6 produced two non-overlapping confidence volumes (indicated by arrows) each of which were accurately localised to the posterior bank of the central sulcus. 140
- Figure 3.32 Dipole localisations across a temporal sequence for right median nerve data for control subjects 1 and 2. Latencies of dipole fits are indicated in the graph legends. The position of the central sulcus in relation to the closest placed confidence volume is indicated by arrows on the x-y axis. The relative size of the confidence volumes at each latency is represented by the size of the data icon in the graph. 142
- Figure 3.33 Dipole localisations across a temporal sequence for right median nerve data for control subjects 3 and 4. Latencies of dipole fits are indicated in the graph legends. The position of the central sulcus in relation to the closest placed confidence volume is indicated by arrows on the x-y axis. The relative size of the confidence volumes at each latency is represented by the size of the data icon in the graph. 143
- Figure 3.34 Dipole localisations across a temporal sequence for right median nerve data for control subjects 5 and 6. Latencies of dipole fits are indicated in the graph legends. The position of the central sulcus in relation to the closest placed confidence volume is indicated by arrows on the x-y axis. The relative size of the confidence volumes at each latency is represented by the size of the data icon in the graph. 144
- Figure 3.35 Talairach co-ordinates for Right Median nerve data from six control subjects. Co-ordinates within the given temporal window were averaged. The temporal window was centred on consistent peaks of activation seen in all six subjects. 146
- Figure 3.36 Magnetic field waveforms (Top) following left median nerve stimulation in control subject 1. Waveforms from channels 1 and 2 are shown in black and those from channels 7 and 15 are grey. Number array (Lower left) represents the magnetometer array with dipole localisation at 19 milliseconds shown in black and the 22.7 millisecond dipole in grey. The MRI (Lower right) shows the co-registered localisations for the confidence volumes derived by Monte Carlo analysis. The colours correspond to those used in the neighbouring images and the arrow depicts the predicted central sulcus. 148

- Figure 3.37 Dipole localisations across a temporal sequence for right posterior tibial nerve data for control subjects 1 and 3. Latencies of dipole fits are indicated in the graph legends. The position of the central sulcus in relation to the closest placed confidence volume is indicated by arrows on the x-y axis. The relative size of the confidence volumes at each latency is represented by the size of the data icon in the graph. 150
- Figure 3.38 Dipole localisations across a temporal sequence for left posterior tibial nerve data for control subject 4 and 5. Latencies of dipole fits are indicated in the graph legends. The position of the central sulcus in relation to the closest placed confidence volume is indicated by arrows on the x-y axis. The relative size of the confidence volumes at each latency is represented by the size of the data icon in the graph. 151
- Figure 3.39 Hemisphere asymmetry was estimated by the subtraction of the mean Talairach co-ordinates of right and left median nerve trials. 152
- Figure 3.40 fMRI subtraction image showing an area of high image signal over the left post central gyrus. The time course plot of signal intensity calculated from this area is shown on the right . 154
- Figure 3.41 Plates a) and b) show the final subtraction images from two MRI slice levels with a clear area of high activity seen over the left post central gyrus in each slice. Plates c) and d) show phase contrast venugrams from the same two MRI slices which clearly show the presence of a large vein in close proximity to the fMRI activation sites. 155
- Figure 3.42 Subject 4: Co-registration of fMRI activity (blue/pink) with the smallest MEG confidence volume following right median nerve stimulation (green). 156
- Figure 3.43 Subject 4: Left plate shows confidence volumes achieved from right and left median nerve stimulation with the position of the central sulci indicated by arrows. Right plate shows MEG (green) and fMRI (blue/red) co-registration, both positioned over the post central gyrus. 157
- Figure 3.44 Gibrilins SEP morphology 158
- Figure 3.45 Figure from Talairach and Tournoux (1988) showing the location of the Rolandic fissure from 20 brains stereotactically localised using the normalised proportional grid. 164
- Figure 3.46 The sigmoidal shape of the upper portion of the central sulcus in control subject 6 was localised as the hand area from MEG measurements. 166

## CHAPTER 3 TABLES

- Table 3-1 Latencies and baseline to peak amplitudes (femtoTeslas; 10-15 Tesla) of components 108

Table 3-2 Latencies yielding smallest confidence ellipses following Right Median nerve stimulation are shown. The distance of the mean point of this ellipse from the posterior bank of the central sulcus in each control subject is indicated. 'Plus' or 'minus' signs in the 'Distance from CS' column represents anterior to, or posterior to the posterior bank of the Central Sulcus respectively. The signal-to-noise ratio of the data at the latency indicated is shown for comparison.	126
Table 3-3 Latencies yielding smallest confidence ellipses following Left Median nerve stimulation are shown. The distance of the mean point of this ellipse from the posterior bank of the central sulcus in each control subject is indicated. 'Plus' or 'minus' signs in the 'Distance from CS' column represents anterior to, or posterior to the posterior bank of the Central Sulcus respectively. The signal-to-noise ratio of the data at the latency indicated is shown for comparison.	127
Table 3-4 Latencies yielding smallest confidence ellipses following Right and Left Posterior Tibial nerve stimulation are shown. The distance of the mean point of this ellipse from the posterior bank of the central sulcus in each control subject is indicated. 'Plus' or 'minus' signs in the 'Distance from CS' column represents anterior to, or posterior to the posterior bank of the Central Sulcus respectively.	133
Table 3-5 Group Mean Talairach co-ordinates	134
Table 3-6 Latencies yielding closest position to the central sulcus following Right Median nerve stimulation are indicated and compared with the distance of the smallest confidence volume achieved. Plus or minus signs in the 'Distance from CS' column represents anterior to, or posterior to the posterior bank of the Central Sulcus respectively.	145
Table 3-7 Student t-test probability comparison of Talairach co-ordinates across four temporal windows of activation for right median nerve data.	147
Table 3-8 Latencies yielding closest position to the central sulcus following Right Posterior Tibial nerve stimulation are indicated in bold type and compared with the distance of the smallest confidence volume achieved. Where no applicable data from the Right Posterior Tibial nerve could be used, the Left sided data was substituted. This data is shown in plain italics. Plus or minus signs in the 'Distance from CS' column represents anterior to, or posterior to the posterior bank of the Central Sulcus respectively.	149

## CHAPTER 4 FIGURES

- Figure 4.1 Control subject 1. Magnetic field waveforms following right index finger (a-c) and left index finger (d-f) flexions. 19 channels of a single trial are shown superimposed in waveforms a) and d) with waveforms following separate trials superimposed for comparison (b and e). Waveforms c and f show channels and latencies of maximum dipolar field strength. 174
- Figure 4.2 Control subject 2. Magnetic field waveforms following right index finger (a-c) and left index finger (d-f) flexions. 19 channels of a single trial are shown superimposed in waveforms a) and d) with waveforms following separate trials superimposed for comparison (b and e). Waveforms c and f show channels and latencies of maximum dipolar field strength. 175
- Figure 4.3 Control subject 6. Magnetic field waveforms following right index finger (a-c) and left index finger (d-f) flexions. 19 channels of a single trial are shown superimposed in waveforms a) and d) with waveforms following separate trials superimposed for comparison (b and e). Waveforms c and f show channels and latencies of maximum dipolar field strength. 176
- Figure 4.4 Plot of magnetic field distribution at 10 millisecond intervals across 350 milliseconds of the acquisition window in each subject. Red / yellow represents magnetic field towards the magnetomete and blue / pink away from the magnetometer. 179
- Figure 4.5 Right index finger movement data. Upper graph shows a plot of the signal-to-noise ratio of data at each datapoint of acquisition. The lower graph depicts the latencies in each subject which yielded the smallest confidenc volumes following Monte Carlo analysis. The size of the circles represent the relative size of confidence volumes and these are plotted as a function of the signal to noise ratio of the data at the respective latencies. 180
- Figure 4.6 Left index finger movement data. Upper graph shows a plot of the signal-to-noise ratio of data at each datapoint of acquisition. The lower graph depicts the latencies in each subject which yielded the smallest confidenc volumes following Monte Carlo analysis. The size of the circles represent the relative size of confidence volumes and these are plotted as a function of the signal to noise ratio of the data at the respective latencies. 181
- Figure 4.7 Subject 1. Right index (a) and Left index (b) finger movement confidence volumes for component MF are shown as black ellipses. Both are shown together in a single axial slice in plate c). The smallest median nerve condidence volumes are shown for comparison as white ellipses in all three plates. 183
- Figure 4.8 Subject 2. Right index (a) and Left index (b) finger movement confidence volumes for component MF are shown as black ellipses. Both are shown together in a single axial slice in plate c). The smallest median nerve condidence volumes are shown for comparison as white ellipses in all three plates. 184

- Figure 4.9 Subject 6. Right index (a) and Left index (b) finger movement confidence volumes for component MF are shown as black ellipses. Both are shown together in a single axial slice in plate c). The smallest median nerve confidence volumes are shown for comparison as white ellipses in all three plates. 185
- Figure 4.10 Control subject 1 (C1). Comparison of Talairach co-ordinates for right median and right index finger movement dipole fits (graph left) and left median with left index finger movement dipole fits (graph right). Icons in grey depict median nerve dipole localisations with black icons depicting finger movement. Latencies are shown in legends with the appropriate finger movement wave component labelled prior to latency. Icon sizes reflect relative confidence volumes. 187
- Figure 4.11 Control subject 2 (C2). Comparison of Talairach co-ordinates for right median and right index finger movement dipole fits (graph left) and left median with left index finger movement dipole fits (graph right). Icons in grey depict median nerve dipole localisations with black icons depicting finger movement. Latencies are shown in legends with the appropriate finger movement wave component labelled prior to latency. Icon sizes reflect relative confidence volumes. 188
- Figure 4.12 Control subject 6 (C6). Comparison of Talairach co-ordinates for right median and right index finger movement dipole fits (graph left) and left median with left index finger movement dipole fits (graph right). Icons in grey depict median nerve dipole localisations with black icons depicting finger movement. Latencies are shown in legends with the appropriate finger movement wave component labelled prior to latency. Icon sizes reflect relative confidence volumes. 189
- Figure 4.13 Enlarged portion of a sagittal slice (G.33mm) from a sample brain obtained from the stereotaxic atlas of Talairach and Tournoux (1988). The mean and standard deviation error bars for right median (black), left median (black and white) and combined right and left index finger movement data for component MF (red) are shown for comparison. 190

## CHAPTER 4 TABLES

- Table 4-1 Latencies of components measured from right and left index finger flexion. Latencies in bold type produced strong dipolar field patterns. 177
- Table 4-2 Comparison of mean Talairach atlas co-ordinates 191

## CHAPTER 5 FIGURES

- Figure 5.1 Patient PR. a) Shows two trials of right median nerve waveforms superimposed for comparison. b) Upper waveforms show 19 channels of MEG waveforms superimposed following a trial of right median nerve stimulation. Lower waveform shows the Global Field Power plot for this dataset. 200
- Figure 5.2 Patient PR. a) Shows two trials of right posterior tibial nerve waveforms superimposed for comparison. b) Upper waveforms show 19 channels of MEG waveforms superimposed following a trial of right posterior tibial nerve stimulation. Lower waveform shows the Global Field Power plot for this dataset. 201
- Figure 5.3 Talairach co-ordinate lines were constructed from the location of the anterior and posterior commissures in a midline sagittal slice. 202
- Figure 5.4 Matching digitised head shape with midline MRI slice to test co-registration. 202
- Figure 5.5 a) Shows the smallest 95% confidence volumes from two trials of median nerve stimulation at a latency of 22 milliseconds. These are shown in relation to the VCA and VCP lines of the Talairach co-ordinate system. b) Smallest confidence volumes shown on an axial slice. c) Shows the smallest confidence volumes on a coronal slice. d) Sagittal slice showing four confidence volumes obtained at latencies of 22 (x2), 43 and 44ms. These are shown in relation to the predicted line of the central sulcus depicted by the white curved trace. 203
- Figure 5.6a-c. a) Shows the smallest 95% confidence volumes from two trials of posterior tibial nerve stimulation at latencies of 42 and 77 milliseconds. These are shown in relation to the VCA and VCP lines of the Talairach co-ordinate system. 204
- b) Depicts volumes obtained from right posterior tibial nerve stimulation at 42, 43, 77 and 80 milliseconds with the predicted line of the central sulci shown.
- c) Shows the smallest confidence volumes from median nerve and posterior tibial nerve stimulation superimposed onto a surface rendered image of the cortex. The bold black line indicates the predicted line of the central sulcus. 204
- Figure 5.7 Median nerve localisations in patient PR. Relative sizes of the localisation icons reflect the proportional sizes of the corresponding confidence volumes. The double arrow indicates the Neuro-Radiologically predicted position in the x-y axis of the line of the central sulcus. 205
- Figure 5.8 Posterior Tibial nerve localisations in patient PR. Relative sizes of the localisation icons reflect the proportional sizes of the corresponding confidence volumes. The double arrow indicates the Neuro-Radiologically predicted position in the x-y axis of the line of the central sulcus. 206

- Figure 5.9 indicates the location of maximal fMRI activation (yellow) following a finger-thumb opposition sequence, together with the MEG localisation following Median nerve stimulation (green). Upper right image shows the juxtaposition of the functional locations with respect to the predicted line of the central sulcus traced with a black line. 207
- Figure 5.10 Surgical area in patient PR. White labels indicate areas of positive sensory - motor responses from the patient following electrical stimulation of the cortex. Labels to the right of the surgical field yielded motor responses while those to the left were predominantly sensory. 207
- Figure 5.11(top) shows magnetic field waveforms following Left Median nerve stimulation. The lower figure shows the corresponding Global Field Power analysis of the data. The latencies indicated are those from which single equivalent dipole models were calculated. 210
- Figure 5.12(upper) shows magnetic field waveforms following Left Posterior Tibial nerve stimulation. The lower figure shows the corresponding Global Field Power analysis of the data. The latencies indicated are those from which single equivalent dipole models were calculated. 210
- Figure 5.13 Talairach co-ordinate base lines computed for patient DT. 211
- Figure 5.14 The four figures above indicate source localisations for Left Median nerve from three independent trials (Yellow, Green and White ellipses). Left Posterior Tibial nerve localisation is also indicated (red ellipse). The three yellow ellipses are source localisations from a single trial of Left Median nerve stimulation but at three latencies (22.0ms, 23.0ms and 35.0ms). 212
- Figure 5.15 Patient DT. From the cluster of smallest confidence volumes from three trials of median nerve stimulation and one of posterior tibial nerve stimulation, a prediction of the line of the central sulcus was made. This is indicated on the images by the marker labelled CS. 213
- Figure 5.16 Median nerve and Posterior Tibial nerve localisations in patient DT. Relative sizes of the localisation icons reflect the proportional sizes of the corresponding confidence volumes. The double arrow indicates the predicted position in the x-y axis of the line of the central sulcus. 214
- Figure 5.17 Photograph (left) of the display screen of the surgical ISG wand system taken during surgery on patient DT. Yellow cross hairs indicate the position of the hand held wand (right). 215
- Figure 5.18 Patient SM. Separate trials of right median nerve (left upper) and right posterior tibial nerve (right upper) magnetic field waveforms are superimposed for comparison. Magnetic field waveforms (middle) from 19 simultaneously acquired MEG channels following Right Median nerve together with the corresponding Global Field Power analysis of the data. The latencies indicated are those from which single equivalent dipole models were calculated. 218



- Figure 5.19 Plates a) and b) show digitised head shape files acquired during MEG acquisition superimposed onto the MRI. This was used to check the quality of the matching transformation matrix. Plates c) and d) show the baselines for the Talairach co-ordinate system superimposed onto the mid-line MRI slice. 219
- Figure 5.20 Patient SM: Smallest confidence volume for Right median nerve stimulation co-registered with the MRI. Sagittal slice in plate a) shows the confidence volume with respect to the Talairach co-ordinate baselines. The predicted line of the central sulcus is indicated. In plate b), the predicted line of the central sulcus is indicated by the white line. 220
- Figure 5.21 Right median nerve localisations in patient SM. Relative sizes of the localisation icons reflect the proportional sizes of the corresponding confidence volumes. The double arrow indicates the predicted position in the x-y axis of the line of the central sulcus. 221
- Figure 5.22 19 MEG channels of data superimposed following Left median nerve stimulation in patient JC (upper traces). Beneath, the corresponding Global Field Power plot is shown. The latencies indicated are those from which single equivalent dipole models were calculated. 224
- Figure 5.23 Plates show the baselines for the Talairach co-ordinate system superimposed onto the mid-line MRI slice. 224
- Figure 5.24 MEG dipole localisations for patient JC. Plate a) shows the smallest confidence volume at 29.0 milliseconds co-registered with the appropriate MRI slice. The bilateral positions of the predicted line of the central sulcus are indicated. This data is shown in the respective sagittal (plate b) and coronal planes (plate c). 225
- Figure 5.25 Since no dipole localisations could be made directly following right median nerve stimulation, an approximation of location of function in the left hemisphere was made based on symmetry of response in the opposite hemisphere. 226
- Figure 5.26 Left median nerve localisations in patient JC. Relative sizes of the localisation icons reflect the proportional sizes of the corresponding confidence volumes. The double arrow indicates the predicted position (in the x-y axis only) of the line of the central sulcus. 227
- Figure 5.27 Upper figure shows the magnetic field waveforms following Right median nerve stimulation in patient TH. The lower figure shows the corresponding Global Field Power plot. The latencies indicated are those from which single equivalent dipole models were calculated. 230
- Figure 5.28 Talairach co-ordinate lines were constructed from the location of the anterior and posterior commissures in a midline sagittal slice. 230
- Figure 5.29 Right median nerve source localisations for patient TH. Ellipses were obtained at 24.0 ms (smallest volume) and 40.0 ms. 231

- Figure 5.30 Neuro-Radiological prediction of the line of the central sulcus in the right hemisphere from symmetry of functional localisation computed for the left hemisphere. 232
- Figure 5.31 Median nerve localisations in patient TH. Relative sizes of the localisation icons reflect the proportional sizes of the corresponding confidence volumes. The double arrow indicates the predicted Neuro-Radiological position in the x-y axis of the line of the central sulcus. 233
- Figure 5.32 Upper traces show magnetic field waveforms following Right (right side traces) and Left Median nerve stimulation. Below these are the corresponding Global Field Power analysis of the data. The latencies indicated are those from which single equivalent dipole models were calculated. 235
- Figure 5.33 MEG-MRI matching matrix confirmation by superimposition of digitised headshape file acquired during MEG measurements. 236
- Figure 5.34 Talairach co-ordinate lines were constructed from the location of the anterior and posterior commissures in a midline sagittal slice. 236
- Figure 5.35 Several trials of each stimuli were performed to assess reliability of response. Latencies from the two trials shown above were at 31.0ms (Trial 1, green ellipse) and 30.5ms (trial 2, blue ellipse). 237
- Figure 5.36 Smallest confidence volumes from both right (green ellipse) and left median nerve stimulation were co-registered with the MRI and the predicted line of the central sulcus indicated. Latencies of the right and left hemisphere confidence volumes were 30.0 and 32.0 milliseconds respectively. 237
- Figure 5.37 Smallest confidence volumes from two trials of Right Median nerve localisations and one Left median trial in patient AS. Relative sizes of the localisation icons reflect the proportional sizes of the corresponding confidence volumes. The double arrow indicates the predicted position in the x-y axis of the line of the central sulcus. 238
- Figure 5.38 Patient AS. Labelling following electrical stimulation of the surface of the cortex to monitor motor function. A= arm, H= hand, Th = thumb. 239
- Figure 5.39 Magnetic field waveforms for Left (upper left) and right (upper right) median nerve stimulation. Beneath are the corresponding Global Field Power plots. 241
- Figure 5.40 Left Posterior Tibial nerve data in patient AD. The latencies indicated in the Global Field Power plot are those from which single equivalent dipole models were calculated. Unfortunately, at no latency were dipole fits at significance levels ( $r < 0.95$ ). 242
- Figure 5.41 Headshape files co-registered with the MRI of patient AD. Clearly, a positional error had been introduced in the first MRI (left plate a)). It later became clear that a mobile dental plate had been responsible for the misalignment of the bite bar in the mouth. The second MRI at 1.5mm slice thickness (b) shows the correct alignment. 242

- Figure 5.42 Talairach co-ordinate lines were constructed from the location of the anterior and posterior commissures in a midline sagittal slice. 243
- Figure 5.43 Source localisations for patient AD for right and left median nerve stimulation superimposed upon single slices for ease of comparison. The predicted line of the central sulcus (CS) is indicated. 244
- Figure 5.44 Smallest confidence volumes from trials of Right and Left Median nerve localisations in patient AD. Relative sizes of the localisation icons reflect the proportional sizes of the corresponding confidence volumes. The double arrow indicates the predicted position in the x-y axis of the line of the central sulcus. 245
- Figure 5.45 Magnetic Field waveforms following Right median nerve stimulation in patient DB. a) shows two separate trials superimposed to show repeatability. b) 19 channels of MEG data superimposed following a single trial of right median nerve stimulation and c) shows the corresponding Global Field Power plot for trial b). 247
- Figure 5.46 Patient DB. Plate a) shows digitised head shape file, acquired at the time of the MEG acquisition, co-registered with the MRI. Plate b) shows the CA-CP and VCA-VCP lines of the Talairach co-ordinate system positioned on a mid-line slice. 248
- Figure 5.47 Two separate trials of Right median nerve source localisations for patient DB co-registered with the MRI. Smaller confidence ellipse was achieved at a latency of 29.0 ms and the other at 21.0ms. Predicted location of the Central Sulcus is indicated (CS). 249
- Figure 5.48 Prediction of the location of the Central Sulcus in patient DB was made on the basis of assumed symmetry between hemispheres. The predicted location for the left median nerve is shown in the sagittal plate on the right. 250
- Figure 5.49 Smallest confidence volumes from trials of Right Median nerve localisations in patient DB. Relative sizes of the localisation icons reflect the proportional sizes of the corresponding confidence volumes. The double arrow indicates the predicted position in the x-y axis of the line of the central sulcus. 251
- Figure 5.50 19 channels of magnetic field data following single trials of Left Median nerve (upper left) stimulation and Right Median nerve stimulation (upper right). The figures beneath these waveforms (lower left and right) show the corresponding Global Field Power plots of the data. 253
- Figure 5.51 Left Posterior Tibial nerve data from patient CJ. 19 MEG channels from a single trial are superimposed (upper) with the corresponding Global Field Power plot below. 253
- Figure 5.52 Patient CJ. Plate a) shows digitised head shape file, acquired at the time of the MEG acquisition, co-registered with the MRI. Plate b) shows the CA-CP and VCA-VCP lines of the Talairach co-ordinate system positioned on a mid-line slice. 254

- Figure 5.53 Patient CJ. Plates a-c, co-registration of smallest volume at 25.0ms following Left median nerve stimulation. Plates d-f show localisations following separate trials of right median nerve stimulation (20.0ms and 19.5ms). 255
- Figure 5.54 Upper plates a-c show co-registration of Left Posterior Tibial nerve data at 41.5ms. Lower plates d and e show predicted line of the central sulcus with right median nerve confidence ellipse shown on the sagittal slice and both right and left median nerve data co-registered to a single axial slice for ease of comparison. 256
- Figure 5.55 Right and Left median nerve with Left Posterior Tibial nerve localisations in patient CJ. Relative sizes of the localisation icons reflect the proportional sizes of the corresponding confidence volumes. The double arrow indicates the predicted position (in the x-y axis only) of the line of the central sulcus. 257
- Figure 5.56 19 channels of superimposed MEG data (upper) following Left median nerve stimulation in patient PP. Below is the corresponding Global Field Power plot. 259
- Figure 5.57 Patient PP. Plate a) shows digitised head shape file, acquired at the time of the MEG acquisition, co-registered with the MRI. Plate b) shows the CA-CP and VCA-VCP lines of the Talairach co-ordinate system positioned on a mid-line slice. 260
- Figure 5.58 Patient PP. Localisations following two trials of Left Median nerve stimulation. Sources computed at a latency of 18.0ms. The predicted line of the central sulcus is indicated (CS). 261
- Figure 5.59 Left median nerve localisations in patient PP. Relative sizes of the localisation icons reflect the proportional sizes of the corresponding confidence volumes. The double arrow indicates the predicted position (in the x-y axis only) of the line of the central sulcus. Legend indicates separate trials of Left Median nerve stimulation (T1 and T2). 262
- Figure 5.60 Magnetic field waveforms following Left Median nerve (upper left) and Right Median nerve stimulation (upper right). Below are the corresponding Global Field Power plots. 264
- Figure 5.61 Figures show the magnetic field waveforms following self paced movement of the Left (upper figure) and Right (lower figure) index finger. The vertical line indicates the point at which an electrical contact was made as part of the movement and was defined as time zero. Latencies were calculated with respect to this point. 265
- Figure 5.62 Patient RL. Plate a) shows digitised head shape file, acquired at the time of the MEG acquisition, co-registered with the MRI. Plate b) shows the CA-CP and VCA-VCP lines of the Talairach co-ordinate system positioned on a mid-line slice. 265

Figure 5.63 Plates A and D show the location of three separate trials of Left Median nerve stimulation (white ellipses) with plates B and E showing the location of two separate trials of Left index finger movement confidence volumes. Plates C and F show the juxtaposition of sensory and movement evoked confidence volumes.

267

Figure 5.64 Right Median nerve and Right index finger movement confidence volumes (white and black respectively) are shown in plate A. Plate B shows right and left sensory and motor localisations with respect to the predicted line of the central sulcus. Plate C shows the extent of outline of the astrocytoma (cross in centre of plate) 6- 7millimetres superior to the indicated slice.

268

Figure 5.65 Graph A) shows the relative size and positions of separate trials of median nerve data over a range of latencies with Graph B) showing the corresponding index finger movement data. Graph C gives the mean positions of the previous data for ease of comparison. Icon size represents the proportional confidence volumes with the double arrows indicating the predicted lines of the Central Sulcus.

269

Figure 5.66 Sagittal section showing Left index finger localisation with respect to the lesion in patient RL.

270

Figure 5.67 Magnetic field waveforms following Left Median nerve stimulation (upper a). The corresponding Global Field Power analysis of the data is shown beneath the MEG plots. The latencies indicated are those from which single equivalent dipole models were calculated.

Below (b), the MEG waveforms following Right (upper traces) and Left self paced index finger movement. The vertical line indicates the moment of contact formed by depression of a contact switch and corresponds to time zero for the purposes of latency presentation.

272

Figure 5.68 Patient JS. Plate a) shows digitised head shape file, acquired at the time of the MEG acquisition, co-registered with the MRI. Plate b) shows the CA-CP and VCA-VCP lines of the Talairach co-ordinate system positioned on a mid-line slice.

273

Figure 5.69 Patient JS: Two trials of right median nerve stimulation both locate to what is predicted to be the post-central gyrus in this patient.

274

Figure 5.70 The juxtaposition of right median (white ellipse) with right index finger movement (black ellipse) confidence volumes are shown in the left and middle plates. Left index finger localisation is shown in the right sagittal plate.

275

Figure 5.71 Smallest median nerve confidence volume (white ellipse) together with index finger movement confidence volumes (black)

are shown on this axial and sagittal slice. The predicted positions of the central sulci are indicated by the arrows. The lesion is clearly visible

in the enlarged sagittal slice (right) and appears to lie in the gyrus posterior to the sensory cortex.

276

Figure 5.72 Right median nerve (RMED) and right and left index finger movement localisations (RINDEX and LINDEX) in patient JS. Relative sizes of the localisation icons reflect the proportional sizes of the corresponding confidence volumes. The double arrow indicates the predicted position (in the x-y axis only) of the line of the central sulcus.	278
Figure 5.73 Patient DO. Two trials of Left median nerve stimulation (top) are superimposed to allow comparison.	280
Figure 5.74 19 MEG channels superimposed following a single trial of Left median nerve stimulation with the corresponding Global Field Power plot with the Right median nerve data alongside to the right.	280
Figure 5.75 Top traces show two separate trials of Left index finger movement data superimposed for comparison. Beneath are 19 MEG channels from a single trial superimposed. Latencies are calculated from the moment that a button switch was depressed as part of the finger movement and represents time zero. Vertical axis is in femtotesla ( $10^{-15}$ T).	281
Figure 5.76 Patient DO Plate a) shows digitised head shape file, acquired at the time of the MEG acquisition, co-registered with the MRI. Plate b) shows the CA-CP and VCA-VCP lines of the Talairach co-ordinate system positioned on a mid-line slice.	281
Figure 5.77 Mean Talairach co-ordinates for dipole localisation in patient DO.	283
Figure 5.78 Patient DO. Plates a) and b) show 95% confidence volumes for localisations of Left Median nerve stimulation (white ellipses) and Left index finger movement (black ellipses). Plate c) shows Left and Right median somatosensory confidence volume localisations with white ellipses and that of the Left index finger movement with the black confidence ellipse. The white lines superimposed on the axial slice indicate the predicted line of the central sulcus.	284

## CHAPTER 5 TABLES

Table 5-1 Summary of pre-surgical evaluation data	285
Table 5-2 Summary of pre-surgical evaluation data	286

## CHAPTER 6 FIGURES

Figure 6.1 Evoked magnetic field waveforms from subject 2 for proximal and distal oesophageal stimulation. Separate trials of each evoked response are superimposed for comparison. The nomenclature adopted by Aziz et al (1985) for evoked potential data is used. The units on the vertical amplitude (x) axis on the scale bar are in femtoTesla ( $10^{-15}$ Tesla).	301
---	-----

- Figure 6.2 95% confidence ellipses were co-registered with the MRI of that individual. For ease of comparison, ellipses were plotted on a single slice of the sagittal, axial and coronal planes. White ellipses show proximal oesophageal data and black ellipses show the distal segment data. The mid-point of the ellipse represents the mean dipole source location following 50 iterations of Monte-Carlo analysis. 303
- Figure 6.3 95% confidence ellipses were co-registered with the MRI of that individual. For ease of comparison, ellipses were plotted on a single slice of the sagittal, axial and coronal planes. White ellipses show proximal oesophageal data and black ellipses show the distal segment data. The mid-point of the ellipse represents the mean dipole source location following 50 iterations of Monte-Carlo analysis. 304
- Figure 6.4 95% confidence ellipses were co-registered with the MRI of that individual. For ease of comparison, ellipses were plotted on a single slice of the sagittal, axial and coronal planes. White ellipses show proximal oesophageal data and black ellipses show the distal segment data. The mid-point of the ellipse represents the mean dipole source location following 50 iterations of Monte-Carlo analysis. 305
- Figure 6.5 95% confidence ellipses were co-registered with the MRI of that individual. For ease of comparison, ellipses were plotted on a single slice of the sagittal, axial and coronal planes. White ellipses show proximal oesophageal data and black ellipses show the distal segment data. The mid-point of the ellipse represents the mean dipole source location following 50 iterations of Monte-Carlo analysis. 307
- Figure 6.6 95% confidence ellipses were co-registered with the MRI of that individual. For ease of comparison, ellipses were plotted on a single slice of the sagittal, axial and coronal planes. White ellipses show proximal oesophageal data and black ellipses show the distal segment data. The mid-point of the ellipse represents the mean dipole source location following 50 iterations of Monte-Carlo analysis. 308
- Figure 6.7 95% confidence ellipses were co-registered with the MRI of that individual. For ease of comparison, ellipses were plotted on a single slice of the sagittal, axial and coronal planes. White ellipses show proximal oesophageal data and black ellipses show the distal segment data. The mid-point of the ellipse represents the mean dipole source location following 50 iterations of Monte-Carlo analysis. 309
- Figure 6.8 To more readily compare the source localisations between subjects, the three dimensional proportional grid system of Talairach and Tournoux (1988) was employed. Upper graph shows the relative localisations of superiorly placed sources with the lower graph depicting laterally located sources. 310

Figure 6.9 Segmentation of surface rendered 3- dimensional MRI images illustrate the juxta-position of dipole sources. White diamonds represent the mean dipole location following proximal oesophageal stimulation and the black diamonds represent the distal oesophageal data.

313



### 1. The Anatomy and Physiology of Sensory-Motor pathways

#### 1.1 The receptors

There is still much debate as to the anatomical sources of the somatosensory derived potentials, particularly at the cortical level. Anatomical pathways that are considered to be involved in somesthesia and the 'grey' areas of knowledge will now be outlined

**The skin** contains several forms of sense organs as well as free nerve endings. These receptors are classified in a number of ways. Three main divisions are Exteroceptors, Proprioceptors and Interoceptors. The latter constitute the receptor end organs of the visceral afferent components and detect internal events such as changes in blood pressure; we will not consider these further. Exteroceptors respond to stimuli from the external environment and are therefore found at or close to the surface of the body. These include the encapsulated and non-encapsulated terminals in the skin and around hairs; examples of the encapsulated terminals are i) Tactile Corpuscles of Meissner - found in papillae of skin of all parts of the hand and foot. ii) Lamellated Corpuscles of Pacini - subcutaneous tissue of the palmer aspects of the hand and planter aspects of the digits, generally accepted as pressure receptors and probably sensitive to vibration. iii) Bulbous corpuscles of Krause. iv) Ruffini endings (Figure 1.1)

|| | | | |



Aston University

Illustration has been removed for copyright restrictions

*Figure 1.1 Cross section of the skin indicating the variety of sensory receptors. From  
McNaught and Callander (1983).*

## Chapter 1

Proprioceptors respond to stimuli arising in deeper tissues. They are concerned with movement, position and pressure and include the neurotendinous organs of Golgi, the neuromuscular spindles and deeply placed Pacinian corpuscles. They are stimulated by the activity of the muscles, movements of the joints and changes in the position of the body as a whole or in part. They are essential to the co-ordination of muscles, the grading of muscular contraction and the maintenance of equilibrium.

Free nerve endings occur in many different sites in the body. In the skin they are generally regarded as 'pain receptors' or '*nociceptors*' since they have a high sensory threshold and only potentially traumatic stimuli will cause a high level of activity in these fibres. Many nociceptors may be specialised chemoreceptors that are excited by tissue substances released in response to noxious stimuli; such substances include histamine, bradykinin, serotonin, acetylcholine, substance P and high concentrations of  $K^+$ .

The other receptors may also be classified on the basis of their properties as afferent units, such as *mechanoreceptors* that fire maximally following mechanical deformation or *thermoreceptors*, firing maximally following temperature change.

Mechanoreceptors can be further subdivided into Rapid adapting and Slow adapting types based on their type of response and distribution. Rapid adaption indicates that the unit is firing only as long as the stimulus is moving or active whereas slow adaption indicates that the unit also fires when the stimulus is held constant. It has been suggested that tactile corpuscles (Meissners) and the nerve endings around hair follicles respond to touch (Rapid adaption), the bulbous corpuscles to cold, the Ruffini type of receptor organ to warmth (Slow adaption) and the free nerve endings in the epidermis and dermis to pain. The lamellated corpuscles are sensitive to deformation. However, it is suggested that the appreciation of the different modalities of cutaneous sensation depends more on the pattern of the impulses arriving at the sensory cortex, including their number and spatial and temporal arrangements. For example, touch, heat, cold and pain can be appreciated in the cornea where only free nerve endings exist.

## Chapter 1

All cutaneous sensors and many proprioceptors are thought to be of one structural type. This is where the neuronal receptor is itself a primary sensory neuron with a perikaryon situated in a craniospinal ganglion and a long peripheral process, the ending of which constitutes the actual sensory terminal.

### 1.1.1 Receptors of proprioception

The problem of which receptors are responsible for mediating proprioception is still debated in the literature. Joint receptors, once thought entirely dominant in this role, are losing ground to both muscle and cutaneous receptors. Moberg (1983) made many observations on patients during four decades of reconstructive limb surgery, together with the results of some simple experiments, also on man, and mainly by blocking the afferent input from different parts of the forearm and hand, have suggested that the role of cutaneous receptors in position sense and kinaesthesia has been greatly underestimated. The following contribution is from a review by Matthews (1988) who examines a number of these factors.

Table 1.1 (overleaf) lists the numerous receptors that transmit signals whenever we move. The question is which of them contribute significantly to position sense.

The standard neurological test of position sense, namely waggling the patients passive finger, does not correspond to any commonly occurring natural stimulus. The detection of such essentially external stimuli cannot be the prime function of the internally placed proprioceptors. A priori, this would seem to fall equally within the sphere of action of the cutaneous receptors.

#### 1.1.1.1 Cutaneous receptors

Recent observations, shown by recording from single fibres in man, is that for the hand virtually all of the receptors are excited whenever we move it. It is reasonable to suppose that the sensation during movement bears no relation to that elicited by an external stimulus.

# Chapter 1

Table 1-1 RECEPTORS THAT TRANSMIT SIGNALS DURING MOVEMENT (MATTHEWS 1988)

POSITION SENSE	POSSIBLE NEURAL INPUTS
1. Joint	In capsule In ligaments
2. Skin	Fast adapting I and II Slow adapting I and II
3. Muscle	Spindle: primary and secondary Tendon organ
4. Motor centres	Corollary discharges.

## 1.1.1.2 Joint Receptors

As mentioned earlier, these are now out of favour as producing a significant contribution to position sense. This is largely due to work in animals on studies of the knee that intimates that they are only effectively excited by moving the joint to one or other of its extremes. In the middle of the range most, if not all, are normally quite silent, including while the joint is being moved (Burgess and Clark 1969; Grigg and Greenspan 1977).

## 1.1.1.3 Muscle receptors

Their sensory contribution would be expected to be in the genesis of sensations of force and effort rather than position. Of undoubted importance however are the

## Chapter 1

muscle spindle afferents that lie in parallel with the main muscle and so signal its length; in addition they can be specifically excited by the fusimotor system or gamma efferents.

### 1.2 The Peripheral Nerve

There are pure sensory nerves, pure motor nerves and mixed nerves. The skin is innervated by cutaneous nerves; most but not all of them are branches from mixed sensory-motor nerves. In cutaneous nerves about 50% of the sensory fibres originate from nociceptors.

Mixed peripheral nerves have been classified according to total fibre diameter and conduction velocity. The three main classifications are A,B and C. Class B comprises the myelinated preganglionic fibres of the autonomic nervous system and we will consider these no further.

**Class A** fibres can be further subdivided and we will consider the afferent sensory fibres within this classification.

Group I The thickest myelinated A fibres ( type A alpha) vary from 1 $\mu$ m to 20 $\mu$ m in diameter. Their excitability threshold is low and their conduction velocity is high - as much as 100 m/sec. They include the primary sensory fibres from muscle spindles (subgroup Ia) and from tendon organs (Ib).

Group II The diameters of group II fibres range from 5 to 15 $\mu$ m, and their conduction velocities from 20 to 90 m/sec. Includes cutaneous afferent fibres from various mechanoreceptors such as touch and Pacinian corpuscles, receptors associated with larger, 'guard' hair follicles and fibres of the secondary endings on the intrafusal muscle fibres of muscle spindles.

Group III (A delta fibres) Their diameters range from 1 to 7 $\mu$ m and their conduction speeds from 12 to 30 m/sec. Fibres innervate follicle receptors associated with finer hair, sensory endings in the walls of some blood vessels, and a variety of nociceptors.

## Chapter 1

### Group IV (type C fibres)

These are non-myelinated nerve fibres with diameters ranging from 0.2µm to about 1.5µm and conduction velocities of 0.3-1.6 m/sec. Such fibres include autonomic efferents which are postganglionic in position, and both visceral and somatic sensory fibres, many of which are 'pain' fibres serving all the tissues of the body except the interior of the central nervous system.

Each sensory neurone works on the 'all or none' principle; all impulses in a given neuron are identical to one another, and the only variables will be the number of impulses transmitted along the neurone per second, and the pattern of this discharge. Since neurones do not vary the amplitude or size of the nerve impulse, an increase in a sensory stimulus is transmitted to the CNS as more impulses per second.

#### 1.2.1 Somatosensory activity in peripheral nerve.

With electrical skin stimuli in the glabrous skin of the hand and the microelectrode positioned in the appropriate median nerve fascicle, the response in A-alpha fibres can be recorded at the threshold for perception of the stimulus ( Valbo et al 1979). At this weak stimulus strength the subjects report tactile sensations, described as tapping, flutter or vibration, dependent on the stimulation frequency. At 5-10 times threshold, A-delta fibres are recruited. Single stimuli are felt to be sharp and pricking, and repetitive stimulation at 50 hz causes severe pain. Further increase in stimulus intensity up to 15-20 times threshold recruits C fibre deflections. Single shocks are described as heavy sharp pain followed by an aching "afterpain". In the radial nerve some A delta and C fibre deflections may be activated by non-painful skin stimuli just above threshold for perception indicating that impulses in thin fibres need not necessarily be associated with pain.

## Chapter 1

### 1.2.2 Proprioceptive activity in peripheral nerve

Most units encountered in muscle nerve fascicles are mechanoreceptive afferents of muscular origin. They do not respond to skin stimuli or local joint pressure, but they do respond to mechanical stimulation of the receptor bearing muscle by passive stretch and local pressure and to an isometric voluntary contraction of this muscle. Muscle receptors responding in this way are likely to be either primary spindle endings, secondary spindle endings, or Golgi tendon organs. Sudden light taps on the muscle belly or tendon are usually sufficient to induce a spindle discharge.

Some characteristics of proprioceptive receptor stimulation are;

#### 1) Primary muscle spindle endings

- a) High dynamic sensitivity to passive muscle stretch, the firing rate increasing with speed of movement.
- b) Silence during the rising phase and discharge during the falling phase of an electrically induced twitch contraction of the receptor bearing muscle.

#### 2) Secondary muscle spindle endings

- a) Have a position sensitivity similar to that of the primary endings but a much smaller dynamic sensitivity to sudden stretches or relaxations.
- b). Silence during the rising phase of an electrically induced twitch contraction of the receptor bearing muscle.

#### 3). Golgi tendon organs

- a). No resting discharge at intermediate muscle length and relatively low dynamic sensitivity to passive stretch.
- b). Close relation between discharge rate and contraction force.
- c). Discharge during the rising phase of an electrically induced muscle twitch.



# Chapter 1

## 1.3 Dorsal Nerve Roots

Sensory and motor nerves run for the greater part of their route as a mixed nerve with motor and sensory fibres in adjacent bundles, although they have separate spinal cord roots. Motor nerves have their cells of origin in the anterior horn of grey matter of the spinal cord. These nerves leave via the ventral nerve roots. Sensory nerves have their cells of origin outside the spinal cord in the spinal ganglia, entering the cord via the dorsal nerve roots.

Each ganglion cell possesses a single nerve process that divides in the form of a "T", with a central branch running to the spinal cord and a peripheral branch coming from a receptor organ or organs. There are no synapses in a spinal ganglion.

The area in which the dorsal root fibres enter the spinal cord, in the region of the dorsolateral sulcus, is called the dorsal root zone. The largest and most heavily myelinated fibers generally occupy the most medial position in this zone, and the small myelinated and unmyelinated fibres are the most lateral.

The subsequent pathways after dorsal root entry, now depend on the type of sensation.

## 1.4 Pathways mediating sensation.

Tactile sensations are complex in nature because they involve a blending of light cutaneous contact and variable degrees of pressure, depending upon the intensity of the stimuli. Two different forms of touch sensibility are recognised: simple touch and tactile discrimination. Simple touch involves a sense of light contact with the skin associated with light pressure and a crude sense of tactile localisation. Tickling and itching sensations are related to pain sense. Tactile discrimination conveys the sense of spatial localisation and perception of the size and shape of objects.

At least three different spinal cord pathways mediate tactile sensation (Figure 1.2):

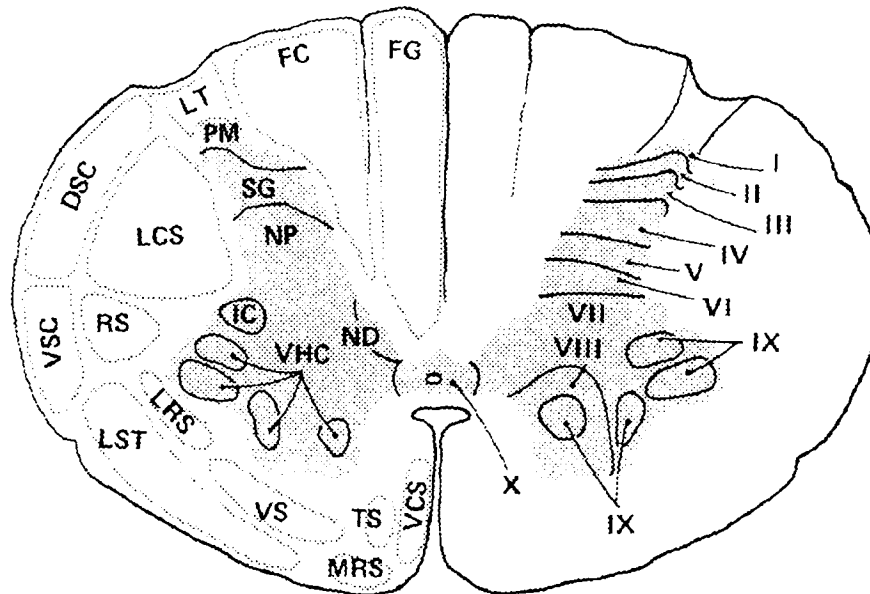


Figure 1.2 Cross section of spinal cord at approximately the C8/T1 segmental level. Tracts and nuclei of the cord are illustrated on the left; Rexed's laminar organisation of the grey matter are illustrated on the right. DSC= dorsal spinocerebellar tract; FC= fasciculus cuneatus; FG= fasciculus gracilis; IC=intermediolateral cell column; LCS= lateral corticospinal tract; LRS= lateral reticulospinal tract; LST= lateral spinothalamic tract; LT= Lissauer's tract; MRS= medial reticulospinal tract; ND= nucleus dorsalis; NP= nucleus proprius; PM= posteromarginal nucleus; RS= rubrospinal tract; SG= substantia gelatinosa; TS= tectospinal tract; VCS= ventral corticospinal tract; VHC= ventral horn cell columns; VS= vestibulospinal tract; VSC= ventral spinocerebellar tract. Adapted from Gilman and Newman (1987)

## Chapter 1

The LEMNISCAL PATHWAYS are concerned with the discriminative aspects of touch, including place, contour and quality of the stimulus, and identification of objects and numbers on the hand. This latter sensory capacity is stereognosis.

The ANTEROLATERAL SYSTEM, comprising the lateral and ventral spinothalamic tracts subserves simple touch sensation. The other component of the anterolateral system, the spinoreticular projections, is concerned with responses to noxious stimuli.

Finally the LATERAL CERVICAL SYSTEM (Spincervicothalamic pathway) is thought to mediate touch sensation as well as vibratory and proprioceptive senses.

We will now consider these pathways individually:

### 1.4.1 Lemniscal System.

This pathway comprises two large ascending tracts, the fasciculi gracilis and cuneatus, which are separated from each other by the postero-intermediate septum. (Figure 1.3). The fasciculus gracilis receives fibres from the lower thoracic, lumbar, sacral and coccygeal segments and we will consider this no further.

The fasciculus cuneatus commences in the mid thoracic region and derives its fibres from the dorsal roots of the upper thoracic and cervical nerves and in consequence is situated laterally to the fasciculus gracilis. The fasciculus is heavily myelinated and contain the central processes from cells in the spinal ganglia, and these pass without interruption or decussation to the medulla oblongata, where they terminate in the cuneate nuclei.

The dorsal column nuclei are not simple 'relay nuclei' as was long supposed - afferent information is separated in channels which are discrete both for spatial origin and stimulus specificity (Uddenberg 1968) - in the cat, those fibres conducting impulses from hair receptors being most superficial, followed by fibres mediating tactile and vibratory sensibility in successively deeper layers.

## Chapter 1

All the large calibre fibres of the dorsal funiculus (excepting some of the medially placed ones), have collaterals which pass through the medial two thirds of laminae I, II and III.

The internal structure of the spinal cord changes gradually to that of the **medulla oblongata**. The posterior region is divisible into caudal and cranial levels. The caudal part, consists of the upward continuation of the fasciculi gracilis and cuneatus of the spinal cord. These two fasciculi are at first vertical but at the caudal end of the fourth ventricle they diverge from the median plane, and each presents an elongated swelling; that on the fasciculus cuneatus is termed the cuneate tubercle and is caused by a nucleus of grey matter termed the nucleus cuneatus. Most of the fibres of the fasciculus end by forming synapses in this nucleus. The somatotopic arrangements in the tracts is also evident in the nuclei, within which there is also a specific distribution of terminals on the basis of sensory modalities, including hair displacement, light touch, pressure, vibration and joint movement.

New fibres arise in the nucleus and constitute the second neurons on the pathway of tactile and proprioceptive sensibilities. These internal arcuate fibres emerge from the ventral aspects of the nuclei and, curving forwards and laterally at first round the central grey matter, they bend medially to reach the median plane, where they decussate with the corresponding fibres of the opposite side.

The fibres of the medial lemniscus, after emerging from the lemniscal decussation, turn upwards on each side in the form of a flattened tract. In this position they ascend to the pons, increasing in number as additional fibres join them from the upper levels of the decussation.

The spinocerebellar, spinotectal, vestibulospinal, rubrospinal and lateral spinothalamic tracts (spinal lemniscus), are all in the anterolateral area.

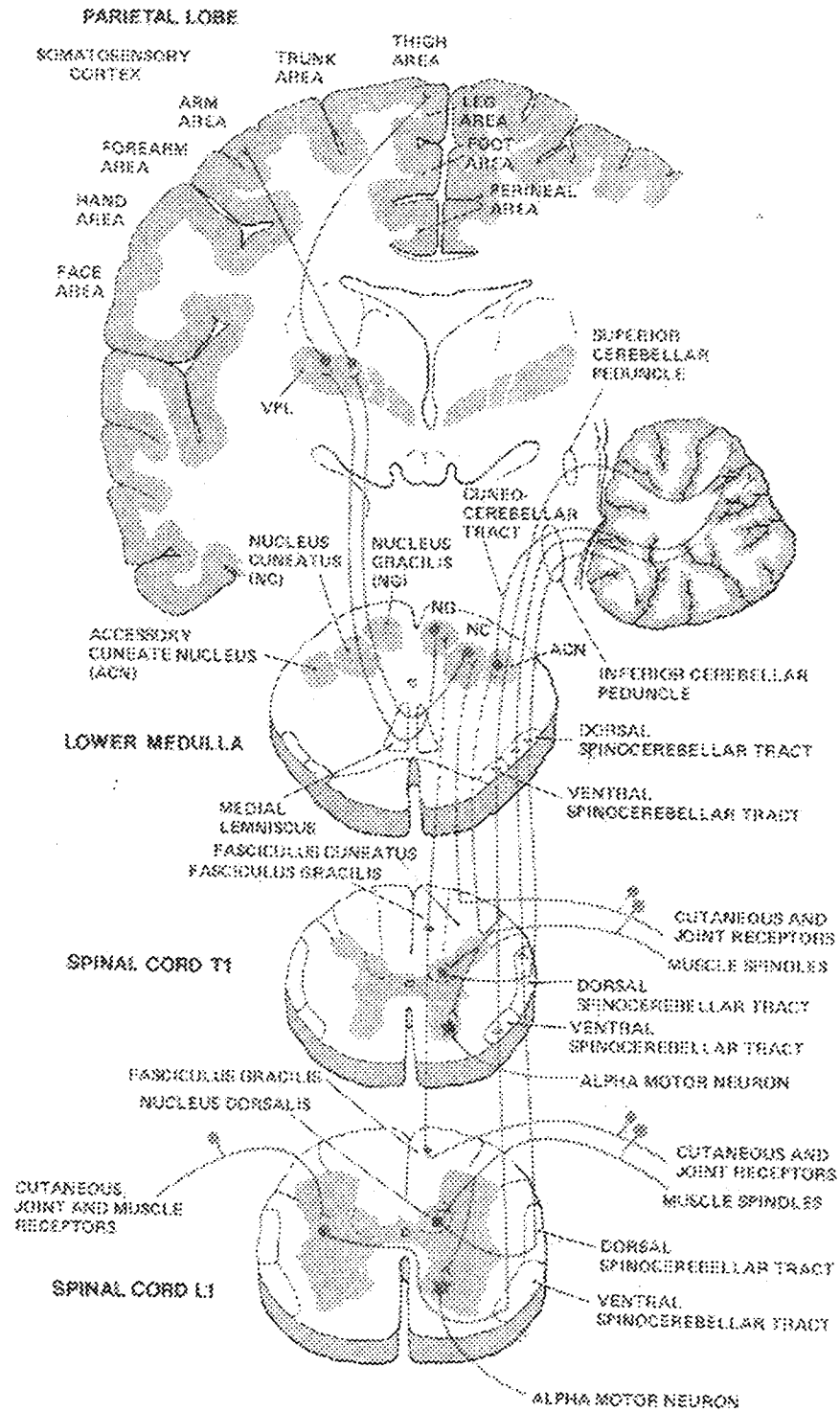


Figure 1.3 The central nervous system pathways mediating proprioception and stereognosis.

NG= nucleus gracilis; NC= nucleus cuneatus; ACN= accessory cuneate nucleus; VPL= thalamic nucleus ventralis posterolateralis. Adapted from Gilman and Newman (1987).

## Chapter 1

Inferiorly the pons is continuous with the medulla oblongata. Here the medial lemniscus is joined by the second neuron fibres from the principal sensory nucleus of the trigeminal nerve, which convey proprioceptive, tactile and pressure impulses from the receptive field covered by it.

The somatotopic lamination is maintained throughout the passage of the tracts through the medulla oblongata and the pons. In the midbrain however, the fibres from the lower limbs extend dorsally, and in this part of their course it is possible for the surgeon to divide the pain and temperature fibres of the upper limb and trunk without injury to the corresponding fibres of the lower limb.

The ascending somatosensory fibres terminate in the **ventral group of thalamic nuclei** (See section 1.5).

### 1.4.2 Anterolateral System

The sensations of pain, temperature and crude touch are mediated by the anterolateral system (Figure 1.4). The system contains pathways that include the lateral and ventral spinothalamic tracts. Other components of the anterolateral pathway, mainly spinoreticular, do not reach the thalamus and thus cannot be termed "spinothalamic".

Portions of the anterolateral system are phylogenetically old. The system consists of the "paleospinothalamic tract" which projects to the medial portions of the thalamus (the intralaminar nuclei), and the "neospinothalamic tract" which projects to the ventral posterolateral region of the thalamus.

The anterolateral system is predominantly a slowly conducting, polysynaptic system. In humans, a small percentage of fibres go directly to the thalamus, but most synapse in the medial aspect of the reticular formation throughout its length in the brain stem.

## Chapter 1

Neural responses to noxious stimuli mediated by A delta and C peripheral nerve fibres enter the spinal cord through the lateral part of the dorsal root zone and divide at once into short ascending and descending branches that run longitudinally in the Tract of Lissauer (posterolateral fasciculus). Within a segment or two, these fibres leave this tract to make synaptic connections with neurons in the dorsal horn, including interneurons in laminae I, II and III (substantia gelatinosa), IV and V. The interneurons project to neurons in laminae V through VIII and there make synaptic connection upon the cells of origin of the anterolateral system, including the lateral and ventral spinothalamic tracts and the spinoreticular projections.

The axons of the spinothalamic tract cells cross anterior to the central canal in the ventral white commissure and then rostrally in the antero-lateral funiculus.

The subsequent projection of the anterolateral system to the thalamus is organised somatotopically so that the upper body is located medial to that from the lower body.

The lateral spinothalamic tract extends through the spinal cord and brain stem, supplying inputs to the reticular formation, the superior coliculus and several thalamic nuclei, including the intralaminar nuclei, the posterior nuclear complex (PO), and the ventral posterolateral nucleus (VPL) (See section 1.5.0).

Previously, the lateral and ventral components of the spinothalamic tract were thought to subserve different functions, with the lateral spinothalamic tract mediating nociceptive information and the ventral spinothalamic tract mediating tactile sensation. Recent evidence indicates no functional difference between the lateral and ventral components of the spinothalamic tract. Both are capable of mediating nociceptive and tactile sensation.

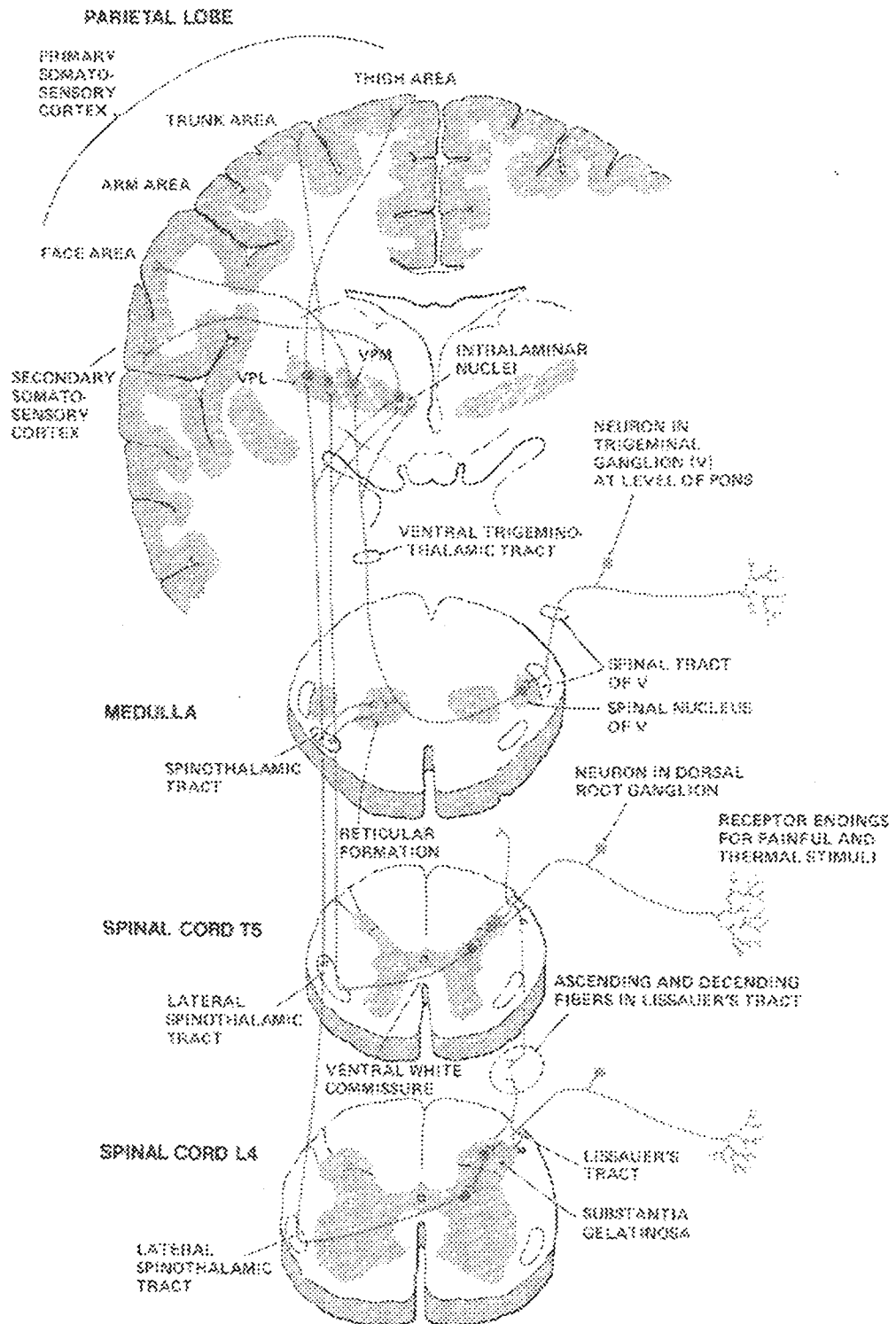


Figure 1.4 The central nervous system pathways that mediate the sensations of pain and temperature. Adapted from Gilman and Newman (1987).



### 1.4.3 Lateral Cervical System

Almost all of the cells of the lateral cervical system (Figure 1.5) are sensitive to light mechanical stimulation of the skin of the ipsilateral side of the body, but a few are activated by noxious stimuli. Peripheral nerve fibres entering this system make synaptic connections in the dorsal horn (laminae III, IV and V) throughout the length of the spinal cord. Heavily myelinated second-order neurons arise in these laminae and ascend ipsilaterally in the most medial corner of the dorsal lateral funiculus to terminate in the lateral cervical nucleus. This nucleus is located just lateral to the dorsal horn of the first and second cervical segments (see Figure 1.5). The axons of these cells cross the spinal cord to join the contralateral medial lemniscus and, with it, terminate within the thalamus. The fibres of the entire lateral cervical system conduct very rapidly.

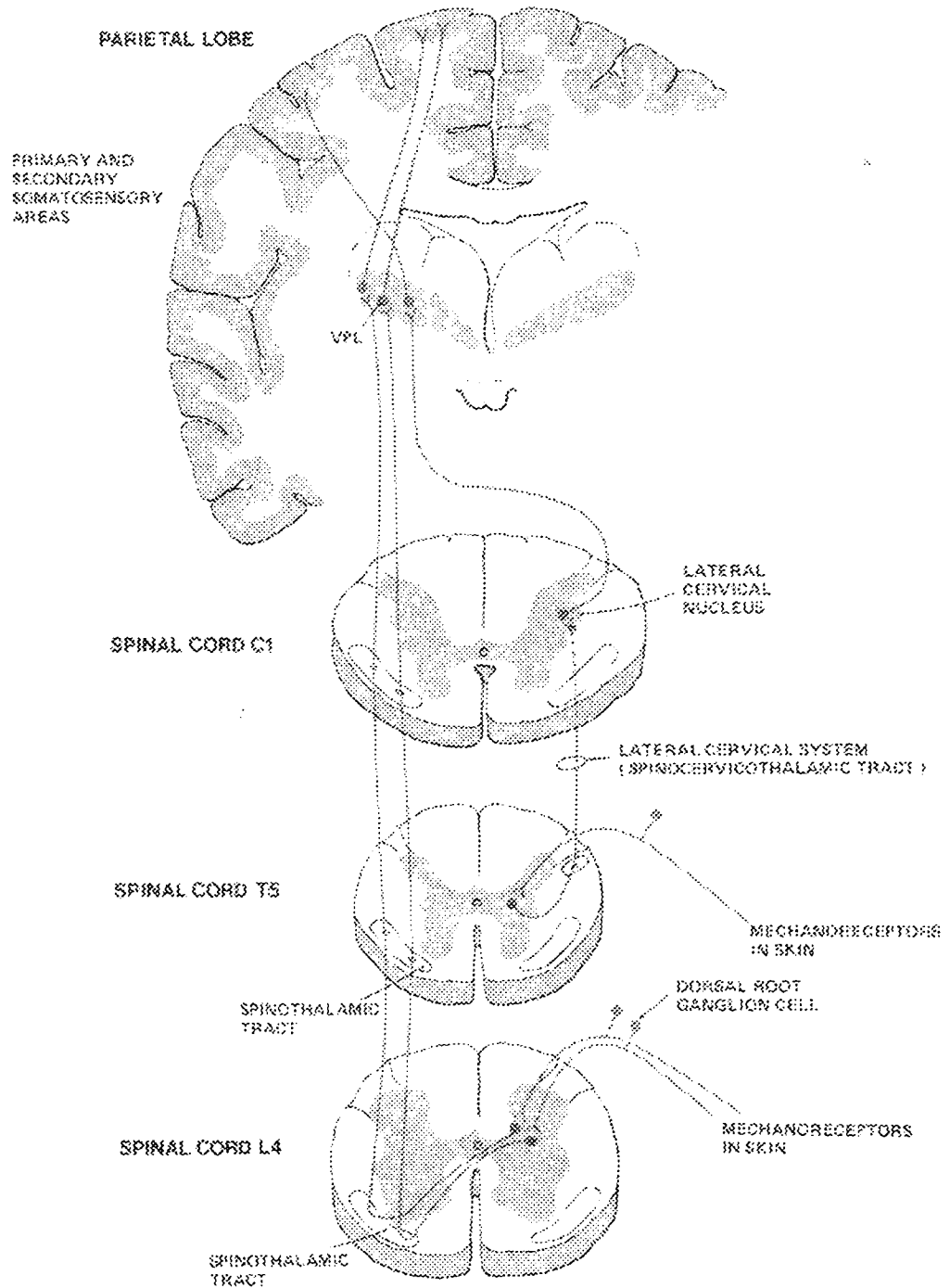


Figure 1.5 The central nervous system pathways mediating tactile sensation except for the lemniscal system. The lateral and ventral components of the lateral spinothalamic tract are shown. Adapted from Gilman and Newman (1987).

### 1.5 Thalamic Nuclei

The ventral group of thalamic nuclei form a craniocaudal sequence of three main nuclei; the Ventralis anterior (VA), the Ventralis Intermedius (VI), also known as the Ventralis Lateralis (VL) and the Ventralis Posterior (VP). The latter can be subdivided into the Ventralis Posterior Lateralis (VPL) and the Ventralis Posterior Medialis (VPM). There are additional nuclei in this group which are inferior and oral in position (Figure 1.6)

The terminations of the medial lemniscus and spinothalamic tract fibres show contrasting features. The lemniscal fibres are wholly crossed, originating exclusively in the gracile and cuneate nuclei of the opposite side and their terminals are confined to the VPL. Whilst the majority of the spinothalamic tract fibres are also crossed, an appreciable number ascend on the same side and terminate in the ipsilateral thalamus.

VPL cells are highly specific for both the type of stimulus and the bodily site of origin. In monkeys, units respond to contralateral stimulation of the skin or hairs, or joint movement or static joint position or sinusoidal tissue vibration, but never to two of these varieties. Receptive fields from medial lemniscus activity are small and sharply localised, the smallest being recorded by stimulation of the terminal segments of the limbs. Units responding to spinothalamic tract activity in general show rather larger receptive fields and are somewhat less modality specific.

Transmission in the nuclei may be modulated by activity in descending corticothalamic fibres.

The main thalamocortical radiations from the VPL and VPM proceed through the posterior limb of the internal capsule to the primary somatic sensory areas of the cerebral cortex. Throughout this radiation the precise somatotopic organisation continues to be preserved. The same cortical projection areas project corticothalamic fibres back to the nuclei. Unfortunately, the thalamic projections to the secondary somatic sensory areas cannot yet be regarded as settled.

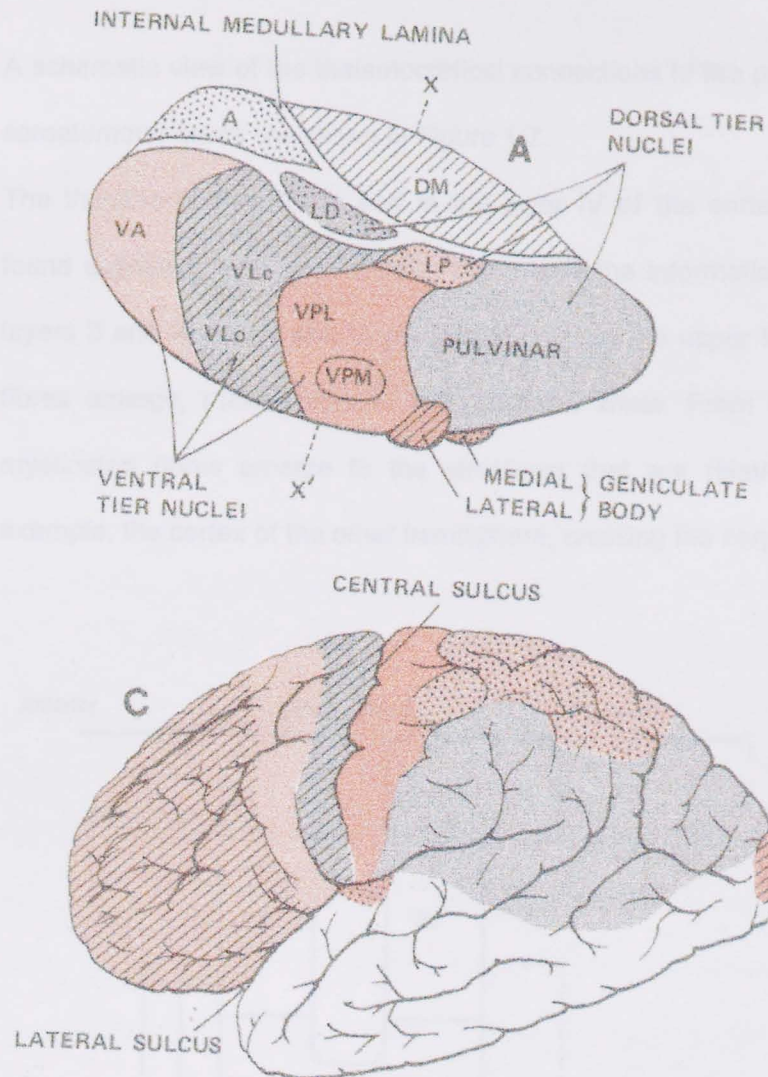


Figure 1.6 Thalamic nuclei. (A) A schematic dorsolateral view of the thalamus, which has been dissected from the left side of the brain, showing the boundaries of the thalamic nuclei. A= anterior nuclear group; CM= centromedian nucleus; DM= dorsomedial nucleus; LD= lateral dorsal nucleus; LP= lateral posterior nucleus; VA= ventral anterior nucleus; VLc= ventral lateral pars caudalis; VLo= ventral lateral pars oralis; VPL= ventral posterolateral nucleus; VPM= ventral posteromedial nucleus. Thalamic projections to the cortex are represented by the matching colours shown on the schematic brain C. Adapted from Gilman and Newman (1987).

## Chapter 1

### 1.6 Thalamo - Cortical and Cortico - Cortical Projections

A schematic view of the thalamocortical connections to the primary somatosensory / somatomotor areas are shown in Figure 1.7.

The thalamo-cortical tracts end in the layer IV of the cortex where synapses are found especially with stellate cells. From here the information is transported to the layers II and III and V and VI respectively. From the upper layers, the so-called U-fibres emerge, making contact with adjacent areas. From the lower layers large myelinated fibres emerge to the structures that are relatively far away as, for example, the cortex of the other hemisphere, crossing the corpus callosum.

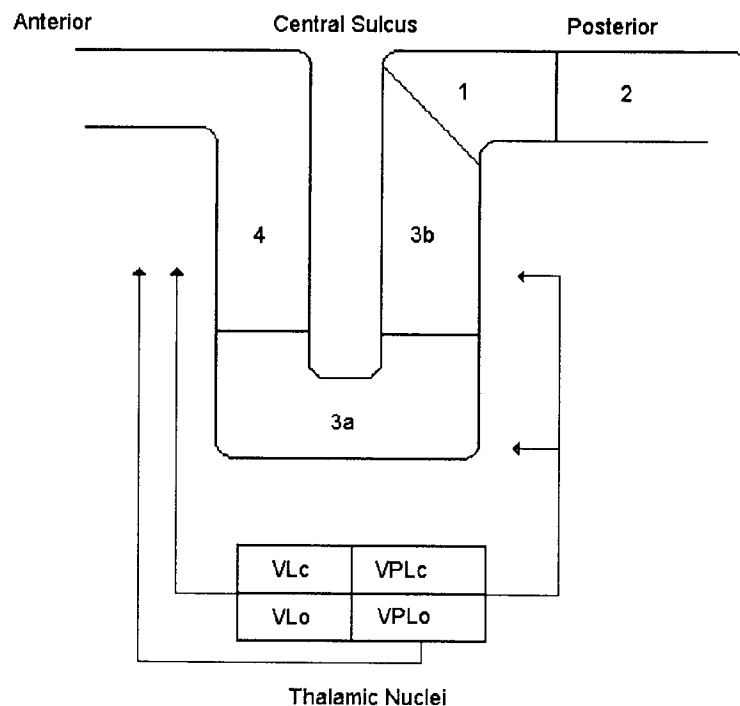


Figure 1.7 Schematic transverse cross section of the central sulcus showing Brodman areas and thalamocortical projections in the human brain. VLc= ventral lateral pars caudalis; VLo= ventral lateral pars oralis; VPLc= ventral posterolateral pars caudalis; VPLo= ventral posterolateral pars oralis.

### 1.7 Sensory - Motor Cortex

Evidence over the last 30 years has shown that the areas receiving or originating projection fibres for somesthesia are much more extensive than the initial classical studies indicated. Furthermore, the division into 'receiving' and 'originating' projection areas is by no means so distinct as at first appeared. The postcentral gyrus is not the only area to which a somatosensory thalamic projection is directed and the distinction of motor and sensory areas still favoured in simplistic description is erroneous. In 1933 Dusser de Barenne demonstrated motor responses to stimulation of the 'sensory' areas, and projection of efferent pyramidal fibres from the same postcentral area were described by Levin and Bradford in 1938.

#### 1.7.1 Somatosensory cortex

In the postcentral gyrus **Sml** is the primary sensory area. Much work has been done using ablation techniques to study the projections of this area of cortex. In the main somatic areas, as in the visual sensory areas, it is apparent that there is an anatomical segregation of "building blocks" of different types in that neurons with similar response properties tend to be grouped in different architectonic subdivisions of the primary sensory areas. A schematic transverse section of the central sulcus showing the relative locations of the Brodmann classification of this area is shown in Figure 1.7.

Its anterior part (Brodmann area 3), borders the central sulcus and extends into its depths to meet the agranular cortex of area 4. It is of the granular type but also contains numbers of scattered medium and small pyramidal cells.

The posterior part of the postcentral gyrus (areas 1 and 2) differs particularly in its smaller content of less densely packed granular or stellate cells. The precise boundary, if such exists, between the pre and post central areas in the central sulcus (area 3a) is still subject to much experimentation.

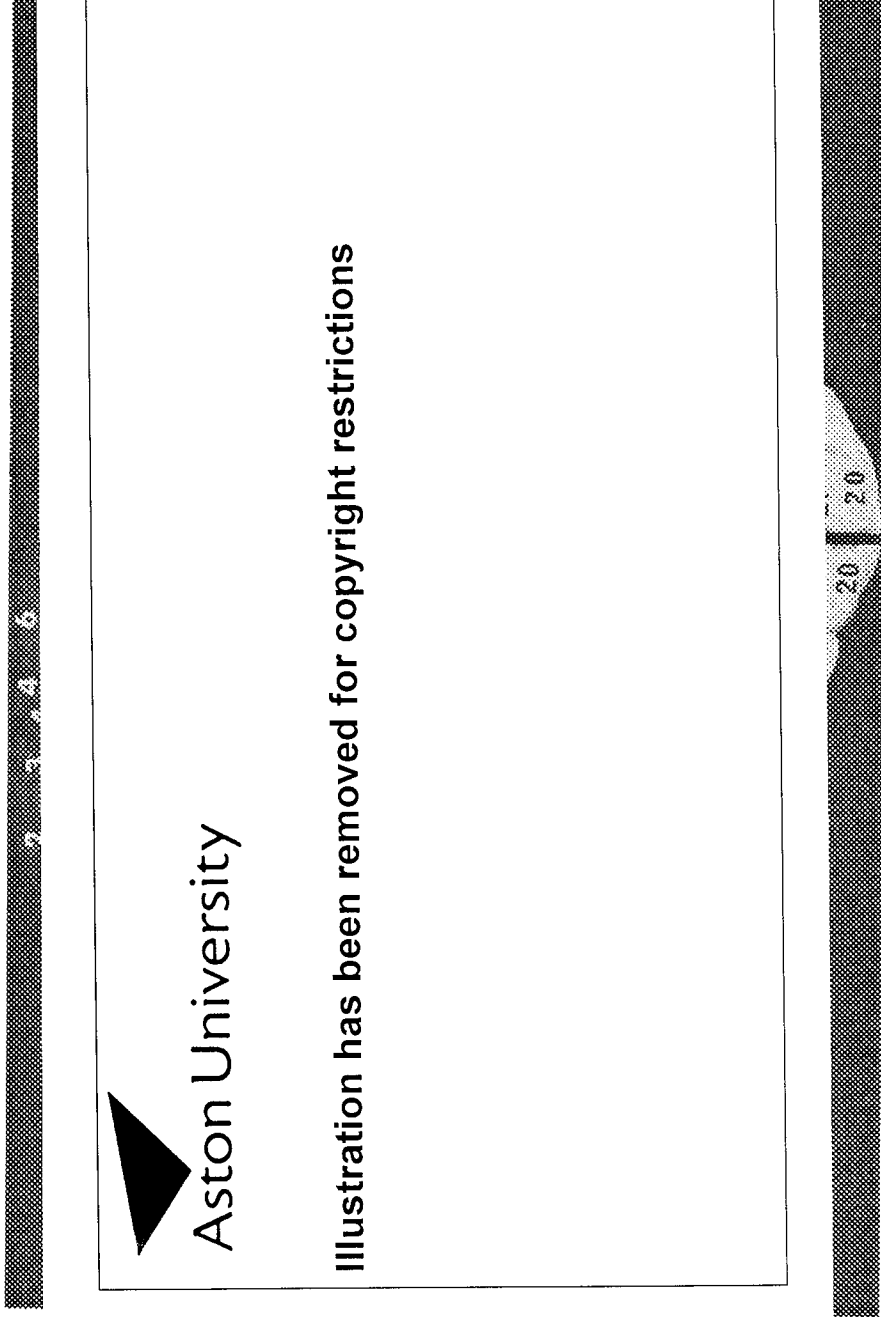


Figure 1.8 Brodmann cortical area classifications shown on a brain surface (from Talairach and Tournoux 1988).

## Chapter 1

The primary somatosensory cortex, as previously mentioned, receives its main input from the thalamic ventrobasal complex. In the monkey the projection to area 3b is heavy and made up of singularly coarse fibres, whereas the fibres to areas 1 and 2 are much fewer in number and finer in calibre (Hyvarinen 1982). It is possible that the fibres to areas 1 and 2 are branches of the coarser fibres passing to area 3b (Jones and Powell 1969a). The most anterior part of Sml, area 3a, also receives a projection from the ventrobasal complex from the subnucleus ventralis posterolateralis, pars oralis (VPLo), (Jones and Porter 1980). Area 3a differs from the more posterior part of Sml in that it receives a strong afferent input from muscles (Phillips et al., 1971), whereas the muscles have little or no representation in areas 3b and 1.

The number of neurones with complex cutaneous receptive fields increase posteriorly within Sml. Most movement sensitive neurones that do not differentiate between directions are located in area 1. The more complex cell types specifically sensitive to direction of movement or to orientation of an edge are not observed in area 3b and their number increase posteriorly (Hyvarinen 1982). Anatomical data therefore suggests that an increase in the complexity of the information handled occurs in the cytoarchitectural subdivisions of Sml with successive intracortical projection steps from area 3 to areas 1 and 2.

Inferior to Sml lies **SmlI**, found in the superior lip of the posterior limb of the lateral fissure. Evoked potentials indicate a somatotopic organisation in SmlI, with the face area most anterior and the leg at the posterior or caudal end of the area. Single units associated with tactile and vibration senses have been identified, and stimulation of Pacinian corpuscles evokes higher potentials than in the primary somatosensory area (McIntyre et al 1967). This second somatosensory area projects to the thalamus, but its connections and their reciprocal nature have not yet been studied in detail. It also projects to the dorsal column nuclei.



## Chapter 1

### 1.7.1.1 Ipsilateral Cortical Connections

The primary somatosensory cortex is organised strictly somatotopically. Its neurons have rather small receptive fields that facilitate accurate localisation of stimuli, and they respond briskly, indicating precisely the timing of sensory events. Moreover, in Sml different submodalities are segregated in columns giving a localizational basis for stimulus quality.

Jones and Powell (1969a) demonstrated in the monkey that Sml and SmlI areas are connected with one another and with area 4 in a reciprocal organised manner and that each has a further projection to the supplementary motor area, MslI. Sml alone sends fibres outside the sensorimotor region - to area 5. The fibres passing from Sml to the above areas arise in all three of its architectonic subdivisions (areas 3,1 and 2). In addition, areas 3,1 and 2 are interconnected with one another and with the transitional field between sensory and motor cortex, area 3a, by intracortical association fibres. Functional columns in area 3, the majority of which respond preferentially to light tactile stimuli are firmly and reciprocally interconnected with those areas 1 and 2 which respond mainly to deep stimuli, that is pressure or rotation of a joint (Powell and Mountcastle 1959; Hyvarinen 1982)

SmlI receives fibres from areas 3,1 and 2 and from the ventrobasal complex of the thalamus.

It seems possible that area 3a may be a specific cortical projection area in Sml for Group I muscle afferents (Jones and Porter 1980) in much the same way as area 3 is the main receiving area for cutaneous afferents and areas 1 and 2 for afferents from deep tissues.

Area 2 represents a transitional zone between the anterior postcentral gyrus and the posterior parietal area 5. The latter is an associative somasthetic area that combines inputs from the joints with input from various submodalities to represent different somatosensory patterns arising during movement.

## Chapter 1

### 1.7.1.2 Contralateral Cortical Connections

It has been demonstrated in the monkey that in both Sml and Smll areas, only the parts of the cortex containing the representation of regions close to the mid-line are connected commissurally. In Sml, at least, those regions of cortex containing the representation of the distal, freer parts of the limbs neither receive nor send callosal fibres (Jones and Powell 1969b, Pandya and Vignolo 1968).

Projections from Sml and Smll are restricted to somatic sensory regions in the opposite cortex, Sml projecting in a topographically organised manner to both Sml and Smll of the contralateral side. The precise organisation of the commissural fibres may respect both the topographic and functional properties of individual cell columns. Smll, on the other hand, may be a region for interhemispheric convergence for all somatic sensory modalities.

### 1.7.2 Motor cortex

The **primary motor area**, also known as Brodmann's area 4, is located in the precentral gyrus of the frontal lobe. It extends from the lateral fissure upward to the dorsal border of the hemisphere and a short distance beyond to the medial surface of the frontal lobe in the rostral aspect of the paracentral lobule. The left motor strip controls the right side of the body, and the right strip controls the left side. The larynx and tongue are influenced by neurons in the lowest part of this strip, followed in upward sequence by the face, thumb, hand, forearm, arm, thorax, abdomen, thigh, leg and foot. The neurons controlling leg, foot and perineal muscles are in the paracentral lobule. In humans, areas for the hand, tongue and larynx are disproportionately large because of the elaborate motor control of these muscle groups.

Immediately rostral to area 4 is the premotor cortex, which consists of areas 6 and 8. Area 6 is involved in movement of the body musculature, and area 8 influences eye movements. The most medial aspect of area 6 can be seen on a midsagittal section

## Chapter 1

of the brain just rostral to the paracentral lobule. This is the location of the supplementary motor area. Another motor area is referred to as the secondary motor area and is present on the most ventral aspect of the precentral and postcentral gyri near the lateral fissure. This overlaps the secondary somatosensory cortex.

Area 4 is concerned with the performance of movements, particularly those of the distal joints of the limbs, and confers skill, precision and agility upon those movements. The activity of neurons in area 4 results in precisely fractionated muscle contractions, which are needed for individual finger movements. The discharge frequency of individual neurons in this area is related to the force that is generated during a movement.

The supplementary motor area and the premotor cortex are concerned with the planning and programming of movement performance. Both of these areas are thought to provide signals that influence the output of area 4. The functions of supplementary motor area neurones are related to complex movements of the limbs, including movements of the limbs simultaneously on both sides of the body. Movements of the contralateral limbs can be elicited from the supplementary motor areas in monkeys and in man. There is a bilateral projection to the thalamus and to the gracile, cuneate and pontine nuclei, contrasting with the similar but unilateral projections from the primary somatomotor cortex. Efferent fibres from this area have been traced into the spinal column in cats. Much is still to be discovered of the complete nature of this area.

### 1.8 Motor control fibres from the cerebral cortex and brain stem

Skeletal muscle activity results from the net influence of higher nervous system structures upon the alpha and gamma motoneurons of the spinal cord and upon the motor components of the cranial nerve nuclei. Collectively, these are the neurons

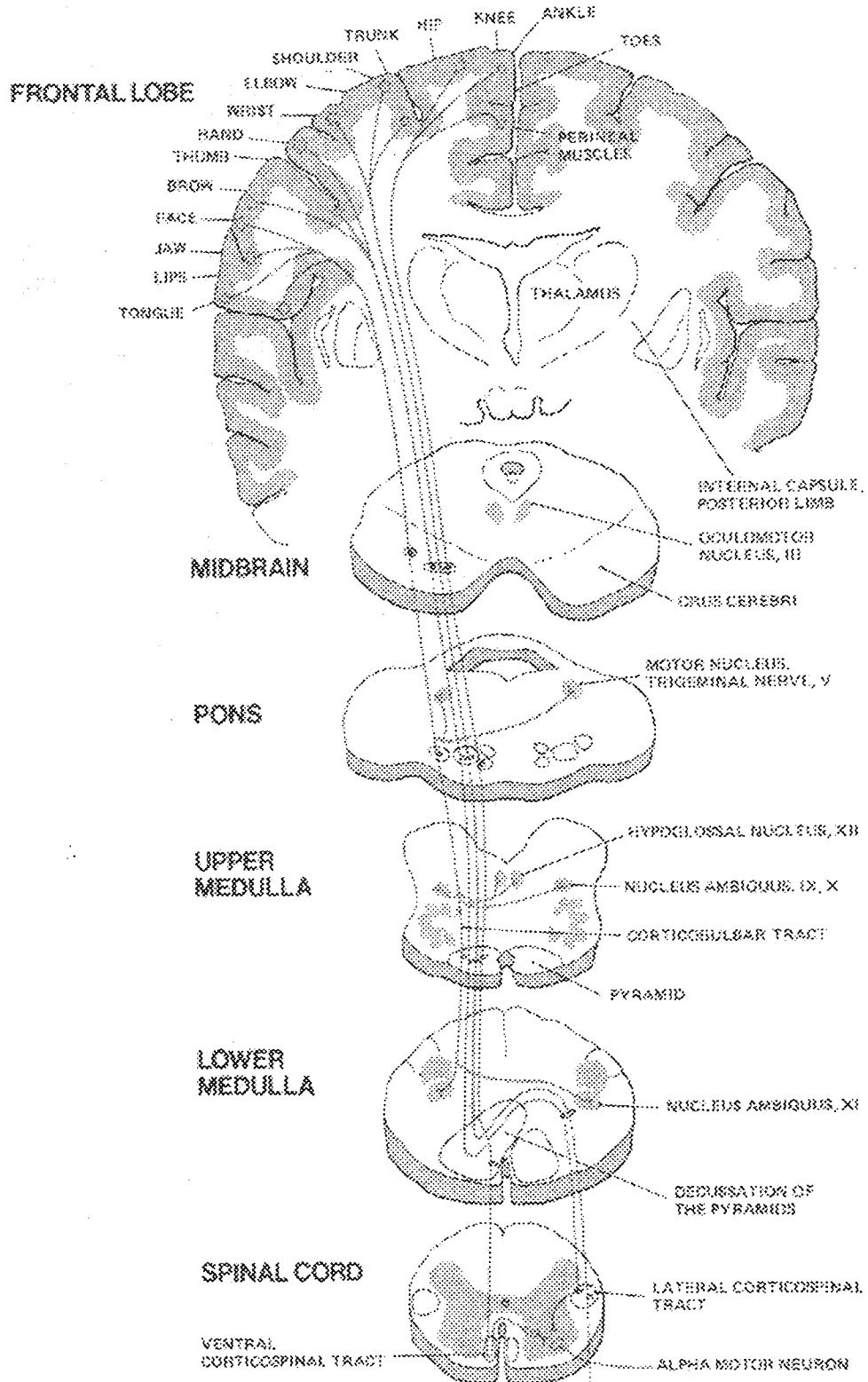


Figure 1.9 Descending pathways. Adapted from Gilman and Newman (1987)

## Chapter 1

that provide the final direct link with muscles through myoneuronal junctions (motor end plates). Such neurons are referred to as lower motor-neurons (LMN's). Their cell bodies reside within the central nervous system, and their axons make synaptic contact with extrafusal and intrafusal fibres of somatic origin.

A number of descending motor pathways regulate lower motor neuronal activity, which in turn controls somatic muscles (Figure 1.9). These descending pathways are controlled directly or indirectly by the cerebral cortex, cerebellum, or basal ganglia. The neurons in all such pathways should be termed upper motorneurons (UMNs). Upper motorneurons operate directly, or through interneurons, upon alpha and gamma motorneurons and upon motor components of the cranial nerve nuclei. They are contained completely within the central nervous system.

### 1.8.1 Corticospinal Tract

The corticospinal tract, also termed the pyramidal tract, was once considered to be the pathway that initiated and controlled all 'voluntary' muscular activity. It is now known to be concerned primarily with skilled movements of the distal muscles of the limbs and, in particular, with facilitation of the alpha and gamma motorneurons that innervate distal flexor musculature. Approximately one third of the axons in this tract arise from area 4, the primary motor cortex, and about 3 percent of these fibres originate from unusually large pyramidal cells, called Betz cells, which are located in the fifth layer of the cortex. Another one third of the fibres arise from area 6, and the remainder of the fibres originate from the parietal lobe, primarily areas 3,1 and 2 of the postcentral gyrus.

The corticospinal tract passes through the posterior limb of the internal capsule and the middle of the crus cerebri. It then breaks up into bundles in the basilar portion of the pons and finally collects into a discrete bundle forming the pyramid of the medulla. This pathway was originally named the pyramidal tract because of its passage through the medullary pyramid, and not because of its origin from pyramidal cells in the cortex. In the lower levels of the medulla, most of the corticospinal tract

## Chapter 1

decussates to the opposite side. This region is referred to as the level of the motor or pyramidal tract decussation. Approximately 90 percent of the fibres cross at this level and descend through the spinal cord at the lateral corticospinal tract, which passes to all cord levels in the lateral funiculus and synapses in the lateral aspect of laminae IV through VIII. Many of the cells in these laminae are interneurons that synapse on alpha and gamma motoneurons in lamina IX. In primates, a small percentage of the fibres (perhaps arising from Betz cells) synapse directly upon the alpha and gamma motoneurons in lamina IX. These motoneurons innervate the muscles in the distal parts of the extremities (hands and feet).

The 10 percent of corticospinal fibres that do not decussate in the medulla descend in the anterior funiculus of the cervical and upper thoracic cord levels as the ventral corticospinal tract. However, at their respective levels of termination, the fibres in this pathway decussate through the anterior white commissure (ventral white commissure) prior to synapsing upon interneurons and motoneurons. The number of fibres in both lateral and ventral corticospinal tracts decreases in successively lower cord segments as more and more fibres reach their terminations.

The corticospinal tract is not purely motor. It also sends fibres to synapse on interneurons in laminae IV, V, and VI of the spinal cord. These interneurons can influence local reflex arcs and cells of origin of ascending sensory pathways. Thus, the cerebral cortex can control motor output and can also modify sensory input reaching the brain.

The corticospinal tract exerts both facilitatory and inhibitory influences on the spinal interneurons and motoneurons it contacts. Activation of the corticospinal tract generally evokes excitatory postsynaptic potentials in interneurons and motoneurons of flexor muscles and inhibitory postsynaptic potentials in those of extensor muscles. The discharge rate of cerebral cortical neurons of the corticospinal tract is directly related to the force exerted by a limb during an active movement. The facilitatory effects of the corticospinal tract are thought to be mediated by the neurotransmitter, glutamate.

# Chapter 1

## 1.8.2 Corticobulbar Tract

The fibres of the corticobulbar tract arise from neurons in the ventral lateral part of areas 4 and 6, and from area 8. The axons start out in company with the corticospinal tract but take a divergent route at the level of the midbrain. The fibres of this pathway terminate in the brain stem, where they influence (but not by direct, or monosynaptic, connections) the motor nuclei of cranial nerves.

## 1.8.3 Corticorubral and Rubrospinal Tracts

The corticorubral and rubrospinal tracts represent an indirect route from the cerebral cortex to the spinal cord. Fibres originating from the same cortical areas that give rise to the corticospinal tract form the corticorubral tract. This tract projects to the ipsilateral red nucleus in the tegmentum of the midbrain. The red nucleus gives rise to the rubrospinal tract, the fibres of which cross the midline in the ventral tegmental decussation and descend through the lateral tegmentum of the pons and midbrain. In the spinal cord, this crossed pathway is found just anterior to the lateral corticospinal tract in the lateral funiculus. Its fibres synapse at all cord levels in the lateral aspect of laminae V, VI, and VII and thus overlap part of the termination of the corticospinal tract. In fact, the rubrospinal tract is functionally similar to the corticospinal tract in that it facilitates flexor and inhibits extensor alpha and gamma motoneurons, particularly those innervating the distal parts of the arms. The red nucleus is also a way station between the cerebellum and ventral lateral nucleus of the thalamus.

## 1.8.4 Corticoreticular and Reticulospinal Tracts

The reticular formation (a matrix of nuclei in the core of the brain stem) receives a large input from corticoreticular fibres, which accompany the corticospinal tract. Two areas of the reticular formation send major projections into the spinal cord. The

## Chapter 1

pontine reticular formation gives rise to the uncrossed pontine reticulospinal tract. In the brain stem, this pathway travels just ventral to the medial longitudinal fasciculus. In the spinal cord, it passes through the ventral funiculus to all cord levels. Its fibres synapse in laminae VII and VIII. This tract is mainly facilitatory for extensor alpha motoneurons, particularly those innervating the midline musculature of the body and the proximal parts of the extremities, and it provides an important input to gamma motoneurons.

The medial aspect of the medullary reticular formation gives rise to the medullary reticulospinal tract, which is primarily uncrossed but has a small crossed component. This tract passes to all cord levels in the lateral funiculus just anterior to the rubrospinal tract. It synapses in laminae VII and IX. There is controversy regarding the exact function of this pathway with respect to the alpha and gamma motoneurons. The tract conveys autonomic information from higher levels to the preganglionic sympathetic and parasympathetic neurons to influence respiration, circulation, sweating shivering, and dilatation of the pupils, as well as the function of the sphincteric muscles of the gastrointestinal and urinary tracts. Autonomic functions are also influenced directly by hypothalamic projections to the spinal cord from the paraventricular and other hypothalamic nuclei.

### 1.9 The Brain Gut Axis

Gut function is modulated by extrinsic as well as intrinsic neural pathways. The myenteric and the submucous plexi provide the intrinsic innervation and are involved in local reflexes, whereas, the extrinsic innervation is provided by the splanchnic 'sympathetic' and vagal-sacral 'parasympathetic' nerves. The proximal oesophagus and the external anal sphincter are composed of striated muscle and motor function in these regions is regulated entirely by vagal and sacral nerves respectively. The rest of the gastrointestinal tract is composed of smooth muscle, has its own intrinsic innervation and shows less dependence on extrinsic innervation. Nevertheless, the enteric neural network is subject to descending neural control by the central nervous system (CNS) which helps to co-ordinate motility in different regions of the gut.



## Chapter 1

Sectioning the extrinsic nerves does not paralyse the gut but seriously disrupts its function.

Afferent information from the gastrointestinal tract is carried via both vagal and spinal afferents. Cell bodies of vagal afferents lie in the nodose ganglia while cell bodies of the spinal afferents lie in the dorsal root ganglia. The central processes of vagal afferents terminate in the brain stem nucleus of the solitary tract (NTS) from which second order neurons pass both ipsilaterally and contralaterally to the cingulate as well as the supracingulate cortex, especially the orbitofrontal and the insular cortex. This cortical projection is mediated mainly via the thalamic nuclei, however, some projections also pass via the hypothalamus, tegmentum and the reticular formation. Vagal afferents also constitute the sensory limb of the circuitry involved in vago-vagal reflexes and are connected to the motor limb via projections from the NTS to the vagal efferent neurons in the dorsal motor nucleus of the vagus (DMN) which in turn project to the intrinsic neural ganglia. Second order neurons of spinal afferents, pass either to the CNS predominantly in the spinothalamic tracts which project to the cortex via the ventral and medial nuclear complex of the thalamus or return via the prevertebral ganglia, to the intrinsic neural plexi of the gut to form spinal reflexes.

### 1.9.1 Gut sensation

The two afferent pathways conduct different information from the gut viscera. Vagal afferents, which constitute 70-90% of the vagus nerve, conduct vegetative data e.g. hunger, satiety, nausea, whereas spinal afferents mediate sensations which inform the brain about potentially noxious events. In contrast to somatic sensation which is well localised, visceral sensation is vague and poorly localised. Visceral afferents are fewer in number than somatic afferents, accounting for only 10% of the total number of spinal afferents despite having a similar surface area to innervate. Due to convergence of visceral and somatic afferents at the level of the spinal cord, visceral sensation is often referred to somatic structures.

Animal studies show that modulation of gut sensation can occur at several sites within the CNS and the peripheral nervous system (PNS). The CNS modulates gut

## Chapter 1

sensation via excitatory and inhibitory descending pathways from the cerebral cortex both to the termination of vagal afferents at the level of the brain stem NTS and to the second order spinal neurons. Modulation of gut sensation can also occur peripherally either at the level of the prevertebral ganglia by descending influences from the higher centres or at the level of the primary afferent fibres within the gut wall by factors such as inflammatory and immune mediators, hormones and neuropeptides which may alter receptor function. In addition, recent animal studies provide evidence for viscerovisceral reflexes such that information encoded within vagal afferents has an inhibitory influence on spinal afferent activity (Randich and Gebhart 1992).

A review of the investigation of the brain gut axis in man is given in Chapter 6.

## 2. Neuroimaging techniques

### 2.1 Introduction

The purpose of this Chapter is to provide an overview of neuroimaging and functional neuroimaging techniques. This will enable the reader to more readily appreciate the current role of Magnetoencephalography in functional imaging as well as to provide an introduction to some of the technology and methodologies employed in the experimental Chapters which follow.

Most functional neuroimaging techniques rely at some point in their analysis on some form of co-registration with a high resolution anatomical image. The current 'gold standard' for this is the technique of Magnetic Resonance Imaging, or MRI, and this will be reviewed first. An overview of Functional Magnetic Resonance Imaging (fMRI) follows as this provides a natural progression from the essential volume acquisition technique. Positron Emission Tomography (PET) and finally MEG or Magnetoencephalography will be discussed. Particular reference to the MEG system used in the studies described in this thesis will be made, together with issues relating to co-registration of functional data with the MRI.

### 2.2 Magnetic Resonance Imaging

#### 2.2.1 Signal origin

The Magnetic Resonance signal arises from the nucleus of the atom. All nuclei possess a property called 'spin angular momentum'. The spin properties of the nucleus cause it to act as a small magnet and the strength of the magnetic moment depends on the type of nucleus. Because of the spin properties of the nucleus, it aligns with a strong external magnetic field, just as a compass needle does.

If a strong magnetic field were applied to a person's body, the normally random arrangement of magnetic dipoles would be aligned along the plane of that magnetic field, thus creating a 'net magnetisation'. The nuclear magnetic moments would therefore be spinning, or more accurately precessing, along the axis of the externally applied field. The frequency of this precession is given by the Larmor equation:

$$f = \gamma B_0$$

where  $B_0$  is the applied magnetic field strength (G) and  $\gamma$  is the gyromagnetic ratio (Hz/G). For protons,  $\gamma = 4,257$  Hz/G. So, for example, a hydrogen nucleus in a 1.5 Tesla field completes 64 million rotations per second.

For a given nucleus, increasing field strength increases the frequency of precession and different nuclei precess at different frequencies in the same magnetic field. This forms the basis of MR image formation.

The hardware involved in producing MR images can be divided into three main categories: the magnet itself, front-end electronics and computers. The MR magnet consists of miles of titanium alloy wire wound around a cylinder that is large enough to surround a person. The interior of the cylinder is called the "magnet bore". By being enclosed in a dewar that contains liquid helium, the titanium wire is supercooled. At near absolute zero temperatures, the titanium alloy becomes superconducting; that is, resistance to the flow of electric current decreases to essentially zero. This allows the unimpeded flow of a large electric current indefinitely. Because movement of an electric charge produces a magnetic field, the case of a cylindrically wound wire produces a magnetic field directed along the long axis, or bore of the magnet. The static magnetic field is known as the ' $B_0$ ' or 'main magnetic field'. Field strengths common in diagnostic imaging range from 0.06 Tesla to 2.0 Tesla.

Having applied the large magnetic field to the body, no signals can be measured because the 'net magnetisation' of the nuclei is a static event. To evoke a

## Chapter 2

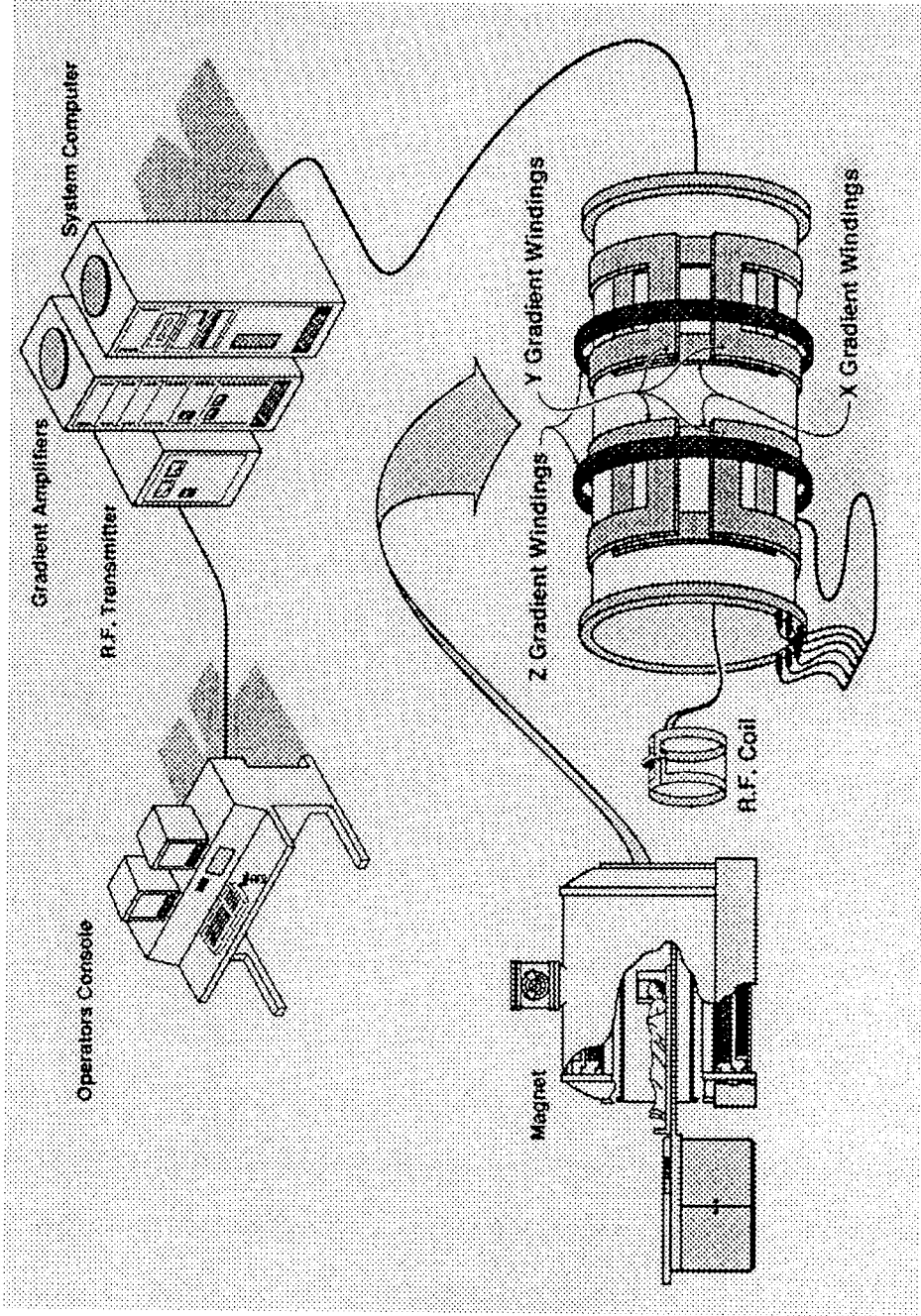


Figure 2.1 Hardware components of a Magnetic Resonance Imaging system

measurable signal, a radio frequency (RF) pulse is applied to rotate the magnetisation in the patients body by 90 degrees. This RF 'nutating' puts the magnetisation into a transverse plane, where it precesses as it recovers to the starting point in the direction of  $B_0$ . This precession causes electrical currents to flow in strategically placed receiver coils and this induced current is the MR signal.

The RF pulse is transmitted from a large coil located just inside the  $B_0$  coil windings. A receiver coil is used to receive a signal from the patient and for imaging the head, a coil that fits closely around the patients head is used. Because the signals are small and in a specific frequency range, the receiver coils are specially tuned for the resonance frequency of each scanner.

### 2.2.2 Image creation

The basis of MR image formation is that the resonant frequency is proportional to the amplitude of the magnetic field ( $f = \gamma B_0$ ). The first step in creating an image is to distinguish between different locations within a patients body. To achieve this a magnetic field gradient is applied during imaging. This is achieved with gradient coils: three pairs of gradient coils are oriented orthogonally to the long axis of the magnet. When current is applied to the gradient coils, a small magnetic field gradient is introduced along the bore of the magnet. The gradient changes the static field into a linear ramp. Because the resonant frequency is proportional to the magnetic field, the resonant frequency is proportional to a spatial position when the gradient is present. This means that when a gradient is applied, it creates a variation in the precession frequencies of magnetic dipoles in the patient.

After the MR signal is collected, it is analysed to find the signal intensity at different frequencies. The signal frequency and phase determine the pixel location, and the amplitude or intensity at each frequency determines the pixel grey scale value. By using a simple model, an MR image is a graph of frequency in two directions, with

## Chapter 2

signal intensity as the image grey scale. The object contrast within the image is determined by the timing of the RF pulses.

### 2.2.3 Longitudinal (T1) and Transverse (T2) Relaxation

Following an RF pulse, a 'relaxation' process occurs; relaxation is the process by which the system of spins reaches thermal equilibrium in the external magnetic field. The two types of relaxation are longitudinal and transverse. Longitudinal relaxation occurs when the magnetisation of dipoles aligned with  $B_0$  are perturbed from this alignment by the RF pulse, and the magnetisation 'recovers' or re-aligns with  $B_0$ . This rate of recovery is identified by a time constant T1: defined as the time at which 64% of the final equilibrium magnetisation has recovered.

Transverse relaxation occurs when components of the magnetisation in the transverse plane following an RF pulse dephase or lose coherence. The rate of signal loss due to this dephasing is identified by a time constant T2. The MR data acquisition technique acquires data at discrete 'echo times' (TE). The amount of signal lost at TE reflects the relative tissue T2 values. Long TE values allow more T2 relaxation to occur and influence image contrast.

T1 and T2 rates are different for different components of the body. Tissues with a long T1 require a longer time for the longitudinal magnetisation to re-align. By re-exciting with an RF pulse before the longitudinal relaxation is complete, we can cause tissues with different T1 values to have different intensities within the image; thus T1 is dependent on repetition time or TR.

MR images are often referred to as 'weighted' by T1 or T2. This weighting means that the contrast in the image is mainly affected by the T1 or T2 times. Since relaxation times vary in pathology, appropriate use of T1 and T2 weightings are clinically important.

### 2.3 Functional Magnetic Resonance Imaging

MRI techniques can be adapted to detect an increase in oxygen that occurs in an area of heightened neuronal activity. The basis for this capacity comes from the way neurons make use of oxygen. Functionally induced increases in blood flow accompanies alterations in the amount of glucose consumed but not in the amount of oxygen used. Therefore, additional blood to the brain without a concomitant increase in oxygen consumption leads to a heightened concentration of oxygen in the small veins draining the active neural centres. The amount of oxygen carried by the haemoglobin affects the magnetic properties of the haemoglobin. In 1990, Seiji Ogawa demonstrated that MRI could detect these small magnetic fluctuations. Deoxyhaemoglobin is paramagnetic, whereas oxyhaemoglobin is diamagnetic. In tissue, deoxyhaemoglobin, like any paramagnetic substance, produces microscopic inhomogeneities in an externally applied magnetic field. These field inhomogeneities lead to more rapid loss of coherent precession of tissue protons during an image acquisition; that is, the effective T<sub>2</sub> relaxation time is shortened. Appropriate pulse sequences were adopted to enhance what has been described as blood oxygen level dependent contrast, or BOLD contrast.

BOLD contrast is dependent on differing levels of deoxyhaemoglobin between active and non-active states. The percentage of haemoglobin molecules that have exchanged O<sub>2</sub> for CO<sub>2</sub> increases as a bolus of blood traverses the capillary bed and is maximum when capillaries coalesce into venules. Therefore, the BOLD effect is more pronounced at the distal capillary and venous level.

A concern with with BOLD imaging has been that the point source of fMRI contrast may be located predominantly in macroscopic draining veins rather than in the microcirculation. This problem is intimately related to the issues of field strength, imaging methods and pulse sequences used. It has been shown that scanners operating at high field strengths ( 3 or 4 Tesla) offer a clear advantage over low field scanners in imaging the microcirculation rather than the macrocirculation.



## Chapter 2

At 1.5 Tesla, the magnitude of the fMRI signal using BOLD gradient echo technique, although small (2-5%), is nonetheless reliably detectable.

### 2.3.1 Echo Planar Imaging

Several of the pioneering groups of investigators in fMRI have used so called 'echo planar imaging' (EPI) techniques. EPI is the fastest MR imaging available. After radiofrequency excitation, the readout gradient is rapidly modulated to create a series of echoes. All the data necessary for reconstructing a complete image can be acquired in a single excitation. EPI is usually associated with high performance gradients and used in combination can produce a complete cross sectional image in less than 100 milliseconds.

### 2.3.2 Artefacts

A major problem in fMRI is movement by the subject. Motion-related artefacts can be divided into two categories: in-train image motion and inter-image motion.

In-train image motion refers to the motion that occurs during the period of time that the views needed to reconstruct a single image are being acquired. For example, some echoes are collected during full inspiration, some in full expiration and some in between. This creates image blurring and can be overcome with single shot EPI techniques.

Inter-image motion occurs between successive images in an fMRI time series. Even EPI cannot compensate for bulk head motion in which the position of the head is shifted over a period of several minutes while the activation task is cycled off and on.

### 2.3.3 Clinical application

Initial fMRI demonstrations used normal volunteers who performed tasks that activated primary cortical areas of sensorimotor, visual and auditory functions (Ogawa et al 1992; Menon et al 1992; Binder et al 1994). Subsequent studies demonstrated that the known somatotopic and retinotopic organisation of these primary cortical areas could be faithfully reproduced (Cao et al 1993; Schneider et al 1993; Engel et al 1994).

fMRI has been applied to the study of pre-surgical planning. Jack et al (1996) studied mapping of the sensorimotor area in 20 patients with epilepsy. Single-slice functional acquisition series using an interleaved EPI sequence was performed. A reasonable functional map of sensorimotor activation was achieved in 9 of 20 patients. The reason for failure in 11 patients were various but head motion corrupted the data in nine of the patients.

A common finding reported by these authors was that fMRI activations that met statistical criteria implicated more than one cortical sulcus, which clearly prohibits adequate location of the motor strip.

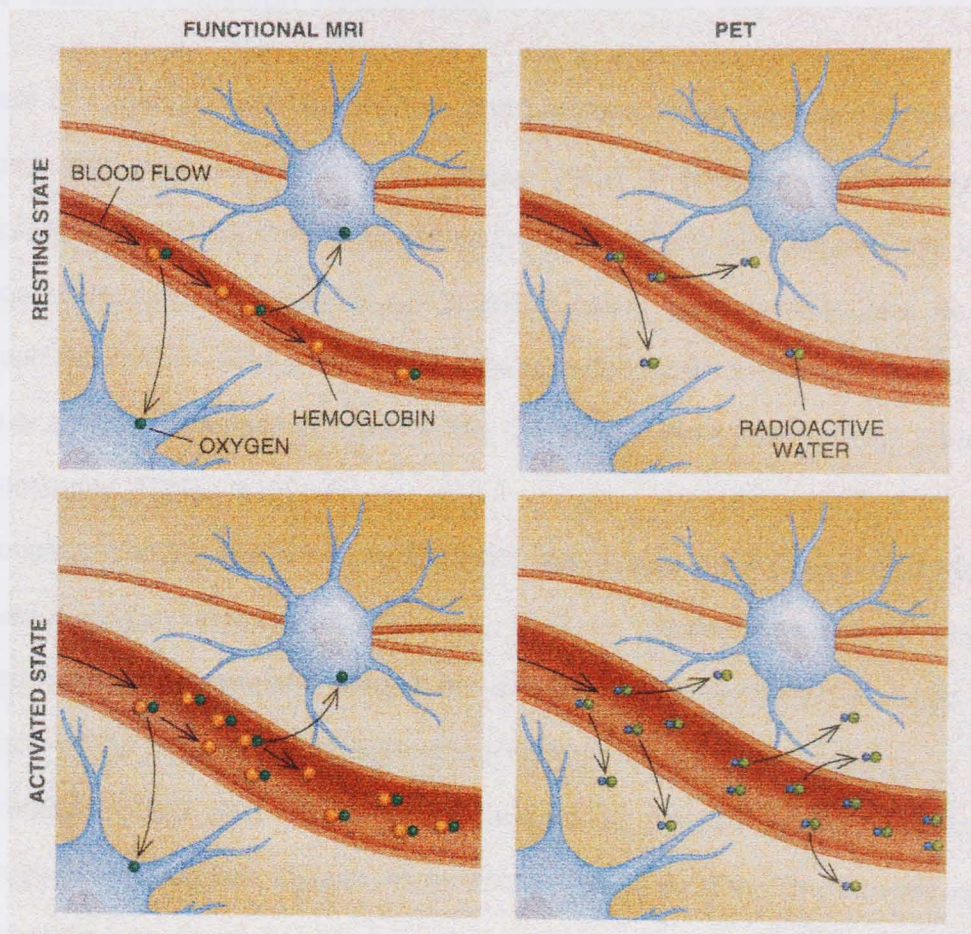


Figure 2.2 Schematic showing the physiological mechanisms upon which fMRI and PET rely to detect cortical changes as a result of a correlated task. (Adapted from Raichle, *Scientific American*, 1994)

### 2.4 Positron Emission Tomography

There is a class of radioisotopes that emit positrons. Positrons resemble electrons except that they carry a positive charge. When a positron combines with a neighbouring electron, they annihilate each other, emitting two gamma rays in the process. Because each gamma ray travels in nearly opposite directions, devices around the sample could detect the gamma rays and locate their origin. The crucial role of positrons in human autoradiography gave rise to the name 'Positron Emission Tomography' (PET).

Throughout the late 1970's and early 1980's, researchers rapidly developed PET to measure various activities in the brain, such as glucose metabolism, oxygen consumption, blood flow and interactions with drugs. Of these variables, blood flow has proved the most reliable indicator of moment to moment brain function.

To measure blood flow, PET relies on radioactively labelled water - specifically, hydrogen combined with Oxygen 15, a radioisotope of oxygen. The labelled water emits copious numbers of positrons as it decays (hydrogen isotopes cannot be used because none emit positrons). The labelled water is administered into a vein in the arm. In just over a minute the radioactive water accumulates in the brain forming an image of blood flow.

Oxygen 15 has a half life of only two minutes: an entire sample decays almost completely in about 10 minutes (five half lives) into a non-radioactive form. The rapid decay substantially reduces the exposure of subjects to the potentially harmful effects of radiation. Moreover, only low doses of the radioactive label are necessary. The fast decay and small amounts permit many measurements of blood flow to be made in a single experiment.

Current PET strategies involve subtraction of blood flow taken before a task is begun from those obtained when the brain is engaged in a task. To achieve reliable data, workers take the average of responses across many individual subjects.

### 2.4.1 Difficulties associated with PET

To perform such studies, a Cyclotron must be available as part of the scanning facility because of the short half lives of Oxygen 15 and Carbon 11.

Obtaining stable and adequate baselines for measurements are problematic and, as with fMRI, the ability to establish appropriate thresholds for differentiating relevant from irrelevant signals may significantly alter the interpretation of the data presented.

Anatomical localisation presents another difficulty and several strategies have been used to combine structural and functional image data. Fox et al (1985) extrapolated the landmarks of a lateral skull radiograph performed with the patient in the PET scanner, to a pneumoencephalographic atlas to obtain anatomical co-ordinates for cerebral blood flow measurements. Images can be obtained using a system of fiducial markers, such as a set of petroleum filled tubes visible on MRI attached to a thermoplastic face mask (Meltzer et al 1990). Most recent approaches have used PET and MRI contour matching (Dann et al 1989) or pixel by pixel alignments (Woods et al 1993).

### 2.4.2 Clinical application

PET uniquely offers data about receptor sites and metabolism by using a range of labelled neurotransmitters and neuropharmacology. Visualisation of receptors in vivo may be the most important contribution of PET to understanding the pathophysiologic basis of human epilepsy.

The most promising areas of development for PET in pre-surgical evaluation is in the study of language. Because specific language tasks cause alterations of cerebral blood flow, attempts have been made to use PET as a substitute for Wada's test in establishing cerebral dominance for language and memory. The results of cerebral

blood flow PET studies in language localisation have been compared with the results of subdural electrode stimulation in epilepsy patients who are candidates for surgery (Bookheimer et al 1993). CT scans were performed with the subdural electrodes in place, and both the PET and CT scans were digitally co-registered with the MR images of each patient. Each point that showed language disruption with electrical stimulation was associated with increased cerebral blood flow. No change was found in cerebral blood flow at grid points that did not include language disruption.

### 2.5 Magnetoencephalography

Magnetoencephalography, or MEG, is a term used to describe the technique of measuring magnetic fields generated by neural activity of the cerebral cortex.

Cortical activation is associated with a primary current source related to the movement of ions due to their chemical concentration gradients. In addition, passive ohmic currents are set up in the surrounding medium. This 'volume current' completes the loop of ionic flow so that there is no buildup of charge. The magnetic field is generated by both the primary and volume currents (Hämäläinen, 1993).

If the primary source and the surrounding conductivity distribution are known, the resulting electric potential (EEG) and magnetic field can be calculated from Maxwell's equation. This is known as the 'forward problem'. Conversely, if the electrical or magnetic field is known, one might deduce the source currents responsible; this is termed the 'inverse problem'. Hermann von Helmholtz showed in 1853 that this problem has no unique solution. One must therefore use source models such as current dipoles in a spherical conductor to interpret the data.

The current dipole is a popular source model in MEG interpretation. It is used to approximate the flow of electrical current in a small area. Williamson and Kaufman in 1987 showed that a current dipole could be used to adequately model a theoretical field distribution with an experimental one and achieve source localisation i.e. solve

the inverse problem. The outcome of this procedure is referred to as the 'equivalent current dipole'. A typical strength of such a dipole caused by the synchronous activity of tens of thousands of neurons is 10 nA m.

### 2.5.1 Direct and Inverse problem

Computation of the estimated source parameters are obtained by means of a least squares regression which yields best fit values. This technique also provides confidence intervals which provide a measure of the uncertainty of dipole localisation (Press et al. 1996).

Since the dependence of the dipole field on dipole parameters is non-linear, the least-squares regression requires an iterative procedure whereby the dipole field must be calculated at each trial value of the parameters. Therefore dipole localisation requires the solution of the direct problem.

Commonly, spherical head models have been used in the inverse solution (Sarvas 1987). Even though the brain is not spherical, some regions of the cortex may be represented by a sphere of appropriate radius.

#### 2.5.1.1 Monte Carlo analysis

The effect of measurement error on fitted model parameters is usually analysed statistically by computing covariances and/or multidimensional confidence regions of the parameters. These statistics can be computed by traditional analytic methods if the measurement errors are additive and normally distributed (Press et al 1986).

However, most MEG source models are non-linear in some of their parameters.

Medvick et al (1990) described a Monte Carlo analysis strategy for analysing localisation errors in MEG which has been adopted for use in this Thesis.

The basic approach of Monte Carlo error analysis can be summarised from the study by Medvick et al as follows.

The measurements used to compute the source model parameters correspond to one particular experimental set of conditions. Because of the random nature of the measurement errors, repetition of the experiment would result in a slightly different

## Chapter 2

set of measurements. Fitting the model to this different set of measurements would result in slightly different values for the model parameters. The most robust method of analysing the effect of measurement errors on the fitted parameters is to repeat the experiment many times and fit the model to each set of the resulting measurements. This would provide a sample of the parameter population that could be directly analysed.

Since repetition of the experiment is usually impractical, the approach of Monte Carlo error analysis is to simulate the measurements that would have been obtained if the experiment had been repeated. Using the parameters found by fitting the model to the real measurement data as surrogates for the unknown 'true' parameters, multiple copies of the 'ideal' field measurements produced by the model are generated. Each of these ideal fields is then perturbed by a different set of simulated errors. These sets of simulated errors are randomly generated on a computer with distributions that mimic those of the errors in the measuring process. The simulated errors can be used to perturb the ideal field additively, as when one simulates the error caused by noise sources, or nonadditively, as when one simulates the error caused by imprecise location of the sensors. (In Appendix I, the errors introduced through sensor position estimation using the bite bar strategy are described.) The result is a number of simulated measurement sets. The source model is then fitted to each measurement set, providing a collection of model parameters. This data set approximates the joint distribution of the parameters, and from it any statistics describing the parameter error can be directly estimated (e.g. variances, confidence regions).

Like all procedures for analysing the effect of measurement error on fitted model parameters, Monte Carlo analysis depends on statistical knowledge of the error processes. As a consequence, the validity of the final results are dependent on the accuracy of this knowledge. Unlike most alternate procedures however, this is the only requirement for the Monte Carlo approach. Error processes do not have to be normal and additive, linear approximations are not required for the source model, and detailed statistical analyses are unnecessary.



### 2.5.2 MEG vs EEG

MEG and EEG field distributions are mutually orthogonal. Data obtained by these two techniques complement each other, and both methods have their own advantages.

In determining the locations of source activity in the brain, MEG has better spatial accuracy than EEG; 1 to 2 mm under favourable conditions. However, the nature and complexity of measurements will greatly influence any comparison (Cohen and Cuffin 1991; Hämäläinen et al 1993).

Electrical potentials measured on the scalp are often strongly influenced by various inhomogeneities in the head, making accurate determination of the activated area difficult. The magnetic field, in contrast, is mainly produced by currents that flow in relatively homogeneous intracranial space. Because of the poor electrical conductivity of bone, the irregular currents in the skull and on the scalp are weak and can be ignored as contributors to the external magnetic field.

Importantly, only the tangential component of the current dipole produces a net magnetic field outside the sphere. This means that MEG is more sensitive to sources located in sulci rather than in gyri. EEG can successfully measure both tangential and radially oriented fields. Determination of the orientation of field source with EEG is limited to the extent that identical potential distributions are seen when measuring fields generated by two radial sources when compared with a single tangentially oriented source.

### 2.5.3 Measuring neuromagnetic fields

The key component of a biomagnetometer is a Superconducting Quantum Interference Device, or SQUID. The SQUID measures the magnetic flux transported into it by the superconducting magnetic flux transformer. This comprises a

## Chapter 2

superconducting coil which collects ambient flux and is connected in series to a second input coil which is tightly inductively coupled to the SQUID itself. The net effect of the circuit is to funnel the flux trapped in the pickup coil into the SQUID loop and thereby to provide an enhanced flux sensitivity. The flux sensitivity of a typical modern SQUID is around  $10^{-20}$  Tm<sup>2</sup>.

For the SQUID devices to achieve superconductivity, they must be supercooled. This is achieved by housing the devices in a dewar filled with liquid helium which maintains an ambient inner temperature of -269° Celsius.

The magnetic signals of the brain are extremely weak compared with the ambient magnetic field variations and so rejection of outside disturbances is vital.

The geometry of the detection coil can be modified in order to achieve partial insensitivity to unwanted magnetic fields still present in the environment. In Figure 2.3, two alternatives to the simple flat coil (namely a magnetometer configuration, usable only with heavy shielding) are shown. These geometries are the most often used, with the second-order gradiometer permitting successful operation even in unshielded environments. The Aston University magnetometer system used in this Thesis comprises 19 such gradiometers in its configuration.

A reduction in overall sensitivity corresponds to a higher degree of spatial discrimination, e.g. second order gradiometers are mostly useful to investigate cortical sources, and can be used in unshielded labs. Conversely, such a configuration negates the ability to measure signals generated by deep sources, such as the brain stem.

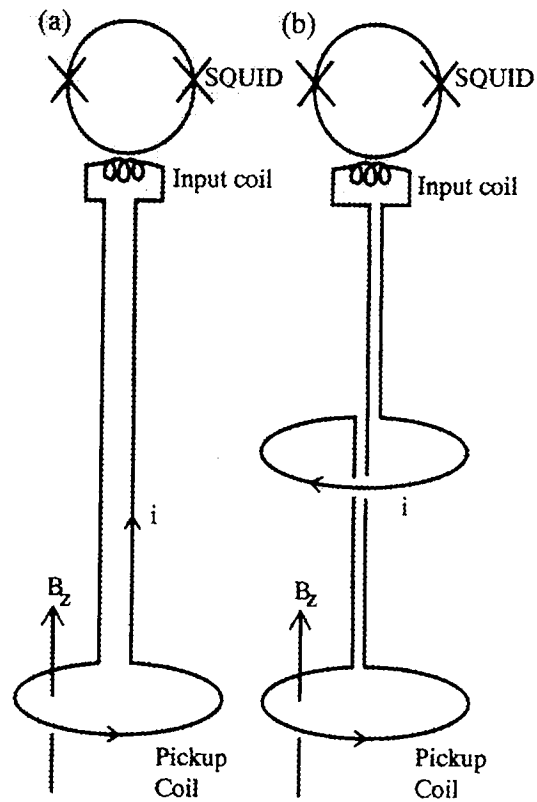


Figure 2.3 Types of Gradiometer array. Two alternatives to the simple flat coil (namely a magnetometer configuration, usable only with heavy shielding) are shown. These geometries are the most often used. The second-order gradiometer (b) permits successful operation even in unshielded environments.

## Chapter 2

The use of shielding is an important way of reducing or eliminating unwanted environmental noise. Shielded rooms comprise a variety of forms; these often consist of one or more layers of a high permeability alloy such as  $\mu$  metal ( a low saturation, high permeability magnetic alloy) which gives good low frequency shielding, together with a high conductivity shield (usually aluminium) to provide eddy-current shielding for higher frequency fields.

The shielded room at Aston University was constructed commercially by Vacuumschmelze™ and comprises an eddy current shielded room lined with a sandwich of  $\mu$  metal. The shielding factor varies from some 50dB at 1Hz to 80dB at 100Hz.

Unwanted noise may be further reduced or eliminated by the use of bandpass filtering; conventional analogue and digital filtering may be applied to the MEG signal. The system at Aston University additionally incorporates a noise rejection system based upon the sampling of environmental noise by three vector magnetometers. These devices were mounted within the same dewar as the gradiometers, but raised away from the recording area so that no neural signal may be detected by them. The vector magnetometers therefore sample environmental noise and the computed noise signal is removed off line from the measured neural data.

Coil configuration within the dewar is frequently a matter of compromise. In addition to maximum sensitivity in every channel, the best configuration for locating accuracy is required: however, increasing the pick-up coil diameter improves field sensitivity but reduces spatial resolution.

The Aston MEG system gradiometers were organised in an hexagonal array beneath a planar baseplate measuring 17.5cm in diameter. Gradiometer baselines were 5cm with a coil diameter of 15mm. Coil separation was 29mm.



Aston University

**Illustration has been removed for copyright restrictions**

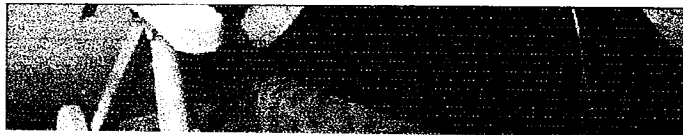


*Figure 2.4 The 19 channel Magnetometer system at Aston University is suspended in a wooden gantry in a magnetically shielded environment. The use of vacuum cushions and a bite bar ensure stability and accuracy of localisation.*

### 2.5.4 MEG-MRI co-registration

The position and orientation of the dewar must be found with respect to a co-ordinate system defined by at least three fixed points on the subjects head. Errors in this method cause systematic errors in the location of the current dipole.

Fixed points on the head that have been used in defining co-ordinates include the ear canals, the nasion, theinion and the front teeth. By the use of a 3D digitising spatial tracking device (e.g. Polhemus 3D Isotrak system), the position of the selected fiducial points can be registered with respect to a fixed electromagnetic source.

An alternative method employs the measurement of magnetic fields produced by small coils attached to the scalp (Erné et al. 1987).

A final crucial step which allows MEG data to provide a true functional neuro-image, is the co-registration of the MEG data with a high resolution MRI. This involves the accurate location of the fiducial points used for MEG recordings within the MRI data set. A common methodology which is applied is to attach Vitamin E capsules to the fiducial points used; these in turn are clearly identified from the MRI and an appropriate translation matrix derived to merge the data sets.

Critically, though, such a methodology may introduce significant error into the data set. Bony landmarks marked with oil capsules present a large target area and slight errors in placement or identification of the precise points used for MEG measurements within the MRI can produce significant location errors.

Work in our lab at Aston University has demonstrated that a dental bite-bar which incorporates a set of fiducial points can substantially improve the stability of co-registration as compared to fixed head markers (Singh et al. 1997). In addition, the bite-bar should reduce additional errors due to head movement during long or repeated MEG acquisitions. Full details of the methodology of the bite-bar strategy

can be found in Appendix I in this Thesis.

Other workers have used different types of external markers to co-register MEG with CT and MR images (van den Elsen et al. 1991; Williamson et al. 1991).

More recently, co-registration methods which involve the transfer of MEG data into the MRI pixel system using a contour fit algorithm and a 3D digitizer (Polhemus Isotrak) have been described (Kober et al., 1993). This method proved accurate with a maximum error of 2mm, in contrast to fits using fiducial points with a maximum error exceeding 2 cm. By comparison, the Aston bite bar system provides co-registration errors of some 2mm.

### 2.6 Summary

The functional imaging techniques of fMRI, PET and MEG each contribute in unique ways to this growth area in Neuroscience.

Functional MRI enjoys the benefit of high spatial resolution and is the spin off of the current 'gold standard' in Neuro-anatomical imaging, the MRI. This makes the potential availability of the technique something which will attract clinicians to explore the clinical benefits of this method.

PET is much more limited in its availability and is a partially invasive technique in the application of radioactivity. Nevertheless, its unique ability to monitor neurometabolism and its application to neuropharmacology will also ensure its success, if only in limited specialist centres

Both EEG and MEG offer the unique advantage over other functional techniques of very high temporal resolution. The ability to visualise with high spatial resolution the millisecond by millisecond changes of neuronal activity ensure that there is a role for both methodologies in the fast and changing field of neuroimaging.

## Chapter 2

MEG is a more expensive technique than EEG but less costly than fMRI or PET, however it is not yet widely available. Its use in clinical trials over the next few years will determine whether it has long term role to play in the clinical domain. Its value as a research tool is already proven.



### **3. Magnetoencephalographic localisation of Somatosensory cortex in Human control subjects**

#### **3.1 Introduction**

Much of what is known today about the functional organisation of the somatosensory cortex is due to the pioneering work of Penfield and colleagues who, as early as 1937, described the somatotopy of somatosensory cortex by electrical stimulation of the cortical surface (Penfield and Boldrey 1937).

In 1947, Dawson first described the form of the Somatosensory Evoked Potential (SEP). These electrical signals were elicited from the cortex following stimulation of peripheral nerves. Through a number of studies (Dawson 1950; 1954 and 1956) he described how the early part of the cerebral response appears over the contralateral Rolandic area, with a maximum some 6-7 cm lateral to the midline for the upper limb. In the 1960's, studies in both America and Europe began to document the morphology and normal ranges of the SEP in man. Most notable of these were Allison 1962; Goff et al., 1962; Shagass and Schwartz 1964; Debecker and Desmedt 1964; Giblin 1964 and Desmedt et al., 1965. There was considerable agreement between the authors and their data has been substantiated since by many workers.

It was Giblin in 1964 who first observed a possible dual configuration of the postrolandic evoked potential in normal controls and described the waveforms as being of the V or W type. Like many studies at that time, Giblin employed electrical shocks to the contralateral median or ulnar nerves at the wrist. Recording electrodes were placed over the 'hand' area of the post-central gyrus which was calculated as being 7cm lateral and 2cm posterior to the vertex point (Cz) according to the international 10-20 system of electrode placement (Jasper 1958).

In 1978, Brenner and colleagues were the first to describe the use of a SQUID (Superconducting Quantum Interference Device) system to measure steady state magnetic responses from the brain following electrical stimulation of the median

nerve. Their data indicated a current source at the contralateral primary somatosensory cortex (SI).

Later, Kaufman et al., (1980), Okada et al., (1981), Hari et al., (1984) and Huttenen et al., (1987) reported that transient responses elicited by median or ulnar nerve stimulation were also localised near the contralateral Rolandic fissure at latencies of 20-250 msec.

Several studies have combined electrical and magnetic recordings (Wood et al., 1985; Baumgartner et al., 1991a; Sutherling et al., 1988) and have confirmed that the waveforms are highly similar in morphology, with spatial distributions centred over sensorimotor cortex.

Authors have also used MEG to determine the functional organisation of the somatosensory cortex non-invasively, using a variety of stimulation sites ( Hari et al., 1984, median and peroneal nerves; Baumgartner et al., 1991b, digits of hand; Narici et al., 1991, median, femoral, tibial and pudendal; Yang et al., 1993, hand and face.)

In 1994, Gallen and co-workers published a detailed study on the intrasubject reliability of somatosensory source localisation using MEG. This important study supported the view that the technique was robust enough to be used in clinical trials.

Recently, Kawamura et al., (1996) has suggested that the technique may be sensitive enough to separate closely spaced dipole sources generated within a given temporal activation sequence following median nerve stimulation.

The current body of data clearly supports the view that MEG provides a sensitive and robust tool for the non-invasive investigation of the functional organisation of primary sensory cortex in man.

## 3.2 Aims

The purpose of the following study was to establish the accuracy and reliability of Magnetometry to localise the sensory-motor cortex in human control volunteers.

Optimum parameters for data acquisition and dipole analysis would be determined

Use of a proportional reference system and correlation with a stereotaxic atlas would be investigated.

The variability of intra- and inter-subject dipole source location, variation of localisation across the temporal sequence of activation and interhemispheric symmetry would be investigated.

Comparison with a functional Magnetic Resonance Imaging paradigm would be made.

Once assimilated, the data would be used as a basis for studying functional organisation of cortex in control subjects and subsequently to study patients with cortical lesions in close proximity to the sensory-motor cortex.

### 3.2.1 Experimental design

Electrical stimulation of nerve trunks was chosen for this study to provide cortical responses from which both electrical potentials and magnetic fields had been studied in detail and whose waveform morphologies and likely cortical generators well documented.

Data would be recorded from stimulation of three nerve sites; the right and left median nerves at the wrist, the right ulnar nerve at the wrist and the posterior tibial nerves from the right and left ankles.

The rationale for the choice of the median and posterior tibial nerves was to provide data about hand and foot sensory-motor function which is clearly critical to healthy mobility and dexterity and for which relatively large cortical areas are devoted. Accurate localisation would also provide points at the apex and middle of the sensory-

motor strip and by matching right and left hemisphere localisations it was hoped that a robust template for the line of the central sulcus could be established.

Choice of the ulnar nerve was to provide a site of similar, but neighbouring function, whose nerve trunk could be readily but separately located for stimulation. The purpose was to examine whether MEG was able to spatially separate such closely spaced cortical functions reliably.

Single equivalent dipole fitting methods were applied to the magnetic field data and Monte Carlo analysis was adopted to generate 95% confidence volumes to enable investigation of optimum criterion for dipole localisation and to assess the accuracy and reliability of dipole fits.

MEG data was co-registered with the MRI of each individual using the strategy of a bite bar.

The proportional co-ordinate system of Talairach and Tournoux (1988) was adopted to provide a millimetric measure which would allow comparison between individuals and to provide a group mean data set for cortical localisation of function.

These strategies were combined to assess the reliability of determining the line of the central sulcus from the combination of median, ulnar and posterior tibial confidence volumes co-registered onto the MRI.

The stereotaxic atlas of Talairach and Tournoux (1988) was used to establish the central sulcus together with anatomical landmarks as outlined by Rademacher et al., 1993.

Functional Magnetic Resonance Imaging was used in three control subjects to investigate the correlation of data with neuroanatomical estimates.

### 3.3 Method and Materials

#### 3.3.1 Magnetometer system

Subjects were seated beneath a Magnetometer comprising 19 independent Second Order Gradiometers linked to DC Superconducting Quantum Interference Devices (SQUID's ) (Matlashov et al., 1993). This system is described in more detail in Chapter 2.

#### 3.3.2 Recording protocol

Nineteen channels of MEG signal was acquired in 64 msec epochs for median and ulnar nerve stimulation and 128 msec epochs for posterior tibial nerve stimulation. Sampling rate was 1Khz with bandpass filters of 0.5 - 212Hz. Data was stored for off line analysis.

To ensure comfort and reliability of recording position, as well as ensuring adequate co-registration with Magnetic Resonance Images (MRI), an acrylic bite bar was manufactured for each subject. This comprised a mouth piece covered with a dental thermoplastic material (Stents™) with two acrylic arms, one on each side of the mouthpiece, projecting backwards along the angle of the jaw. This assembly was mounted in a free standing wooden gantry (see Chapter 2 and Appendix I for a detailed description of this equipment).

Once the subject was seated comfortably in the appropriate recording position, the bite bar was presented to the subject and locked firmly in position.

The precise positional relationship between the magnetometer and subject was achieved using a Polhemus 3D space tracker™ which measured the spatial co-ordinates of 6 markers on the bite bar assembly (Singh et al., 1997).

At the beginning of each study, adhesive stimulating electrodes were applied to the

skin overlying the estimated position of the nerve trunk. The median and ulnar nerves were accessed at the wrist and the posterior tibial nerve at the ankle. In each case, the electrode acting as the anode was placed distally with respect to the cathode with a separation of 2-3 cm.

Electrodes were connected to a Digitimer DS57™ constant current stimulator to enable a pulsed current to be passed between them. The pulse was 0.1msec in duration and delivered at a rate of 1.8 per second. The subjective threshold of the pulse was initially determined and the current increased until a regular moderate contraction of the neighbouring muscle group was obtained. The current required to achieve this was invariably between twice and three times the subjective threshold.

The subject was then seated with the Magnetometer centred over one of three head positions. With reference to the International 10-20 system of electrode placement (Jasper 1958), these positions would include as centre points either C3 (for right median and ulnar nerve stimulation), C4 (for left median nerve stimulation) or Cz (posterior tibial nerve stimulation).

Three trials consisting of 250 stimuli were used for each nerve stimulated.

The subjects were requested to attend to the stimuli throughout each trial.

### **3.3.3 Magnetic Resonance Images (MRI)**

Each subject received a high resolution anatomical T1 weighted MRI scan ( 256 x 256 x128 voxels, 200mm field of view, 1.5 mm slice separation) acquired with the bite bar in situ. The six markers on the acrylic bite bar were filled with cod liver oil to enable them to be clearly visualised on the images and thus enable co-registration with the MEG dataset (Singh et al., 1997 in Appendix I).

### **3.3.4 Functional Magnetic Resonance Imaging**

This paradigm was performed in three control subjects (1, 2 and 4).

Initially a high resolution anatomical MRI volume was acquired (as described in section 3.3.3) and a series of slices were selected as likely to encompass the sensory motor cortex for hand function. Data were collected using a standard Siemens 1.5T clinical scanner.

A T1 weighted BOLD contrast imaging protocol was used and comprised the following settings: TE = 60 msec, TR = 75 msec, Flip Angle = 40 degrees. (Refer to Chapter 2 for further details of this technique).

The activated state for the subject was finger-thumb opposition. In each run, 10 rest images and 10 activated images were acquired, each image consisting of seven seconds of rest or stimulation. The runs were interleaved in blocks of 5.

Functional data was collected from 4 slices, each 5mm thick, and positioned to encompass the region of interest. The same orientation of slices was maintained between the fMRI paradigm and the initial acquisition volume acquisition to aid subsequent MEG-MRI co-registration.

The functional data was analysed by subtraction of the averaged rest image from the averaged activated image. Pixel thresholding was calculated so as to leave only high intensity pixels in the functional image. This final image was then superimposed onto the initially acquired high resolution anatomical MRI. Co-registration of function and anatomy was automatic, as the anatomical image was acquired in the same run as the functional image.

### **3.3.5 Data analysis**

MEG data were averaged off line employing adaptive filtering which incorporated the environmental noise measures acquired by the vector magnetometers.

Global Field Power estimations (Lehmann and Skrandies 1984) were calculated for the nineteen averaged epochs in each run to ascertain latencies likely to yield good source localisation estimations. Field distributions were plotted for the

appropriate latencies. Only those data which showed consistent waveforms when recordings were performed on separate occasions were used in the analysis.

### **3.3.6 Source localisation**

A single equivalent dipole in a homogeneous conducting sphere was used as the source model for localising the cortical generators of the evoked response. 20 discrete scalp points, centred around the measurement area, were digitised using the Polhemus device, and these were used to calculate the radius of the sphere.

Estimation of the dipole parameters was by minimisation of the least squares measure (Chi squared), using the Powell algorithm (Press et al., 1989). A weighting function, based on the signal-to-noise ratio in each channel, was used in the minimisation.

Dipole estimations were made for each trial and all latencies indicating a dipolar field pattern, strong Global Field Power and signal-to-noise ratio's greater than 2:1. After minimisation, the acceptability of the fitted dipole was assessed using the Chi-squared probability and the correlation coefficient,  $r$ , between the measured and estimated magnetic field. Datasets and latencies yielding significant correlations ( $r > 0.95$ ) were taken forward for secondary analysis.

### **3.3.7 Estimation of confidence for the localisation**

Once source localisation was completed, an estimate of the confidence region for the localisation was computed using the method of Monte-Carlo estimation (Medvick et al., 1990). Firstly, the magnitude of the noise in each channel was estimated using the anti-average (Regan 1989). Then, trial datasets were created by adding random gaussian noise of this magnitude to the field from the calculated dipole. These trial datasets were then re-analysed using the same source localisation procedure to yield a spread of dipole positions. Finally, the 95% confidence ellipsoid was calculated such



that 95% of this spread of dipoles was contained within the ellipsoid volume. The benefit of this method was that any noise or uncertainties present in the MEG experiment such as signal noise, positional noise etc. can be factored into the Monte-Carlo analysis. The resultant ellipsoid reflects the true confidence in the localisation parameters.

Following 50 iterations of Monte Carlo analysis, mean dipole estimations and 95% confidence ellipsoids were then superimposed onto the matching slice of the subjects MRI for localisation purposes.

### **3.3.8 Cortical localisation: Reference to co-ordinate systems**

To provide a method of comparing inter-subject source localisations as well as enabling adequate neuroanatomical prediction of the relative position of the central sulcus, reference to a commonly applied stereotaxic atlas was made (Talairach and Tournoux 1988).

Application of the three-dimensional reference system of Talairach and Tournoux (1988) entailed the construction of three reference lines onto the MRI.

The first line passes through the superior edge of the anterior commissure and the inferior edge of the posterior commissure. This line defines the horizontal plane and is defined as the CA-CP line.

The second line is a vertical traversing the posterior margin of the anterior commissure and perpendicular to the CA-CP line. This line is defined as the VCA line

The third line is the midline and is defined by the interhemispheric sagittal plane.

Distances from these planes were then measured in millimetres.

A fourth reference line was also constructed. This was formed by a vertical passing through the posterior commissure also perpendicular to the CA-CP line and defined as the VCP line.

Because of individual variations in height, length and width of human brains, the measurements would only be relevant to one individual brain. Because of this, Talairach and Tournoux (1988) further proposed a proportional grid system to enable comparison between brains. This involved dividing the brain into eighth and quarter segments based on the previously defined base points.

Due to limitations of MRI manipulation by the software tools available, it was not possible to employ the proportional grid system for each measure. Alternatively the three dimensional co-ordinate in Talairach space was used directly for comparison. The individual subject localisations were therefore not 'normalised' for direct intra-subject measure but the group mean data was assimilated into the grid system for comparison with the stereotaxic atlas of Talairach and Tournoux (1988).

In addition, to assist in localising the central sulcus from the MRI, the anatomical reference of Rademacher et al., (1993) was used. These authors detailed the relationships of the primary cytoarchitectonic neocortical areas (namely Brodmann 17, 41, 3b and 4) to salient topographic landmarks reconstructed from serial histological sections in 10 human brains. They described how each of the architectonic fields was found to bear a characteristic relationship to a set of enframing anatomic landmarks, in particular, gyri, fissures and sulci, that could be readily defined by MRI.

To determine the position of the central sulcus in control subjects in this thesis, Talairach co-ordinates were established and the neuroanatomy studied to identify the landmarks highlighted by Rademacher et al., (1993). Below is an illustration from this study detailing the enframing landmarks.

/ {F1} sf \ / / \ \ / / / \



Aston University

Illustration has been removed for copyright restrictions

L ORT - 15 R

L ORT - 20 R

L ORT - 30 R

*Figure 3.1 From Rademacher et al., 1993; the topography of lateral Brodmann area 4: Individual variations of the surface extent of area 4 (hatching) on the lateral cerebral surface in nine left (L) and nine right © hemispheres (view from above, anterior is at the top). Sulci and gyri are labelled only for the first brain. Both the central and precentral sulci take a dorsoventral course from the superior hemispheric margin posteriorly toward the sylvian fissure anteriorly. This course of the precentral sulcus is generally discontinuous. Its intersection with the superior frontal sulcus provides a constant landmark. Abbreviations: F1= Superior Frontal Gyrus , PRG= Precentral Gyrus, POG= Post Central Gyrus, sf= superior frontal sulcus , prc= precentral sulcus, ce= central sulcus , poc= postcentral sulcus.*

## 3.4 Results

### 3.4.1 Magnetic Field waveforms

#### 3.4.1.1 Median nerve evoked components: reproducibility and morphology

Characteristic waveforms were consistently produced following electrical stimulation of the median nerve at the wrist which were highly reproducible both within and between subjects (Figure 3.2). Morphology of the waveforms were consistent with those described for somatosensory evoked potentials.

The first component in each waveform from each subject in this study occurred at around 20 milliseconds (mean 20.9 milliseconds; standard deviation 1.5 milliseconds).

The control group was divided into two morphology types. The first group (comprising subjects 3 and 4) will be described as the 'V' type, with the second major component comprising a single deflection peaking at a mean latency of 33.5 milliseconds with a standard deviation of 1.3 milliseconds.

The second group (control subjects 1, 2, 5 and 6) showed a 'W' shaped waveform formed by a second deflection of mean latency 29.1 milliseconds (s.d. 2.6 msec), a third at 32.7 milliseconds (s.d. 2.8 msec) and a fourth at 40.3 milliseconds (s.d. 2.4 msec).

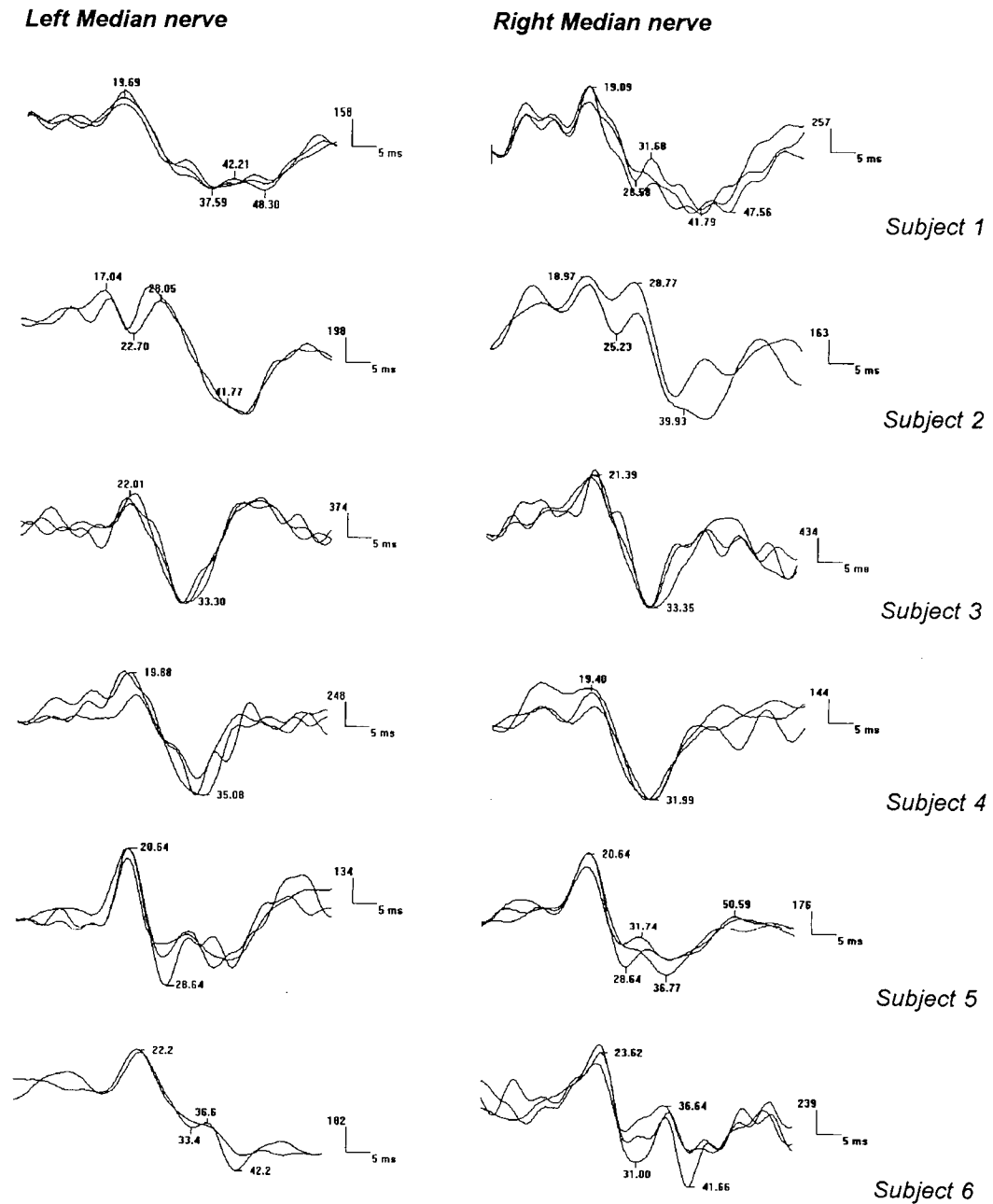
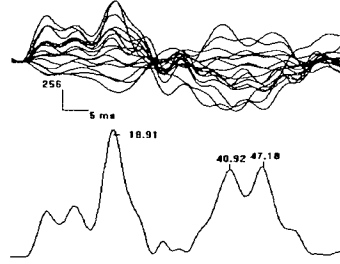
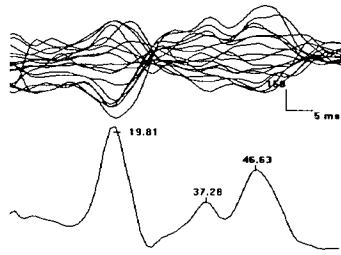


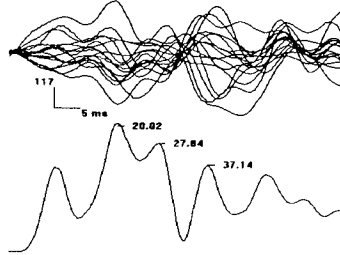
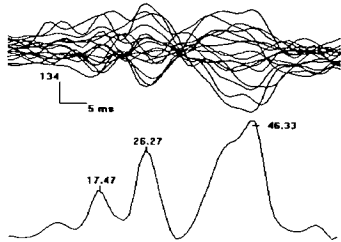
Figure 3.2 Traces in each block show magnetic field waveforms for three separate trials superimposed following right median nerve (right traces) and left median nerve (left traces) stimulation. The vertical scale alongside the waveforms is expressed in femtoteslas (fT).

**Left Median nerve**

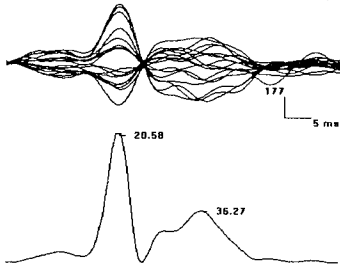
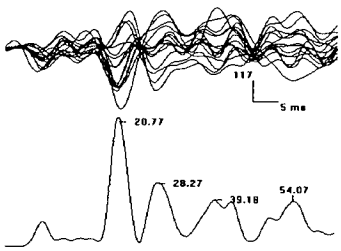
**Right Median nerve**



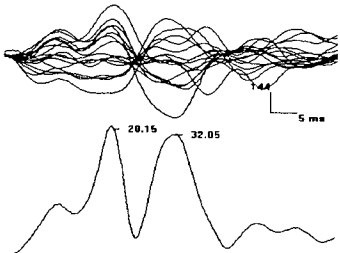
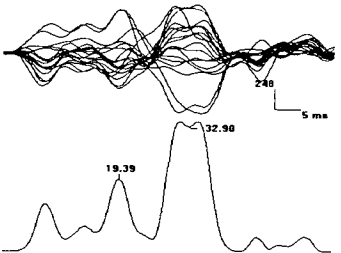
Subject 1



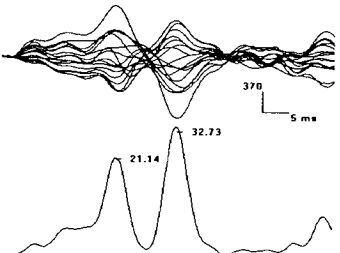
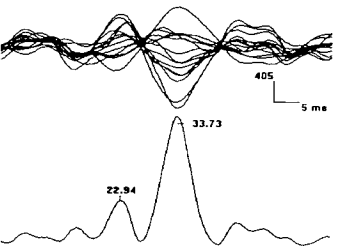
Subject 2



Subject 3



Subject 4



Subject 5

Figure 3.3a (continued overleaf)

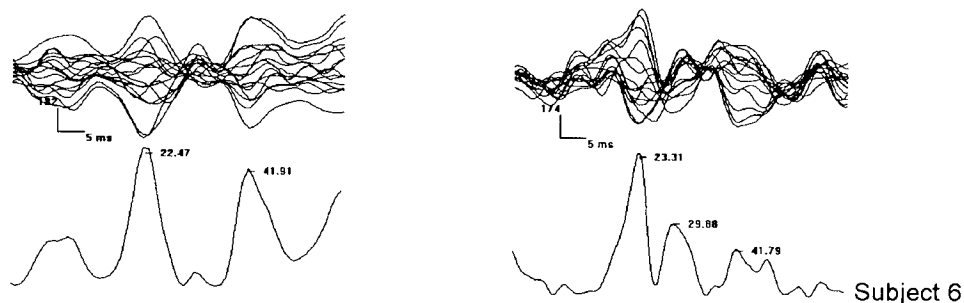


Figure 3.3a&b Group mean waveforms for left median nerve stimulation (left upper traces) and right median nerve stimulation (right upper traces) with their respective integrated global field power plots shown below. The vertical scale alongside the waveforms is expressed in femtoteslas (fT).

Superimposition of the 19 channel neuromagnetic output of the data, as seen in

Figure 3.3a&b, clearly shows that the polarity of the waveforms were equal and opposite in field strength on a number of channels and at various latencies throughout the epoch. Global Field Power plots (Figure 3.3a&b) indicate those latencies at which the field patterns were at a maximum. The two latencies which consistently yielded the strongest dipolar field powers in the control group for both right and left median nerve stimulation were at 20 milliseconds (mean 20.9 milliseconds, s.d. 1.5) and 36 milliseconds (mean 36.9 msec, s.d. 3.7).

As can be seen from the typical magnetic field plots in Figure 3.5, the dipolar appearance of the field pattern remained stable from 20 to 46 milliseconds, becoming unclear and disorganised thereafter.

## 3.4.1.2 Signal to noise ratio of median nerve data

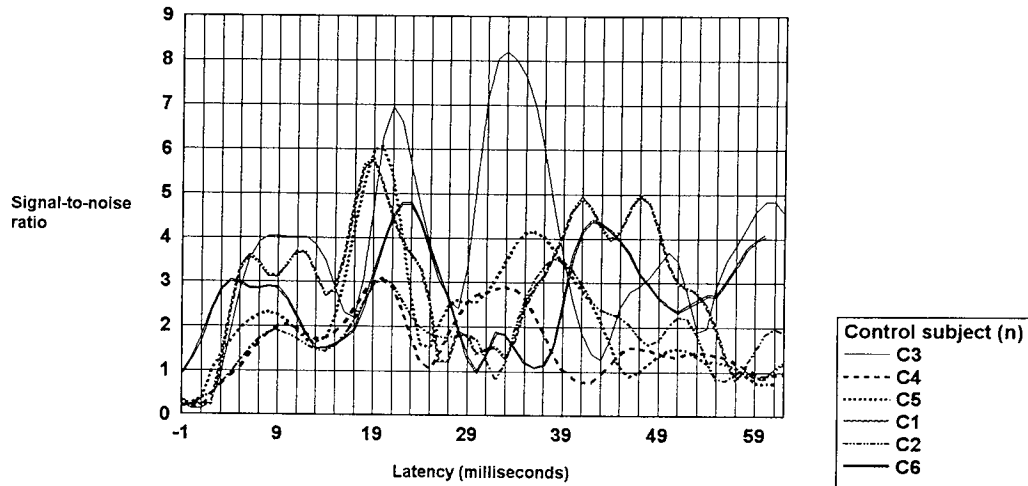


Figure 3.4 A plot of latency versus signal-to-noise ratio's for right median nerve stimulation in six control subjects (C1-C6).

Data in Figure 3.4 for right median nerve stimulation reveals that the largest signal to noise ratios were at 19-24 milliseconds, 31-37 milliseconds and 41-49 milliseconds, with the 19-37msec range consistently providing the strongest signals (> 4:1 ratio).

Peak and mean peak amplitudes for Right Median nerve data are shown in Table 3-1.



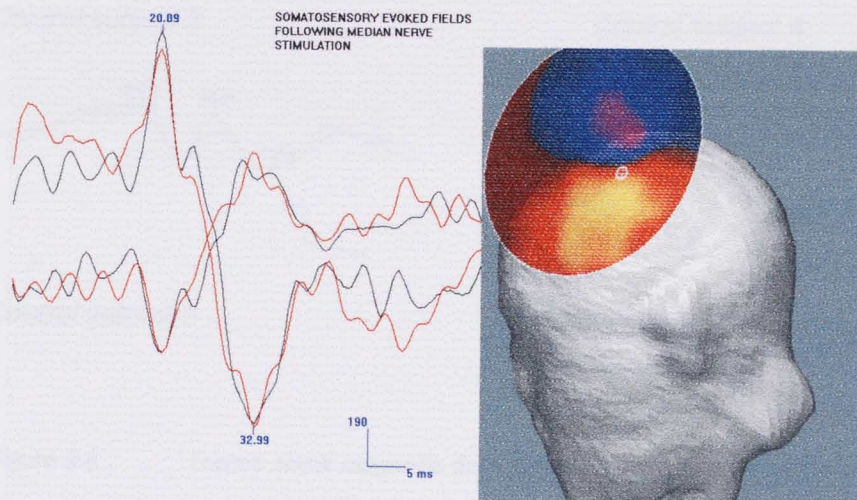
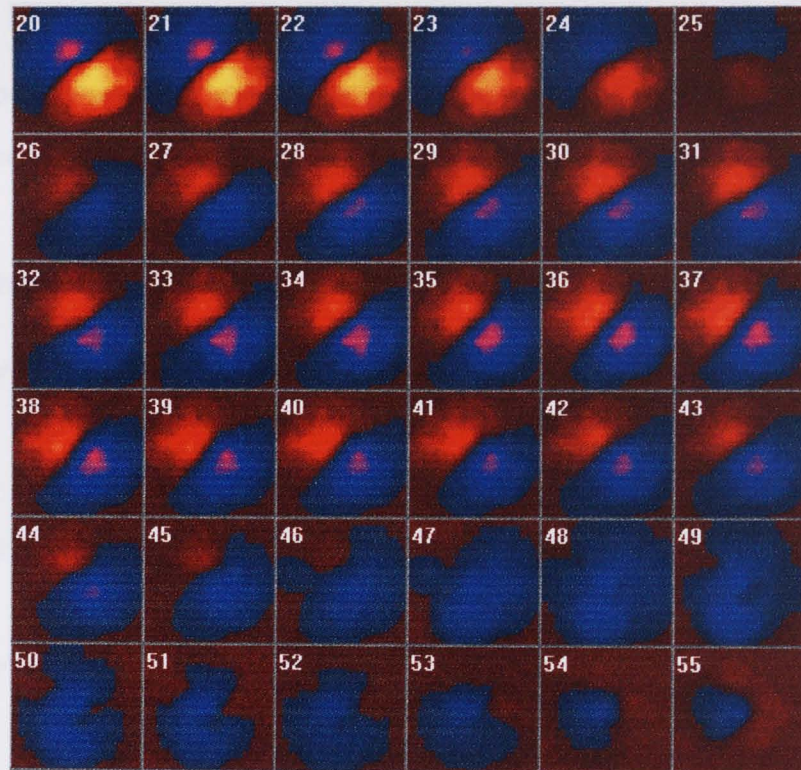
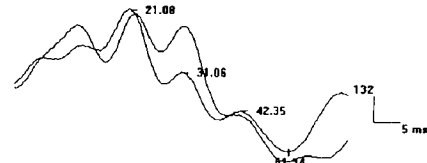
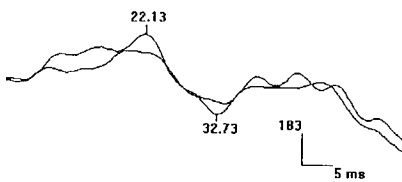
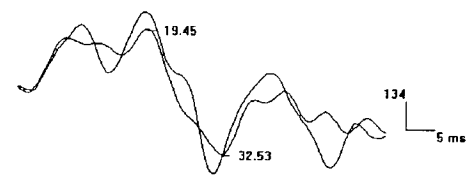
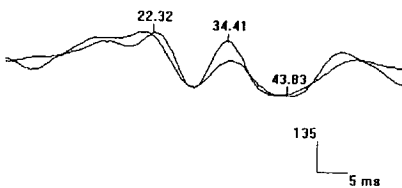
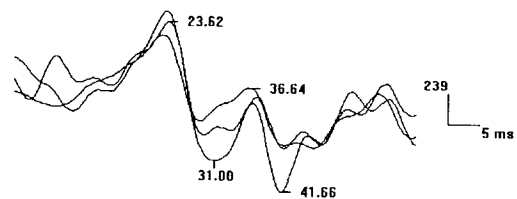


Figure 3.5 Magnetic field distribution between 20 and 55 milliseconds following electrical stimulation of the right median nerve at the wrist. Grid of maps represent the magnetic field distribution across the neuromagnetometer dewar surface with the orientation and location of the dewar depicted in the schematic on the far right. Red and yellow colours represent magnetic field from the head towards the magnetometer and blue/pink represents the return field moving away from the magnetometer.

## 3.4.1.3 Ulnar nerve evoked components: reproducibility and morphology

Data from ulnar nerve stimulation was similar in latency and morphology to the corresponding median nerve data, as can be seen from the waveforms in Figure 3.6.

*Right Ulnar nerve data**Control subject 1**Control subject 2**Control subject 3**Control subject 4**Control subject 5**Control subject 6*

*Figure 3.6* Traces show magnetic field waveforms for two separate trials following right ulnar nerve stimulation. The vertical scale alongside the waveforms is expressed in femtoteslas (fT).

## Morphology of ulnar nerve data

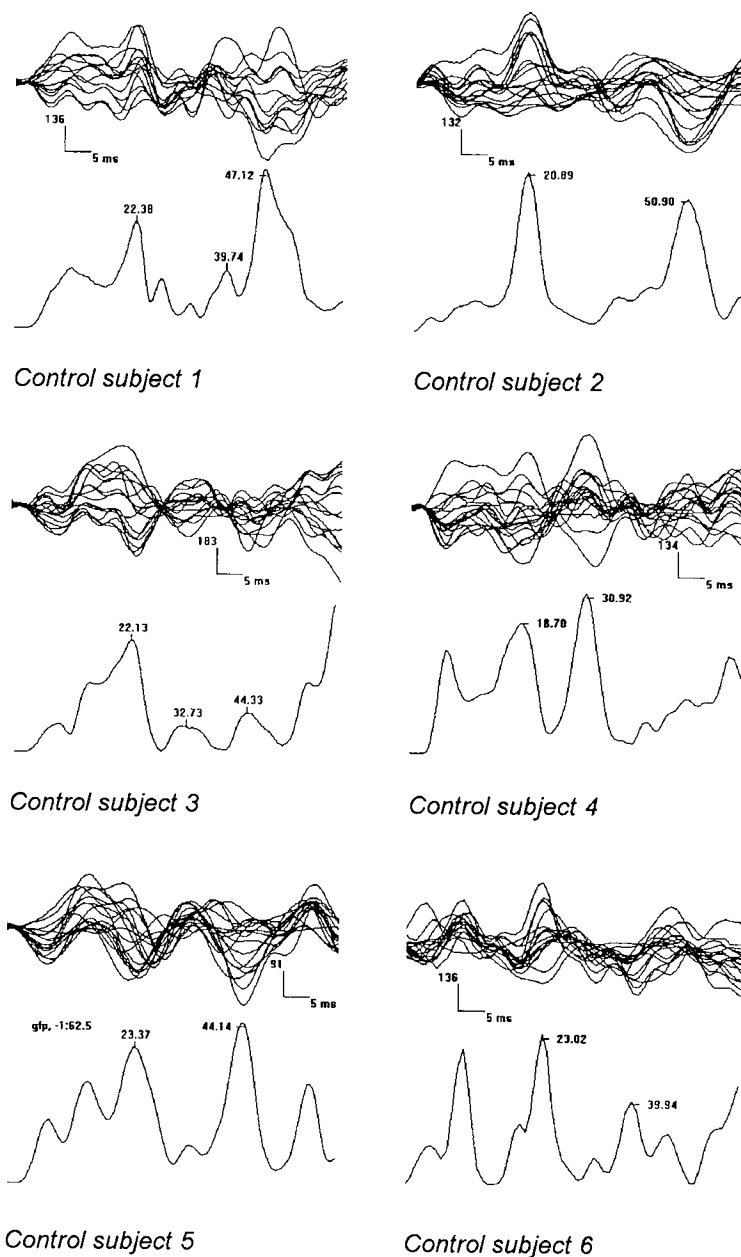


Figure 3.7 Group mean waveforms for right ulnar nerve stimulation (upper traces) with their respective global field power plots shown below. The vertical scale alongside the waveforms is expressed in femtoTeslas (fT).

Global Field Power plots (Figure 3.7) show that the latency interval of 40-50 milliseconds was more of a dominant feature for the ulnar nerve. Unlike the median nerve data, this component (mean 45.5 ms; standard deviation 4.0ms) provided the

strongest dipolar field strength in two subjects. The 20 millisecond component (mean 21.6 ms; standard deviation 1.7ms) provided the other dominant component being largest in three subjects. As with the median nerve data, subjects 3 and 4 showed a 'V' shaped waveform and in subject 4, the first major deflection after the N20m component at 31 milliseconds was the largest signal in this subject.

#### 3.4.1.4 Signal-to-noise ratio of ulnar nerve data

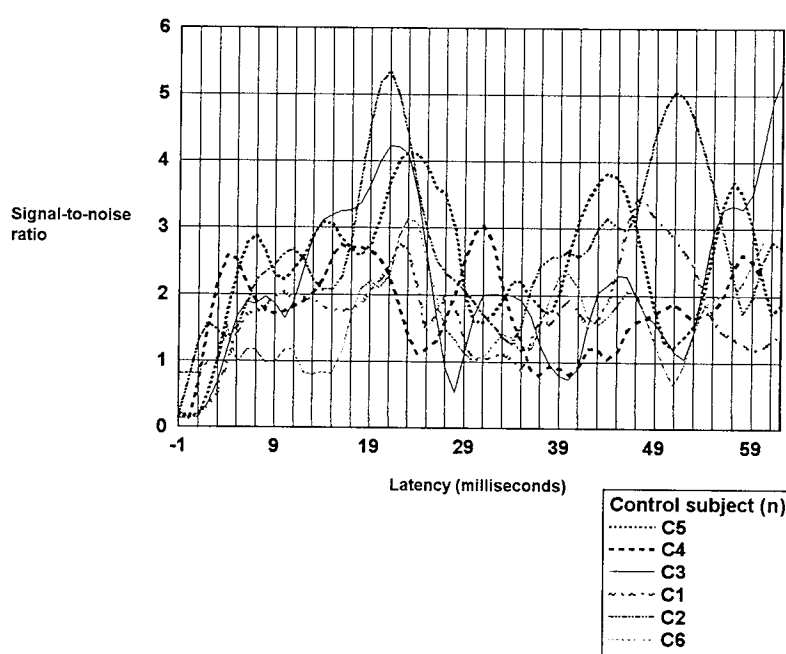


Figure 3.8 A plot of latency versus signal-to-noise ratio's for right ulnar nerve stimulation in six control subjects (C1-C6).

Data in Figure 3.8 for right ulnar nerve stimulation reveals that the largest signal to noise ratios were between 19-24 milliseconds and 43-52 milliseconds, with the earlier components most consistently providing the strongest signals (> 3:1).

Magnetic field strength, and consequently signal-to-noise ratios were greater for median than ulnar nerve data. This data is tabulated overleaf (Table 3-1).

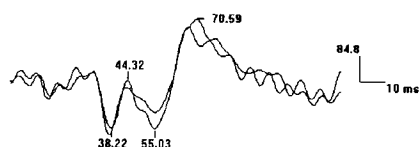
Right Median nerve														
Subject	N20m Latency (ms)	N20m Peak Amplitude (fT)	P27m Latency (ms)	P27m Peak Amplitude (fT)	N33m Latency (ms)	N33m Peak Amplitude (fT)	P45m Latency (ms)	P45m Peak Amplitude (fT)	N45m Latency (ms)	N45m Peak Amplitude (fT)	P45m Latency (ms)	P45m Peak Amplitude (fT)	N45m Latency (ms)	N45m Peak Amplitude (fT)
1	19.8	519.0	30.4	314.0	33.4	273.0	41.0	493.0	47.8	308.0	41.2	342.0	41.2	23.0
2	19.5	303.0	25.2	61.7	29.3	161.0	43.5	342.0						
3	21.3	926.0	33.4	1074.0										
4	19.6	212.0	32.0	421.0										
5	20.1	512.0	28.8	215.0	31.2	165.0	35.5	385.0						
6	23.1	462.0	29.5	269.0	36.5	76.0	42.3	369.0						
Mean	20.6	489.0	29.9	392.5	32.6	168.8	40.6	397.3	44.5	165.5	3.3	57.4	44.5	142.5
STD	1.3	225.3	2.6	323.4	2.7	69.9	3.1							
Right Ulnar nerve														
Subject	N20m Latency (ms)	N20m Peak Amplitude (fT)	P27m Latency (ms)	P27m Peak Amplitude (fT)	N33m Latency (ms)	N33m Peak Amplitude (fT)	P45m Latency (ms)	P45m Peak Amplitude (fT)	N45m Latency (ms)	N45m Peak Amplitude (fT)	P45m Latency (ms)	P45m Peak Amplitude (fT)	N45m Latency (ms)	N45m Peak Amplitude (fT)
1	22.4	313.0	27.2	135.0	35.8	115.5	47.1	406.0						
2	20.1	384.0	27.8	1.1	31.4	60.0	50.9	336.0						
3	22.1	401.0	32.7	122.0										
4	18.7	151.0	32.5	297.0										
5	23.4	163.0	29.0	131.0	34.9	11.2	44.1	175.0						
6	23.0	329.0	31.0	175.0	36.6	76.2	39.9	239.0						
Mean	21.62	290.2	30.0	143.5	34.7	65.7	45.5	289.0						
STD	1.67	98.9	2.2	87.1	2.0	37.4	4.0	88.6						

Table 3-1 Latencies and baseline to peak amplitudes (femtoTeslas;  $10^{15}$  Tesla) of components

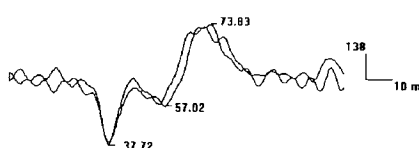
3.4.1.5 Posterior Tibial nerve evoked components: reproducibility and morphology

Characteristic waveforms were consistently produced following electrical stimulation of the posterior tibial nerves at the ankle which were highly reproducible both within and between subjects (Figure 3.9). Magnetic fields for left posterior tibial nerve stimulation were unclear or poorly formed in subjects 2 and 6 and were therefore excluded.

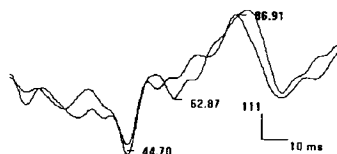
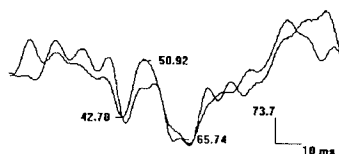
*Left Posterior Tibial*



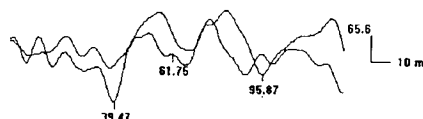
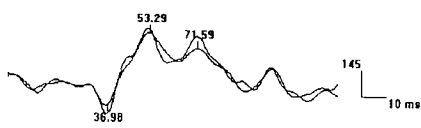
*Right Posterior Tibial*



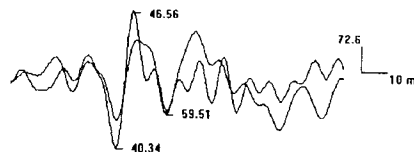
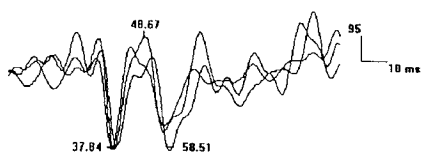
*Control subject 1*



*Control subject 3*



*Control subject 4*



*Control subject 5*

*Figure 3.9 Magnetic field waveforms for two separate trials following left and right posterior tibial nerve stimulation (left and right sided traces respectively). The vertical scale alongside the waveforms is expressed in femtoteslas (fT).*

## Right Posterior Tibial nerve data

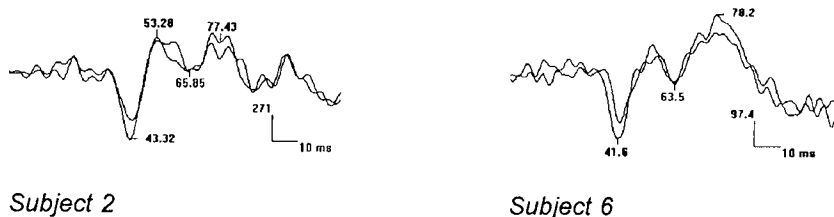


Figure 3.9a Magnetic field waveforms for two separate trials following right posterior tibial nerve stimulation (subjects 2 and 6). The vertical scale alongside the waveforms is expressed in femtoteslas (fT).

Morphology of the waveforms were consistent with those described for somatosensory evoked potentials.

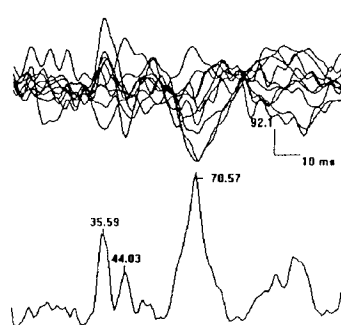
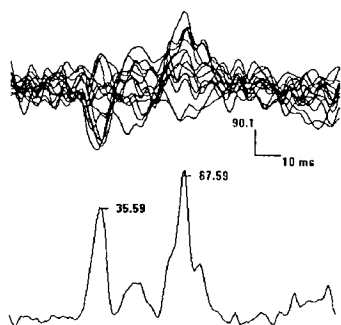
The component with the largest mean amplitude was at a mean latency of 41.2 milliseconds (236.8 +/- 87.2 fT). This compares with 489 +/- 273 fT for the N20m component of median nerve data. (Refer to Table 3-2).

Superimposition of the 19 channel neuromagnetic output of the data, as seen in Figure 3.10, clearly shows that the polarity of the waveforms were equal and opposite in field strength on a number of channels and at various latencies throughout the epoch. Global Field Power plots indicate those latencies at which the field patterns were at a maximum. The component which consistently yielded the strongest dipolar field powers in the control group for both right and left posterior tibial nerve stimulation was the N75m component (n= 6 hemispheres; mean 77.2 ms; s.d. 5.1 ms).

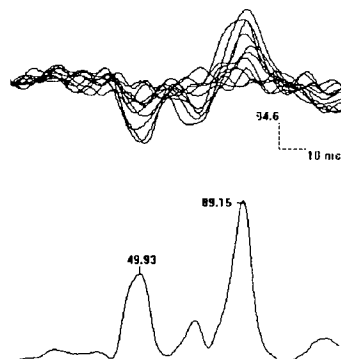
Morphology of posterior tibial nerve data

Left Posterior Tibial

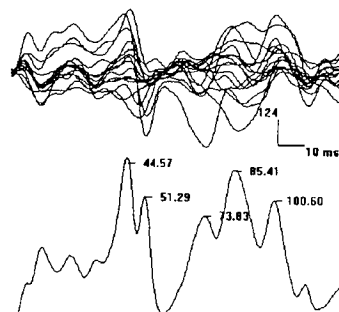
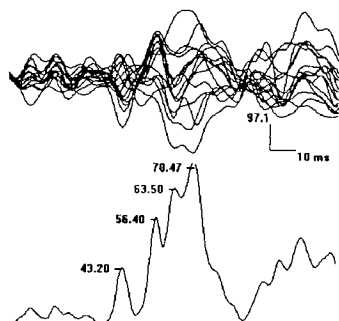
Right Posterior Tibial



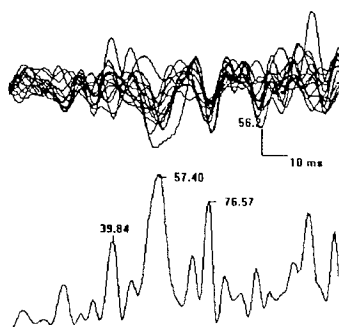
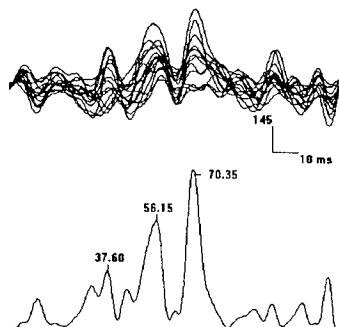
Subject 1



Subject 2



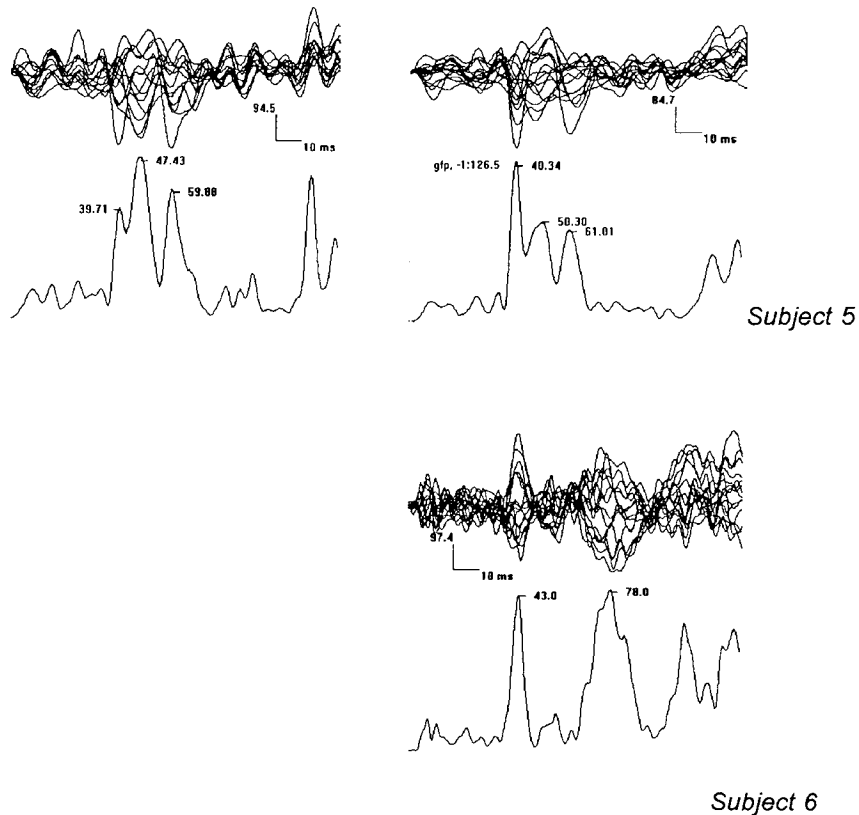
Subject 3



Subject 4

Figure 3.10b (continued over).



*Morphology of posterior tibial nerve data**Left Posterior Tibial**Right Posterior Tibial*

*Figure 3.10 a-c. 19 channels of MEG data are superimposed following a single trial of right and/or left posterior tibial nerve stimulation. Lower traces in each example show the corresponding Global Field Power of the data.*

As can be seen from the typical magnetic field plots in Figure 3.12, the dipolar appearance of the field pattern remained stable between 38 and 64 milliseconds. A dipolar component occurring between 75 and 85 milliseconds was also observed in most trials from control subjects.

## 3.4.1.6 Signal-to-noise ratio of posterior tibial nerve data

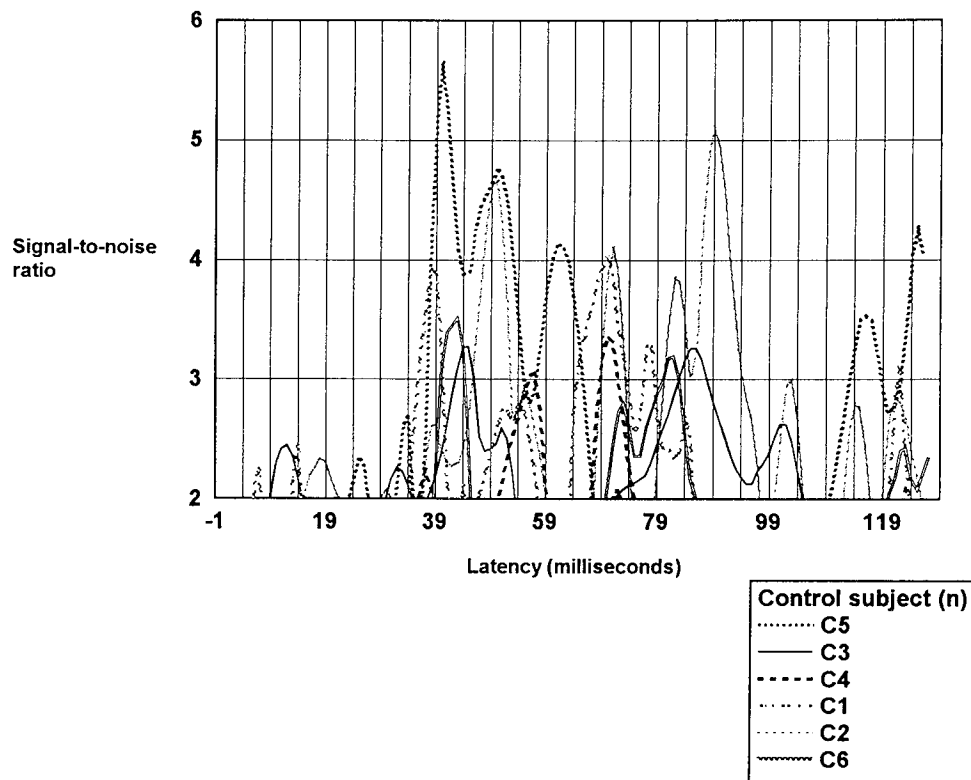


Figure 3.11 A plot of latency versus signal-to-noise ratio's for right posterior tibial nerve stimulation in six control subjects (C1-C6).

The signal to noise ratio plot for posterior tibial nerve data (Figure 3.11) shows a less coherent distribution than median nerve data, though there were two clusters of signal maxima between 40 and 55 milliseconds and between 80 and 95 milliseconds.

Peak and mean amplitudes of right posterior tibial nerve data is shown in Table 3-2 overleaf.

Right Posterior Tibial nerve

Subject	P40m Latency (ms)	P40m Peak Amplitude (fT)	N50m Latency (ms)	N50m Peak Amplitude (fT)	P60m Latency (ms)	P60m Peak Amplitude (fT)	N75m Latency (ms)	N75m Peak Amplitude (fT)
1	37.7	80.8	44.0	95.8	57.0	155.9	73.8	43.2
2	43.3	164.3	53.3	2.7	65.1	99.6	77.4	234.3
3	44.7	275.0	51.3	299.5	62.9	67.3	86.9	336.3
4	39.5	264.8	44.0	236.2	61.8	250.5	76.6	250.5
5	40.3	295.1	46.6	50.7	59.5	177.5	70.4	63.9
6	41.6	338.8	53.1	162.6	63.5	40.7	78.2	311.7
Mean	41.2	236.5	48.7	141.3	61.6	131.9	77.2	206.7
STD	2.3	87.2	4.0	103.3	2.7	71.0	5.1	113.7

Table 3-2 Latencies and baseline to peak amplitudes (femtoTeslas;  $10^{-15}$  Tesla) of Posterior Tibial nerve response components.

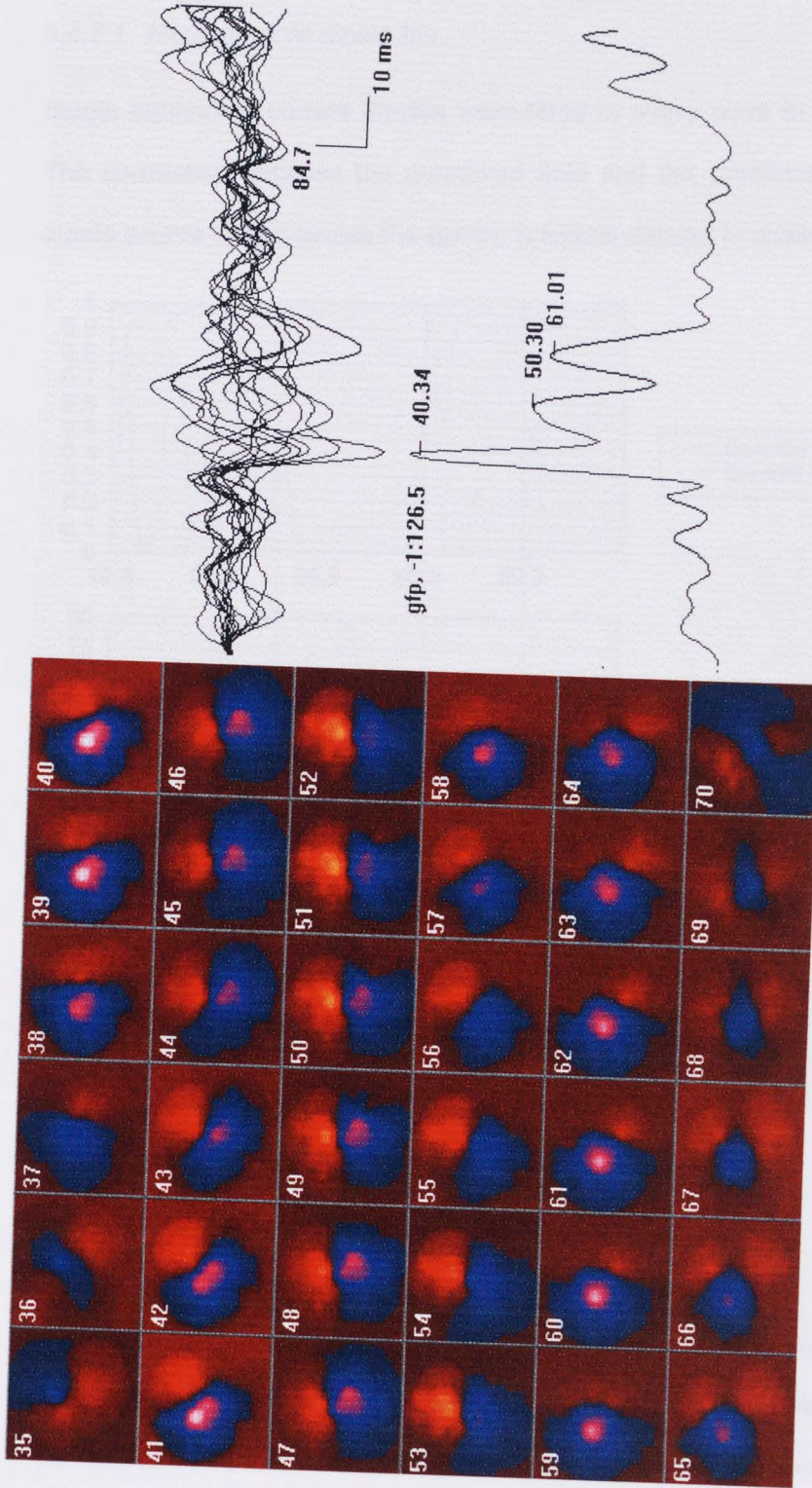


Figure 3.12 Magnetic field distribution between 35 and 70 milliseconds following electrical stimulation of the right posterior tibial nerve at the ankle. Grid of maps represent the magnetic field distribution across the neuromagnetometer dewar surface. Red and yellow colours represent magnetic field from the head towards the magnetometer and blue/pink represents the return field moving away from the magnetometer. Waveforms (right) show magnetic field plot from the 19 magnetometers (upper) with the corresponding Global Field Power plot (lower).

### 3.4.2 Dipole fitting

#### 3.4.2.1 Median nerve dipole fits

Single equivalent current dipoles were fitted to every point of the acquisition epoch. The correlation between the measured field and the predicted localisation's for the dipole source varied across the epoch. A typical dataset is shown in Figure 3.13.

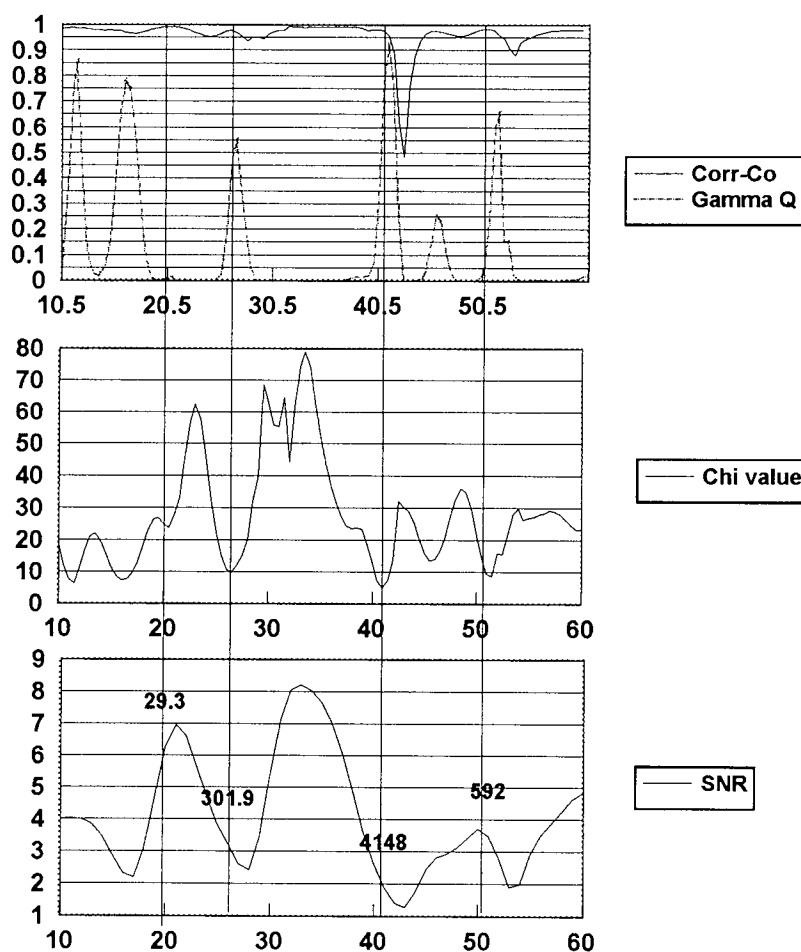


Figure 3.13 Graphs depicting the parameters for Equivalent Current Dipole source localisations across the acquisition epoch. Correlation co-efficients and GammaQ outputs are shown (top) with the Chi values shown below. A plot of signal-to noise ratio's against latency (bottom) also indicates the values for 95% confidence volumes achieved through MonteCarlo analysis (expressed in cubic millimetres). The vertical lines passing through all three graphs indicate the points from which the best confidence volumes were achieved.

The initial criterion for data analysis was a dipole fit correlation coefficient exceeding 0.95. However, a critical value for robust cortex localisation would be the size of the 95% confidence volumes. Consequently, a plot of confidence volumes in relation to signal to noise ratio's was made (Figure 3.14)

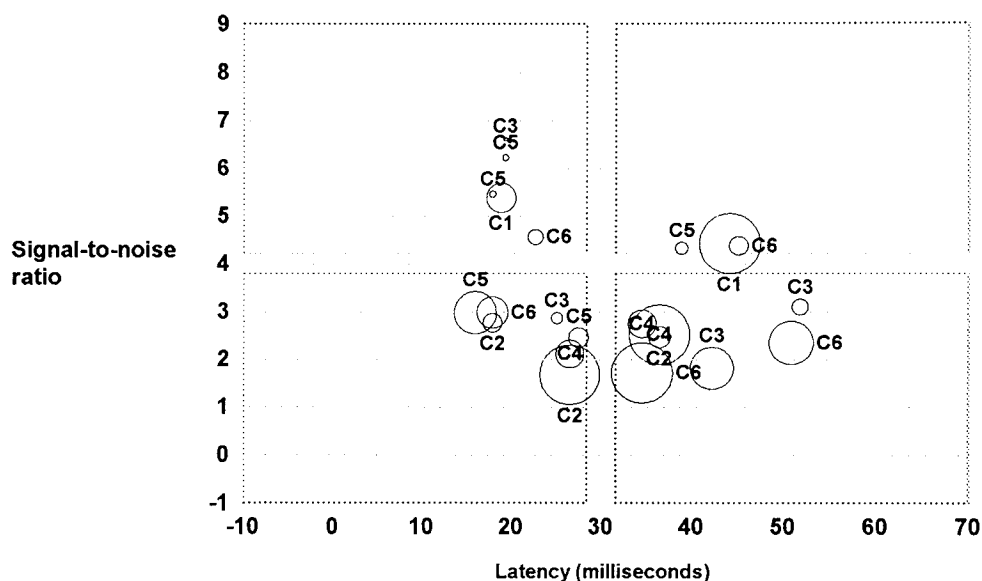


Figure 3.14 Plot of latency versus signal-to-noise ratio for right median nerve data with the sizes of scatter plot points representing the relative 95% confidence volumes (in cubic millimetres) following Monte Carlo analysis of dipole fits. Only confidence volumes of less than  $2 \text{ cm}^3$  were plotted.

Figure 3.14 confirms that the smallest confidence volumes were in conjunction with the largest signal-to-noise ratios and were clustered around the 20 millisecond latency and between 35 and 45 milliseconds. The data also confirmed that a signal-to-noise ratio of greater than 1.8:1 was required for the confidence volumes to be less than  $2 \text{ cm}^3$  and a ratio of 2.5:1 or greater was required for  $1 \text{ cm}^3$  confidence volumes.

Analysis of any single statistic from the dipole fit was inadequate in predicting latencies that would yield confidence volumes of less than  $2\text{cm}^3$ . Both the correlation co-efficient and the GammaQ were relatively insensitive measures, with good confidence volumes being achieved from GammaQ values ranging from 0.01 to 0.99 and confidence volumes ranging from  $2000\text{mm}^3$  to in excess of  $50,000\text{mm}^3$  obtained with correlation co-efficients of 0.96.

Low Chi values provided a more robust indicator with lowest volumes seen in conjunction with Chi values of 25 or less.

The distribution of Chi minima across the control group was plotted (Figure 3.15)

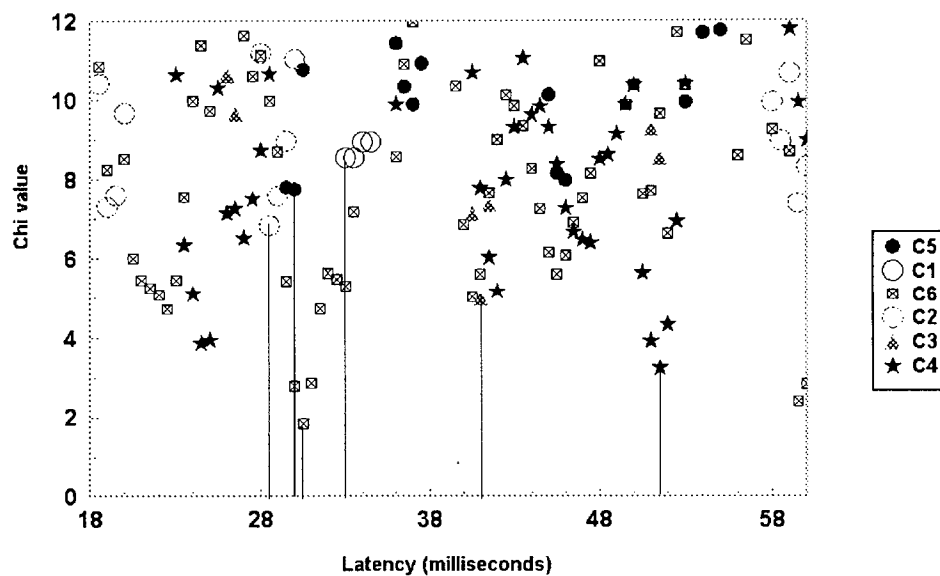


Figure 3.15 Chi values of 12 or less were plotted for each of the control group subjects.

As can be seen from the graph in Figure 3.15, in four subjects the Chi minima were obtained at latencies between 28 and 34 milliseconds.

From analysis of the datasets across the control group, the important combination of data was a correlation coefficient greater than 0.96, a Chi value of less than 25, together with a signal to noise ratio greater than 2:1.

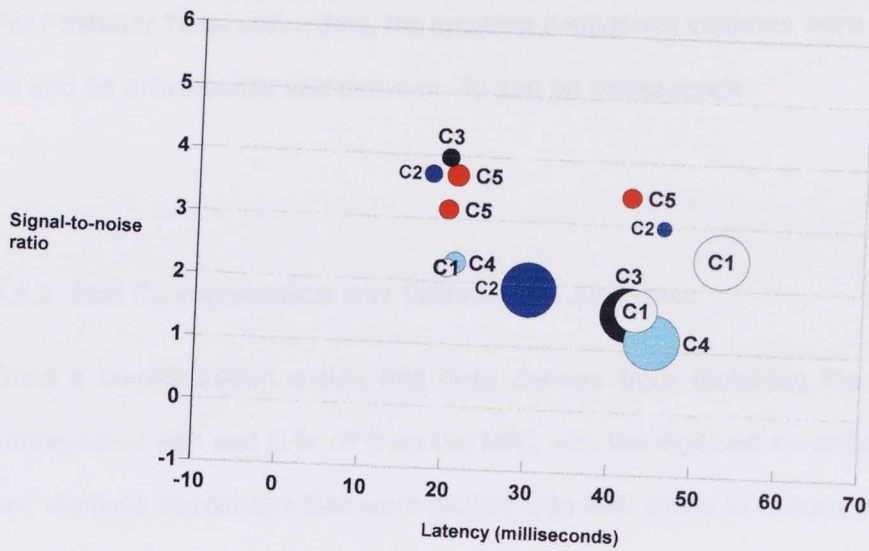


Figure 3.16 Plot of latency versus signal-to-noise ratio for right ulnar nerve data with the sizes of scatter plot points representing the relative 95% confidence volumes (in cubic millimetres) following Monte Carlo analysis of dipole fits. Each subject is shown in a different colour.

3.4.2.3 Posterior Tibial dipole fits

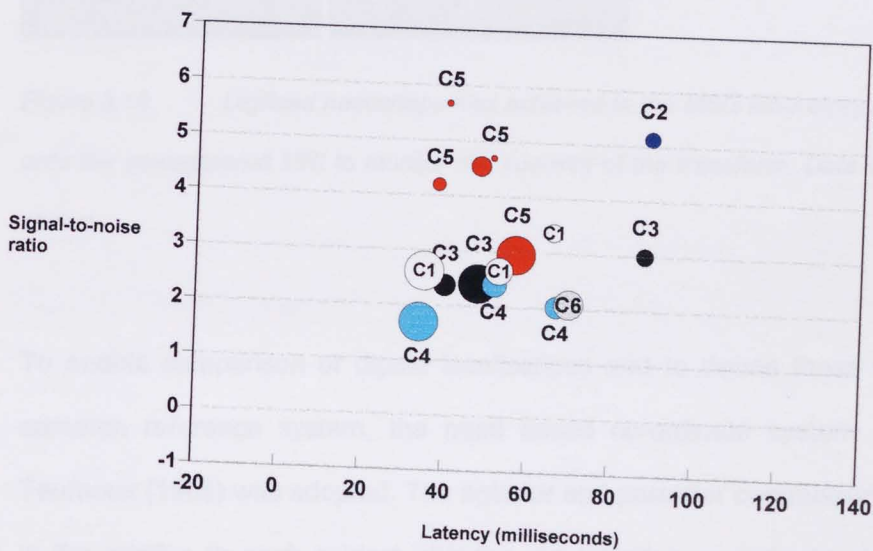


Figure 3.17 Plot of latency versus signal-to-noise ratio for posterior tibial nerve data with the sizes of scatter plot points representing the relative 95% confidence volumes (in cubic millimetres) following Monte Carlo analysis of dipole fits. Each subject is shown in a different colour



For Posterior Tibial nerve data, the smallest confidence volumes were seen between 35 and 55 milliseconds and between 70 and 90 milliseconds.

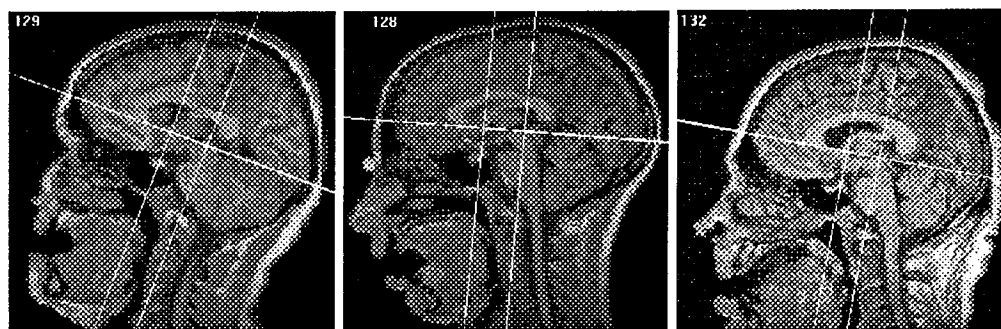
### 3.4.3 MRI Co-registration and Talairach co-ordinates

Once a co-registration matrix had been derived from matching the bite bar points impregnated with cod liver oil from the MRI, with the digitised co-ordinates of the bite bar, digitised headshape files were plotted onto MRI slices to ensure a good match. A typical example is shown below in Figure 3.18.



*Figure 3.18* Digitised headshape files achieved in the MEG laboratory were superimposed onto the co-registered MRI to monitor the success of the transform. Data on control subject 6 shown.

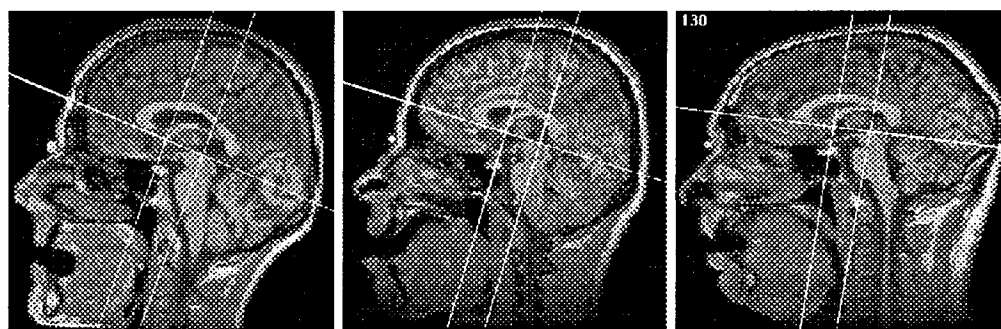
To enable comparison of dipole localisations and to define those localisations in a common reference system, the head based co-ordinate system of Talairach and Tournoux (1988) was adopted. The anterior and posterior commissures were identified in the midline in each subject allowing the baseline co-ordinates to be established. The appropriate midline slices together with the baseline grids established for the control subjects are illustrated in Figure 3.19.



*Control subject 1*

*Control subject 2*

*Control Subject 3*



*Control Subject 4*

*Control Subject 5*

*Control subject 6*

*Figure 3.19 Talairach co-ordinate templates were established for each control subject by identifying the midline position of the anterior and posterior commissures.*

### 3.4.4 Dipole localisations

#### 3.4.4.1 Median nerve localisations

95% confidence ellipses following three separate trials of median nerve stimulation were co-registered with MRI volumes (Figure 3.20a-f). Smallest confidence ellipses from each epoch, if less than  $2\text{cm}^3$  in volume, were plotted.

The following figures illustrate the co-registration of these confidence volumes onto single MRI slices for ease of comparison.

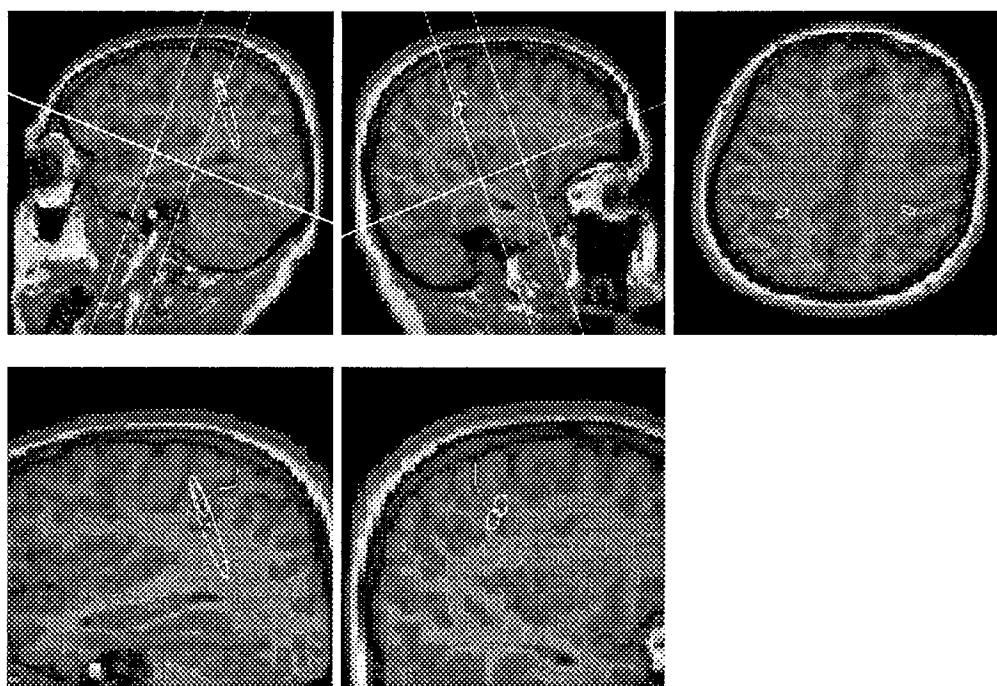


*Figure 3.20a* Smallest 95% confidence ellipses from three trials of right and left median nerve stimulation in control subject 1. The central sulcus has been highlighted in the lower images.

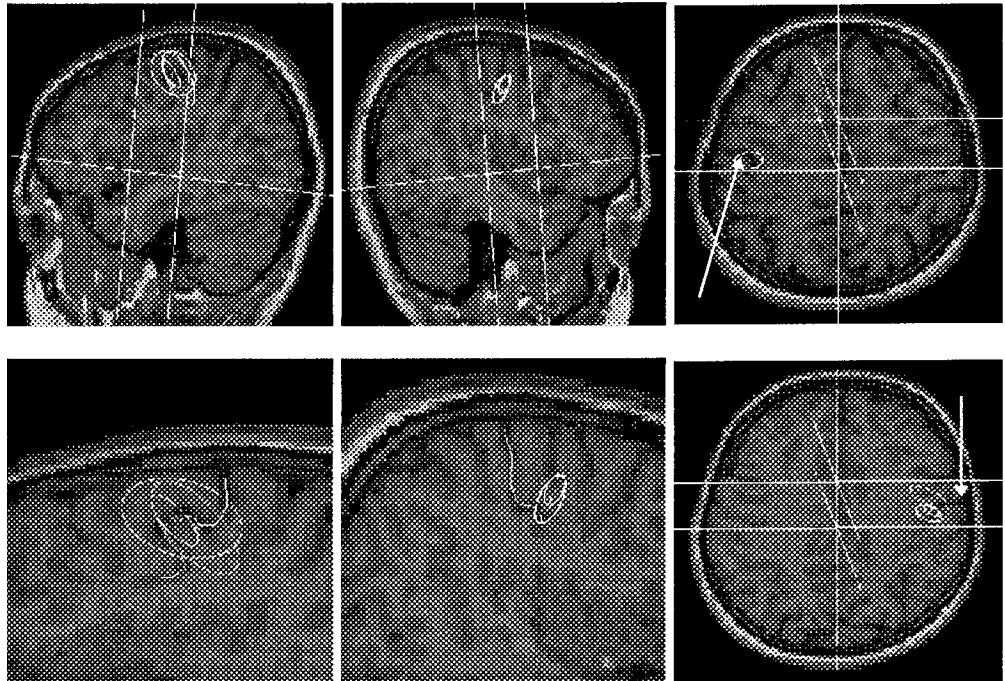


Figure 3.20b Smallest 95% confidence ellipses from three trials of right and left median nerve stimulation in control subject 2.

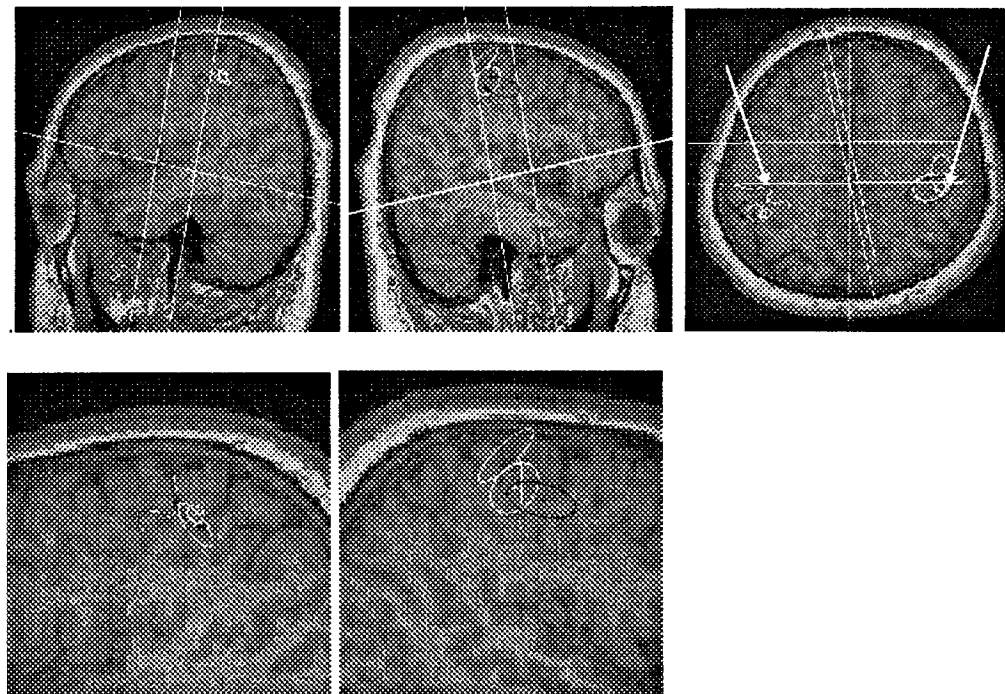


Figure 3.20c Smallest 95% confidence ellipses from three trials of right and left median nerve stimulation in control subject 3..

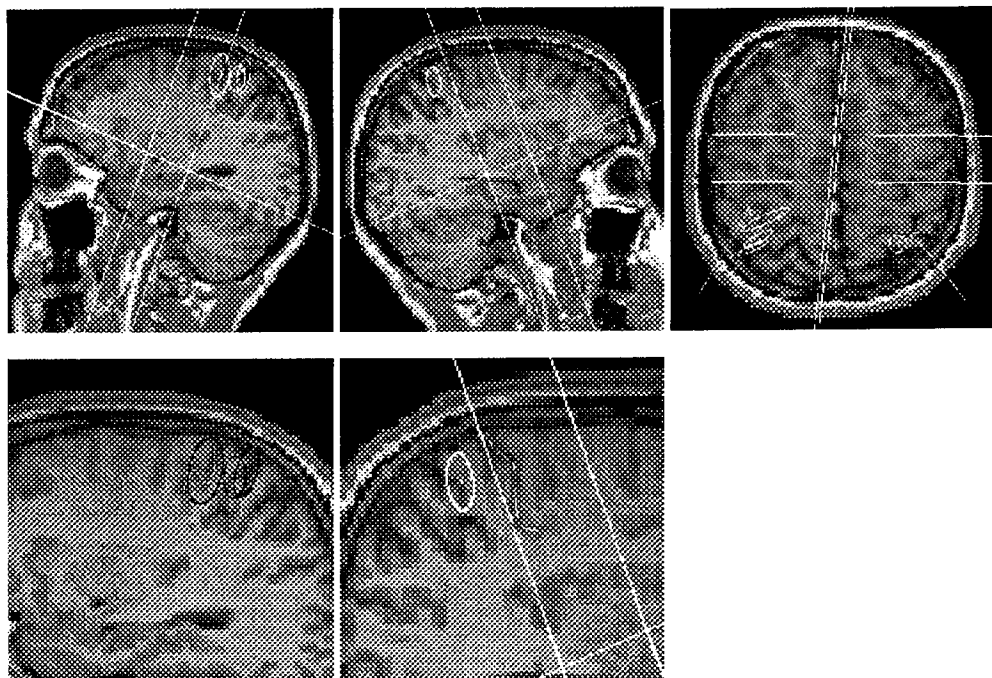


Figure 3.20d *Smallest 95% confidence ellipses from three trials of right and left median nerve stimulation in control subject 4.*

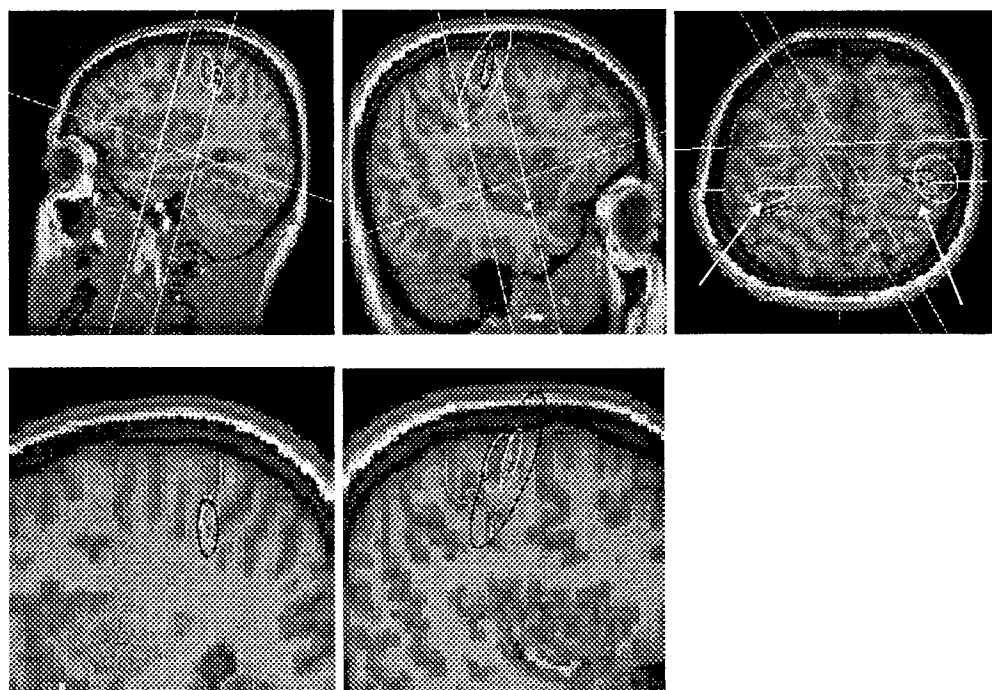


Figure 3.20e *Smallest 95% confidence ellipses from three trials of right and left median nerve stimulation in control subject 5.*

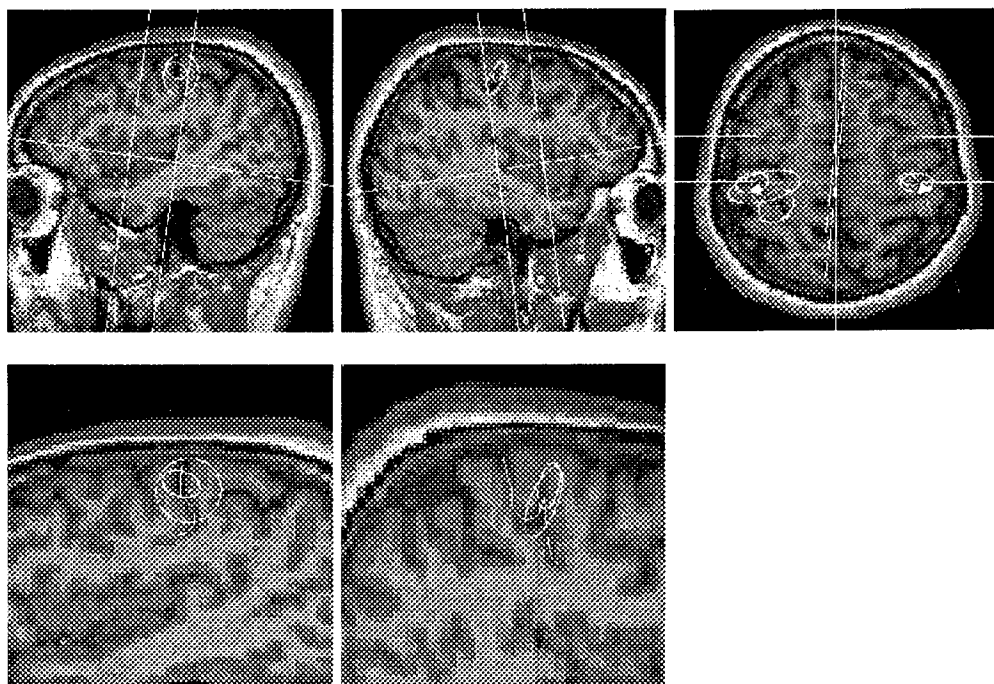


Figure 3.20f Smallest 95% confidence ellipses from three trials of right and left median nerve stimulation in control subject 6.

Figure 3.20 a-f. Median nerve localisations for control subjects. Monte Carlo ellipses for three separate trials of right median nerve stimulation (top left) and the corresponding ellipses for left median nerve stimulation (top middle) are shown. The juxtaposition of right and left median nerve data are shown on a single axial slice for comparison (top right) with the central sulcus line indicated by arrows. Latencies selected for localisations were concomitant with the N20m component. White gridlines indicate the base-planes (AC-PC and VCa-VCp lines) for Talairach (1988) co-ordinates. MRI slices below (lower left and middle) indicate the relative positions of the Central Sulcus as predicted from Talairach atlas co-ordinates.

Following right median nerve stimulation, all confidence ellipses encompassed the postcentral gyrus. Mean localisations within the ellipses were placed either within the posterior bank of the central sulcus, or within the central sulcus itself, for every trial in 5 of the 6 subjects. In one subject, the mean points of all three trial ellipses were located in the precentral gyrus.

For right median nerve stimulation, five of the six subjects yielded the smallest confidence volumes around the 20 millisecond mark.

The distance from the posterior bank of the central sulcus of the single smallest volume achieved from the three trials was measured. The data is summarised in Tables 3-3 and 3-4 below.

### Right Median nerve

Subject	Latency of smallest confidence volume	Smallest Confidence Volume (mm <sup>3</sup> )	Signal to Noise Ratio	Distance from CS
Control 1	20.0msec	38.9	5.9:1	+2.0mm
Control 2	19.0msec	597.0	2.9:1	0.0mm
Control 3	20.5msec	29.3	6.3:1	-4.0mm
Control 4	33.5msec	324.0	2.9:1	-19.0mm
Control 5	20.7msec	92.0	6.1:1	-5.0mm
Control 6	22.5msec	491.7	3.2:1	0.0mm

*Table 3-3 Latencies yielding smallest confidence ellipses following Right Median nerve stimulation are shown. The distance of the mean point of this ellipse from the posterior bank of the central sulcus in each control subject is indicated. 'Plus' or 'minus' signs in the 'Distance from CS' column represents anterior to, or posterior to the posterior bank of the Central Sulcus respectively. The signal-to-noise ratio of the data at the latency indicated is shown for comparison.*

## Left Median Nerve

Subject	Latency smallest confidence volume	Smallest Confidence Volume(mm <sup>3</sup> )	Signal to Noise Ratio	Distance from CS
Control 1	19.0msec	40.8	7.9:1	0.0mm
Control 2	42.0msec	142.0	2.8:1	+3.0mm
Control 3	31.0msec	49.0	6.2:1	0.0mm
Control 4	33.5msec	326.0	2.8:1	-17.0mm
Control 5	28.5msec	478.0	3.1:1	+16.0mm
Control 6	24.0msec	223.0	4.4:1	+5.0mm

*Table 3-4 Latencies yielding smallest confidence ellipses following Left Median nerve stimulation are shown. The distance of the mean point of this ellipse from the posterior bank of the central sulcus in each control subject is indicated. 'Plus' or 'minus' signs in the 'Distance from CS' column represents anterior to, or posterior to the posterior bank of the Central Sulcus respectively. The signal-to-noise ratio of the data at the latency indicated is shown for comparison.*

For left median nerve stimulation, two of the six subjects yielded the smallest confidence volumes between 19 and 24.0 milliseconds; between 28.5 and 33.5 milliseconds in three, and at 42.0 milliseconds in one.

Two subjects (5 and 6) had all three trial confidence ellipses located either entirely or predominantly within the precentral gyrus. In these two subjects, the data between the two hemispheres was asymmetric with the localisations in the left hemispheres lying postcentrally.

In control subject 4, only one trial produced data which was good enough to co-register following left median nerve stimulation. Here, the confidence ellipse was centred 1.6 cm posterior to the central sulcus.



*The group mean distances of the **smallest confidence volumes** (measured from the central mean point of each confidence ellipse) from the posterior bank of the central sulcus were:*

**Right Median nerve 5.0 mm, standard deviation 6.5**

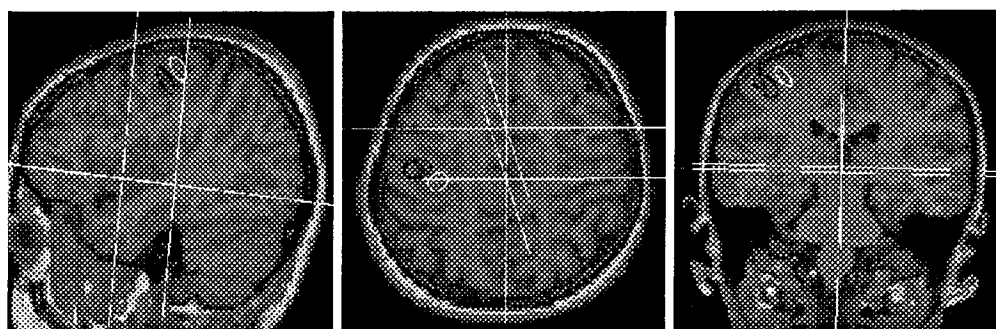
**Left Median nerve 6.8mm, standard deviation 7.1**

The data indicated that cortical localisations of within 0.5cm of the source may be consistently achieved if the criterion of fitting the smallest confidence volume only is applied. However, in subject 4, for both right and left median nerve stimulation, the localisations appeared to be nearly 2cm away from the source predicted by neuroanatomical methods, namely the posterior bank of the central sulcus. Examination of the confidence ellipses from each of the three trials in this subject for right median nerve data (Figure 3.17d) showed that in one trial of larger volume, the localisation was centred only 2 millimetres from the posterior bank of the central sulcus. It is therefore necessary to overlap several confidence volumes from separate trials to ensure validity of localisation.

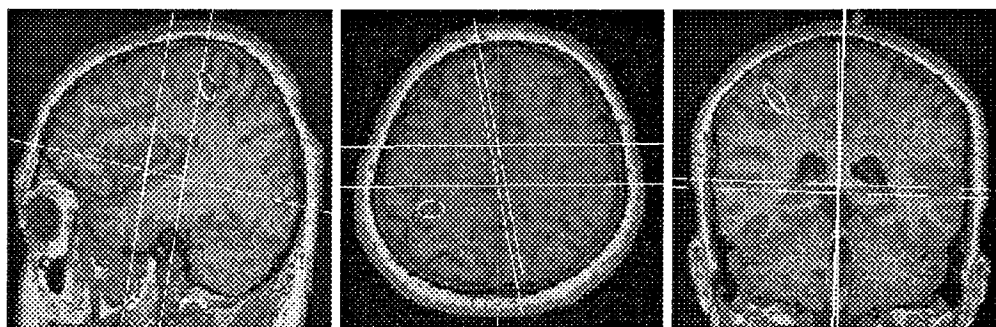
The issue of trial / re-trial variation in localisation is investigated in section 3.4.6

### 3.4.4.2 Ulnar nerve localisations

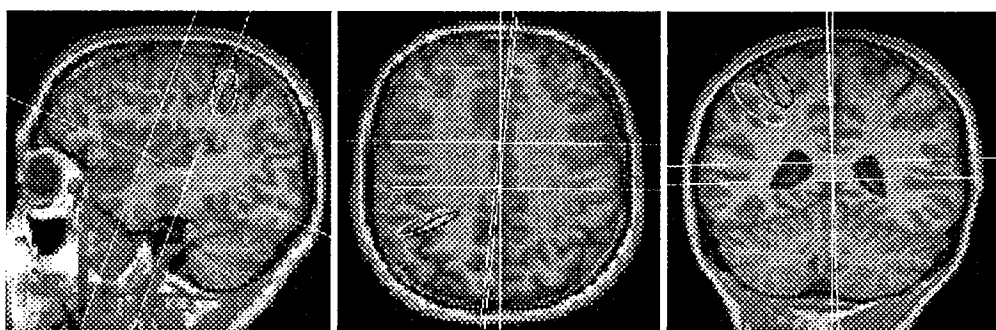
Smallest confidence ellipses for right ulnar nerve data for the 20 millisecond component were all located in close proximity to their right median nerve counterparts (Figures 3.21 & 3.22). All were located in the post central gyrus and except in control subject 4, all were located superiorly to the median nerve ellipses.



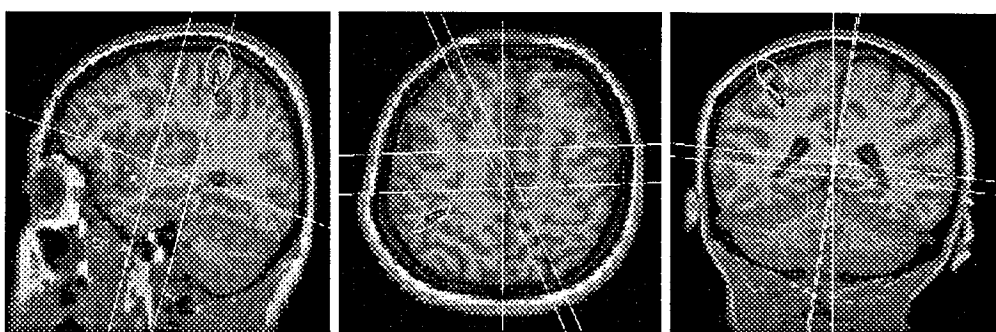
*Control subject 2*



*Control subject 3*

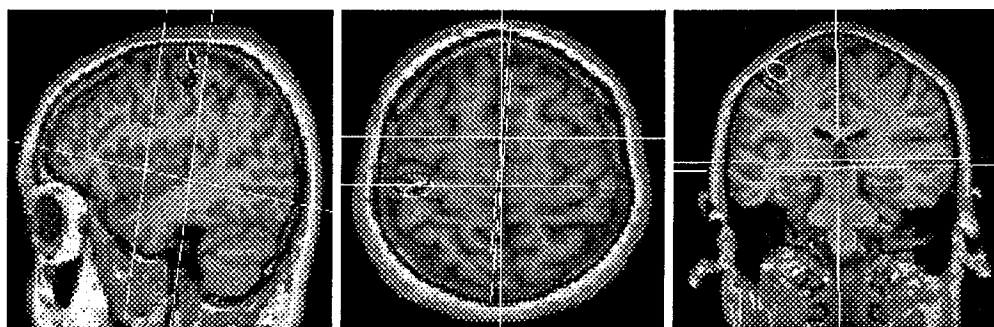


*Control subject 4*



*Control subject 5*

*Figure 3.21 Right ulnar (white) and Right median (black) Monte Carlo confidence ellipses are shown for control subject 2-5 for comparison of localisation.*



Control Subject 6

Figure 3.22 Right ulnar (white) and Right median (black) Monte Carlo confidence ellipses are shown for control subject 6 for comparison of localisation.

### Median and Ulnar nerve localisation differences

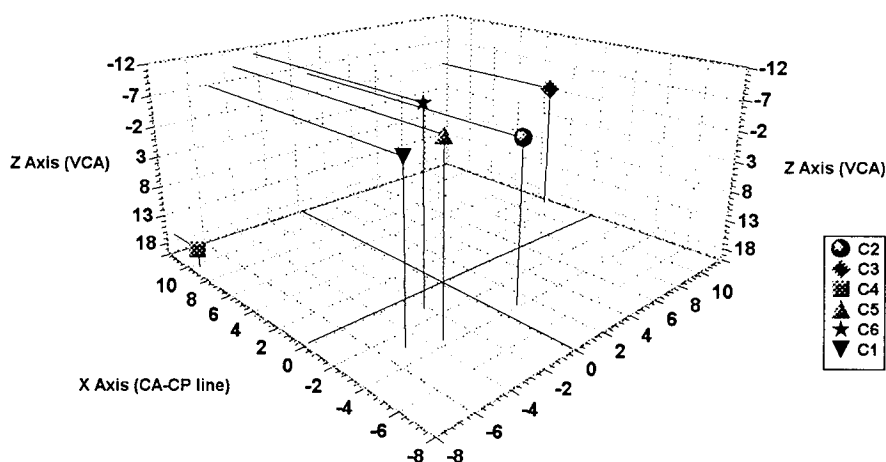
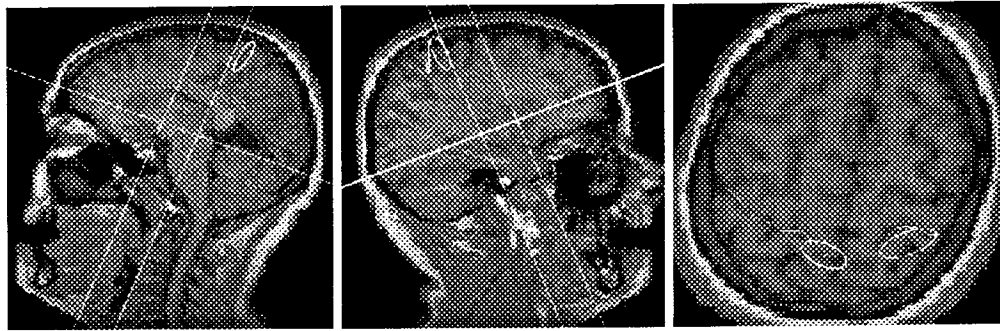


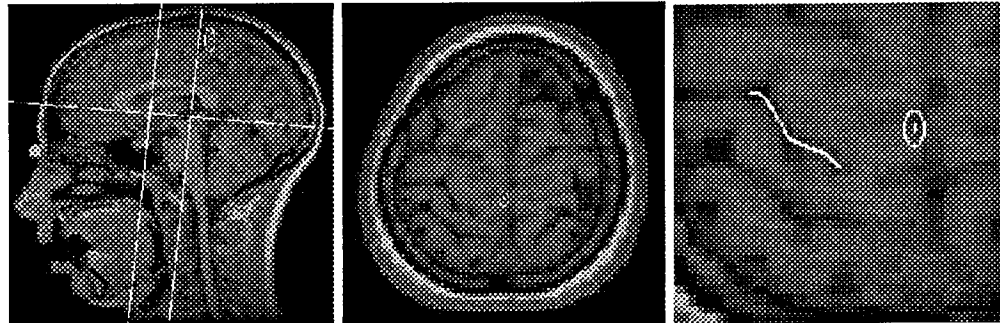
Figure 3.23 Differences in Median and Ulnar nerve localisations are represented in the graph above. Data was provided by the subtraction of the Talairach co-ordinates for the mean point of the smallest confidence volume for ulnar nerve data from the median nerve counterpart in control subjects. Negative values in a given plane therefore indicate a larger Talairach co-ordinate for the ulnar nerve compared to the median nerve counterpart.

Excluding the obvious outlier of control subject 4, the mean displacement of ulnar versus median nerve localisations expressed in Talairach co-ordinate space was 2.9 mm ( $\pm 1.2$ mm) in the CA-CP plane, 4.6 mm ( $\pm 4.1$ mm) in the transverse plane, and 7.1 mm ( $\pm 3.3$ mm) in the VCA-VCP plane.

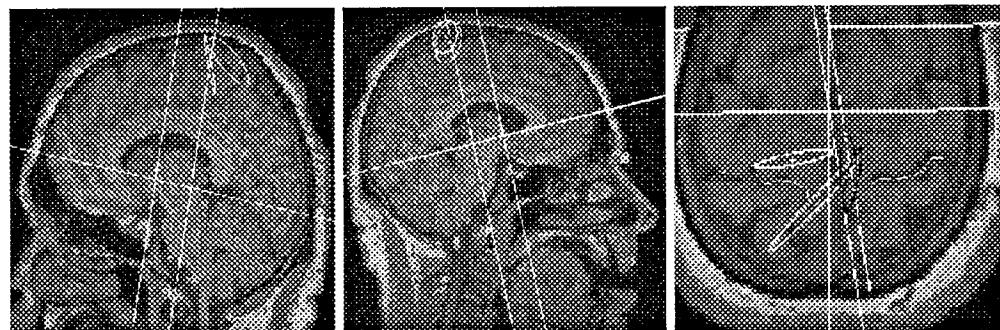
### 3.4.4.3 Posterior Tibial nerve localisations



*Control Subject 1*



*Control Subject 2*



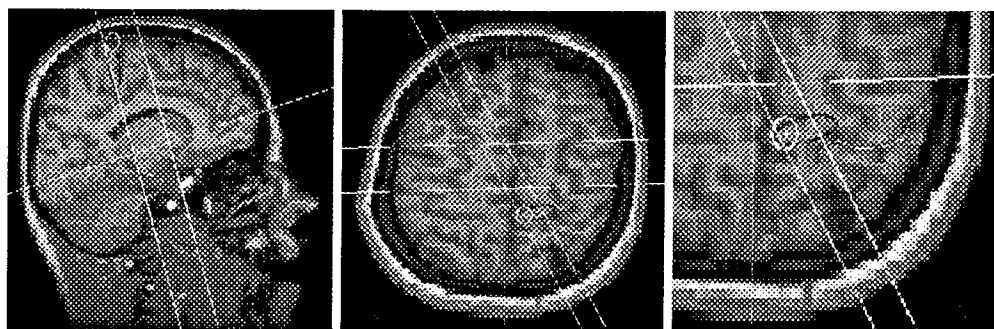
*Control Subject 3*



*Control Subject 4*

*Figure 3.24 a-d Monte Carlo ellipses for separate trials of Right and / or Left Posterior Tibial nerve localisations for each control subject are shown.*

*(Continued over)*



Control Subject 5



Control Subject 6

*Figure 3.24 e-f Monte Carlo ellipses for separate trials of Right and / or Left Posterior Tibial nerve localisations for each control subject are shown.*

In two control subjects (4 and 5) right posterior tibial stimulation produced confidence volumes which exceeded  $8000 \text{ mm}^3$  and so were excluded from the data sets. The same control subjects however did provide acceptable confidence volumes following left posterior tibial stimulation.

In four of the eight successful posterior tibial nerve localisations achieved from the control group (from 12 hemisphere measures), smallest confidence volumes were achieved between 70 and 89 milliseconds.

The **group mean distance** of the smallest confidence volumes from the posterior bank of the central sulcus was **6.25 millimetres (s.d. 4.8mm)**. See Table 3-5 overleaf.

Subject	Right Posterior Tibial			Left Posterior Tibial		
	Latency of smallest confidence volume	Smallest Confidence Volume (mm <sup>3</sup> )	Distance from CS	Latency of smallest confidence volume	Smallest Confidence Volume (mm <sup>3</sup> )	Distance from CS
Control 1	35.0msec	1119.0	0.0	64.0msec	1399.0	-6.0mm
Control 2	89.2msec	1200.0	+4.0mm			
Control 3	88.5msec	1852.0	+6.0mm	73.5msec	669.0	+7.0mm
Control 4		>8000		52.5msec	2619.0	-17.0mm
Control 5		>8000		38.0msec	1558	+8.0mm
Control 6	70.0msec	1545.0	+2.0mm			

Table 3-5 Latencies yielding smallest confidence ellipses following Right and Left Posterior Tibial nerve stimulation are shown. The distance of the mean point of this ellipse from the posterior bank of the central sulcus in each control subject is indicated. 'Plus' or 'minus' signs in the 'Distance from CS' column represents anterior to, or posterior to the posterior bank of the Central Sulcus respectively.

### 3.4.5 Comparison of Talairach co-ordinates

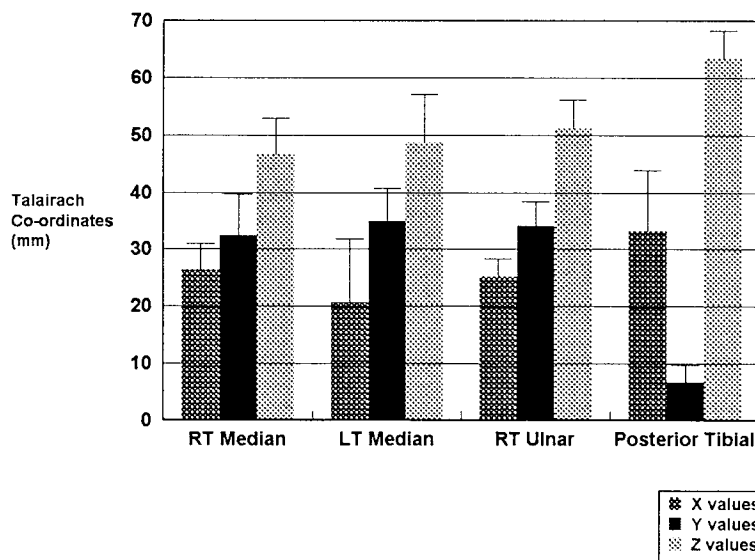


Figure 3.25 Group mean Talairach co-ordinates for Median, Ulnar and Rt + Lt Posterior Tibial nerve data. Error bars show 1 standard deviation from the mean value.

Group Mean Talairach co-ordinates were calculated for comparison between stimulation sites as well as to allow comparison with the Talairach atlas data. Data is plotted graphically (Figure 3.25, previous page) and tabulated below (Table 3-6).

Table 3-6 Group Mean Talairach co-ordinates

Nerve	Co-ordinate	Co-ordinate	Co-ordinate
	CA-CP axis (x) N mm (S.D.)	Lateral (y) axis N mm (S.D.)	VCA-VCP axis (z) N mm (S.D.)
Right Median	26.3 ( 4.7)	32.4 (7.3)	46.6 (6.4)
Left Median	20.7 (11.1)	34.9 (5.8)	48.7 (8.5)
Right Ulnar	25.2 (3.1)	34.2 (4.3)	51.2 (5.0)
Rt + Lt Post. Tibial	33.2 (10.7)	6.7 (3.1)	63.5 (4.8)

No significant difference was observed between right and left median nerve data. Ulnar nerve data was consistently superior in aspect to the median nerve. Posterior Tibial nerve data was consistently located towards the vertex and close to the midline.

The mean and standard deviations for these localisations were matched with the appropriate slices in the sample brain within the Talairach and Tournoux atlas. These comparisons are shown overleaf (Figures 3.26 - 3.29).

It is interesting to observe that although the direct Talairach co-ordinates have been plotted onto the 'typical brain' directly, without conversion to the proportional co-ordinates of Talairach and Tournoux (1988), that the localisations were anatomically relevant when compared with the actual localisations of individual data-sets. This provides evidence of the value of such an atlas and generic data produced from a proportional reference system.

## Chapter 3

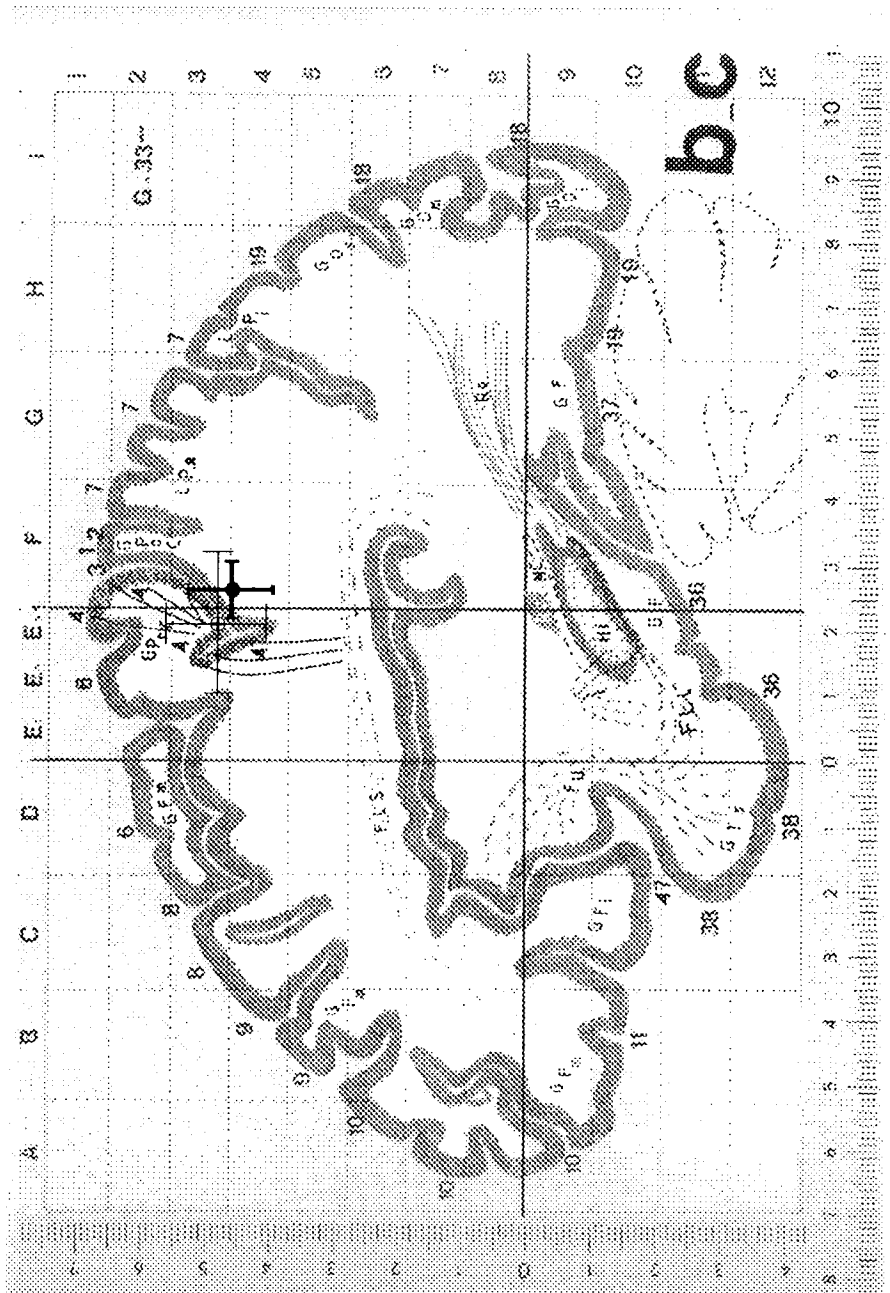


Fig 3.26 Mean localisations for right median (black circle) and left median (white circle with black cross) nerve trials are plotted onto the nearest matching sagittal slice from the Talairach and Tournoux atlas (1988). Error bars represent one standard deviation from the mean. Right hand plate is an enlargement from the full plate.



## Chapter 3

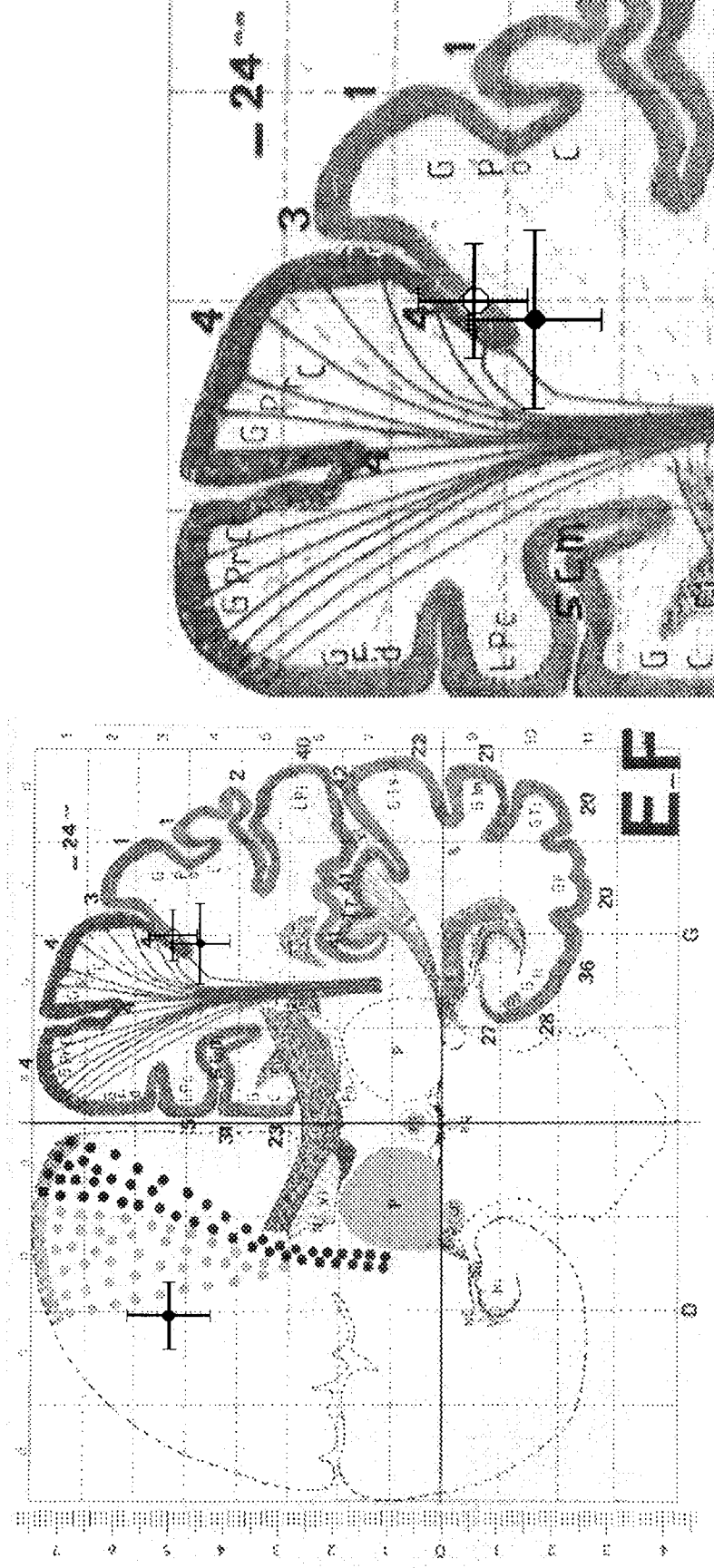
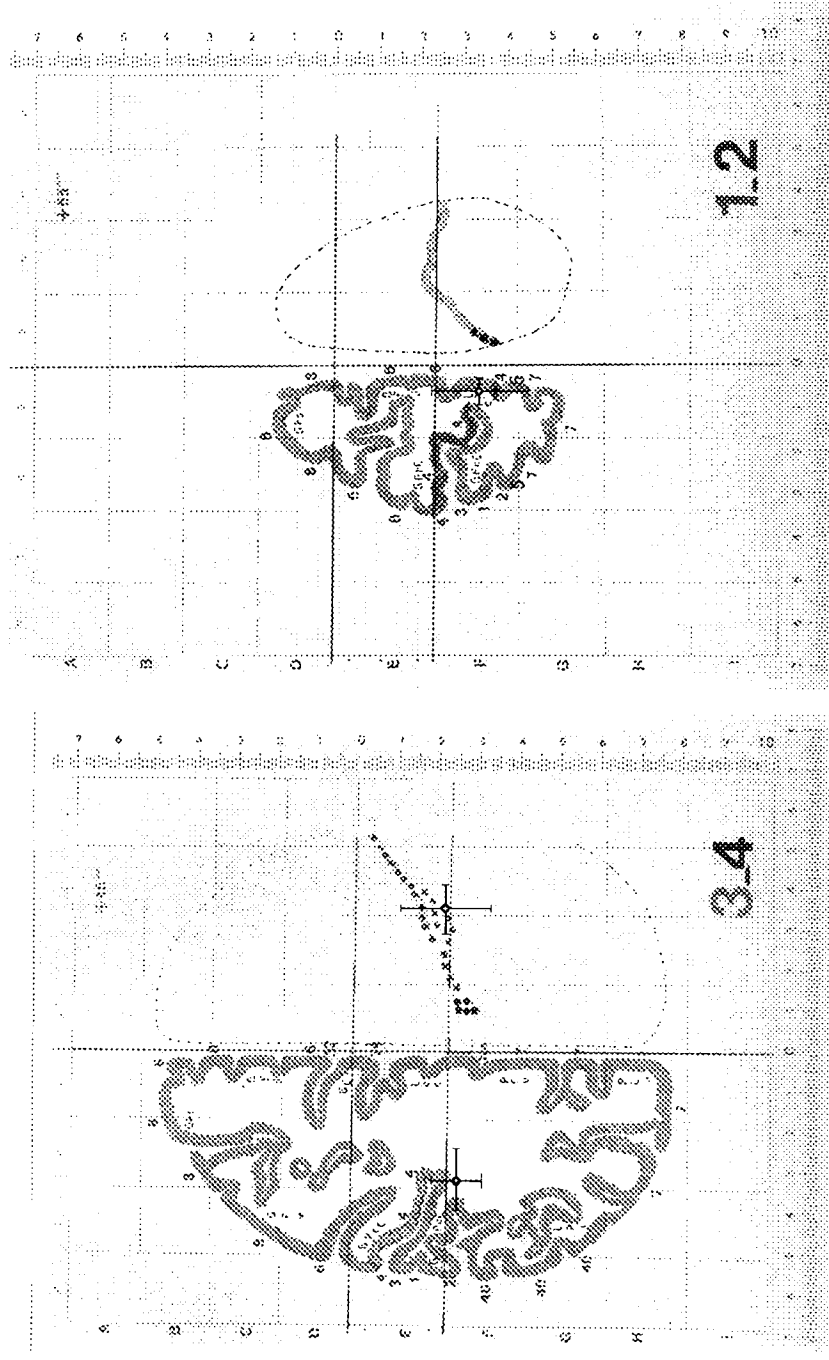


Fig 3.27 Mean localisations for right median (right side of plate) and left median nerve trials are plotted onto the nearest matching coronal slice from the Talairach and Tournoux atlas (1988). Mean ulnar nerve data (white circle) is plotted for comparison. Error bars represent one standard deviation from the mean. Right hand plate is an enlargement from the full plate.

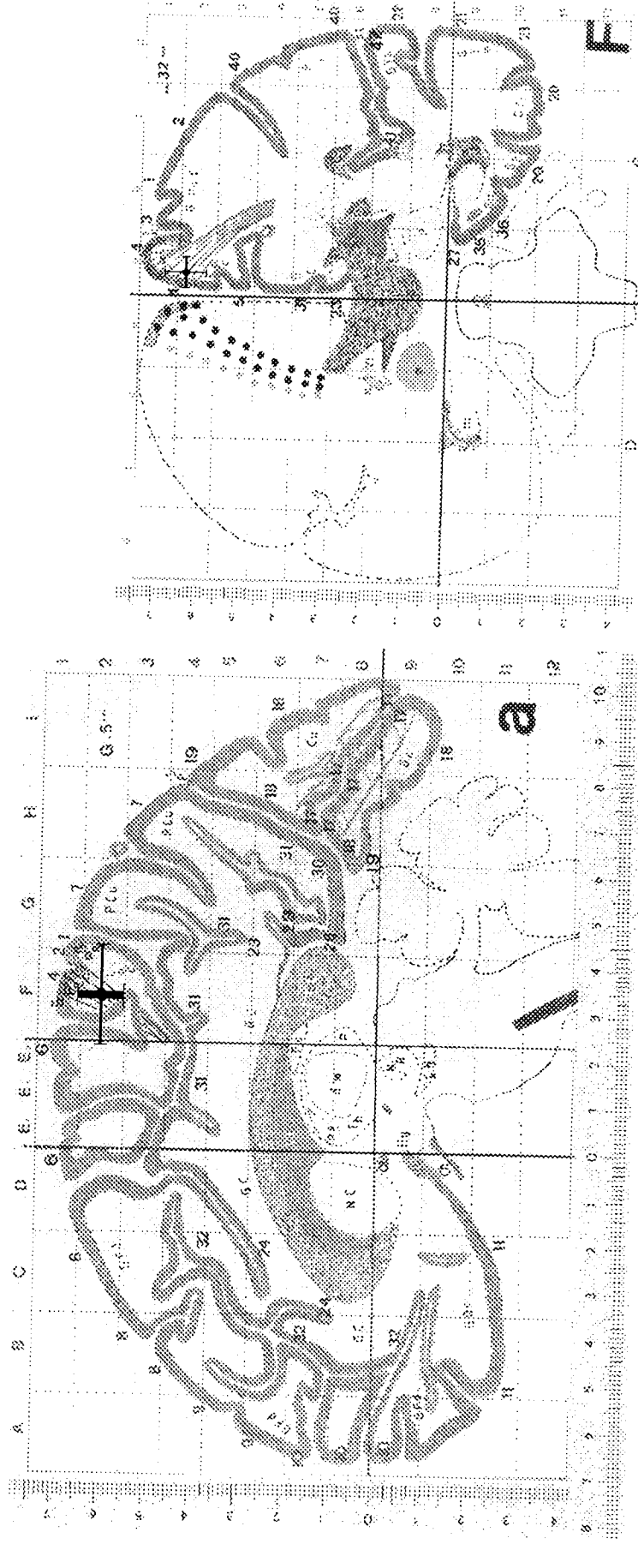
Chapter 3



a) b) c)

Fig 3.28 Plate a) shows mean Talairach co-ordinate localisations for right and left median nerve data. Error bars indicate one standard deviation from the mean. Plate b) shows the mean Talairach co-ordinate localisation for right posterior tibial data with one standard deviation error bars. Plate c) is an enlargement from b).

### Chapter 3



a)

b)

Fig 3.29 Mean Talairach co-ordinate for right posterior tibial nerve data plotted onto the nearest matching sagittal (a) and coronal (b) slices from the Talairach and Tournoux atlas (1988).

3.4.6 Variation in the localisation of repeated trials.

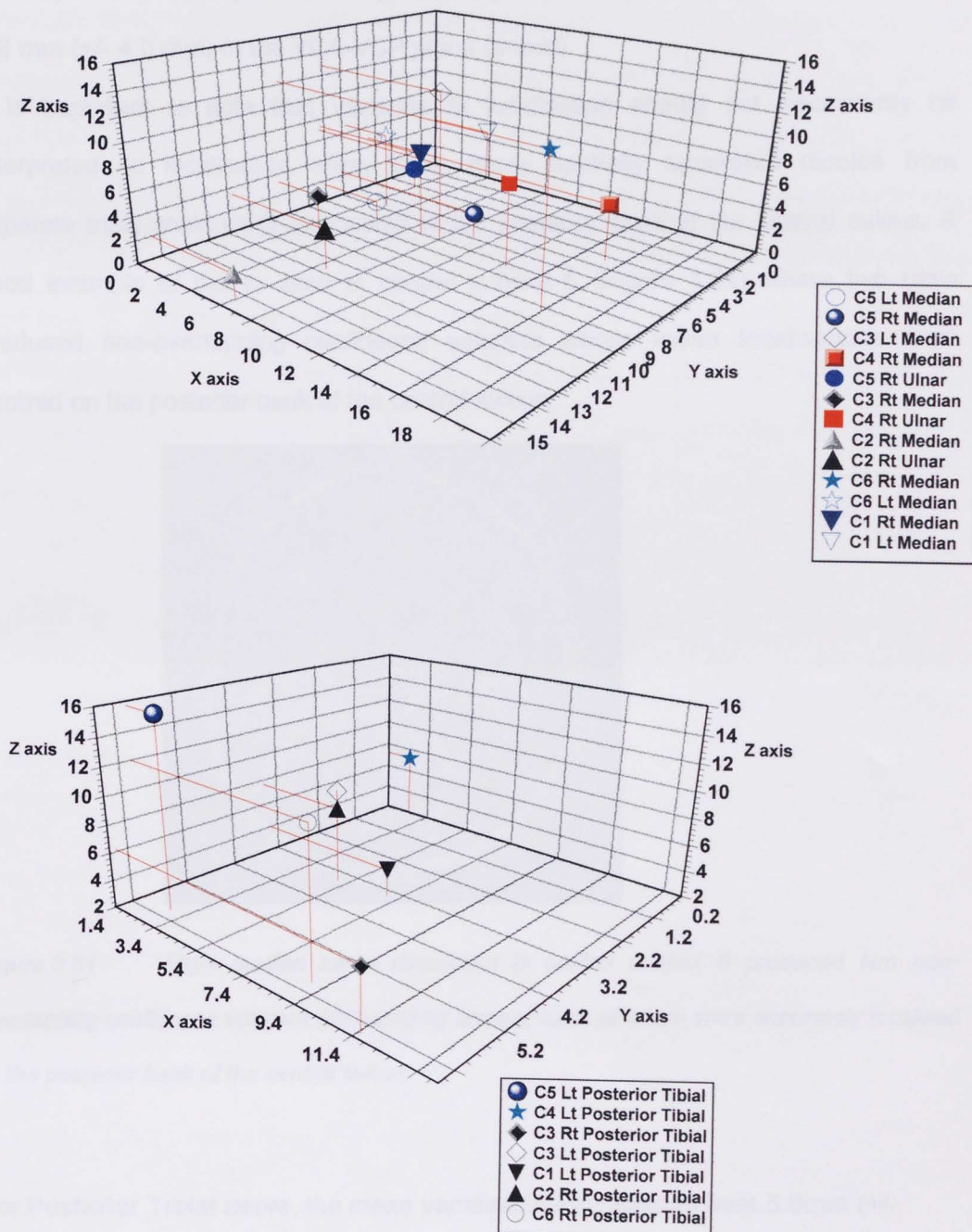
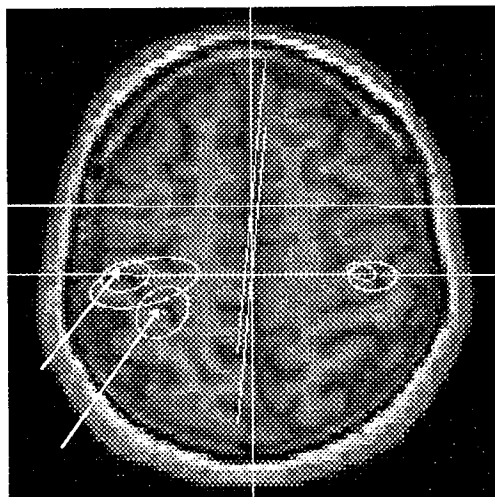


Figure 3.30 To show the spatial separation of dipole fits seen over repeated trials, the minimum x,y and z Talairach co-ordinates were subtracted from the maximum values obtained following three successive trials of nerve stimulation. Right and Left Median nerve data is shown in the upper graph with Right and Left Posterior Tibial nerve data in the lower.

The data shows that sequential stimulation trials resulted in a spread of localisations. For **median nerve** stimulation, the mean variation in localisations were 7.5mm (+/- 4.8mm) in the CA-CP plane (x axis), 7.2mm (+/- 3.9 mm) in the lateral or y-axis, and 5.8 mm (+/- 4.0 mm) in the VCA-VCP plane (z-axis).

It is important to note that variation in localisation should not necessarily be interpreted as localisation error, since many spatially separated dipoles from separate trials could each be located to the posterior bank of the central sulcus. A good example of this is seen in control subject 6 (Figure 3.31) where two trials produced non-overlapping confidence volumes whose mean localisations were centred on the posterior bank of the central sulcus.



*Figure 3.31 Right median nerve stimulation in control subject 6 produced two non-overlapping confidence volumes (indicated by arrows) each of which were accurately localised to the posterior bank of the central sulcus.*

For **Posterior Tibial nerve**, the mean variation in localisations were 5.6mm (+/- 3.8mm) in the CA-CP plane (x axis), 3.9mm (+/- 2.4 mm) in the lateral or y-axis, and 8.2 mm (+/- 4.7 mm) in the VCA-VCP plane (z-axis). This data is closely similar to the median nerve data set.

### **3.4.7 Variation in localisation across the temporal window of acquisition.**

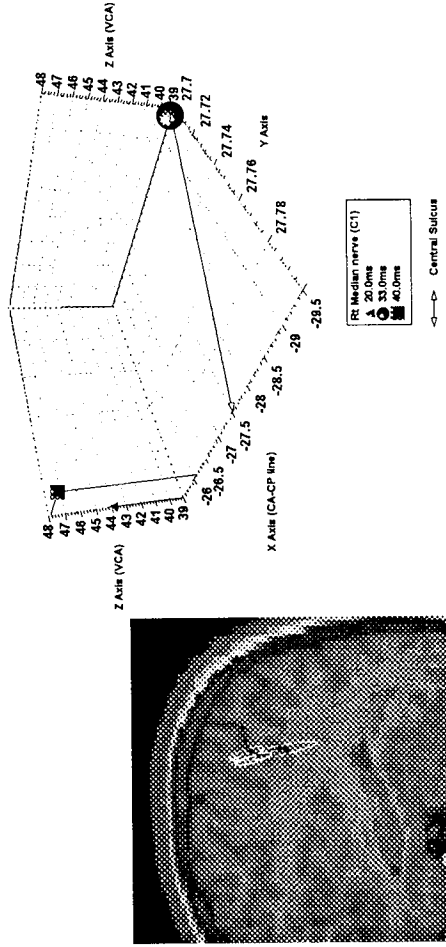
Analysis was required to determine the spatial localisation of dipoles across the temporal window of acquisition and to establish latencies yielding the closest localisation to the central sulcus. Consequently, all confidence volumes from across the entire acquisition epoch producing volumes less than  $2\text{cm}^3$ , were co-registered with the MRI. The trial which had produced the smallest confidence volume was selected for analysis. The Talairach co-ordinate distance from the central mean point of each volume to the posterior bank of the central sulcus was measured and compared with that of the smallest volume. Right Median and Right Posterior Tibial nerve data was used for this analysis.

#### **3.4.7.1 Temporal localisations for right median nerve data**

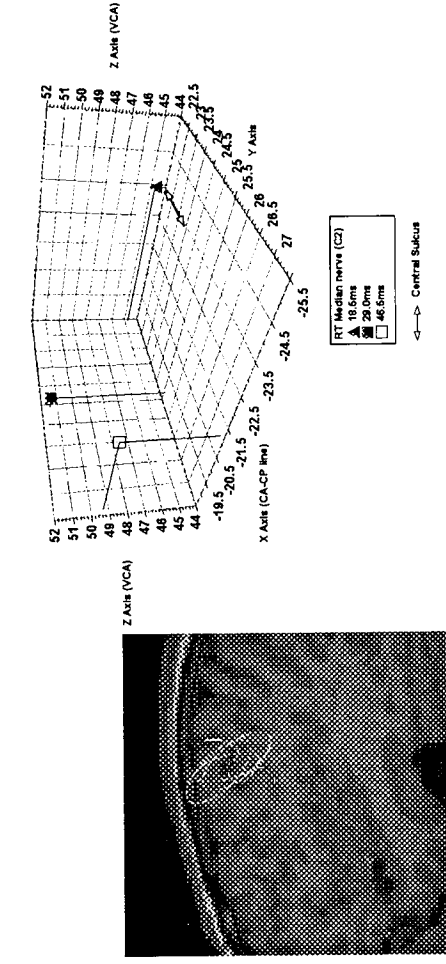
The following figures illustrate the dipole localisations across the temporal window of acquisition for right median nerve stimulation.

3.4.7.1 (Continued)

Variation in localisation across the temporal window of acquisition (Median nerve)



Control subject 1



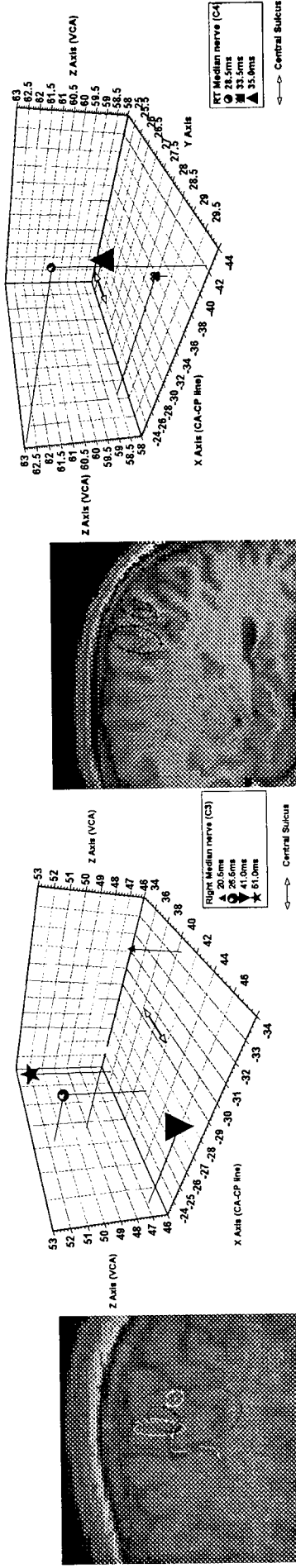
Control subject 2

Figure 3.32 Dipole localisations across a temporal sequence for right median nerve data for control subjects 1 and 2. Latencies of dipole fits are indicated in the graph legends.

The position of the central sulcus in relation to the closest placed confidence volume is indicated by arrows on the x-y axis. The relative size of the confidence volumes at each latency is represented by the size of the data icon in the graph.

Variation in localisation across the temporal window of acquisition (Median nerve)

3.4.7.1. (Continued)



Control subject 3

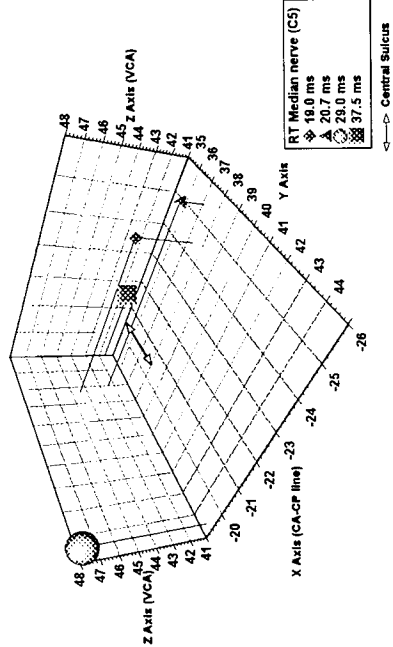
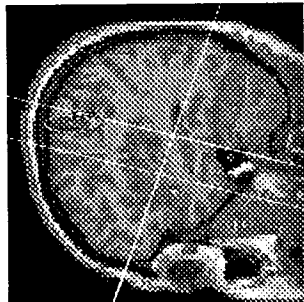
Control subject 4

Figure 3.33 Dipole localisations across a temporal sequence for right median nerve data for control subjects 3 and 4. Latencies of dipole fits are indicated in the graph legends. The position of the central sulcus in relation to the closest placed confidence volume is indicated by arrows on the x-y axis. The relative size of the confidence volumes at each latency is represented by the size of the data icon in the graph.

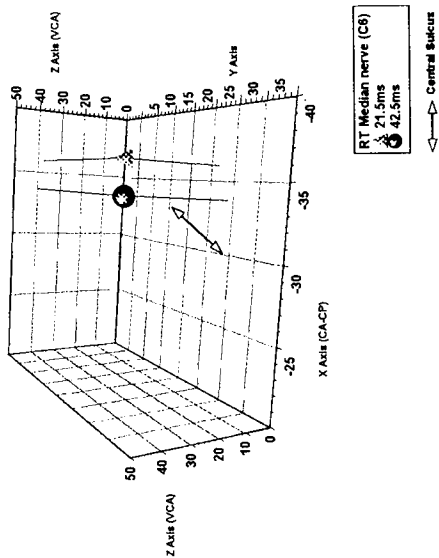
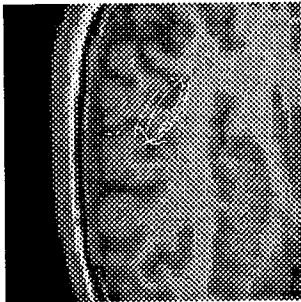


3.4.7.1. (Continued)

Variation in localisation across the temporal window of acquisition (Median nerve)



Control subject 5



Control subject 6

Figure 3.34 Dipole localisations across a temporal sequence for right median nerve data for control subjects 5 and 6. Latencies of dipole fits are indicated in the graph legends. The position of the central sulcus in relation to the closest placed confidence volume is indicated by arrows on the x-y axis. The relative size of the confidence volumes at each latency is represented by the size of the data icon in the graph.

### 3.4.7.1 (Contd) Variation in localisation across the temporal window of acquisition

(Median nerve)

For Right Median nerve data, it was apparent that the mean localisation point of the smallest confidence volumes (centre point of the confidence ellipse) were not always localised nearest to the posterior bank of the central sulcus.

As indicated in section 3.4.4.1., for right median nerve stimulation, five of the six subjects yielded the smallest confidence volumes around the 20 millisecond mark. However, in only one of the six subjects was the mean point of these volumes closest to the posterior bank of the central sulcus when compared with volumes at other latencies. In five subjects, the 33-41 millisecond latency range yielded closest placed volumes as measured from the central mean localisation.

The latencies, distances and volumes of the closest localised confidence ellipses to the central sulcus for right median nerve data are summarised in Table 3-7 below.

#### Right Median Nerve

Subject	Latency of smallest confidence volume	Smallest Confidence Volume (mm <sup>3</sup> )	Chi value/GammaQ	Distance from CS	Latency of closest confidence volume (if not smallest)	Size of Closest Confidence Volume (mm <sup>3</sup> )	Chi value/GammaQ	Distance from CS
Control 1	20.0msec	38.9	14/0.27	+2.0mm	33.0msec	673.0	8.6/0.74	0.0mm
Control 2	19.0msec	597.0	7/0.75	0.0mm				
Control 3	20.5msec	29.3	24/0.01	-4.0mm	41.0msec	4148	4.9/0.9	+1.4mm
Control 4	33.5msec	324.0	12/0.3	-19.0mm	35.0msec	1497.0	8/0.7	-2.0mm
Control 5	20.7msec	92.0	20/0.06	-5.3mm	37.5msec	359	11/0.53	-1.4mm
Control 6	22.5msec	491.7	5/0.94	+2.5mm	33.0msec	3471	5/0.93	+1.0mm

*Table 3-7 Latencies yielding closest position to the central sulcus following Right Median nerve stimulation are indicated and compared with the distance of the smallest confidence volume achieved. Plus or minus signs in the 'Distance from CS' column represents anterior to, or posterior to the posterior bank of the Central Sulcus respectively.*

The group mean distance from the posterior bank of the central sulcus of the closest placed confidence volumes for right median nerve stimulation was **0.97 millimetres** ( $\pm 0.8$  mm). This compared with 5.0 millimetres ( $\pm 6.5$ mm) for the smallest confidence volumes.

The data showed that the 33-41 millisecond components for median nerve stimulation yielded the best fitting dipoles despite poorer signal-to-noise ratio's compared with the earlier components. Chi values of 11 or less with GammaQ values of 0.5 or greater appeared to be a consistent criterion for localisation accuracy of less than 5 millimetres.

To determine whether there were consistent differences in localisation across the temporal window of acquisition, the X (CA-CP axis), Y (Lateral axis) and Z (VCA-VCP axis) Talairach co-ordinates for dipole localisations from the six control subjects were plotted graphically. To enable ease of comparison, the co-ordinates were divided into a series of temporal windows and the data averaged (Figure 3.35).

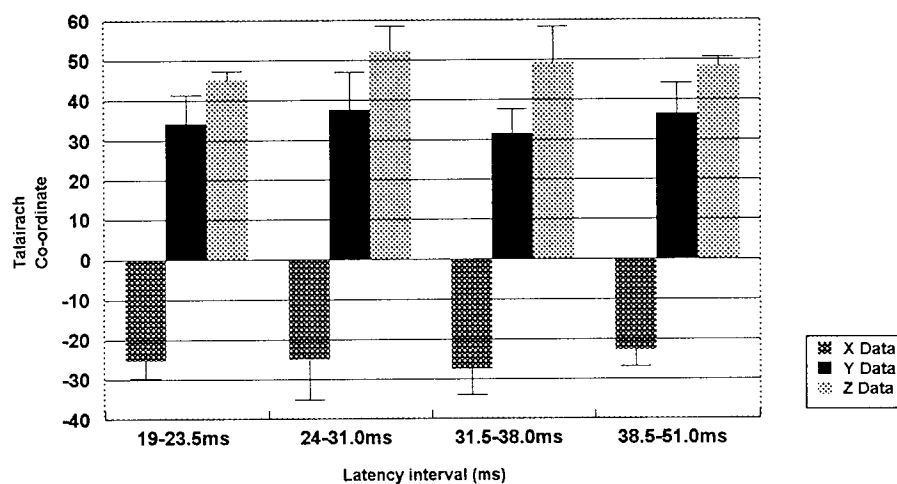


Figure 3.35 Talairach co-ordinates for Right Median nerve data from six control subjects. Co-ordinates within the given temporal window were averaged. The temporal window was centred on consistent peaks of activation seen in all six subjects.

The choice of temporal windows was based on the peaks of activation seen in signal-to-noise ratio plots together with the temporal groupings of dipole localisations seen across the control group.

Using the Student T-Test, each of the four temporal windows within an axis were compared. The probability functions are shown below in Table 3-8.

X Axis data	19-23.5msec	24-31msec	31.5-38.0msec	38.5-51msec
19-23.5msec	x	p=0.92	p=0.57	p=0.27
24-31.0msec	x	x	p=0.65	p=0.65
31.5-38.0msec	x	x	x	p=0.19
Y Axis data	19-23.5msec	24-31msec	31.5-38.0msec	38.5-51msec
19-23.5msec	x	p=0.53	p=0.53	p=0.62
24-31.0msec	x	x	p=0.27	p=0.82
31.5-38.0msec	x	x	x	p=0.28
Z Axis data	19-23.5msec	24-31msec	31.5-38.0msec	38.5-51msec
19-23.5msec	x	p=0.07	p=0.26	<b>p=0.036</b>
24-31.0msec	x	x	p=0.60	p=0.26
31.5-38.0msec	x	x	x	p=0.81

Table 3-8 Student t-test probability comparison of Talairach co-ordinates across four temporal windows of activation for right median nerve data.

As can be seen from the tabulated data for right median nerve stimulation, the only significant difference observed at the 5% level was between the 19-23.5msec window compared with the 38.5-51msec window in the Z (VCA-VCP) axis. Here, the later components were consistently superior in cortical presentation. Individual data for the two intervals were also compared using a paired -t-test and again the data remained significant ( $p < 0.05$ ).

3.4.7.1.1 Cortical sources with temporal overlap

In one control subject (control subject 1), it was evident that there was a marked temporal separation between neighbouring channels of the first peak of activation following Left Median nerve stimulation (Figure 3.36) suggesting multiple source activation.

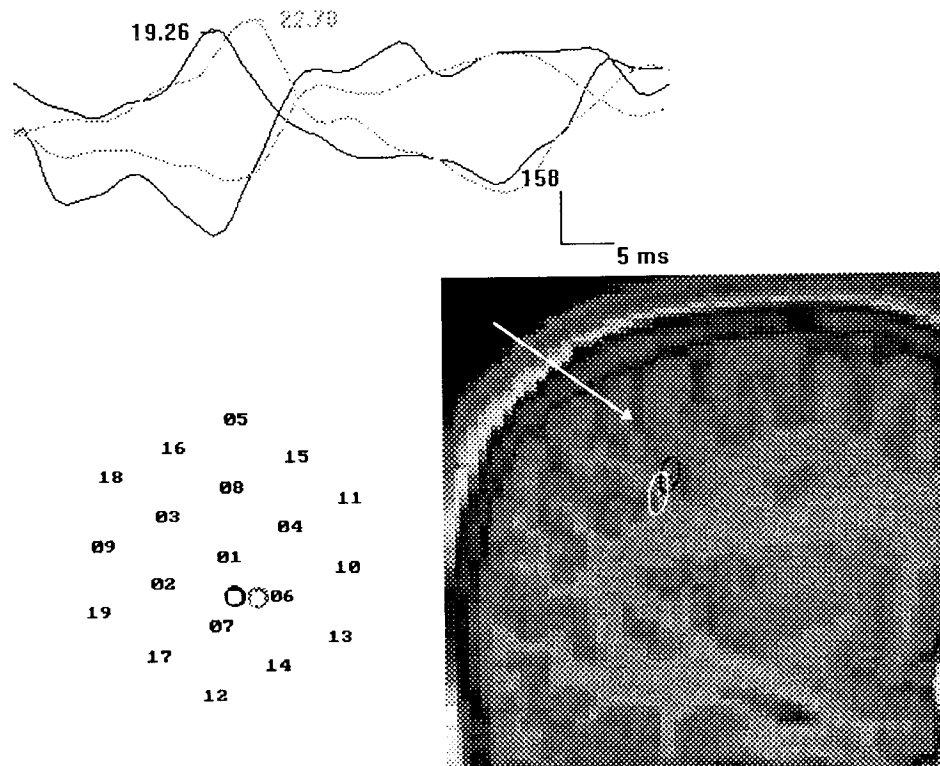


Figure 3.36 Magnetic field waveforms (Top) following left median nerve stimulation in control subject 1. Waveforms from channels 1 and 2 are shown in black and those from channels 7 and 15 are grey. Number array (Lower left) represents the magnetometer array with dipole localisation at 19 milliseconds shown in black and the 22.7 millisecond dipole in grey. The MRI (Lower right) shows the co-registered localisations for the confidence volumes derived by Monte Carlo analysis. The colours correspond to those used in the neighbouring images and the arrow depicts the predicted central sulcus.

Both confidence volumes derived from the two peaks of activation (19.3 msec and 22.7 msec) were located entirely within the postcentral gyrus, and although there was

some spatial separation, the confidence volumes overlapped in part.

A multiple dipole fitting algorithm would be required to ascertain whether there may be separate neural populations generating these dipole fields.

### 3.4.7.2 Temporal localisation for Posterior Tibial nerve data

#### Posterior Tibial Nerve Data (Right or *Left* as indicated)

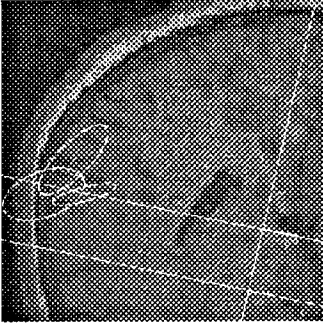
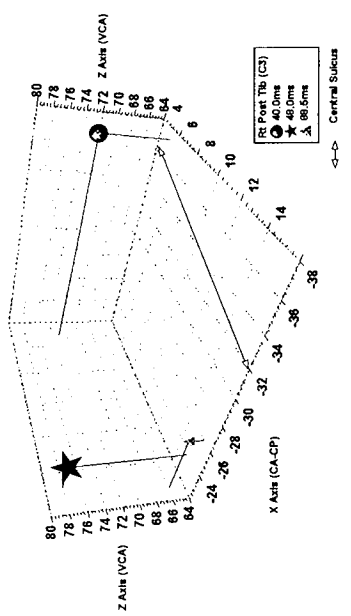
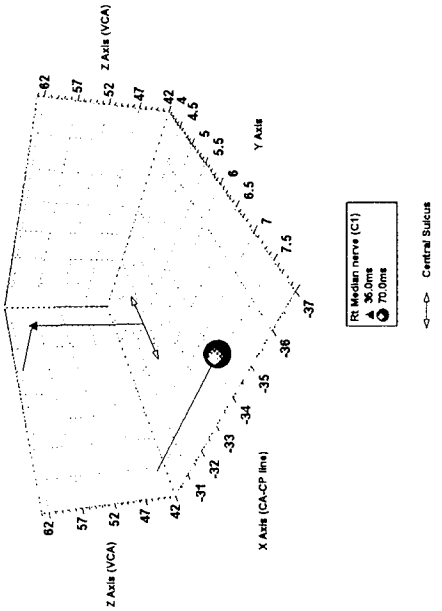
Subject	Latency of smallest confidence volume	Smallest Confidence Volume (mm <sup>3</sup> )	Chi value/ GammaQ	Distance from CS	Latency of closest confidence volume (if not smallest)	Size of Closest Confidence Volume (mm <sup>3</sup> )	Chi value/ GammaQ	Distance from CS
Control 1	<b>35.0msec</b>	<b>1119.0</b>	<b>6 / 0.92</b>	<b>0.0mm</b>				
Control 2	89.2msec	1200.0	5 / 0.9	+4.0mm				
Control 3	<b>88.5msec</b>	<b>1852.0</b>	<b>5 / 0.9</b>	<b>+6.0mm</b>	<b>40.0msec</b>	<b>2997.0</b>	<b>7.5 / 0.7</b>	<b>-1.0mm</b>
Control 4	52.5msec	2619.0	7 / 0.82	-19.0mm	34.5msec	6882.0	4 / 0.96	-17.0mm
Control 5	38.0msec	1558.0	11 / 0.4	+8.0mm	48.5msec	3495.0	4 / 0.97	+6.0mm
Control 6	70.0msec	1700	6 / 0.9	+2.0mm				

*Table 3-9 Latencies yielding closest position to the central sulcus following Right Posterior Tibial nerve stimulation are indicated in bold type and compared with the distance of the smallest confidence volume achieved. Where no applicable data from the Right Posterior Tibial nerve could be used, the Left sided data was substituted. This data is shown in plain italics. Plus or minus signs in the 'Distance from CS' column represents anterior to, or posterior to the posterior bank of the Central Sulcus respectively.*

As with the median nerve data set, smallest confidence volumes were not consistently the closest localisations to the predicted source, namely the posterior bank of the central sulcus. Dipole fits within the latency range of 35-55 milliseconds were consistently localised close to the central sulcus, though there was no consistent spatial separation between components across the window of acquisition (Figures 3.37 & 3.38).

3.4.7.2 (Continued)

Temporal localisations for Posterior Tibial nerve

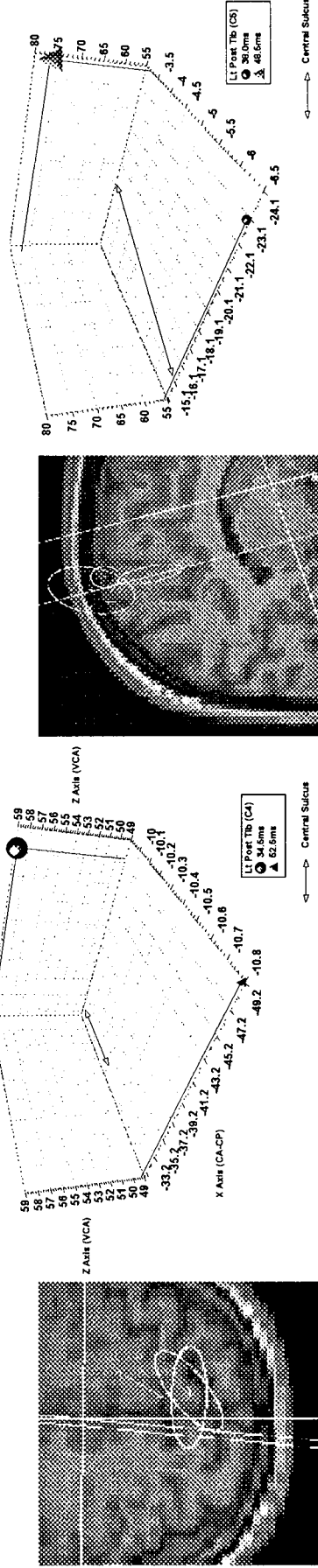


Control Subject 1

Control Subject 3

Figure 3.37 Dipole localisations across a temporal sequence for right posterior tibial nerve data for control subjects 1 and 3. Latencies of dipole fits are indicated in the graph legends. The position of the central sulcus in relation to the closest placed confidence volume is indicated by arrows on the x-y axis. The relative size of the confidence volumes at each latency is represented by the size of the data icon in the graph.

3.4.7.2 (Continued) Temporal localisations for Posterior Tibial nerve



Control Subject 4

Figure 3.38 Dipole localisations across a temporal sequence for left posterior tibial nerve data for control subject 4 and 5. Latencies of dipole fits are indicated in the graph legends. The position of the central sulcus in relation to the closest placed confidence volume is indicated by arrows on the x-y axis. The relative size of the confidence volumes at each latency is represented by the size of the data icon in the graph.



## 3.4.8 Variation in hemisphere localisation (symmetry)

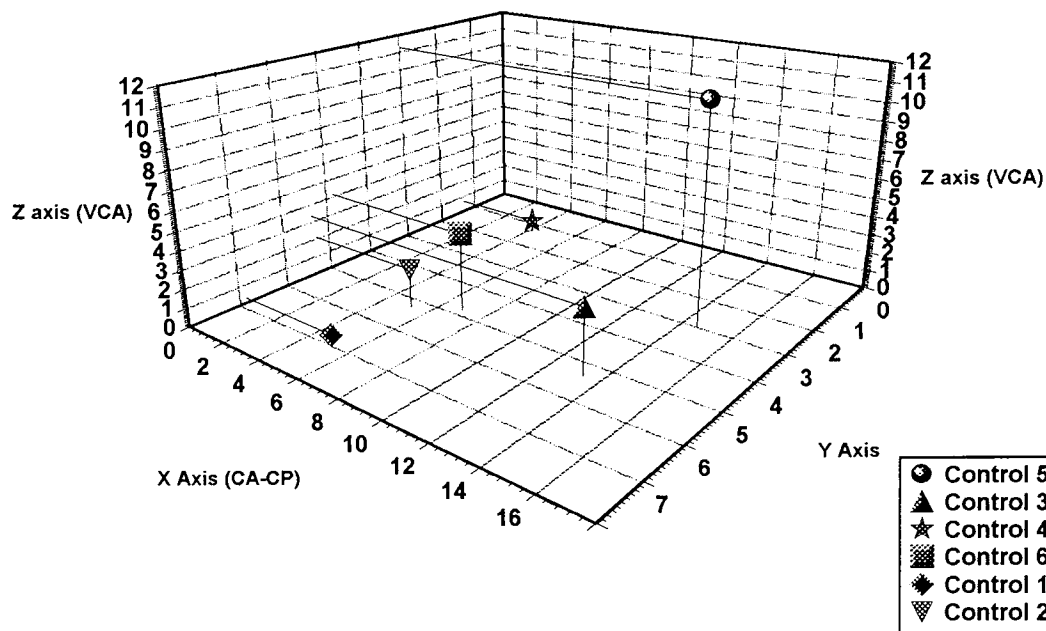


Figure 3.39 Hemisphere asymmetry was estimated by the subtraction of the mean Talairach coordinates of right and left median nerve trials.

Only Median nerve data was examined for the assessment of symmetry of hemisphere localisation because posterior tibial nerve data was localised close to the mid-line making such measurement difficult.

The group mean hemisphere differences were 8.8 mm (+/- 4.9 mm) in the CA-CP axis, 4.3 mm (+/- 2.2 mm) in the Y axis and 4.0 mm (+/- 4.4 mm) in the VCA-VCP axis.

The data included one clear outlier which was the left median nerve localisations from subject 5. Here, the closest fitting dipole was + 16 mm (in the CA-CP plane) from the central sulcus following Left median nerve stimulation.

### 3.4.9 Functional MRI

In each of the three subjects studied, image processing of the fMRI data consisted of simple image subtraction. The 20 images were partitioned into four clusters of five inactive, five active, five inactive and five active images. The active images were then added together and subtracted from the sum of the inactive images. Study of the resultant image was made to observe areas of high pixel image intensity which were used for further examination. In those subsequently selected areas, pixel image intensity was correlated across the activation sequence to observe any consistent and significant change between rest and activation.

In only one subject (subject 4) was a significantly correlated area of high activity observed. In Figure 3.40 (overleaf), an area of high signal intensity in the left sensorimotor cortex was selected from the subtraction image and the corresponding time course plot of signal intensity shown. This clearly demonstrated the correlated cyclic change between the active and inactive states.

A Phase Contrast Venugram was obtained from the corresponding MRI slices to show the juxtaposition of the larger venous drainage vessels in comparison with the high pixel image signals achieved through fMRI. This data is shown in Figure 3.41 and appears to confirm that the fMRI paradigm was highlighting signal changes in smaller capillaries as well as the larger vessels.

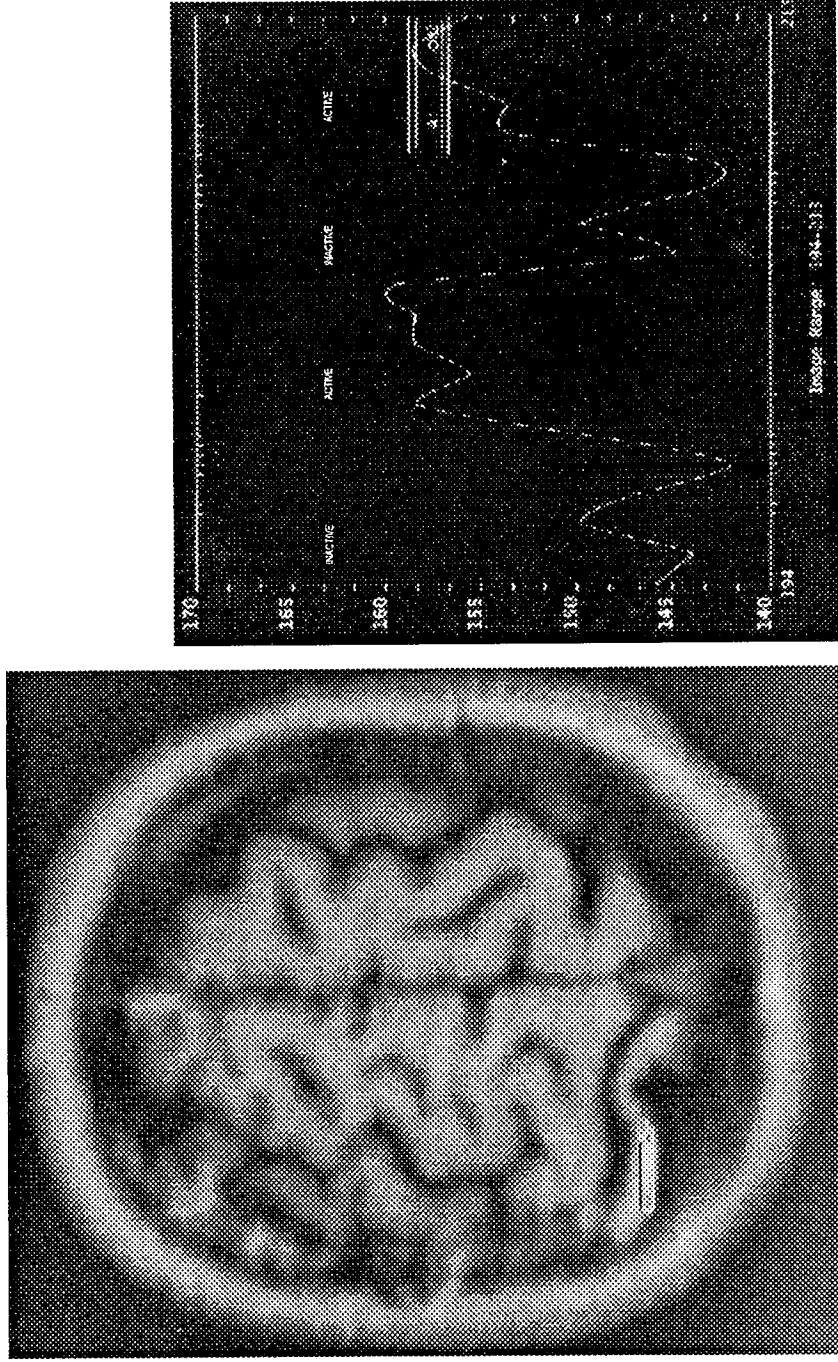
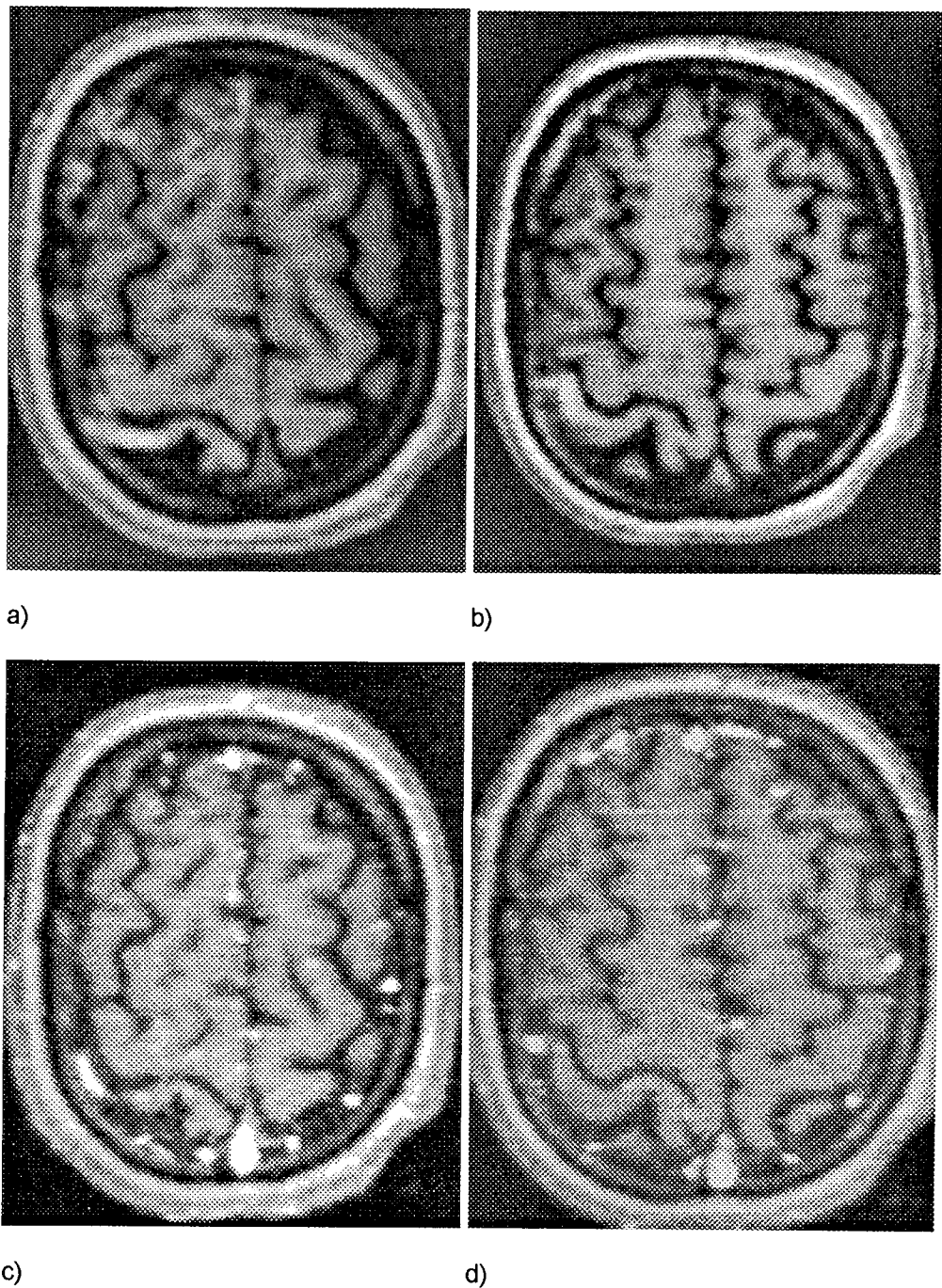


Figure 3.40 fMRI subtraction image showing an area of high image signal over the left post central gyrus. The time course plot of signal intensity calculated from this area is shown on the right .



*Figure 3.41 Plates a) and b) show the final subtraction images from two MRI slice levels with a clear area of high activity seen over the left post central gyrus in each slice. Plates c) and d) show phase contrast venograms from the same two MRI slices which clearly show the presence of a large vein in close proximity to the fMRI activation sites.*

3.4.10 Functional MRI and MEG co-registration.

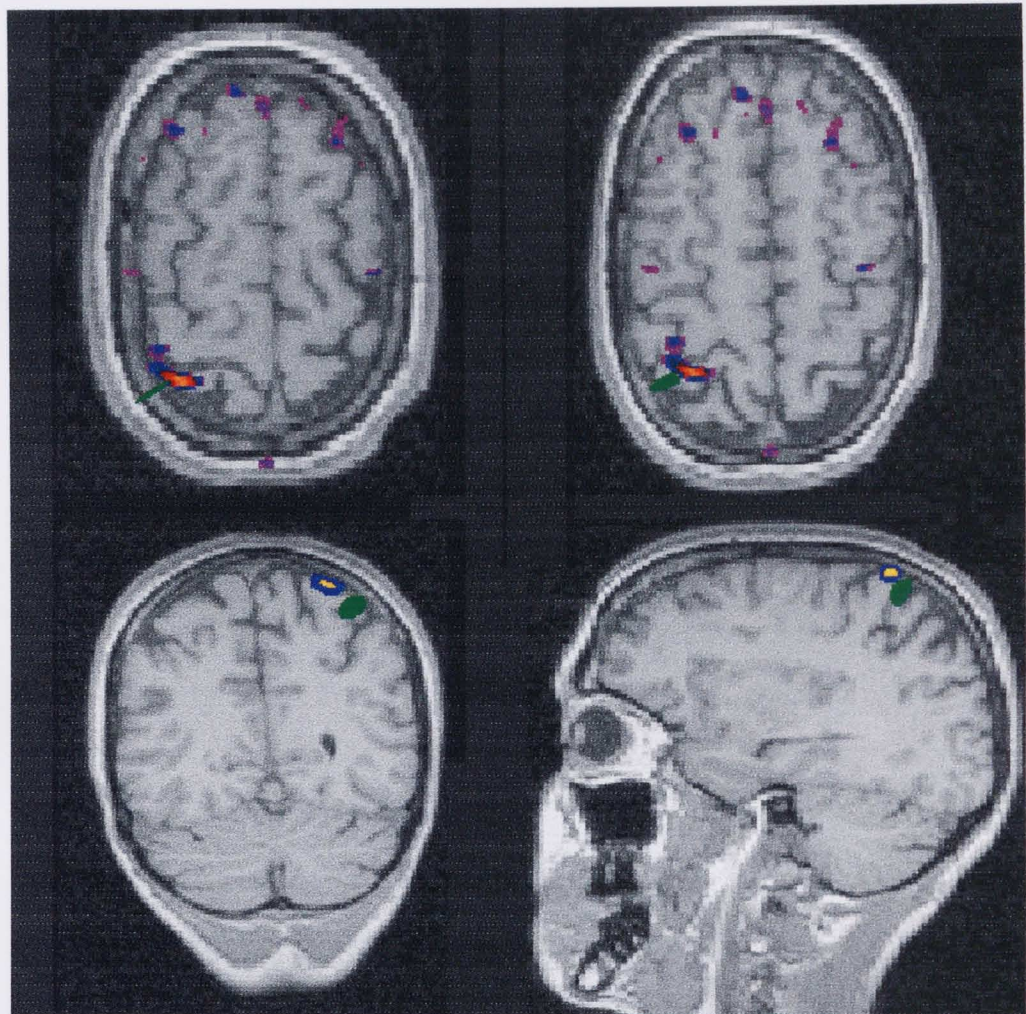


Figure 3.42 Subject 4: Co-registration of fMRI activity (blue/pink) with the smallest MEG confidence volume following right median nerve stimulation (green).

The smallest confidence volume achieved following right median nerve stimulation in subject 4 was co-registered with the fMRI slices. As can be seen in Figures 3.42 and 3.43, MEG and fMRI activations were located closely together in the post-central gyrus in this subject.

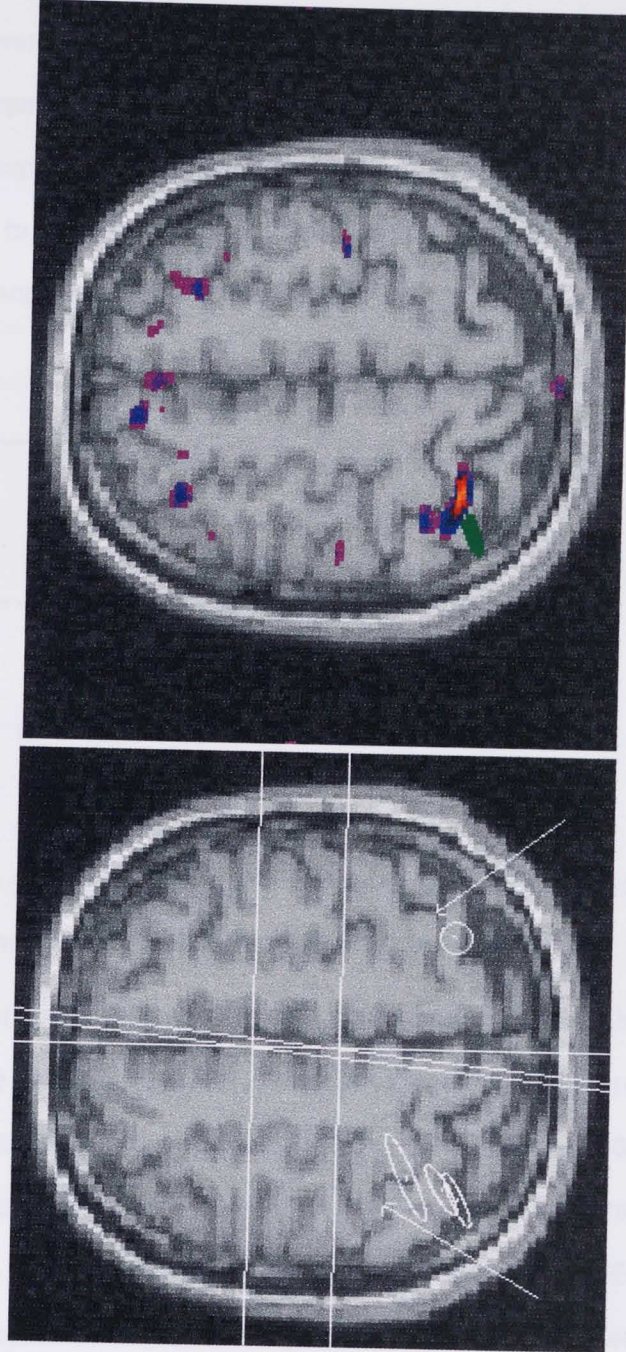


Figure 3.43 Subject 4: Left plate shows confidence volumes achieved from right and left median nerve stimulation with the position of the central sulci indicated by arrows. Right plate shows MEG (green) and fMRI (blue/red) co-registration, both positioned over the post central gyrus.

### 3.5 Summary and Conclusions

#### 3.5.1 Magnetic field waveforms

Consistent with previous studies in this field, the magnetic waveforms produced in this study were easily recognisable in morphology with those of their cortical potential counterparts produced by electrical stimulation of peripheral nerves.

The morphologies described by Giblin as long ago as 1964 (Figure 3.44) adequately suffice to compare with the median nerve magnetic data recorded here with the 'V' shape and 'W' shaped waveforms described.

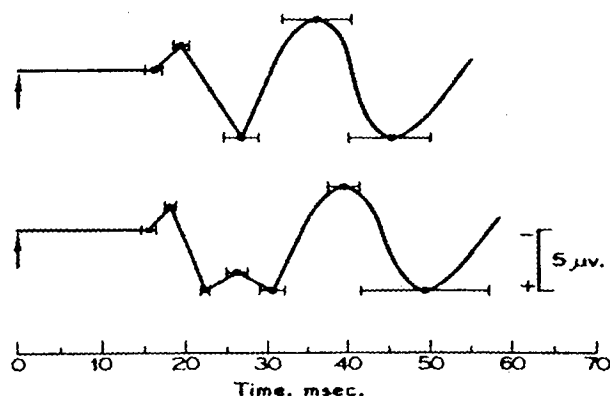


*Figure 3.44 Morphological variations of the postcentral somatosensory evoked potential to median nerve stimulation as described by Giblin (1964).*

The first component measured in all median nerve data in this study corresponds to the N20 potential reported in a large number of evoked potential studies (Allison et al., 1980; Desmedt and Bourguet 1985; Deiber et al., 1986; Wood et al., 1988) and believed to be generated in the posterior bank of the central sulcus, namely Brodmann area 3b. This data was substantiated by a number of MEG studies (Kaufman et al., 1981; Okada et al., 1981;1984; Hari et al., 1984; Wood et al., 1985; Huttenen et al., 1987; Baumgartner et al., 1991c).

The second major component measured is comparable with the previously described 'P27' of Desmedt et al., (1987) or the 'P30' described by Allison et al., (1980), again attributed to Brodmann area 3b.

One important issue which cannot fully be resolved in this study was whether the radially oriented electrical potential known as the 'P22' (Desmedt and Cheron, 1981) or the 'P25 component (Allison et al, 1980), contributes significantly to the MEG signal at this latency.

Sutherling et al., (1988) measured the MEG, Electroencephalogram(EEG) and Electrocorticogram (ECoG) after stimulation of the contralateral median nerve in four patients with partial epilepsy evaluated for surgery. Isopotential fields were plotted for each modality. Each of the three fields appeared to give a different picture of the underlying cortical currents in active somatosensory cortex. MEG was simplest, showing good fits to a single tangential dipole at 20 and 30 msec. EEG detected what the MEG did and in addition detected approximately radial currents at 25msec which required a second dipole fit to the data. However, these authors reported that the MEG appeared more sensitive than previous investigators had expected in detecting in two patients the tangential part of a current source that was predominantly radially oriented.

Baumgartner et al., (1991c) reported that 2 sources were required to adequately model the first 40msec of magnetic field data following median nerve stimulation. The first source was located deeper than the second source and was oriented primarily in the antero-posterior direction, explained a larger amount of variance than the second source, and showed a biphasic time activity with peak latencies of 19 and 29msec. These findings were compatible with a tangential dipole in the posterior bank of the central sulcus generating the N20m-P30m component (m denoting the magnetic field counterpart of the evoked potential component).

The second source was located more superficially, showed no consistent orientation across subjects, explained a smaller amount of variance than the first source, and



also showed a biphasic time activity with peak latencies of 22 and 32 msec. These results were compatible with a radial source generating the P25m-N35m component. Purely radial sources should not generate a recordable magnetic field. However, Tiihonen et al., (1989) reported that slightly tangential components can generate measurable magnetic fields with low-noise recording systems. Data in this thesis recorded from subject 1 strongly suggested a second active source peaking at 22-23 msec, but a single equivalent dipole model was unlikely to adequately represent the spatial separation of the two sources.

Posterior Tibial nerve data was generally of much smaller amplitude than median nerve data and less robust in acquisition and repeatability. The morphology of the components were clearly recognisable and comparable with the evoked potential counterparts. Components at 40 and 75 milliseconds were consistently the most robust both in terms of field strength and dipolar field patterns.

### 3.5.2 Dipole fitting

An important result from the study was to determine optimum protocols for data acquisition and analysis.

Most authors cite the correlation co-efficient in isolation as the essential value for adequate matching of their computed magnetic field with the measured field. The dipole with the highest correlation co-efficient is then co-registered with the MRI. However, the resultant dipole fit gives the independent interpreter no sense of the reliability of the localisation in terms of the area of cortex that may have equally well generated the measured field given the signal to noise values of the data.

Our strategy has been to employ Monte Carlo analysis to the data to provide confidence volumes for localisations based on the signal to noise measures within the data. MRI localisation values were therefore calculated from the mean point of 50 iterations across the noise spectrum.

To this end, a range of statistics were examined in the selection of dipole confidence volumes that were co-registered with the MRI. It was concluded that dipole fitting criterion should meet the following values to ensure reliable localisation;

Signal-to-noise ratio of 1.8:1 or greater; Correlation co-efficient of 0.96 or greater; Chi value of 11 or less; Gamma Q of 0.5 or greater; confidence volume of 6000 mm<sup>3</sup> or less.

### 3.5.3 Repeatability of localisations

One of the few studies to explore issues of trial - re-trial variability was performed by Gallen et al., in 1994. They performed two experiments: In the first, the spatial distribution of dipoles recorded sequentially within a single dewar position were examined and in the second, sequential measures with new dewar positions as well as fiducial points for each trail were assessed. All measures were made in a single individual using a pneumatic piston type of somatosensory stimulus. These authors found that within a single probe placement, the test-retest repeatability gave a standard deviation of 6.7mm. With the experiment set out afresh for each measure, the standard deviation rose to 1.02cm.

Data in this thesis was best compared with the independent measure data of Gallen et al, since two of the three trials were acquired with a single dewar position, but then repeated with the system re-positioned. For median nerve stimulation obtained from six control subjects, the mean variation in localisations were 7.5mm (s.d.4.8mm) in the CA-CP plane (x axis), 7.2mm (s.d. 3.9mm) in the lateral or y-axis, and 5.8mm (s.d.4.0mm) in the VCA-VCP plane of the Talairach co-ordinate system (z-axis).

However, as observed by Gallen et al, much of the spread of localisations were along the wall of the central sulcus and not spread uniformly around the mean. This measure was determined in this thesis by the relative positions of the central mean localisations of confidence ellipses. Importantly, many of the confidence ellipses

themselves were orthogonal rather than perpendicular to the central sulcus and lay predominantly within the post-central gyrus.

### 3.5.4 Localisation accuracy

To assess localisation accuracy of dipole fits, the distance of both the smallest confidence volumes obtained in a sequence of acquisitions as well as the distance of the closest placed dipoles to the central sulcus was made.

For median nerve data, the mean distance to the centre of the smallest confidence volumes from the central sulcus in the CA-CP plane (X axis) was 5.5 millimetres (+/- 5.5mm). For posterior tibial nerve data, the mean distance was 6.25 millimetres (+/- 4.8 mm).

Analysis of dipole localisation across the temporal sequence of activation showed that the 33-41 millisecond components for median nerve stimulation yielded the best fitting dipoles despite poorer signal-to-noise ratio's compared with the earlier components.

The mean distance from the posterior bank of the central sulcus of the closest placed confidence volumes for right median nerve stimulation was 0.97 millimetres ( +/- 0.8 mm).

This data can be compared with a recent study on some 274 cerebral hemispheres using a whole of head MEG system (Nakasato et al., 1996) where the dipole deviation from the central sulcus for median nerve stimulation was 2.3 mm (s.d. 2.6 mm) and for posterior tibial nerve data in 218 cerebral hemispheres, 3.5 mm (s.d. 4.1 mm).

### 3.5.5 Temporal sequence of activation

Analysis of temporal windows of activation showed a trend for a more lateral and superior localisation for median nerve activation across the acquisition epoch. However, data only reached statistical significance ( $p < 0.05$ ) in the VCA-VCP axis of Talairach co-ordinate space between the 19-23.5msec and 38.5-51msec intervals.

These measurements were made with respect to the mean localisations at the centre of Monte Carlo analysis generated confidence volumes, and for the majority of

temporal localisations, there was a considerable overlap of these confidence intervals. It was concluded therefore that components generated within the first 40 msec at least, following median nerve activation, were predominantly generated by a common neuronal population located in the posterior bank of the central sulcus.

The data of Gallen et al., (1994) recorded in a single individual, suggested a slight movement of estimated sources anteriorly and laterally across a 150msec acquisition epoch, but concluded that they were all dipoles were generated by a common source.

In contrast, Kawamura et al., (1996) postulated that while the N20m component was generated in the posterior bank of the central sulcus, a second peak, with a mean peak latency  $7.7 \pm 3.2$  msec after the N20m, was localised 3.7mm medial and 2.0mm superior, placing it in the anterior wall of the central sulcus in Brodmann area 4. This was a statistical measure achieved from 184 hemisphere recordings.

These authors however were applying single equivalent dipole models and made no allowance for the possibility of multiple source interaction for the second component nor calculated confidence regions for the dipole sources.

It may be essential to analyse the temporal window of acquisition with a multiple dipole fitting solution to establish further the possibility of discrete multiple sources of activation.

### **3.5.6 Comparison with stereotaxic atlas**

The application of the 'Co-Planar Stereotaxic Atlas of the Human Brain' of Talairach and Tournoux (1988) served two functions. The first was to provide a three dimensional co-ordinate system that could be readily applied. This would enable easy

definition of localisation, comparison between localisations as well as some comparison between individuals and the collection of group mean data.

The second was to enable a prediction of the location of the central sulcus by use of anatomical landmarks (Rademacher et al., 1993) and with reference to the co-ordinates of the Atlas and the sample brain.

The space between the two perpendicular lines erected through the anterior and posterior commissures have been divided into three zones within the Atlas and have been shown to be able to consistently define the central sulcus (Figure 3.45)

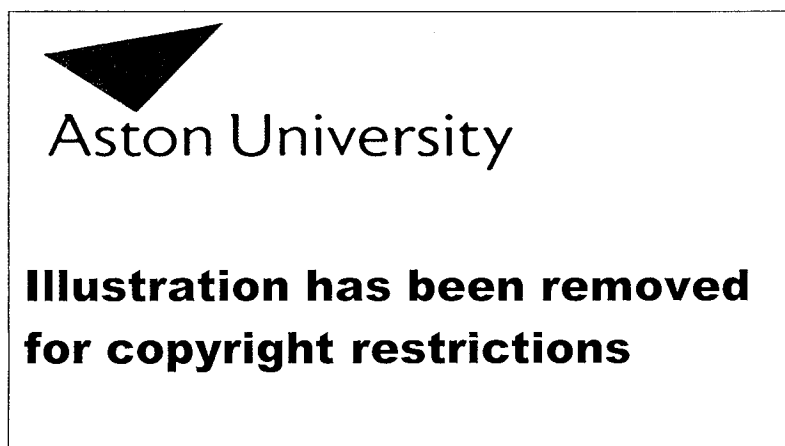


Figure 3.45 Figure from Talairach and Tournoux (1988) showing the location of the Rolandic fissure from 20 brains stereotactically localised using the normalised proportional grid.

Rademacher et al., (1993), in their histological sectioning study of 20 human cerebral hemispheres, makes reference to the limitations of the Talairach co-ordinate system in accomodating Class 1 and Class 2 variabilities of primary cytoarchitectonic neocortical fields. These variabilities were defined as follows:

Class 1 variability - variability that is not predictable from visible landmarks. This type of variability could be applied to the distribution of Brodmann area 4 upon the paracentral lobule.

Class 2 variability - variability that is closely predictable from visible landmarks. This was seen in the marked interindividual or interhemispheric variation in size or shape of a field and was prominent in all fields measured.

These authors recommended the use of the landmarks that framed these fields as providing a more reliable basis for functional mapping reference than a system such as the Talairach Atlas. However, the anatomical boundaries that were defined by Rademacher were necessarily broad. For example, for the motor cortex, the boundaries were the paracentral lobule anteriorly to the end of the corpus callosum posteriorly. Whilst this data provided essential reference landmarks, there was also a need for a proportional millimetric reference scale.

It was clear that a combination of anatomical landmarks together with the normalised grid determined by the Talairach co-ordinate system could be combined to enable a reliable prediction of the line of the central sulcus.

Two difficulties experienced in the application of the Talairach system were; 1) clear identification of the anterior and posterior commissures and 2) MRI images acquired with head placed at a skewed angle to the direction of slice.

The first problem was either as a result of an artefactually distorted MRI acquisition volume or if both commissures were not visible within a single mid-line slice. This relates to the second issue in that as there was not the capability to re-orient the slice angle, if the MRI slices were not on an orthogonal plane to the base lines of the Talairach Atlas co-ordinate system, then direct comparison with Atlas landmarks was difficult.

Despite these difficulties, co-registration with the Talairach Atlas system did provide a most useful reference framework for inter-subject comparison as well as providing confidence boundaries to the likely location of the sensory-motor cortex.

### 3.5.7 Interhemispheric symmetry

There was clear symmetry of localisation of median nerve data across the control subjects which allowed adequate representation of both hemispheric dipoles in a single axial slice in all but one subject (C2). Even allowing for clear asymmetry of function due probably to poor localisation of left median nerve data in subject C5 (left median +15mm to central sulcus compared with right median -5.0mm), the group mean hemisphere differences were only 8.8 mm (+/- 4.9 mm) in the CA-CP axis, 4.3 mm (+/- 2.2 mm) in the Y axis and 4.0 mm (+/- 4.4 mm) in the VCA-VCP axis. In subjects 4,5, and 6, the localisations can be seen to near a distinctive twist in the line of the central sulcus (Figure 3.46). This 'sigmoidal' shape in the upper central sulcus has previously been described as a possible useful landmark of the hand area for clinical correlation (Rumeau et al., 1994).



*Figure 3.46 The sigmoidal shape of the upper portion of the central sulcus in control subject 6 was localised as the hand area from MEG measurements.*

### 3.5.8 Somatotopic organisation of the cortex

Since the classic experiments of Penfield et al., (1937;1950;1954) using direct cortical stimulation, a number of alternative approaches have been applied using both

invasive and non-invasive techniques to study the somatotopic organisation of the cortex.

Recent studies have included the use of somatosensory evoked potential dipole localisation from electrodes placed directly onto the cortical surface. Sutherling et al., (1992) described digit somatotopy together with nerve trunk localisation and observed that median and ulnar nerve stimulation produced better dipole fits than did digital stimulation. Consistent with previous findings these authors reported that median nerve localisations were always nearer the Sylvian fissure than those of the ulnar nerve. This was in agreement with a similar study by Baumgartner et al., (1992) who examined the topography of human hand and lip representation recorded from chronically indwelling subdural grid electrodes.

In a series of experiments, Baumgartner et al., reported the findings on the somatotopy of the human hand studied by scalp EEG and MEG combined (1991a), MEG (1991b) and scalp EEG and ECoG (1993). Their findings showed that the ulnar nerve localisations were always more medial and superior than those for median nerve. The mean distance between the two localisations were 13.2mm for MEG (range 7-19mm) and 10.8mm for scalp EEG (range 7-18mm).

Other MEG studies (Narici et al., 1991, Yang et al., 1993) have further supported the view that MEG can be used to examine in detail the somatotopic organisation of the cortex non-invasively and accurately.

Data in this thesis was consistent with previous findings with regard to the relative mean positions of median, ulnar and posterior tibial representation on the cortex.

Posterior tibial nerve data was always most superiorly placed and close to the midline. For the ulnar nerve, five of the six subjects showed localisations which were superior to the median nerve with a mean distance of 7.1mm (+/- 3.3mm) in the VCA-VCP axis and four of the six with the ulnar nerve more medially placed (mean distance 4.6 mm,



+/- 4.1 mm). 95% confidence volumes for the two nerve trunks frequently overlapped because of the smaller signal-to noise values of the ulnar data.

Once again caution would be urged to other workers in this field when declaring that sources may be spatially separated, that due attention must be made to the inherent noise within the system and duly reflected within the source predictions.

### **3.5.9 Ability to reliably identify the central sulcus**

For clinical studies, the important criterion for dipole localisations would be the ability to accurately determine the sensory-motor cortex when normal anatomical landmarks are unclear and / or when the cortex is displaced or distorted to some degree by pathology.

Whilst the absolute spatial resolution of the technique appeared to be in the order of 1-2 millimetres, the trial -re-trial variability provided an important measure of the possibility of false identification of the generator source.

Success of the technique can only be judged by the ability to accurately locate the posterior bank of the central sulcus from which the majority of the measured signal was known to arise.

From data in this study, given that the post-central gyral width is some 1-1.5cm, the localisation of the smallest volume on its own was adequate to localise the post-central gyrus in 5 of the six subjects following right median nerve stimulation and in four of the six following left median nerve stimulation. The overlap of several trials of Monte Carlo confidence volumes was an important measure of the reliability of the source localisations

Examination of multiple nerve site dipole localisations further improved the confidence of localisations.

### 3.5.10 MEG-fMRI co-registration

In this study, in only one of three control subjects could fMRI data be confidently co-registered with the anatomical MRI because of low or non-correlated signal changes through the activation sequence in two subjects.

This data was less consistent than that reported by Connelly et al., (1993), who employed the same acquisition method also using un-modified clinical MRI equipment. These authors studied 14 control individuals and observed up to 15% signal intensity changes in gray matter following a finger-thumb opposition paradigm. Activation was commonly seen in both the pre and post central gyri.

It is interesting to note that data in our study which employed the same 'motor task' as described by Connelly et al., highlighted activation over the gyral surface of the sensory cortex. Clearly, the finger movement exercise will evoke both sensory and motor activation and one would not expect specific pre-or post central activation.

In a study by Stippich et al., (1996) in comparing somatosensory stimuli of the right index finger using both MEG and fMRI measurements in four control subjects (a pneumatically driven stimulator was used), they observed a mean MEG - fMRI separation of activation of  $15.5 \pm 6.5$ mm in four control subjects. Authors attributed this relatively large separation to the different neurophysiological effects measured by MEG (neural activation) and fMRI (BOLD effect).

In this thesis, in the one control subject in which significant pixel image intensity changes were observed, fMRI correlated closely with the MEG localisations with the centres of activation being separated by only 5mm. Both localisations were overlying the post-central gyrus.

Failure to measure correlated fMRI activity in two control subjects may possibly be due to inappropriate selection of slice angle since all measurements were made in the same plane as the high resolution volume acquisition. Connelly et al., (1993) observed that choice of imaging plane, voxel size and TE strongly influences the percentage increase in signal intensity that is observed. Other factors may include the appropriate thresholding of pixel intensity; very small signal changes might well be lost in noise.

As discussed in Chapter 2, registration of correlated movement artefact may also increase noise levels beyond an acceptable margin, a factor we were unable to control for in this study.

Clearly though, with modified and more sophisticated acquisition techniques, the combination of fMRI together with MEG would provide a potent tool for the non-invasive study of the location and functional organisation of the sensory-motor cortex.

## 4. Voluntary movement related evoked fields

### 4.1 Introduction

From animal studies it is well known that the primary sensory cortex receives afferent inputs to specialised areas. Brodmann areas 1 and 3b mainly respond to cutaneous tactile stimulation (Powell and Mountcastle 1959; Kaas et al. 1981) while it appears that areas 2 and 3a receive projections from proprioceptive fibres (Powell and Mountcastle 1959; Phillips et al 1971; Jones and Porter 1980; Kaas et al 1981). This area of work is detailed more extensively in Chapter 1.

In humans, MEG recordings of somatosensory evoked fields from median nerve digital branch stimulation have shown that the short latency somatosensory components are dominated by cutaneous inputs generating an equivalent dipole in the post-central gyrus, suggesting activation of Brodmann area 3b (Okada et al 1984; Hari et al. 1984; Narici et al. 1991; Baumgartner et al. 1991b).

MEG studies investigating cortical sources related to voluntary movement have described a 'readiness field' starting some 500 ms before movement onset (Deecke et al. 1982) with a larger, so called 'motor field', peaking about 100 ms after movement onset (Cheyne and Weinberg 1989). It has been proposed by some authors that the motor field (MF) reflects a sensory input from the moving body part (Cheyne and Weinberg 1989; Kristeva et al. 1991) and that the cortical source underlying MF should be located in the subdivision of SI, mainly area 3a, (Kristeva-Feige et al. 1996) known to receive predominant input from muscle receptors activated during movement (Jones and Porter 1980; Arezzo and Vaughan 1981).

Other authors have attributed the underlying source of the motor field equivalent to MF as lying precentrally in motor cortex (MI) (Chiarenza et al. 1991; Kassubek et al. 1996), either reflecting an 'efferent copy' of the motor cortex to the sensorimotor

cortex or a refferent input from the proprioceptors and muscle afferents to motor cortex (Chiarenza et al. 1991).

### 4.2 Aims

To investigate the source localisation of cortical evoked magnetic fields following self paced flexion of the index finger in human control volunteers and to compare these localisations with those obtained from stimulation of the median nerve at the wrist

### 4.3 Method

A software tool was developed in our lab to enable the constant acquisition of 19 MEG channels together with a marker channel. The incoming analogue signals were continuously and seamlessly buffered from the ADC (Analogue - Digital Conversion device) to be permanently stored onto a hard disk storage medium. Data was sampled at a rate of 500 Hz with bandpass filters of DC-106Hz. The baseline of the waveforms was computed from a section of the interstimulus interval values.

Finger movements were registered by a microswitch mounted on a plastic box which could be comfortably accommodated within the palm of the hand allowing the index finger to be rested on a small plunger. A finger flexion of 5 millimetres was required to depress the plunger and activate the microswitch; this in turn provided a 5 volt TTL pulse to the ADC.

The software tool was programmed to detect the rising edge of the trigger pulse created by activation of the microswitch and a 1 second epoch centred on this rising edge was 'back-averaged' to create an evoked response. Thus, the epoch revealed 500 milliseconds before and 500 milliseconds following the depression of the switch.

Subjects were seated beneath the magnetometer and positioned onto their personalised bite bar as detailed previously (Chapters 2 and 3). The trigger box was

located in the palm of the hand with the arm and lower trunk fully supported by a vacuum cushion, thus preventing finger flexion being translated into body or head movement.

The subject was requested to depress and release the plunger on the trigger box at a rate of about 1 per second in a smooth manner, never releasing the finger completely from the plunger. This ensured that finger flexion excursions were always in the order of 5 millimetres.

Data was acquired until a total of 200 flexions had been performed. The position of the head with respect to the magnetometer was determined after each run by use of the Polhemus 3D space tracker device as described in previous Chapters. The experiment was repeated until three separate trials of both right and left index finger flexion had been acquired.

A dipole fitting sequence was performed across the entire acquisition epoch for each run. Where dipole correlations coefficients were greater than 0.95, and the signal to noise ratio exceeded 2, then further Monte Carlo analysis was performed to assess 95% confidence volumes. Confidence volumes of less than 2 cm<sup>3</sup> were coregistered with the subjects MRI and compared with the previous localisations achieved through median nerve stimulation at the wrist.

## 4.4 Results

## 4.4.1 Waveform morphology

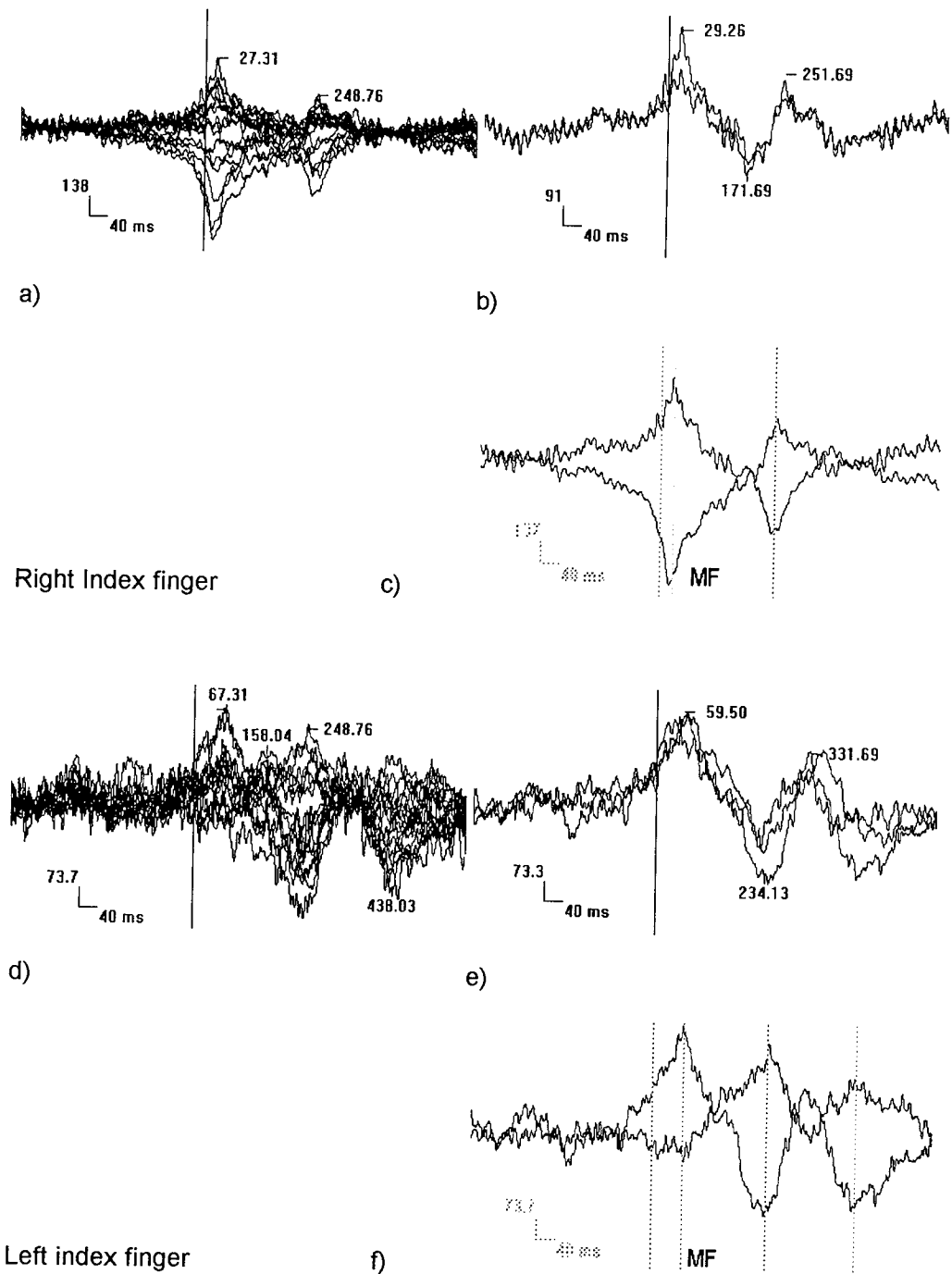


Figure 4.1 Control subject 1. Magnetic field waveforms following right index finger (a-c) and left index finger (d-f) flexions. 19 channels of a single trial are shown superimposed in waveforms a) and d) with waveforms following separate trials superimposed for comparison (b and e). Bold vertical line indicates moment of switch contact by button depression. Waveforms c and f show channels and latencies of maximum dipolar field strength.

Control subject 2

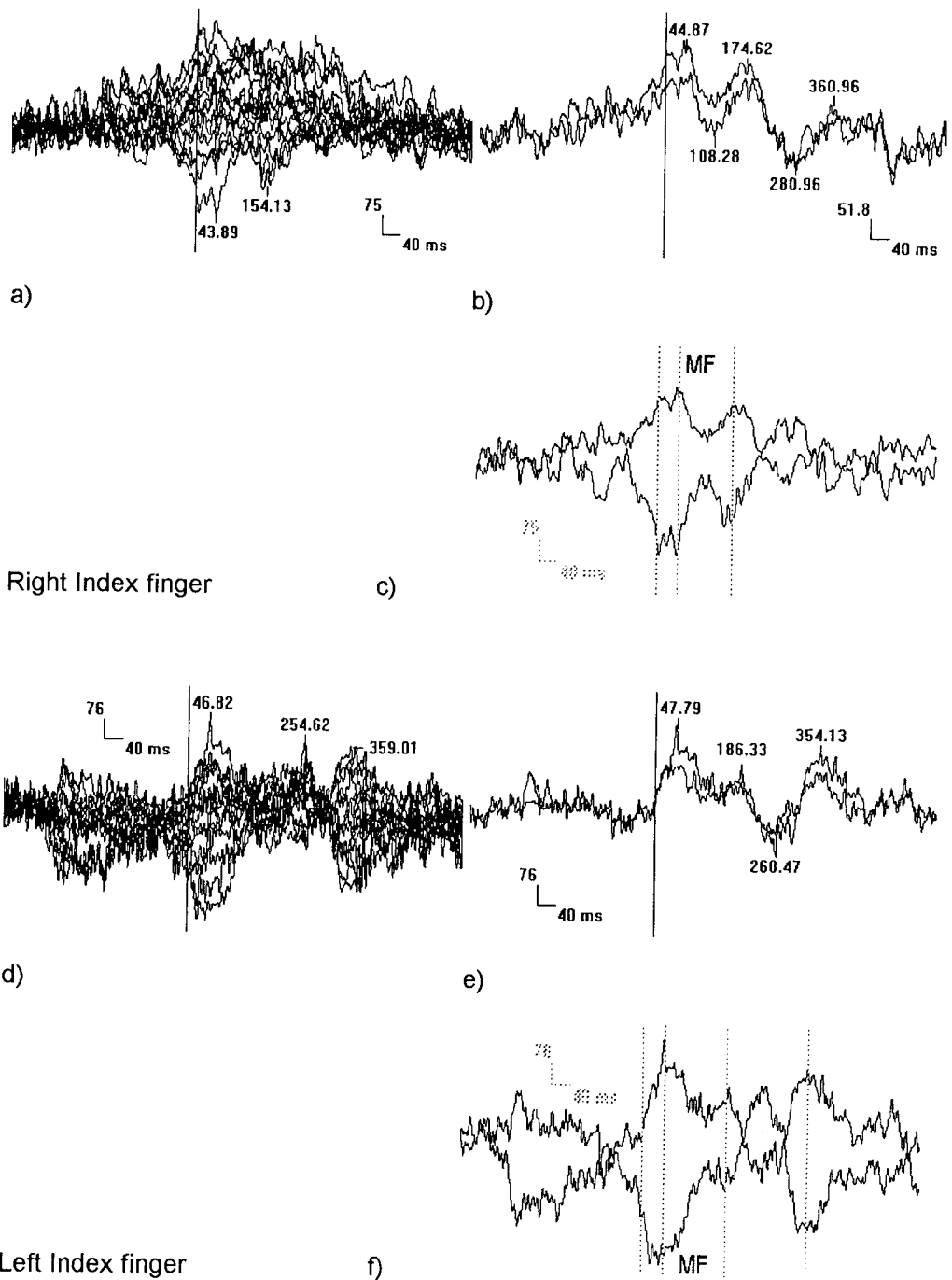


Figure 4.2 Control subject 2. Magnetic field waveforms following right index finger (a-c) and left index finger (d-f) flexions. 19 channels of a single trial are shown superimposed in waveforms a) and d) with waveforms following separate trials superimposed for comparison (b and e). Waveforms c and f show channels and latencies of maximum dipolar field strength.



## Control subject 6

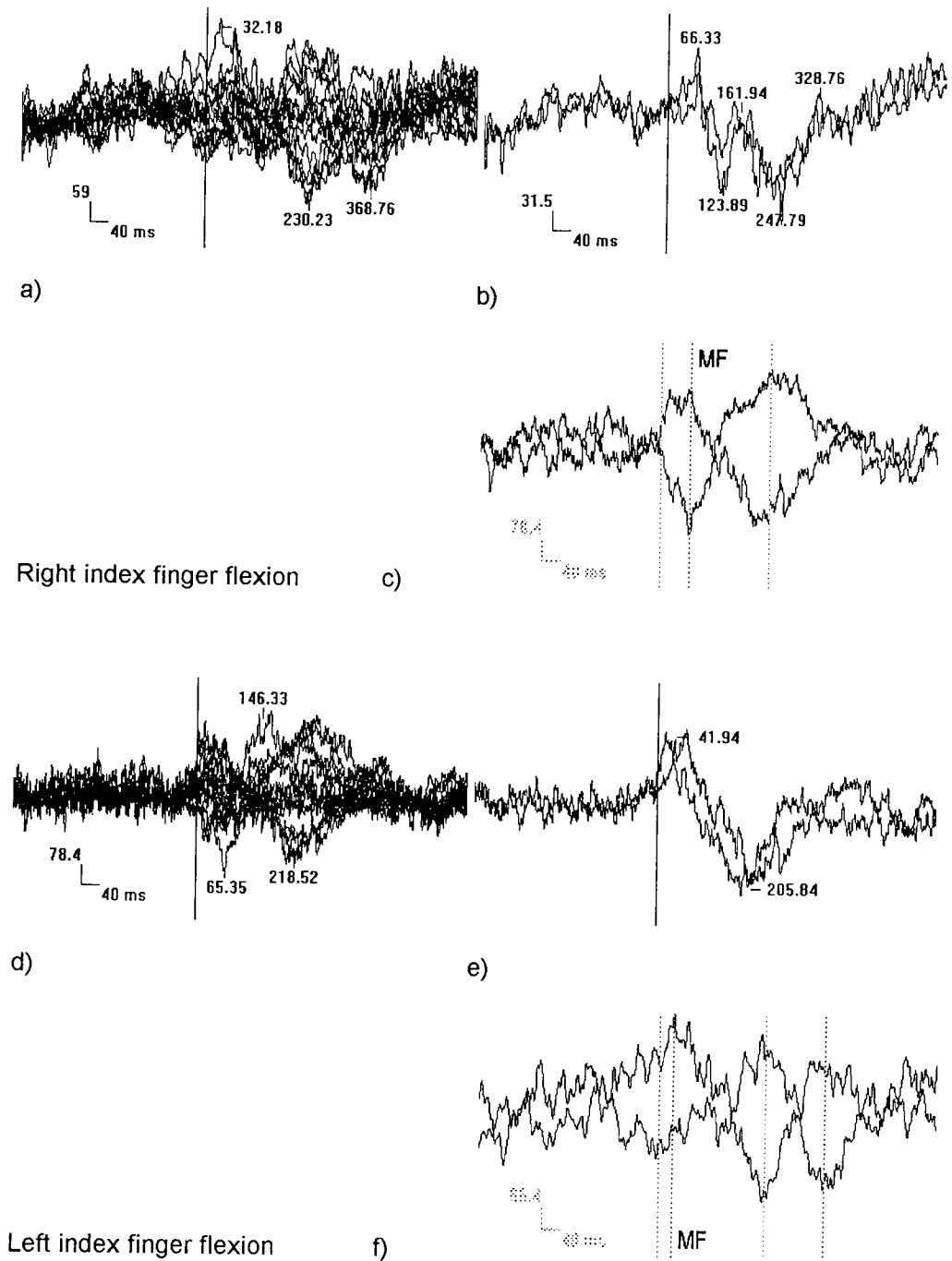


Figure 4.3 Control subject 6. Magnetic field waveforms following right index finger (a-c) and left index finger (d-f) flexions. 19 channels of a single trial are shown superimposed in waveforms a) and d) with waveforms following separate trials superimposed for comparison (b and e). Waveforms c and f show channels and latencies of maximum dipolar field strength.

**Table 4-1** Latencies of components measured from right and left index finger flexion.

Latencies in bold type produced strong dipolar field patterns.

<b>Right Index Finger</b>					
Subject	MF Latency	Wave I	Wave II	Wave III	Wave IV
1	<b>29.3</b>		<i>171.7</i>	<b>251.7</b>	
2	<b>44.8</b>	<i>108.3</i>	<b>174.6</b>	<b>281.0</b>	
6	<b>66.3</b>	<i>123.9</i>	<b>161.9</b>	<b>247.8</b>	<i>329.0</i>
Mean	46.8	116.1	169.4	260.2	
SD	15.2	7.8	5.4	14.8	
<b>Left Index Finger</b>					
Subject	MF Latency	Wave I	Wave II	Wave III	Wave IV
1	<b>59.5</b>	<i>158.0</i>	<b>234.1</b>	<i>331.7</i>	<b>438.0</b>
2	<b>47.8</b>	<i>120.3</i>	<b>186.3</b>	<b>260.4</b>	<b>354.1</b>
6	<b>41.9</b>	<i>146.3</i>	<b>250.0</b>	<b>340.0</b>	
Mean	49.7	141.5	223.5	310.7	396.1
SD	7.3	15.8	27.1	35.7	41.9
Group Mean	48.3	131.4	196.4	285.4	365.3
Group SD	12.0	14.2	33.3	37.2	42.9

In each subject, the first waveform to be generated began to be formed some 50 milliseconds prior to the button depression (time zero) and peaked 30-60 milliseconds afterwards (group mean latency 48.3 ms +/- 12.0 ms). This component was termed the MF component using the nomenclature adopted by previous authors. At latencies concomitant with the peak of the MF component, a strong dipolar field pattern was seen in each subject (Figure 4.4) and was always the strongest field generated throughout the measured epoch. The **group mean amplitude** of this component was 435fT (+/- 153.2). However, this figure included one measure from subject 1 from the right index finger which was at least double the amplitude of any other measure made, including the same subject from the left finger. Excluding this one measure, the group mean amplitude for component MF was 369 fT (+/- 47fT). The MF component was the most consistent component in terms of latency and amplitude of any measured across the subject group.

In subjects 1 and 6, a wave of opposite polarity was observed between 109-124 milliseconds following right index finger flexion, and in all three subjects following left finger flexion (range 120-158 ms); this was termed wave I. However, in none of the

subjects did wave I yield a dipolar field pattern of sufficient strength to enable source localisation modelling.

Three further components were measured (labelled II-IV and detailed in Table 3-1) and in at least two of the three subjects, strong dipolar fields were measured at each of their respective peak latencies (see Figure 4.4).

### 4.4.2 Dipole fitting

Dipole modelling techniques were applied to each trial of index finger movement recordings. From the experience obtained from somatosensory evoked measurements described in Chapter 3, dipole fitting was restricted to data points where the signal to noise ratios exceeded 1.8 : 1. Subsequently, datapoints where the goodness -of -fit correlation coefficients were 0.96 or greater and Chi values were less than 25, were selected for Monte Carlo analysis. Monte Carlo analysis data, where 95% confidence volumes were  $2\text{cm}^3$  or less, were selected for co-registration with the individual subjects MRI.

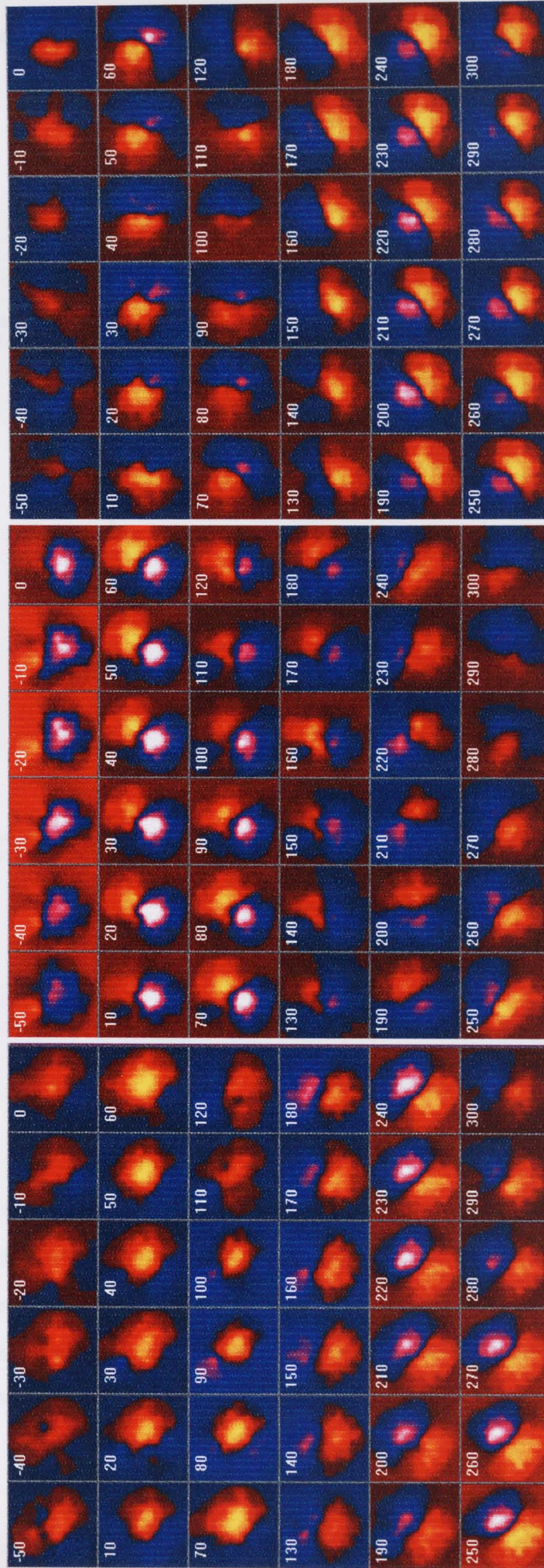
Signal to noise ratio plots and latencies yielding the smallest confidence volumes are detailed graphically in Figures 4.5 and 4.6.

Signal to noise ratio plots for right index finger data showed two clear peaks across subjects; these occurred between 0 and 50 milliseconds and 200-275 milliseconds. The smallest confidence volumes were similarly clustered predominantly within these latency bands.. The 0-50 millisecond window corresponded to component MF. The second latency window encompassed waves II and III.

A similar picture was seen in the left index finger data with the edition of small confidence volumes seen at the 350 millisecond mark (wave IV) from subject 2.

It should be noted that there were large right left differences in signal to noise ratio's in subjects 1 and 2, with large signals on the right in subject 1 and on the left in subject 2. Such difference might be explained by the relatively crude triggering paradigm used which may have caused a smearing of temporal activation of cortical events.

# Chapter 4



**Subject 1**

**Subject 2**

**Subject 6**

Figure 4.4 Plot of magnetic field distribution at 10 millisecond intervals across 350 milliseconds of the acquisition window in each subject. Red / yellow represents magnetic field towards the magnetometer and blue / pink away from the magnetometer.

## Right Index finger movement data

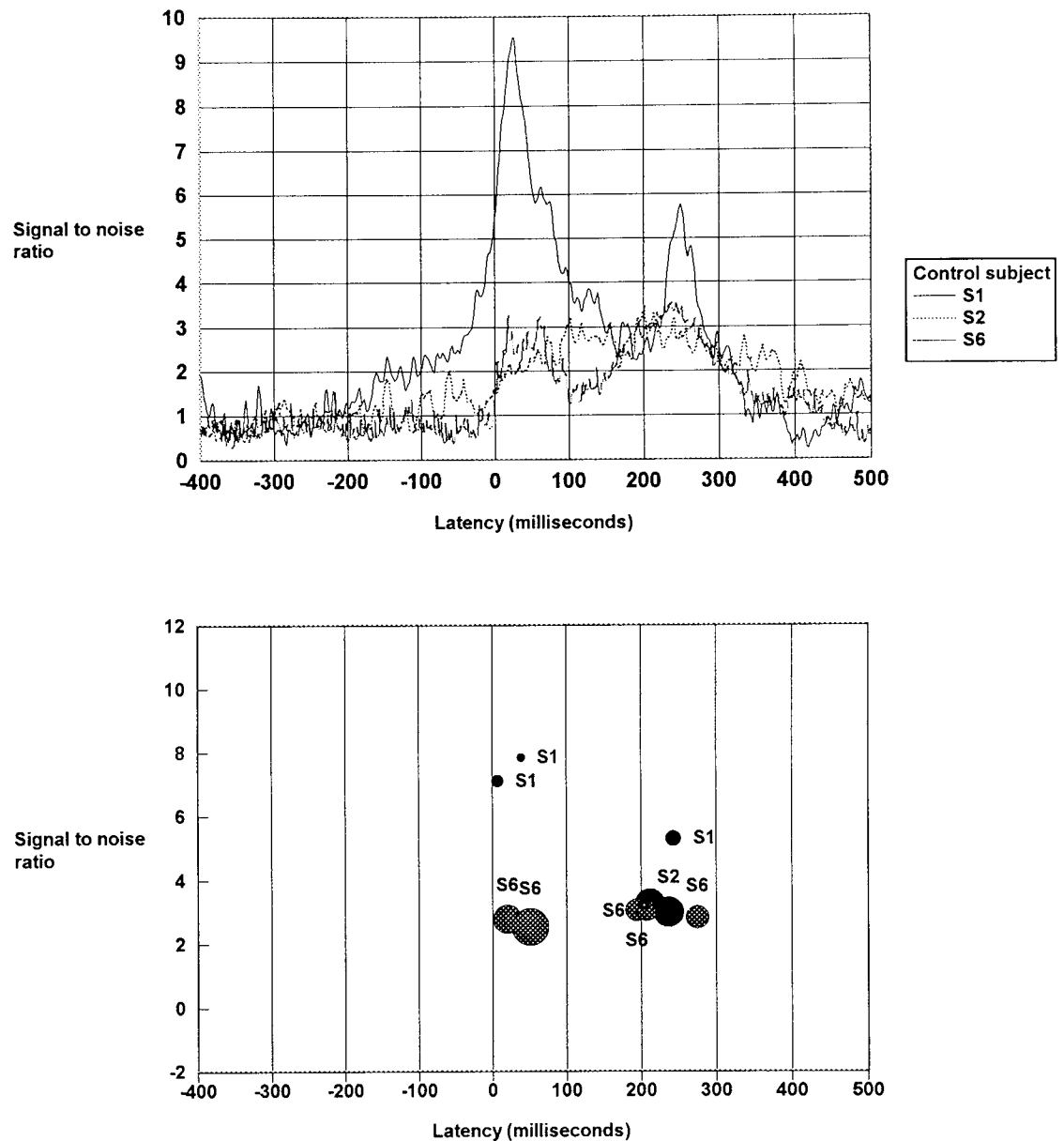


Figure 4.5 Right index finger movement data. Upper graph shows a plot of the signal-to-noise ratio of data at each datapoint of acquisition. The lower graph depicts the latencies in each subject which yielded the smallest confidence volumes following Monte Carlo analysis. The size of the circles represent the relative size of confidence volumes and these are plotted as a function of the signal to noise ratio of the data at the respective latencies.

## Left Index finger movement data

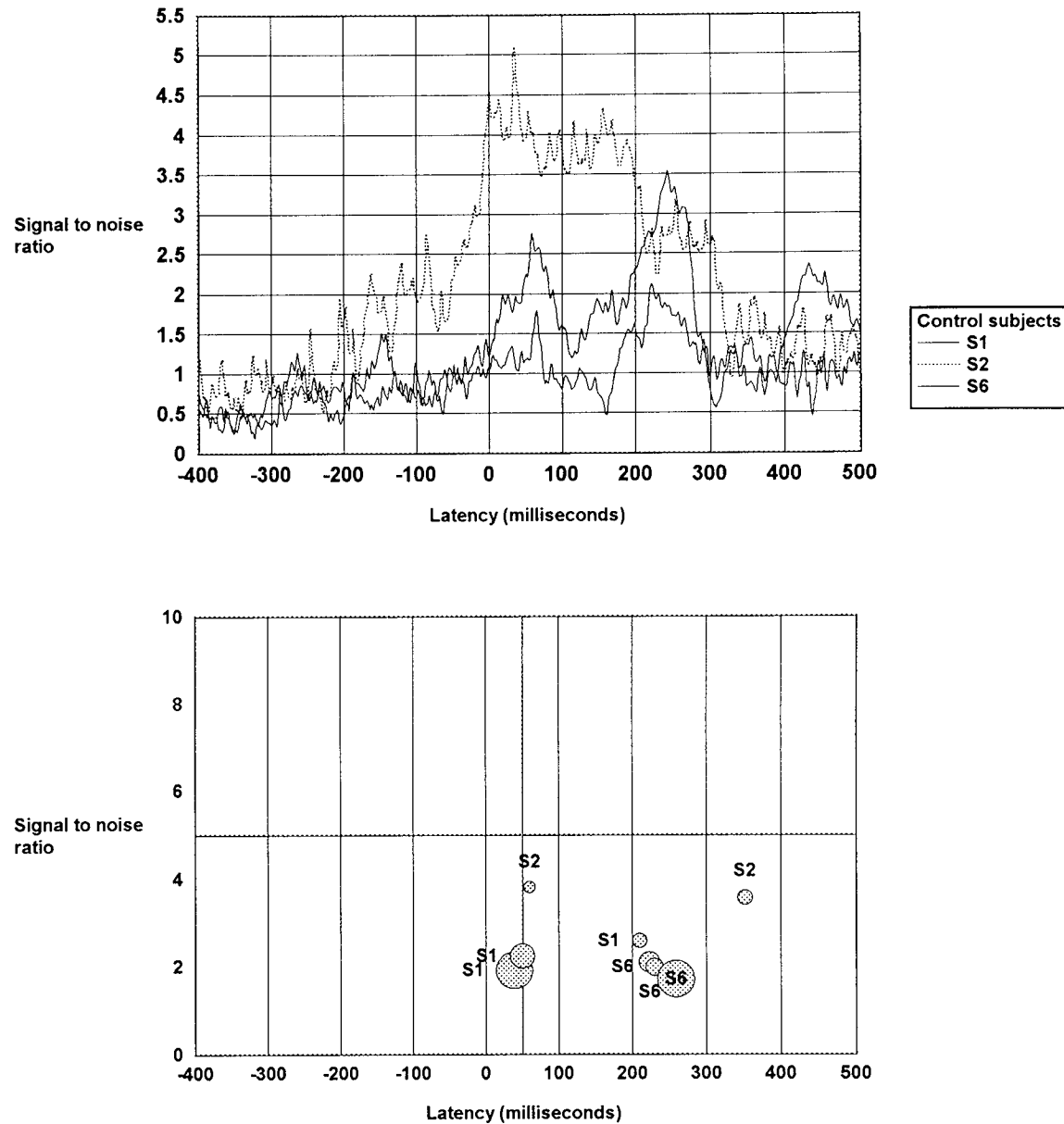


Figure 4.6 Left index finger movement data. Upper graph shows a plot of the signal-to-noise ratio of data at each datapoint of acquisition. The lower graph depicts the latencies in each subject which yielded the smallest confidence volumes following Monte Carlo analysis. The size of the circles represent the relative size of confidence volumes and these are plotted as a function of the signal to noise ratio of the data at the respective latencies.

### 4.4.3 MRI Co-registration and Talairach co-ordinates

Monte Carlo analysis confidence volumes were co-registered with the MRI of the individual subject. Methodology for co-registration was the same as that employed for somatosensory evoked magnetic fields described in Chapter 3. Similarly, using the co-ordinate system of Talairach and Tournoux (1988), three dimensional proportional co-ordinates for the movement related evoked fields were measured and compared with those obtained through median nerve stimulation.

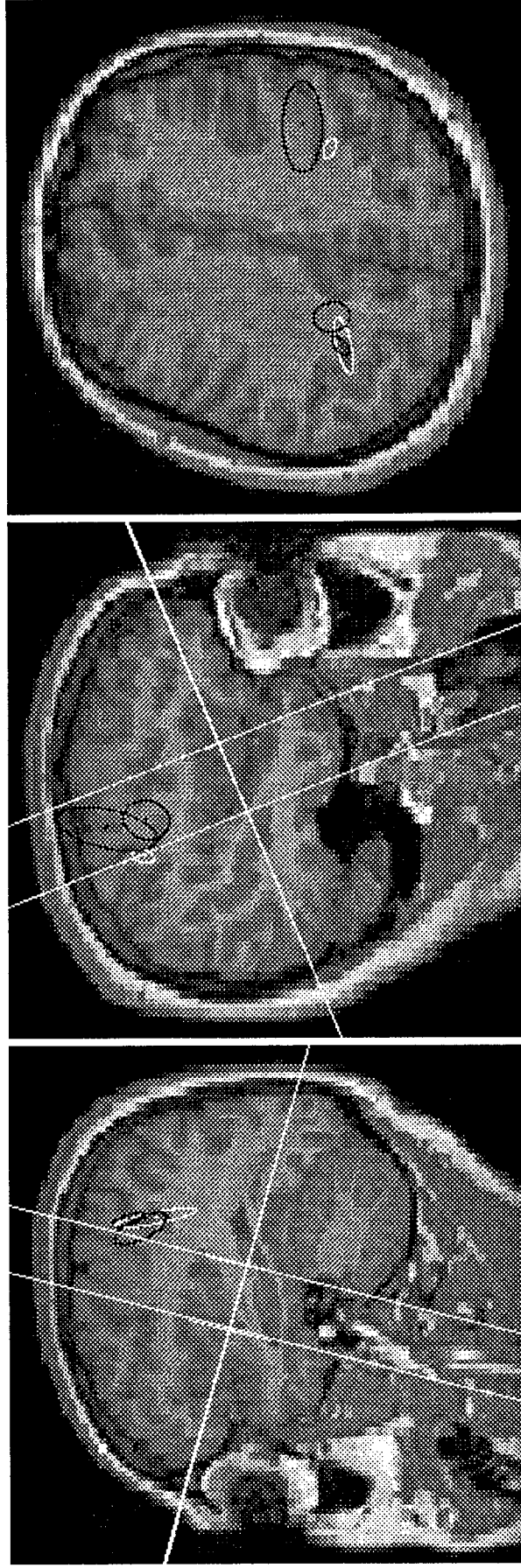
### 4.4.4 Index finger movement localisations

The smallest confidence volumes from three trials of index finger movement, if less than  $2\text{cm}^3$  in volume, were coregistered with the MRI. For ease of comparison between right and left index finger movement data, and for initial comparison with median nerve data, localisations achieved from dipole fitting of the MF component were used where possible.

A comparison of dipole localisations across the temporal window of acquisition was also made and detailed in the next section (4.4.4.1).

The figures overleaf (Figs 4.7-4.9) illustrate the co-registration of the confidence volumes with the MRI. Motor and sensory data is illustrated together on single sagittal, axial and coronal slices for ease of comparison.

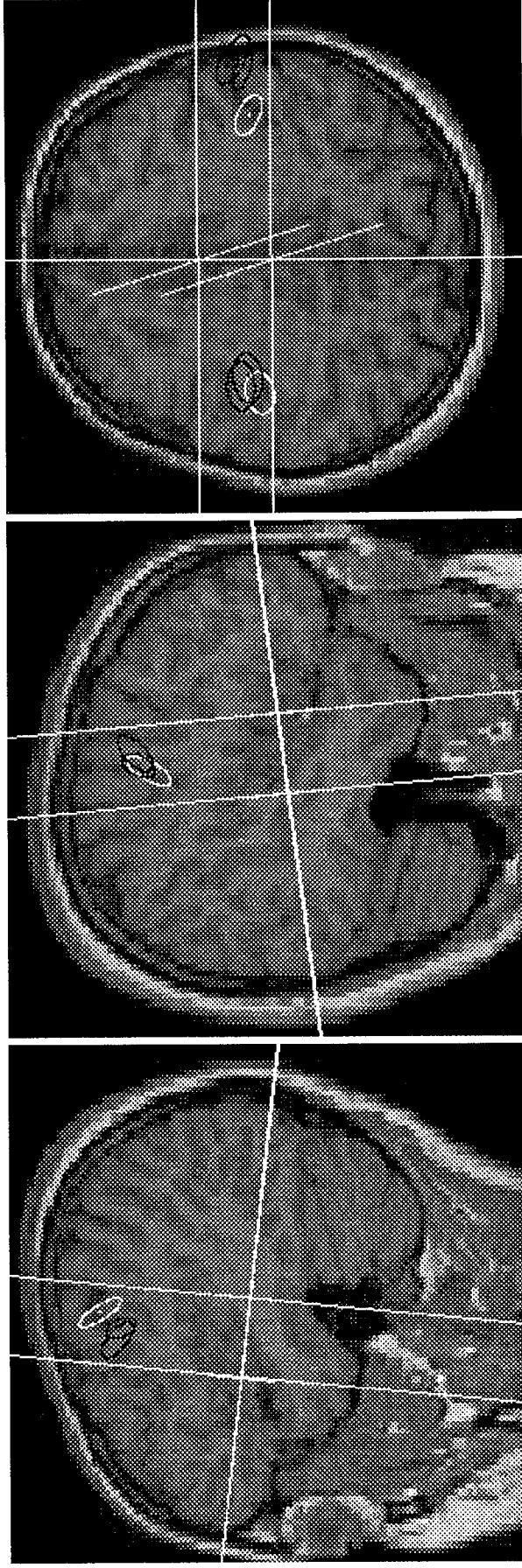
## Chapter 4



a) b) c)  
Figure 4.7 Subject 1. Right index (a) and Left index (b) finger movement confidence volumes for component MF are shown as black ellipses. Both are shown together in a single axial slice in plate c). The smallest median nerve confidence volumes are shown for comparison as white ellipses in all three plates.



## Chapter 4



a) b) c)  
Figure 4.8 Subject 2. Right index (a) and Left index (b) finger movement confidence volumes for component MF are shown as black ellipses. Both are shown together in a single axial slice in plate c). The smallest median nerve confidence volumes are shown for comparison as white ellipses in all three plates.

## Chapter 4

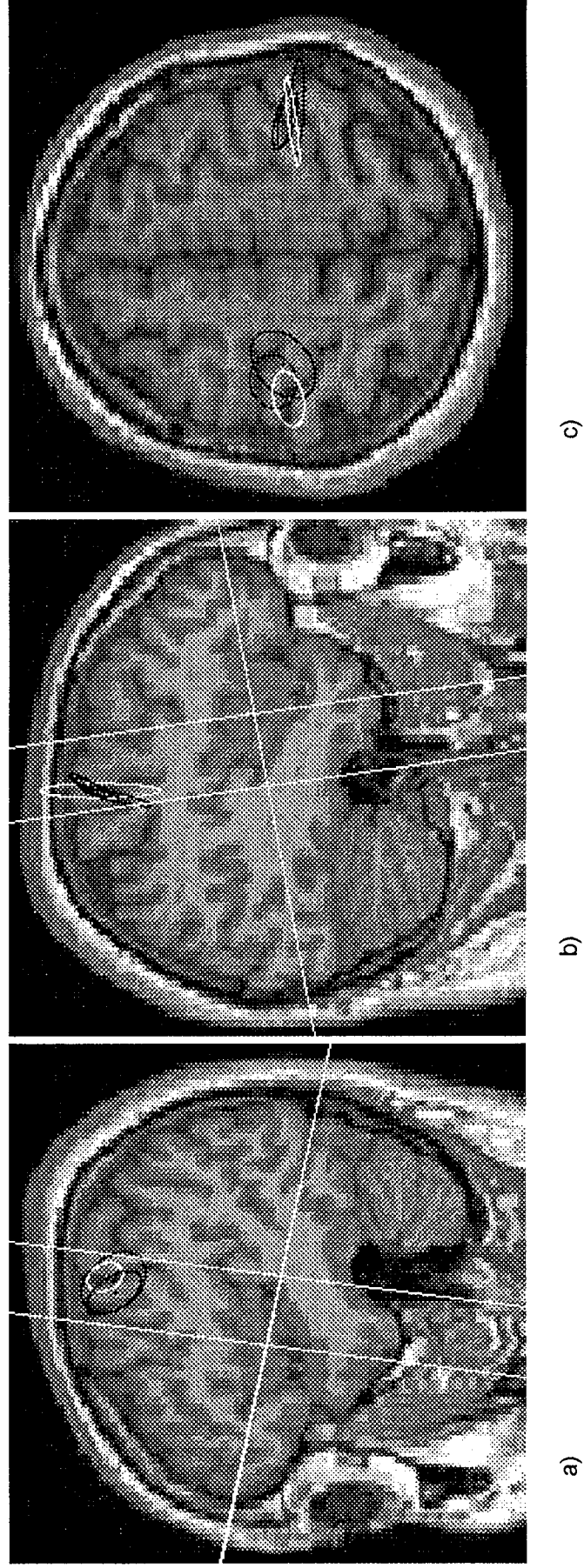


Figure 4.9 Subject 6. Right index (a) and Left index (b) finger movement confidence volumes for component MF are shown as black ellipses. Both are shown together in a single axial slice in plate c). The smallest median nerve confidence volumes are shown for comparison as white ellipses in all three plates.

### 4.4.4 (continued) Index finger movement localisations.

As can be seen from the preceding figures, the centre of the confidence volumes representing the mean localisation of component MF were always anterior to the median nerve counterpart. However, confidence volumes of median nerve and index finger movement frequently overlapped, only being entirely separate in the right hemisphere in subject 1 and the left hemisphere in subject 2..

### 4.4.5 Localisations across the temporal window of acquisition

Analysis of dipole localisation across the temporal window of acquisition was made. All confidence volumes from across the entire acquisition epoch, producing volumes of  $2\text{cm}^3$  or less, were co-registered with the MRI. The Talairach co-ordinate distance from the central mean point of each volume to the centre of the central sulcus was measured. This data was compared with the smallest confidence volumes from median nerve trials. The data from this exercise is shown overleaf in graphical form. The most salient feature of the data was that where the MF component was of sufficient quality to be co-registered with the MRI (4 out of 6 hemispheres measured), it was always seen in an anterior location to any somatosensory localisation and always in a pre-central cortical location. The localisations of waves I to IV were less consistent, with both pre- and post-central positions recorded.

# Chapter 4

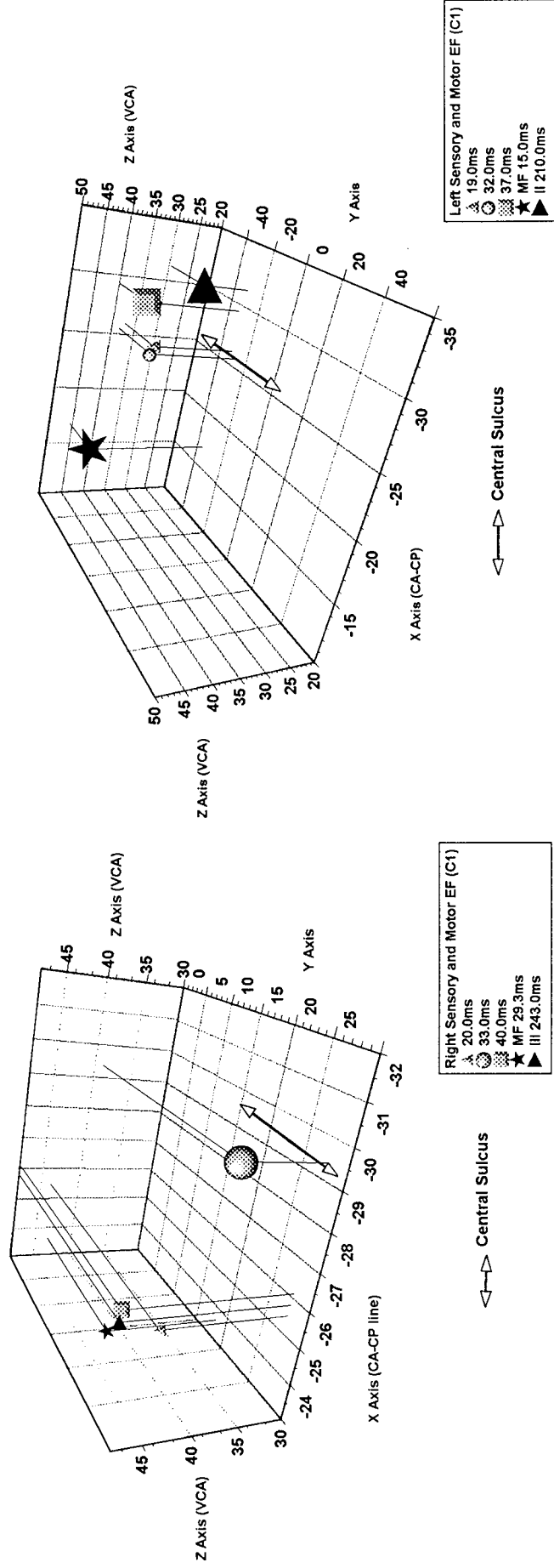


Figure 4.10 Control subject 1 (C1). Comparison of Talairach co-ordinates for right median and right index finger movement dipole fits (graph left) and left median with left index finger movement dipole fits (graph right). Icons in grey depict median nerve dipole localisations with black icons depicting index finger movement. Latencies are shown in legends with the appropriate finger movement wave component labelled prior to latency. Icon sizes reflect relative confidence volumes.

# Chapter 4

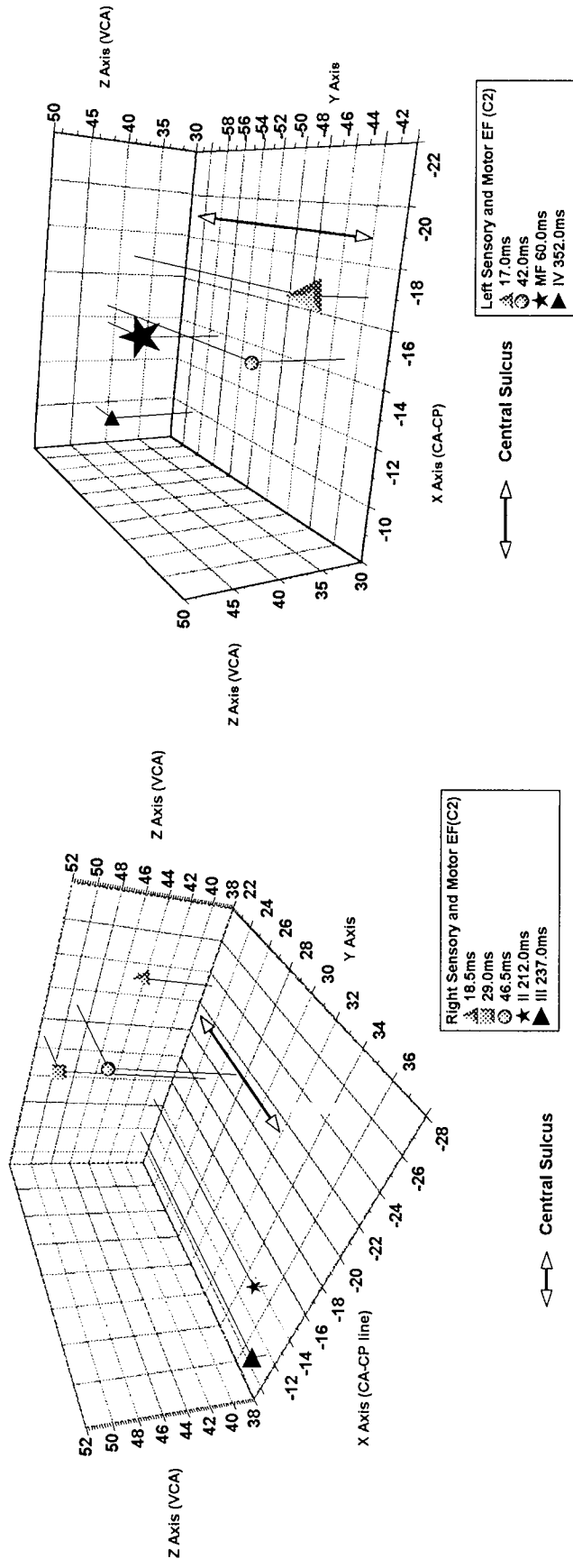


Figure 4.11 Control subject 2 (C2). Comparison of Talairach co-ordinates for right median and right index finger movement dipole fits (graph left) and left median with left index finger movement dipole fits (graph right). Icons in grey depict median nerve dipole localisations with black icons depicting finger movement. Latencies are shown in legends with the appropriate finger movement wave component labelled prior to latency. Icon sizes reflect relative confidence volumes.

# Chapter 4

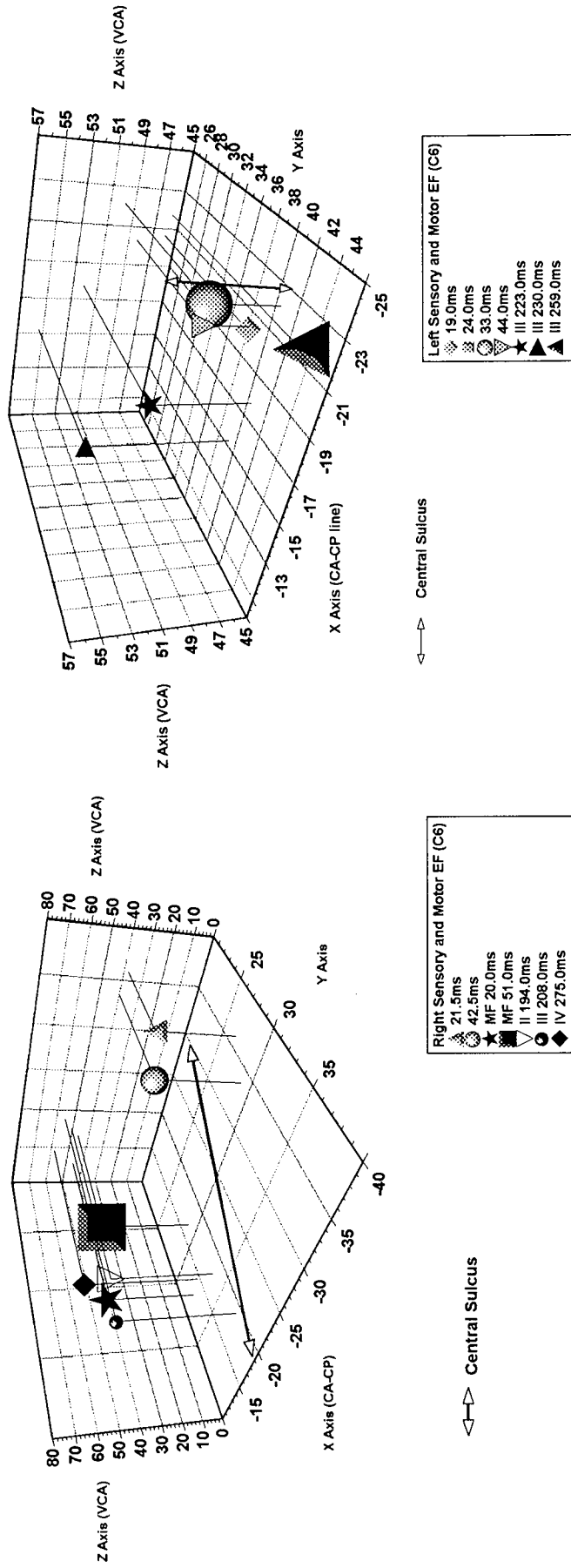


Figure 4.12 Control subject 6 (C6). Comparison of Talairach co-ordinates for right median and right index finger movement dipole fits (graph left) and left median with left index finger movement dipole fits (graph right). Icons in grey depict median nerve dipole localisations with black icons depicting finger movement. Latencies are shown in legends with the appropriate finger movement wave component labelled prior to latency. Icon sizes reflect relative confidence volumes.

#### 4.4.6 Comparison of Talairach co-ordinates

Because of the small amount of data available from this study and the variability in latency and location of many of the components generated from finger movement, little could be made of the statistical variation of Talairach co-ordinates between components. However, reliable dipole fits were achieved from component MF in four of the six hemispheres studied. By combining the right and left hemisphere data (two measures in each, the following means and standard deviations were obtained:

CA-CP plane (x axis): -16.8 (+/- 4.2); Lateral (y axis): 35.4 (+/- 13.1); VCA-VCP plane (z axis): 44.1 (+/- 2.0).

This data was plotted onto a sample brain slice from the Talairach atlas (1988) to compare the mean localisation data obtained from right and left median nerve stimulation. This data is shown below in Figure 4.13.

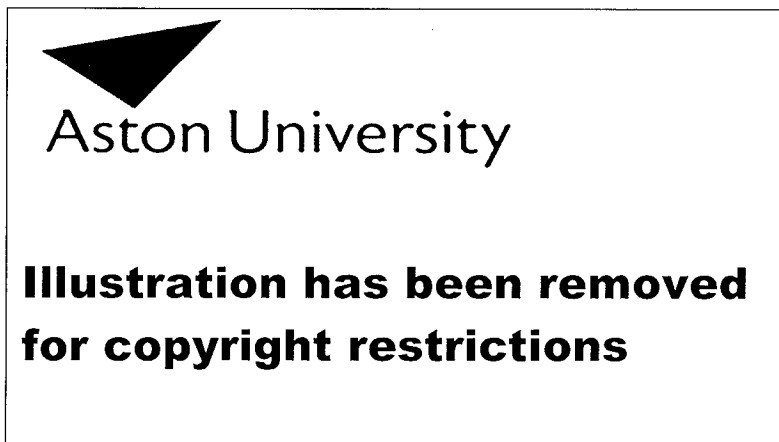


*Figure 4.13 Enlarged portion of a sagittal slice (G.33mm) from a sample brain obtained from the stereotaxic atlas of Talairach and Tournoux (1988). The mean and standard deviation error bars for right median (black), left median (black and white) and combined right and left index finger movement data for component MF (red) are shown for comparison.*

Comparison of the mean Talairach co-ordinates across the recording modalities is shown in Table 4-2 below.

*Table 4-2 Comparison of mean Talairach atlas co-ordinates*

<b>Nerve</b>	<b>Co-ordinate CA-CP axis (x) N mm (S.D.)</b>	<b>Co-ordinate Lateral (y) axis N mm (S.D.)</b>	<b>Co-ordinate VCA-VCP axis (z) N mm (S.D.)</b>
Right Median	-26.3 ( 4.7)	32.4 (7.3)	46.6 (6.4)
Left Median	-20.7 (11.1)	34.9 (5.8)	48.7 (8.5)
Right Ulnar	-25.2 (3.1)	34.2 (4.3)	51.2 (5.0)
Rt + Lt Post. Tibial	-33.2 (10.7)	6.7 (3.1)	63.5 (4.8)
<b>Rt+Lt Index Move</b>	-16.8 (4.2)	35.4 (13.1)	44.1 (2.0)

#### 4.5 Summary and Conclusion

Small flexions of the index finger in either hand was seen to generate cortical evoked fields which were highly reproducible on an intra-subject basis, and some components were comparable on an inter-subject basis.

The so-called 'Bereitschaft' or 'readiness potential' reported by several authors from electrical and MEG studies was not readily discernable from data in this thesis. The trigger point, or zero latency, was formed towards the end of the finger flexion as the finger depressed a plunger making an electrical contact. Allowing for time for the 5mm flexion to occur, no clear preceding component was seen in any trial. One explanation for this may be the uncontrolled nature of the finger movements in this study. No 'prompting' or 'feedback' stimuli was used to control the timing of the movements and averaging was determined by the act of button depression rather than using the EMG to measure movement onset. The latter point might explain the



## Chapter 4

wide differences in amplitude of the signals seen between trials in subject 1, since considerable latency smearing may have been introduced into the averaging paradigm.

The first measurable component in this study, labelled MF, is comparable to that reported in a number of previous studies by other authors, beginning to form at the onset of finger flexion and peaking at a mean latency of 48 milliseconds after flexion. The group mean peak amplitude of component MF (excluding one outlier measure) was 369 fT (+/- 47 fT) which compared with a mean peak amplitude of 435 fT (+/- 153 fT) for the right median N20m component. These amplitudes suggested that the components may be readily measured from a wide population of non-control subjects.

The significantly higher amplitude achieved in one measurement of right index finger movement (subject 1) suggested that larger signals would be achieved if triggering and finger movements were refined to yield better synchronisation for averaging.

The small sample size involved in this study prohibited any meaningful interpretation of statistical comparison of means and standard deviations of localisation between median nerve stimulation and index finger movement data. Nevertheless, for component MF of index finger movement, there was compelling evidence that a different neuronal population was involved in the generation of this component than for the median nerve stimulation counterparts. The consistent localisation of this component anterior to somatosensory localisations, and always within the pre-central gyrus, supports the view that MF is generated, in part at least, by Brodmann area 4.

In this respect, the data conflicts with some previous reports which suggest that MF is generated in the somatosensory cortex by 'feedback and feedforward' mechanisms with the motor cortex (Okada et al., 1982; Cheyne and Weinberg 1989; Kristeva et al. 1991) and that the cortical source underlying MF should be located in the subdivision of SI, mainly area 3a, (Kristeva-Feige et al. 1996).

## Chapter 4

Data in this thesis is most consistent with the findings of Chiarenza et al., (1991) who describe an MEF field peaking at 90-120 ms after EMG onset and whose equivalent dipole source was located precentrally. These authors also suggested that the 'readiness field', (RF) is generated in part by radial sources in the convexial part of the premotor gyrus; this may explain differences in signal strength of the RF component between MEG and EEG measurements.

Further analysis of finger movement data was made from studies in three neurosurgical patients described in detail in Chapter 5.

### 5. Presurgical localisation of Sensory-Motor Cortex

#### 5.1 Introduction

Precise localization of key functional areas of cortex is important in surgical treatment of epilepsy, space occupying lesions and vascular malformations, if permanent neurological deficit is to be avoided. In many cases, computerised tomography (CT) or magnetic resonance imaging (MRI) provides adequate localisation of the central sulcus as well as the lesion. In some cases, though, it is impossible to determine anatomically whether a lesion is pre-or postcentral or whether the surgical approach to the lesion traverses functionally important cortex. This is particularly true where the central sulcus or other functionally important cortical areas have been displaced by the lesion, or reorganisation through cortical plasticity occurred.

The 'gold standard' for cortical location of function is intra-operative measurement. The technique with the longest track record is cortical electrical stimulation of the sensory-motor cortex in awake patients under local anaesthesia. This was pioneered by Penfield and colleagues in the 1930's (Foerster and Penfield 1930; Penfield and Boldrey 1937).

More recently the sensorimotor region was identified under local and general anaesthesia by electrical stimulation and cortical surface recording of evoked potentials (Gregorie and Goldring 1984) or cortical surface evoked potentials alone (Allison et al 1980; Wood et al 1988).

Other workers have advocated that direct motor cortex stimulation under general anaesthesia also provides an entirely acceptable outcome (Ebeling et al 1989).

A number of non-invasive techniques have been applied to the problem of functional mapping for pre-surgical evaluation. These include positron emission tomography (PET) (Fox et al 1987), Functional Magnetic Resonance Imaging (fMRI) (Jack et al

1994), evoked potentials using dipole source analysis (Buchner et al 1994) and Magnetoencephalography (MEG).

Following a large quantity of data from a number of laboratories describing how MEG may be used to determine somatotopic organisation in human cortex (described in detail in Chapter 3), a small number of workers described their experiences in the use of MEG in pre-surgical evaluation in patients together with post-surgical outcome.

In 1992, Orrison et al described two case studies of 'Magnetic Source Imaging' in patients with large space occupying lesions in close proximity to sensory-motor cortex. For both patients, median nerves were stimulated at the wrist and the magnetic N20m components used for source localisation. In the first patient, a large right parieto-temporal mass displaced the sensorimotor cortex anteriorly. MEG localisation of sensory cortex was confirmed as accurate during surgery. In a second patient, a right fronto-parietal lesion displaced the sensorimotor cortex posteriorly which again was accurately predicted by pre-surgical MEG recordings.

These experiences using sensory stimulation were soon extended and confirmed by Gallen et al (1993) and Baumgartner (1993) and more recently by Ganslandt et al (1996).

Rezai et al 1996 described the integration of MEG data acquired pre-surgically into a frame-based stereotaxic system (COMPASS™) as well as a frameless stereotaxic system (REGULUS™). In this way they were able to present the MEG localisations to the surgeon intraoperatively in a form that allowed easy integration into existing techniques and greatly improved the usefulness of the data.

Following the description of MEG and self paced finger movement paradigms by Deecke et al (1982), a number of studies have explored this technique to examine functional localisation and organisation of human motor cortex (Sullivan et al 1989; Orrison et al 1990; Cheyne et al 1991; Kristeva-Feige et al 1996. This data is reviewed in Chapter 4).

Few studies to date have reviewed the effectiveness of the technique in pre-surgical localisation of motor cortex. Kassubek et al (1966) described self paced index finger

movements from 9 control subjects and from two neurosurgical candidates with lesions in close proximity to the sensory-motor cortex. Activity peaked in their data at a mean latency of 100ms following EMG onset (range 30-160ms). This activity was localised to the precentral gyrus in both healthy controls and in the neurosurgical patients.

The conclusions from the Kassubek study differ from some authors in attributing activity after movement onset to the motor cortex. It has been suggested that movement evoked fields peaking at about 100ms after movement onset, described as MEFI, most probably reflects a sensory input from the moving body part.

Potentially there is considerable value in non-invasive pre-surgical evaluation of cortical function. The main advantages are:-

1. The ability to plan in advance the surgical approach to a lesion and possibly to determine the extent of acceptable excision.
2. To support current intraoperative location techniques in patients.

Cortical stimulation of sensory cortex may yield motor signs and conversely, motor cortex stimulation may yield sensory signs. Additional functional imaging could provide useful supportive data. This would also be of value where lesions have displaced the cortex or with chronic lesions, functional anatomy may be grossly atypical. Surgical time may be reduced with the aid of additional supportive data.

3. To avoid the need for patient feedback during invasive cortical stimulation under local anaesthesia.
4. To provide functional location in children where conventional intraoperative cortical stimulation techniques are unsuitable.

### 5.2 Aims

The aim of this study was to establish whether the technique of cortical source localisation within sensory-motor cortex using Magnetometry was robust and reliable enough to be of practical clinical value. In particular, the pre-surgical localisation of somatosensory / motor cortex in patients with lesions or proposed surgical fields close to, or involving, somatosensory cortex. Comparison with presurgical localisation of the central sulcus by Neuro-Radiological assessment would be made and both methods compared to intraoperative localisation techniques.

### 5.3 Methods

#### 5.3.1.1 MEG acquisition

The methodologies described in Chapters 3 and 4 for MEG acquisition was adopted for patient use. Protocols were modified only in so far as some patients were unable to tolerate prolonged recording sessions through fatigue and/ or recurrent seizures. This necessarily curtailed the quantity of data that could be acquired and so the most affected limbs were prioritised for recordings with additional data acquired if possible.

Thirteen patients were assessed in total and these are presented in chronological order of assessment. Three patients (11, 12 and 13) undertook median nerve stimulation together with self-paced finger movement paradigms. Only these patients could benefit from this dual procedure because the acquisition and analysis tools were unavailable earlier in the study.

#### 5.3.1.2 fMRI acquisition

Patient 1 was able to undertake an fMRI paradigm which was performed in the identical manner described in Chapter 3.

### 5.3.1.3 Neuro-Radiographic localisation of the central sulcus

Pre-surgically, the position of the central sulcus was determined in axial MRI slices by a Consultant Neuroradiologist (Dr S.Renowden, Frenchay Hospital, Bristol). Subsequently, the position of the MEG localisation with respect to this determination was made. Both MEG and Neuro-Radiological assessments were compared with intra-operative measures.

### 5.3.1.4 Surgical localisation of sensory-motor function

Two methods of surgical co-registration of MEG data were employed. In patients referred from the Queen Elizabeth hospital in Birmingham (patients 1 and 12), the Neurosurgeon (Mr A.R.Walsh) performed electrical stimulation of the cortex following an awake craniotomy. Here, the patient would be aroused from anaesthesia following the application of local anaesthetic around the surgical wound. A bipolar probe was placed on the surface of the cortex and a 50Hz current passed: the patient would be asked to describe any sensation and any motor signs would be observed by the anaesthetist. In this way, the sensory or motor signs would be mapped onto the cortex thus providing the required functional location (see Figure 5.10). MEG localisations were compared intraoperatively with the gyral patterns observed.

All other patients were referred from the Frenchay Hospital in Bristol. Here, the Neurosurgeon (Mr D Sandeman) employed two methods of cortex mapping. Electrical stimulation of the cortex was used, but here, EMG was measured to determine the motor response. Sensory function was localised by stimulation of the median and posterior tibial nerves at the wrists and ankles and recording the ensuing somatosensory cortical evoked response from recording electrodes placed on the surface of the cortex. In this way, it was rarely required to arouse the patient from anaesthesia to obtain verbal feedback.

MEG co-registration with intraoperative cortical mapping was made by the use of an ISG image guided wand system linked to an Allegro workstation (ISG Technologies;

Toronto, Ontario, Canada). Intra-operative cortical measurements could therefore be compared directly with the MEG localisations during the surgical procedure.

### 5.4 Case Study Results

#### 5.4.1 Case study 1: Patient PR

##### 5.4.1.1 Clinical History

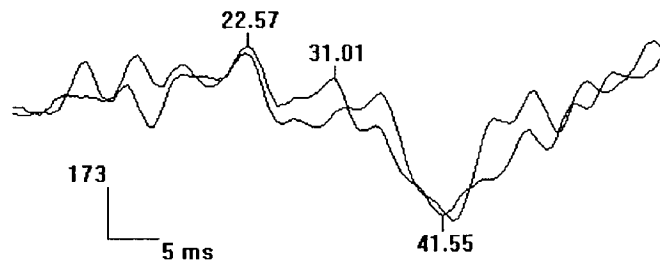
The patient was a 44 year old right handed male who presented with a history of tonic-clonic seizures and partial seizures involving myoclonic jerks of the right hand and arm. An MRI scan revealed what appeared to be a large cystic tumour in close proximity to the sensory-motor cortex. The seizures were partially controlled with anti-convulsants but the seizure frequency remained unacceptable. A surgical option was considered.

The proximity of the lesion to the sensory-motor cortex was a cause for concern and in order to investigate the precise juxtaposition of the functional anatomy, Magnetoencephalography (MEG) and Functional Magnetic Resonance Imaging (fMRI) were performed.

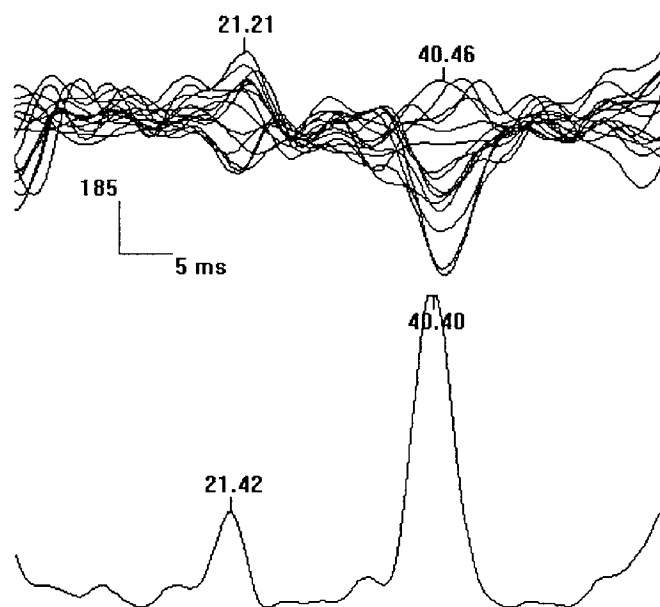
##### 5.4.1.2 MEG Results - Patient PR

Stimulation of the right median nerve at the wrist yielded reproducible evoked responses (Fig. 5.1a) which were within normal limits for latency and amplitude in comparison with the control group. Two clear peaks of activation were noted at 21ms and 40ms and single equivalent dipole source localisations were calculated at these latencies (Figure 5.1b). Significant correlation coefficients ( $r > 0.96$ ) and low Chi values ( $<12$ ) were obtained following single equivalent dipole analysis.





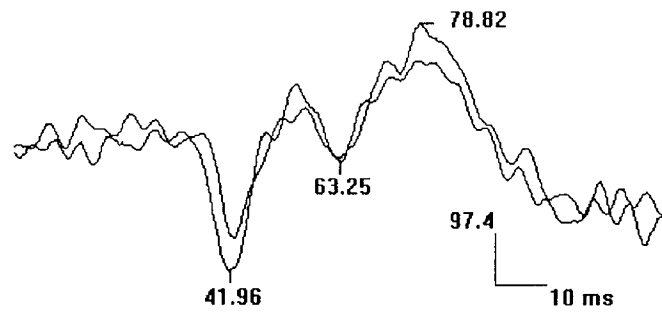
a)



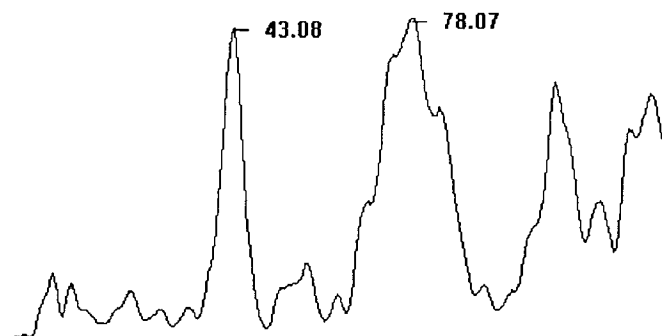
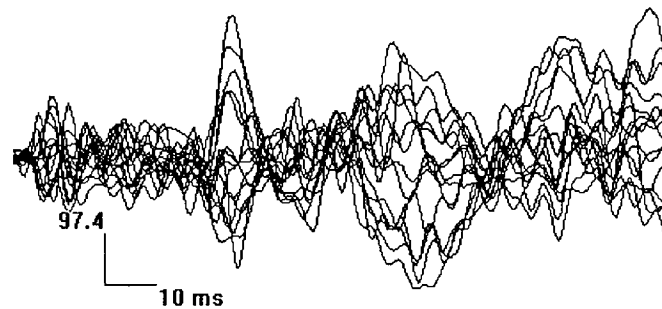
b)

Figure 5.1 Patient PR. a) Shows two trials of right median nerve waveforms superimposed for comparison. b) Upper waveforms show 19 channels of MEG waveforms superimposed following a trial of right median nerve stimulation. Lower waveform shows the Global Field Power plot for this dataset.

Stimulation of the right posterior tibial nerve at the ankle produced repeatable evoked responses which were within normal limits for latency and amplitude (Fig.5.2a)



a)



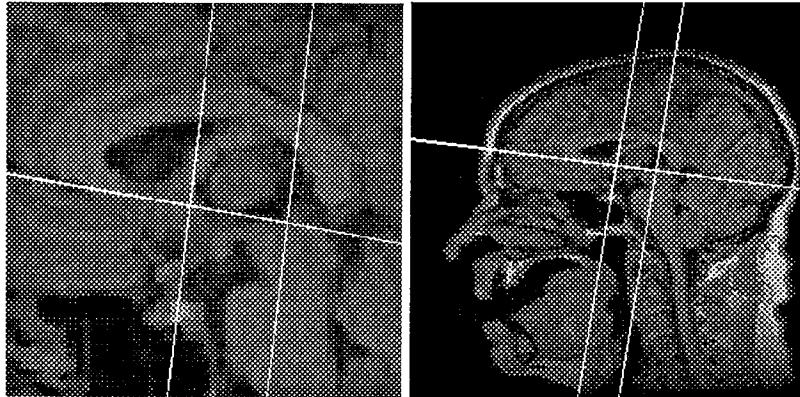
b)

Figure 5.2 Patient PR. a) Shows to trials of right posterior tibial nerve waveforms superimposed for comparison. b) Upper waveforms show 19 channels of MEG waveforms superimposed following a trial of right posterior tibial nerve stimulation. Lower waveform shows the Global Field Power plot for this dataset.

Two clear peaks of activation were noted at 43ms and 78ms and single equivalent dipole source localisations were calculated at these latencies (Figure 5.2b). Significant correlation coefficients ( $r > 0.96$ ) and low Chi values ( $< 12$ ) were obtained and confidence volumes for the source localisations at these latencies were less than  $2\text{cm}^3$ . These were co-registered with the MRI (Fig.5.5 and 5.6).

## 5.4.1.3 MEG -MRI co-registration

A mid-line sagittal slice was selected to identify the anterior and posterior commissures. CA-CP and VCA lines were constructed (Figure 5.3).



*Figure 5.3 Talairach co-ordinate lines were constructed from the location of the anterior and posterior commissures in a midline sagittal slice.*

Bite bar markers were located from the MRI and a matching matrix derived. This match was checked by plotting a digitised head shape onto the MRI (Figure 5.4).

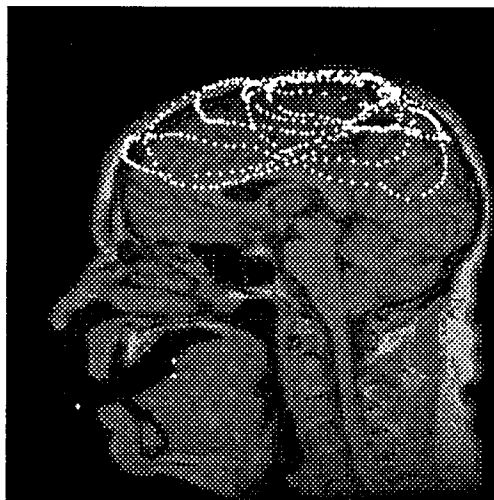


*Figure 5.4 Matching digitised head shape with midline MRI slice to test co-registration.*

## MEG-MRI Source localisation

95% confidence volumes ( $< 2\text{cm}^3$ ) for right median and right posterior tibial nerve data were then co-registered with the MRI. These are shown in Figures 5.5 and 5.6.

## Chapter 5

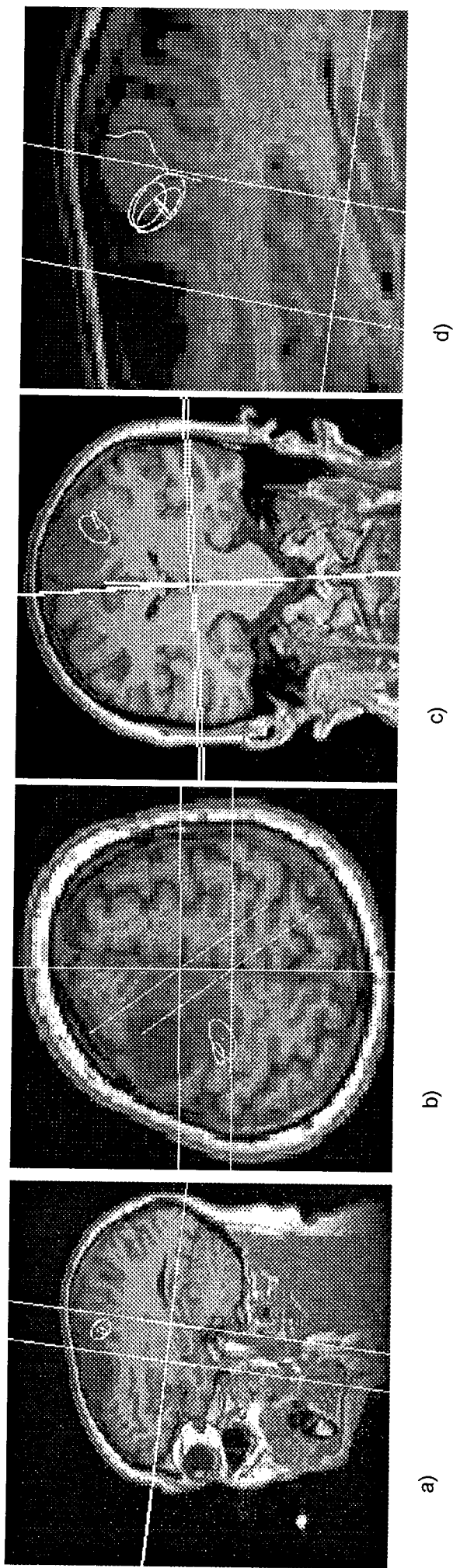


Figure 5.5 a) Shows the smallest 95% confidence volumes from two trials of median nerve stimulation at a latency of 22 milliseconds. These are shown in relation to the VCA and VCP lines of the Talairach co-ordinate system. b) Smallest confidence volumes shown on an axial slice. c) Shows the smallest confidence volumes on a coronal slice. d) Sagittal slice showing four confidence volumes obtained at latencies of 22 (x2), 43 and 44ms. These are shown in relation to the predicted line of the central sulcus depicted by the white curved trace.

## Chapter 5

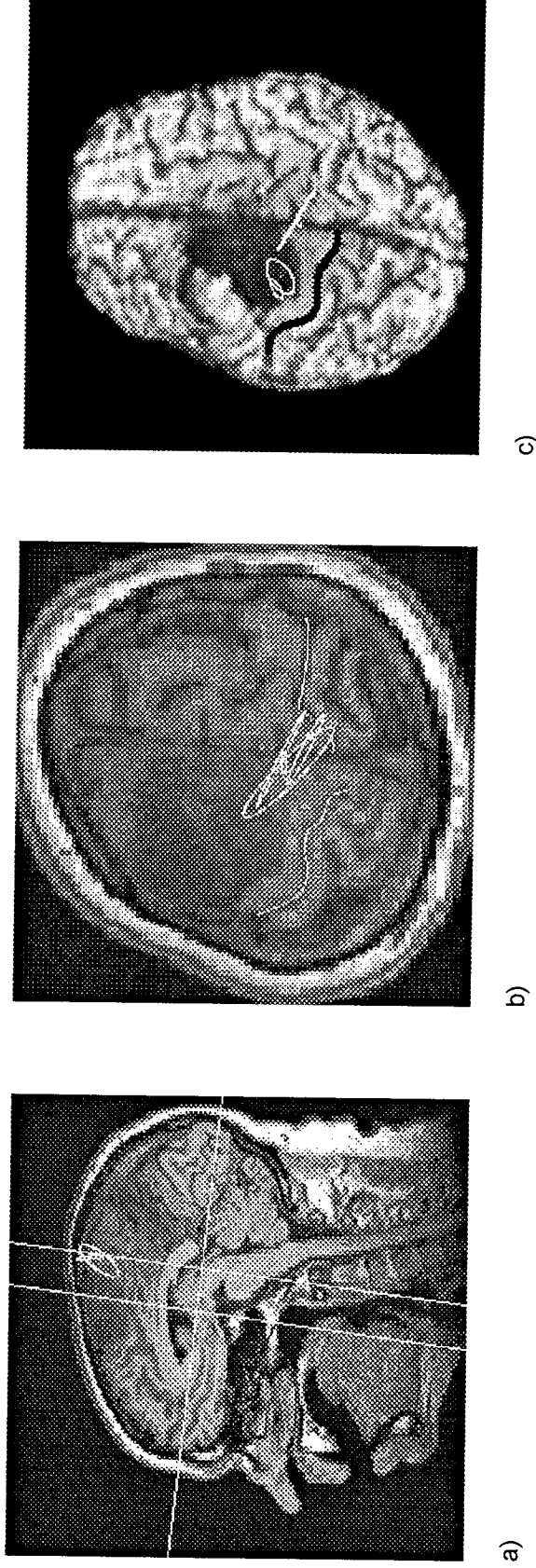


Figure 5.6a-c. a) Shows the smallest 95% confidence volumes from two trials of posterior tibial nerve stimulation at latencies of 42 and 77 milliseconds. These are shown in relation to the VCA and VCP lines of the Talairach co-ordinate system.

b) Depicts volumes obtained from right posterior tibial nerve stimulation at 42, 43, 77 and 80 milliseconds with the predicted line of the central sulci shown.

c) Shows the smallest confidence volumes from median nerve and posterior tibial nerve stimulation superimposed onto a surface rendered image of the cortex. The bold black line indicates the predicted line of the central sulcus.

## 5.4.1.4 Patient PR - Predicted location of the central sulcus

Localisations for both median nerve and posterior tibial stimulation fell within the gyrus immediately posterior to the lesion.

Mean Talairach co-ordinates for the four confidence volumes for median nerve stimulation co-registered with the MRI were:

CA-CP axis: -16.0 mm      Lateral axis: 30.6 mm      VCA-VCP axis: 50.8 mm.

The corresponding values for posterior tibial data were:

CA-CP axis: -26.3 mm      Lateral axis: 3.4 mm      VCA-VCP axis: 64.8 mm.

Neuro-Radiological assessment of the MRI together with Talairach co-ordinate data suggested that the dipoles were localised to the pre-central gyrus in this patient. This is depicted graphically below (Fig 5.7) and overleaf (Fig 5.8).

## Patient PR- Median Nerve data

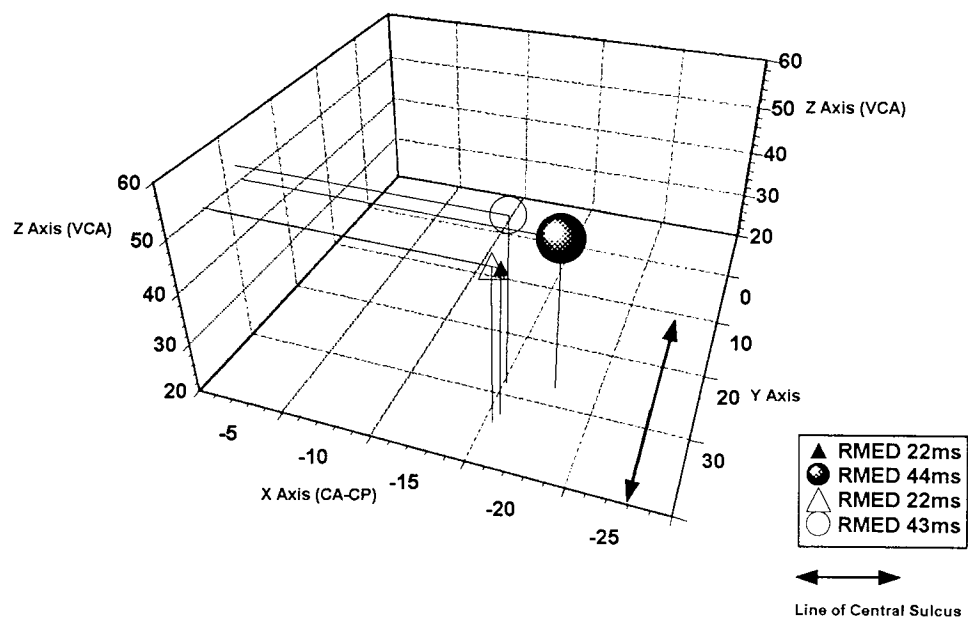


Figure 5.7 Median nerve localisations in patient PR. Relative sizes of the localisation icons reflect the proportional sizes of the corresponding confidence volumes. The double arrow indicates the Neuro-Radiologically predicted position in the x-y axis of the line of the central sulcus.

## Patient PR - Right Posterior Tibial nerve

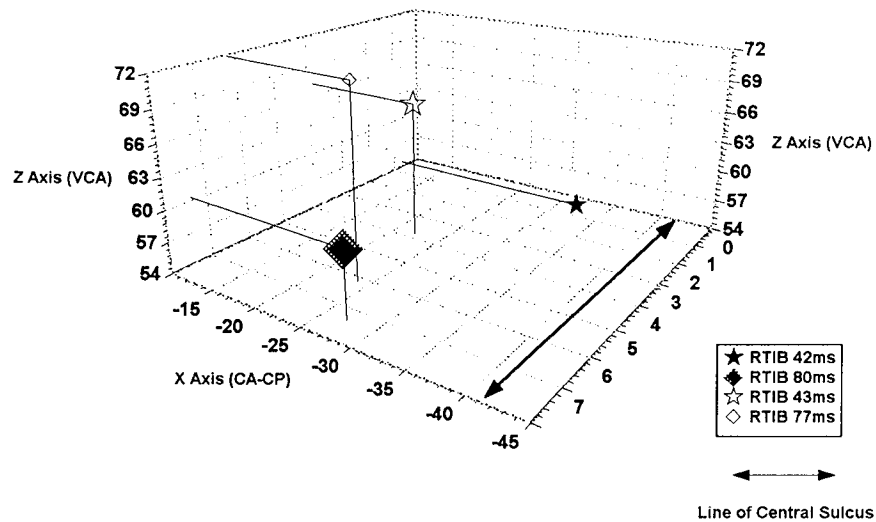


Figure 5.8 Posterior Tibial nerve localisations in patient PR. Relative sizes of the localisation icons reflect the proportional sizes of the corresponding confidence volumes. The double arrow indicates the Neuro-Radiologically predicted position in the x-y axis of the line of the central sulcus.

## 5.4.1.5 Functional Magnetic Resonance Imaging

Analysis of pixel image intensity in relation to the activation sequence revealed areas of significant activation in the sensory-motor cortex region.

fMRI slices were matched with MEG slices for comparison and this data is shown in Figure 5.9. As can be seen, MEG localisation was clearly anterior to the fMRI localisation.

## 5.4.1.6 Surgical validation

A large craniotomy was performed over the left fronto-temporo-parietal regions to expose both the lesion and the expected area encompassing the sensory-motor cortex. Once the cortex was exposed, the patient was aroused from general anaesthesia to respond to direct electrical stimulation of the cortex. A bipolar probe delivering an alternating current at 50Hz was used.

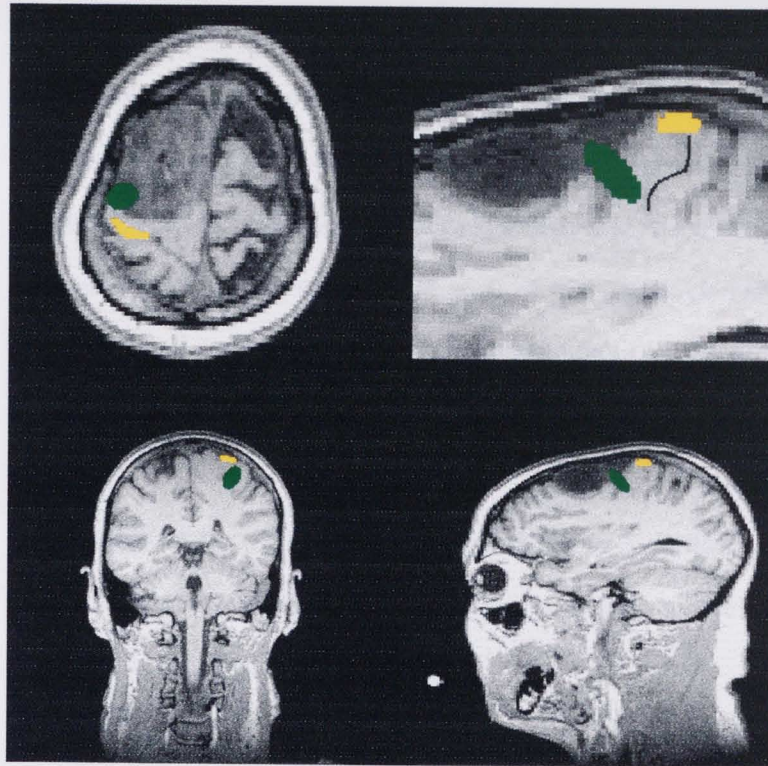


Figure 5.9 indicates the location of maximal fMRI activation (yellow) following a finger-thumb opposition sequence, together with the MEG localisation following Median nerve stimulation (green). Upper right image shows the juxtaposition of the functional locations with respect to the predicted line of the central sulcus traced with a black line.

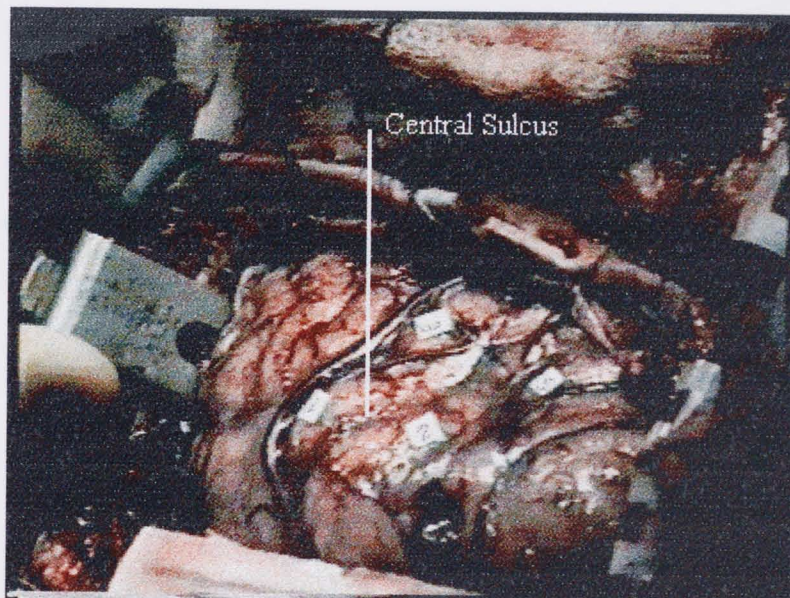


Figure 5.10 Surgical area in patient PR. White labels indicate areas of positive sensory - motor responses from the patient following electrical stimulation of the cortex. Labels to the right of the surgical field yielded motor responses while those to the left were predominantly sensory.



### Surgical validation (continued)

Verbal feedback to sensory stimulation and observation of motor signs enabled mapping of the cortex which was labelled with numeric indicators. For validation purposes, the surgical area was photographed and the gyral patterns compared with 3 dimensional surface rendered images of the cortex derived from the MRI. Using this technique, the Rolandic fissure was determined as the first sulcus posterior to the lesion. This confirmed the predicted line of the central sulcus shown in the previous figures.

Histological section of the lesion determined it to be a low grade Astrocytoma. This was successfully excised and the patient made a complete recovery with no permanent neurological deficit.

#### 5.4.1.7 Patient PR - Summary.

In patient PR, the MEG localisations were located in the pre-central gyrus. This was confirmed by intra-operative cortical mapping which suggested that the MEG data was displaced anteriorly by 8-9mm from the posterior bank of the central sulcus for median nerve localisations and by 10-20mm for Posterior Tibial nerve responses.

fMRI localisation appeared to implicate the gyral surface of Brodmann 4.

A possible explanation for the MEG displacement would be that the Astrocytoma was a large conductivity perturbation and so the true conductivity profile may not have been represented by the homogeneous sphere model used in the source localisation algorithm.

### 5.4.2 Case Study 2: Patient DT

#### 5.4.2.1 Clinical history

Tonic/clonic seizures preceded by aura of sensation in LT arm. Seizures initiated with jerking of Left arm and Left leg with subsequent Jacksonian-like spread. Patient had undergone a previous surgical intervention involving the right parietal cortex

#### 5.4.2.2 Investigations

Magnetometry was performed at the Clinical Neurophysiology Unit at Aston University on 27th April 1995 to localise Left hand and foot function using Somatosensory Evoked Response techniques.

#### 5.4.2.3 MEG Results - Patient DT

Stimulation of the Left Median nerve at the wrist and Left Posterior Tibial nerve at the ankle yielded reproducible magnetic field waveforms (Figs 5.11 and 5.12). Inverse solution algorithms were applied to the data to obtain source localisation coordinates. Goodness of fit analysis indicated statistically significant correlation coefficients ( $p > 0.95$ ) between 21.5 milliseconds and 35.0 milliseconds for Left median nerve stimulation and at 75.5 milliseconds for Left Posterior Tibial nerve stimulation.

Monte Carlo analysis was performed on the data to assess 95% confidence boundaries for the source localisation's. Confidence ellipses with volumes of less than  $2\text{cm}^3$  were then superimposed onto the MR images. The lowest volumes for Left median nerve data was obtained at 23.5ms ( $541\text{ mm}^3$ ) and for Left Posterior Tibial nerve data at 75.5ms and measured  $1822\text{ mm}^3$ .

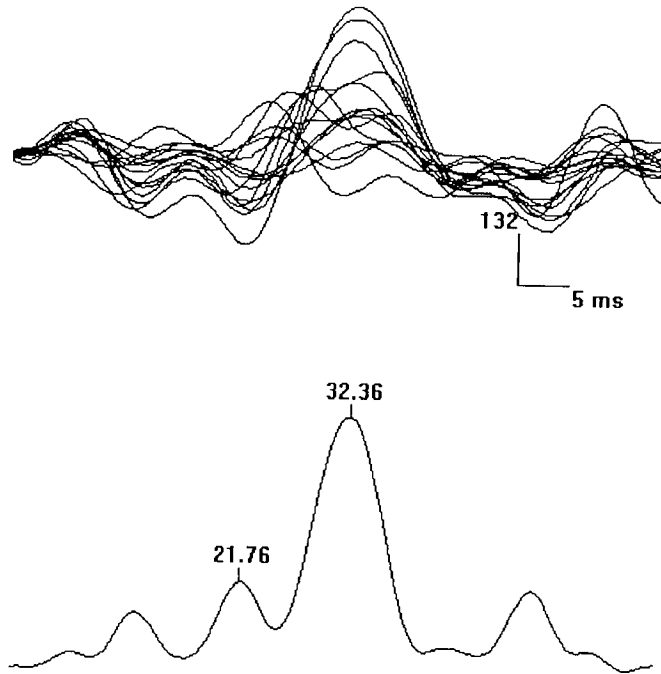


Figure 5.11(top) shows magnetic field waveforms following **Left Median nerve** stimulation. The lower figure shows the corresponding Global Field Power analysis of the data. The latencies indicated are those from which single equivalent dipole models were calculated.

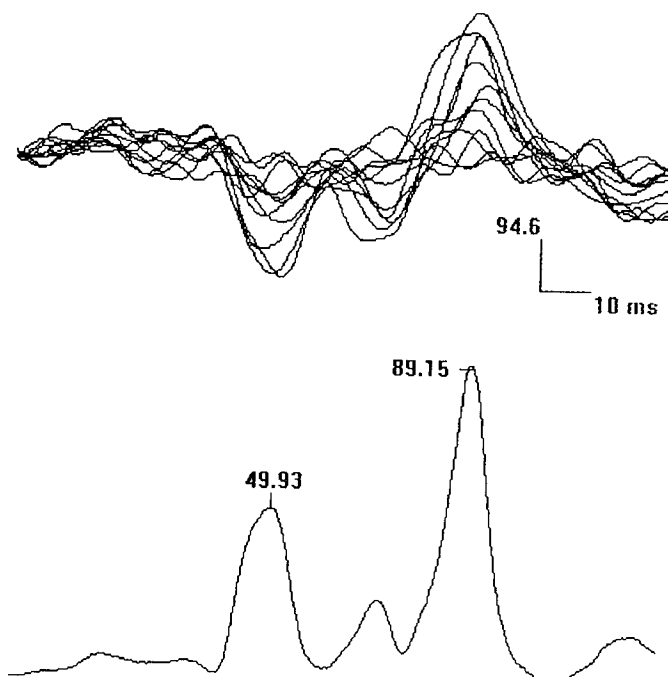


Figure 5.12(upper) shows magnetic field waveforms following **Left Posterior Tibial** nerve stimulation. The lower figure shows the corresponding Global Field Power analysis of the data. The latencies indicated are those from which single equivalent dipole models were calculated.

#### 5.4.2.4 MRI Co-Registration

MRI's were acquired with the co-registration bite bar in situ. Slice thickness of the MRI was 3mm.

Talairach co-ordinate baselines were estimated from the midline (slice 128) and are shown below (Fig 5.13)

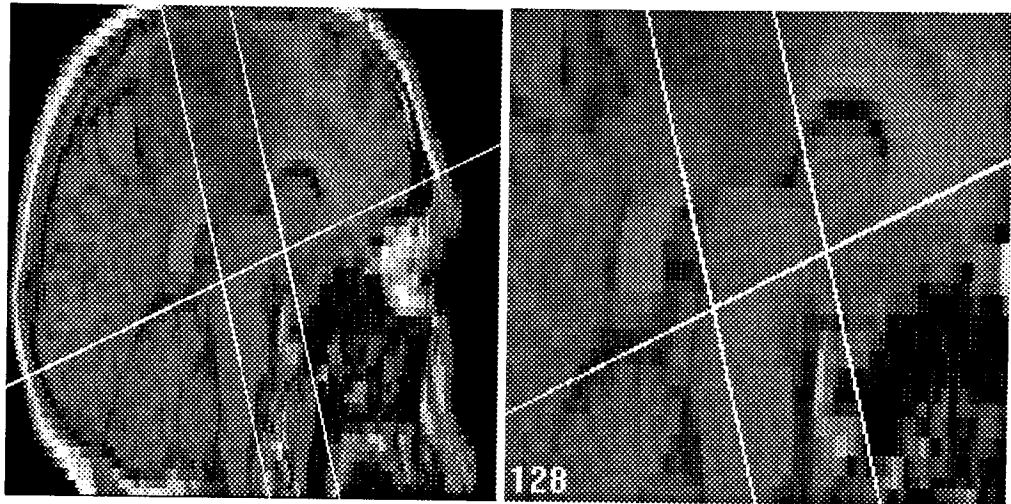


Figure 5.13 Talairach co-ordinate base lines computed for patient DT.

#### 5.4.2.5 Predicted location of the central sulcus

Co-registration of MEG confidence volumes with the MRI are shown on single slices for ease of comparison in Figure 5.14.

From the cluster of smallest confidence volumes from each trial, an estimation of the line of the central sulcus was estimated. These are shown in Figure 5.15.

The mean Talairach co-ordinates for MEG localisations were:

Median nerve:

CA-CP axis: -36.6 mm; Lateral (y) axis: -35.2 mm; VCA-VCP axis: 54.5 mm.

Posterior Tibial nerve:

CA-CP axis: -28.8 mm; Lateral (y) axis: 10.7 mm; VCA-VCP axis: 77.6 mm.

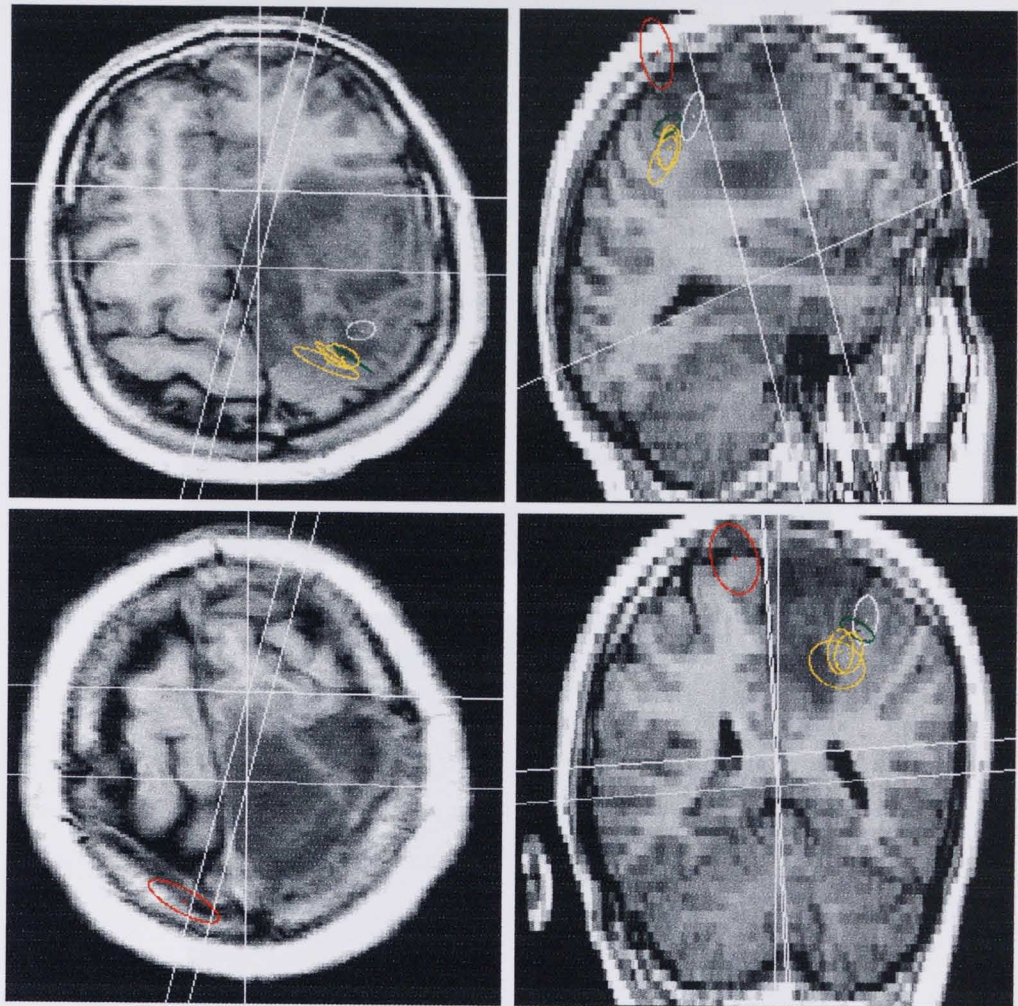


Figure 5.14 The four figures above indicate source localisations for **Left Median nerve** from three independent trials (Yellow, Green and White ellipses). **Left Posterior Tibial nerve** localisation is also indicated (red ellipse). The three yellow ellipses are source localisations from a single trial of Left Median nerve stimulation but at three latencies (22.0ms, 23.0ms and 35.0ms).

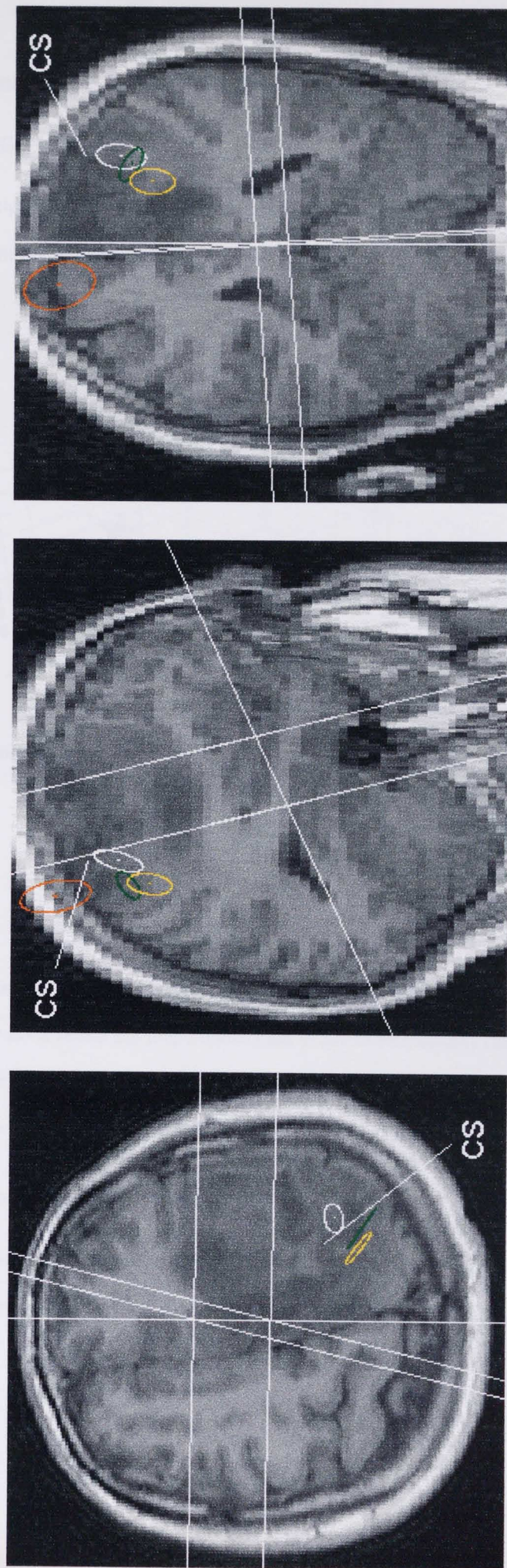


Figure 5.15 Patient DT. From the cluster of smallest confidence volumes from three trials of median nerve stimulation and one of posterior tibial nerve stimulation, a prediction of the line of the central sulcus was made. This is indicated on the images by the marker labelled CS.

Predicted location of the central sulcus (continued)

#### 5.4.2.5.1 MEG Prediction

The relationship of MEG localisations with respect to the predicted line of the central sulcus is shown graphically below (Figure 5.16).

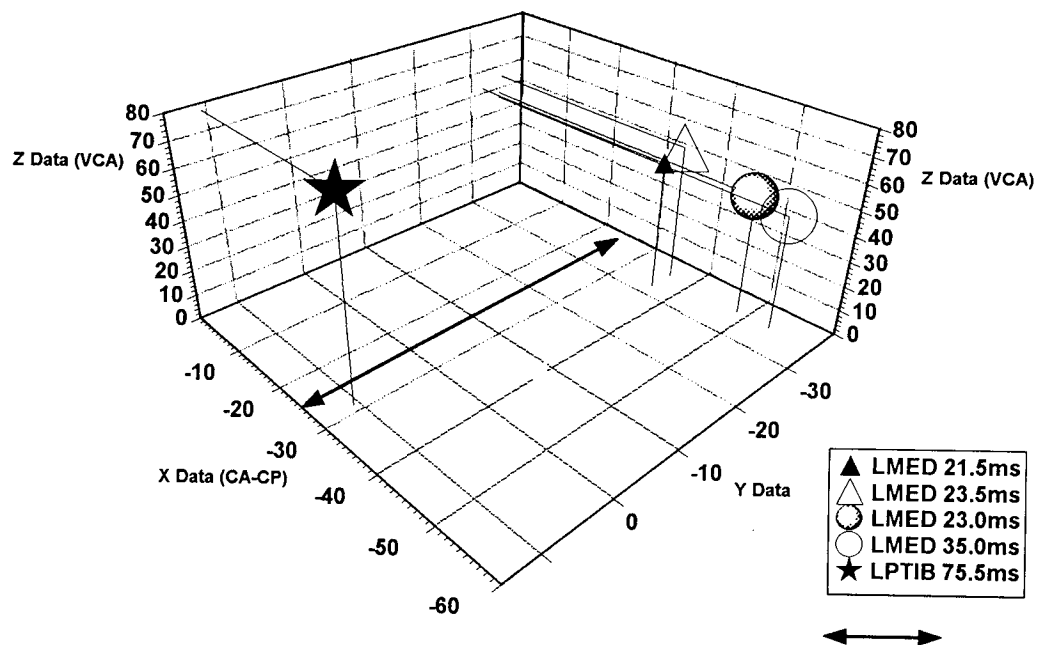


Figure 5.16 Median nerve and Posterior Tibial nerve localisations in patient DT. Relative sizes of the localisation icons reflect the proportional sizes of the corresponding confidence volumes. The double arrow indicates the predicted position in the x-y axis of the line of the central sulcus.

#### 5.4.2.5.2 Neuro-Radiological prediction

Neuro-Radiological assessment of the MRI predicted that the MEG localisations were located in the **pre-central gyrus** and not post-centrally as detailed above.

## Chapter 5

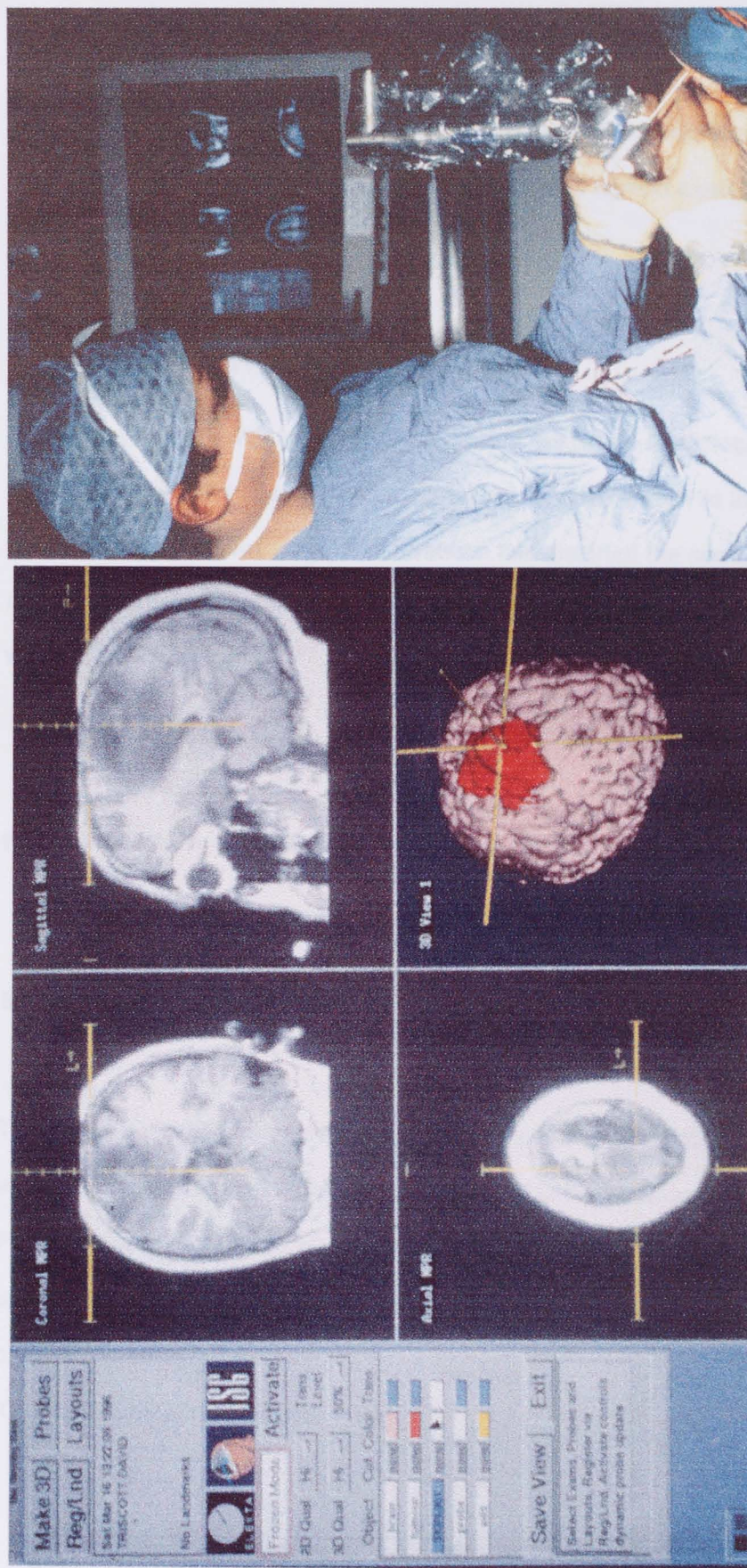


Figure 5.17 Photograph (left) of the display screen of the surgical ISG wand system taken during surgery on patient DT. Yellow cross hairs indicate the position of the hand held wand (right).



#### 5.4.2.6 Surgical validation

Use of the ISG wand confirmed that cortical surface stimulation together with intra-operative somatosensory evoked potential measures agreed exactly with the sensory localisation from MEG measures.

#### 5.4.2.7 Summary - Patient DT

In patient DT, there was a discrepancy between the Neuro-Radiological assessment of hand function and that predicted by MEG which appeared to lie in the pre-central gyrus. Clearly, previous surgical intervention had distorted the normal neuroanatomical landmarks. However, intra-operative measures confirmed that MEG was entirely accurate.

### **5.4.3 Case Study 3: Patient SM**

#### 5.4.3.1 Clinical History

This 38 year old woman presented with a history of onset of epilepsy at age 9 years, with generalised seizures almost certainly related to birth trauma.

Presented with Right sided weakness with shorter limbs. MRI showed a lesion in the upper left hemisphere possibly responsible for focal motor seizures. Surgical removal of lesion planned.

IQ of 129 (superior) and intact memory.

#### 5.4.3.2 Investigations

EEG's in the past had shown Left posterior temporal and Left medial temporal involvement.

SPECT showed hypoperfusion in medial aspect of Rt temporal lobe with minor reduction in Lt cortex.

Sphenoidal EEG showed bilateral activity.

MRI showed small area of high signal in corona radiata and at junction of grey and white matter in the upper Left hemisphere.

WADA was suggestive of Left hemisphere dominance for language but Right hemisphere not tested due to complications. Memory was intact for both hemispheres.

Magnetometry was performed at the Clinical Neurophysiology Unit at Aston University on 25th July 1995 to localise Right hand and foot function using Somatosensory Evoked Response techniques.

#### 5.4.3.3 Magnetometry Results - Patient SM

Stimulation of the Right Median nerve at the wrist and Right Posterior Tibial nerve at the ankle produced reproducible magnetic field waveforms (Fig. 5.18). Those for posterior tibial stimulation were much reduced in amplitude in comparison with the control population. Inverse solution algorithms were applied to the data to obtain source localisation co-ordinates. Goodness of fit analysis indicated statistically significant correlation coefficients ( $p > 0.95$ ) between 22.0 milliseconds and 48.5 milliseconds for Right median nerve stimulation and at 89.5 milliseconds for Right Posterior Tibial nerve stimulation.

Monte Carlo analysis was performed on the data to assess 95% confidence boundaries for the source localisation's. Confidence ellipses with volumes of less than  $2 \text{ cm}^3$  were then superimposed onto the MR images. The lowest volumes for Right median nerve data was obtained at 47.5ms ( $8000 \text{ mm}^3$ ).

Confidence boundaries for Right Posterior Tibial nerve data exceeded the volume criterion limit and so could not be regarded as robust.

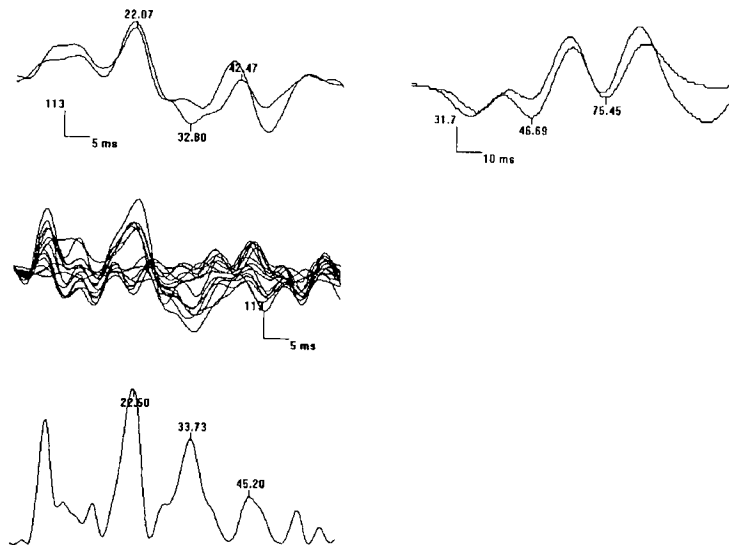
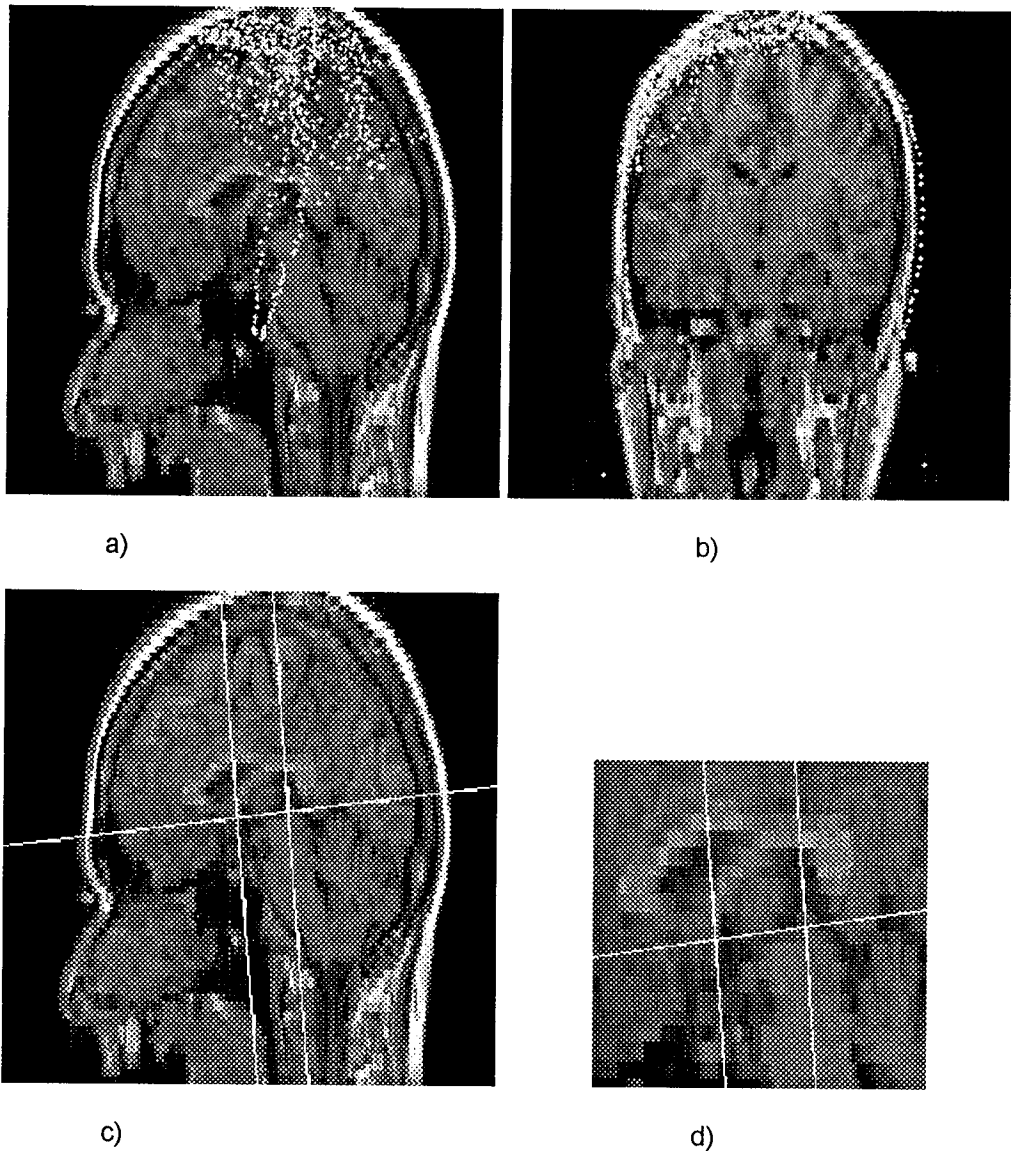


Figure 5.18 Patient SM. Separate trials of right median nerve (left upper) and right posterior tibial nerve (right upper) magnetic field waveforms are superimposed for comparison. Magnetic field waveforms (middle) from 19 simultaneously acquired MEG channels following Right Median nerve together with the corresponding Global Field Power analysis of the data. The latencies indicated are those from which single equivalent dipole models were calculated.

#### 5.4.3.4 MEG-MRI Co-Registration

MRI's were acquired with the bite bar in situ. Bite bar markers were located from the MRI and a matching matrix derived. This match was checked by plotting a digitised head shape onto the MRI (Figure 5.19 a & b)

Slice thickness of the MRI was 3mm. Using a midline slice (131), co-ordinate matching as defined by Talairach was attempted (Figure 5.19 c & d).



*Figure 5.19 Plates a) and b) show digitised head shape files acquired during MEG acquisition superimposed onto the MRI. This was used to check the quality of the matching transformation matrix. Plates c) and d) show the baselines for the Talairach co-ordinate system superimposed onto the mid-line MRI slice.*

Having matched the MEG and MRI co-ordinate systems, MEG dipole localisations were co-registered with the MRI. These are shown overleaf in Figures 5.20a-c).

## Chapter 5

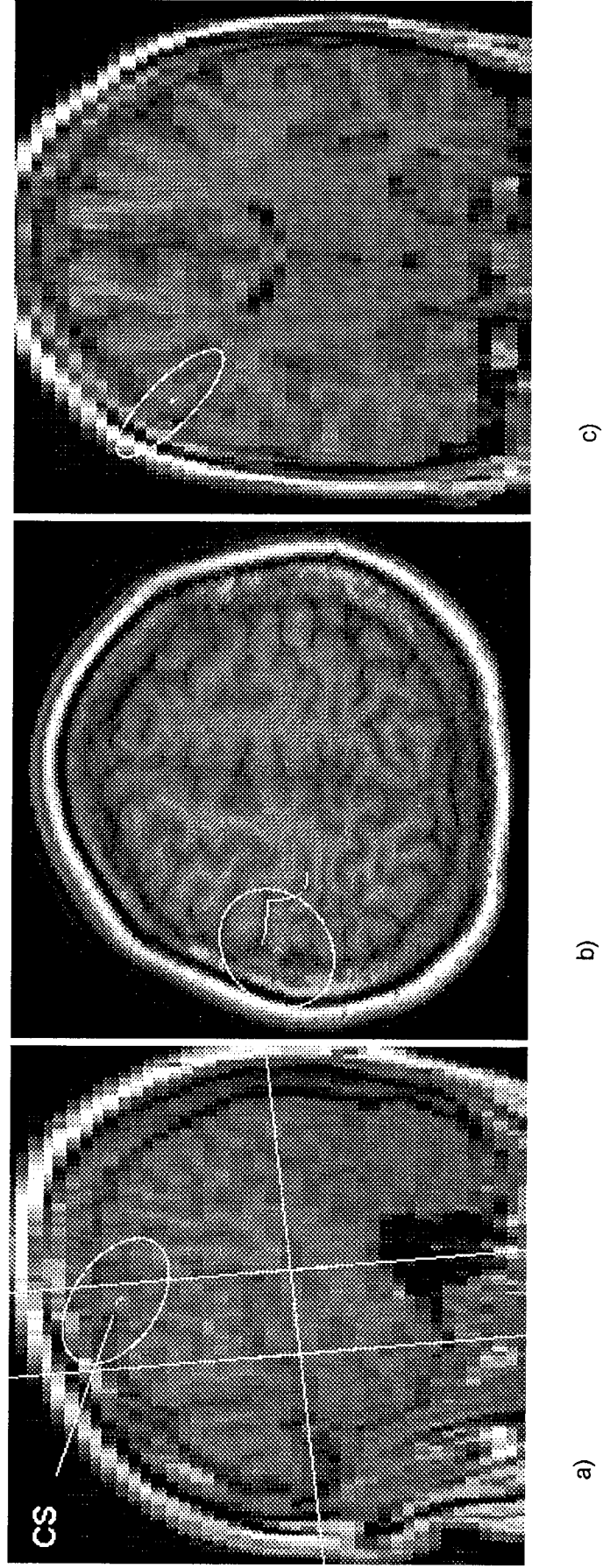


Figure 5.20 Patient SM: Smallest confidence volume for Right median nerve stimulation co-registered with the MRI. Sagittal slice in plate a) shows the confidence volume with respect to the Talairach co-ordinate baselines. In plate b), the predicted line of the central sulcus is indicated by the white line.

## 5.4.3.5 Predicted line of the central sulcus

Localisations for median nerve (at latencies of 40.5 and 47.5ms) yielded a mean Talairach co-ordinate of:

CA-CP axis: -23.5 mm      Lateral axis: 43.9 mm      VCA-VCP axis: 43.6 mm.

Neuroanatomical inspection of the MRI together with Talairach co-ordinate data suggested that the dipoles were localised to the post-central gyrus in this patient. This is depicted graphically below (Fig 5.21).

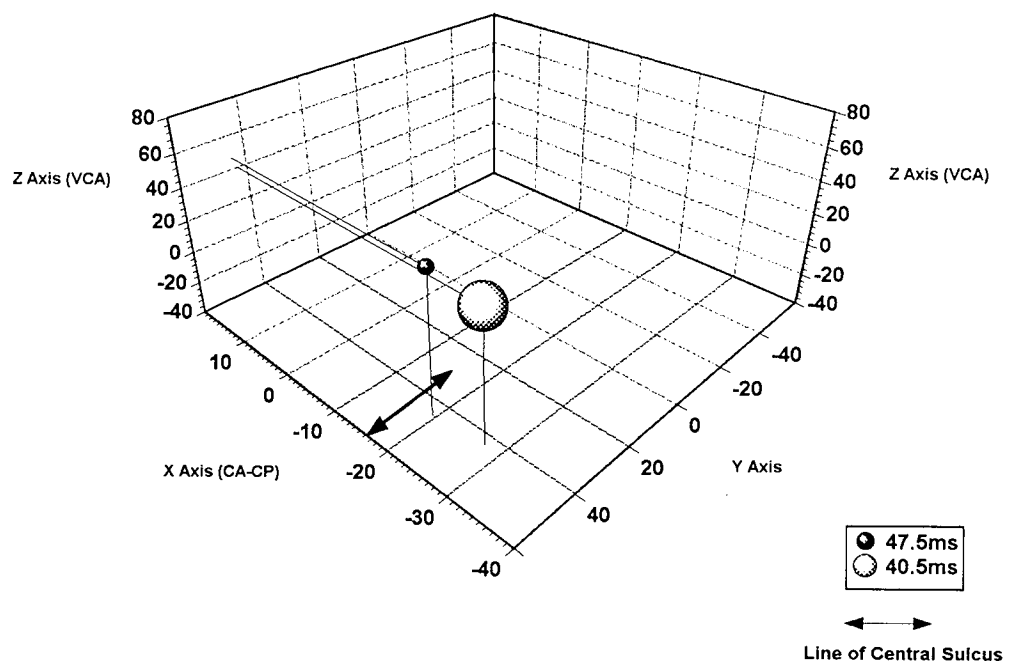


Figure 5.21 Right median nerve localisations in patient SM. Relative sizes of the localisation icons reflect the proportional sizes of the corresponding confidence volumes. The double arrow indicates the predicted position in the x-y axis of the line of the central sulcus.

## 5.4.3.6 Surgical validation

A craniotomy was performed over the left fronto-temporo-parietal regions to expose both the lesion and the expected area encompassing the sensory-motor cortex. Once the cortex was exposed, strips of electrodes were placed across the cortical surface in the area around the sensory-motor region. Somatosensory evoked potentials were recorded to confirm the line of the central sulcus.

Cortical SEP's confirmed the predicted position of the central sulcus from Magnetometry and Neuro-Radiographic assessment.

### 5.4.4 Case study 4: Patient JC

#### 5.4.4.1 Clinical History:

This 28 year old man presented with Right hemiplegia with some wasting and shortening of the Right limbs together with Right hemiathetosis brought out by voluntary movement. Diagnosed as a Thalamic infarct.

Of normal delivery, had first Tonic-Clonic seizure in 1979 with occasional episodes since. In 1987 had 3 days of almost continuous partial status.

Current seizure pattern include twitches in the Right hand every day which may last all morning. Episodes of head turning to the Right for up to one hour.

Episodes of loss of memory and vagueness for approximately 1 minute, occurring once per week.

Very disabled. Unable to work, ride bike, difficulty in dressing etc.

#### 5.4.4.2 Investigations

Routine EEG (15/7/94) shows repeated runs of Left fronto-central high voltage rhythmical sharp waves.

MRI (1.5 tesla) (19/5/95) Right hemisphere normal. Left hemisphere reduced in size with mild corresponding decrease in size of vault on this side. There is ex vacuo dilation of Left lateral ventricle and a large well defined area of tissue loss conforming to the MCA territory consistent with a major birth infarct.

SPECT (23/2/95) Striking loss of blood flow in the Left posterior frontal and temporal regions. In addition there is some hypoperfusion in the posterior temporal region on the right.

Neuropsychology: WMS -R performances severely impoverished for both verbal and non-verbal material. Evidence of extra-temporal dysfunction. Extremely poor verbal fluency.

**Magnetometry** was performed at the Clinical Neurophysiology Unit at Aston University on November 30th 1995 to localise Right hand function using Somatosensory Evoked Response techniques.

### 5.4.4.3 Magnetometry Results - Patient JC

The Right median nerve was stimulated but despite numerous attempts, clear signals could not be elicited. Left median nerve stimulation was also measured for comparison and clear, reproducible signals were obtained from this side (Fig. 5.22)

Inverse solution algorithms were applied to the data to obtain source localisation coordinates. Goodness of fit analysis indicated statistically significant correlation coefficients ( $p > 0.95$ ) between 23.5 milliseconds and 29.0 milliseconds for Left median nerve stimulation.

Monte Carlo analysis was performed on the data to assess 95% confidence boundaries for the source localisation's. Confidence ellipses with volumes of less than  $2 \text{ cm}^3$  were then superimposed onto the MR images. The smallest confidence volumes for Left median nerve data were obtained at 24.0ms ( $1941 \text{ mm}^3$ ).



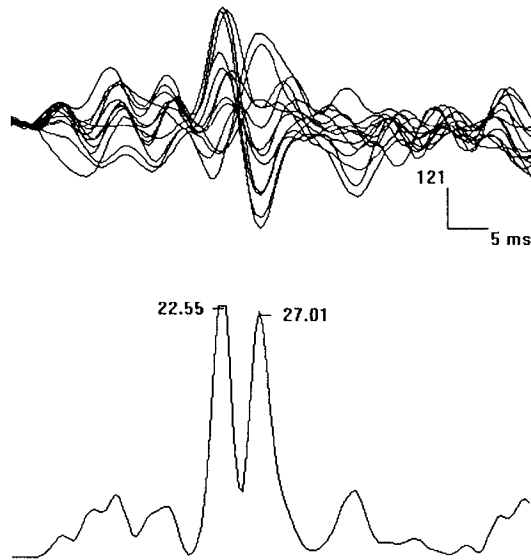


Figure 5.22 19 MEG channels of data

superimposed following Left median nerve stimulation in patient JC (upper traces). Beneath the corresponding Global Field Power plot is shown. The latencies indicated are those from which single equivalent dipole models were calculated.

#### 5.4.4.4 MEG-MRI Co-registration

MRI's were acquired with the bite bar in situ. Bite bar markers were located from the MRI and a matching matrix derived. This match was checked by plotting a digitised head shape onto the MRI

Slice thickness of the MRI was 2mm. Using a midline slice (127), co-ordinate matching as defined by Talairach was attempted (Figures below)

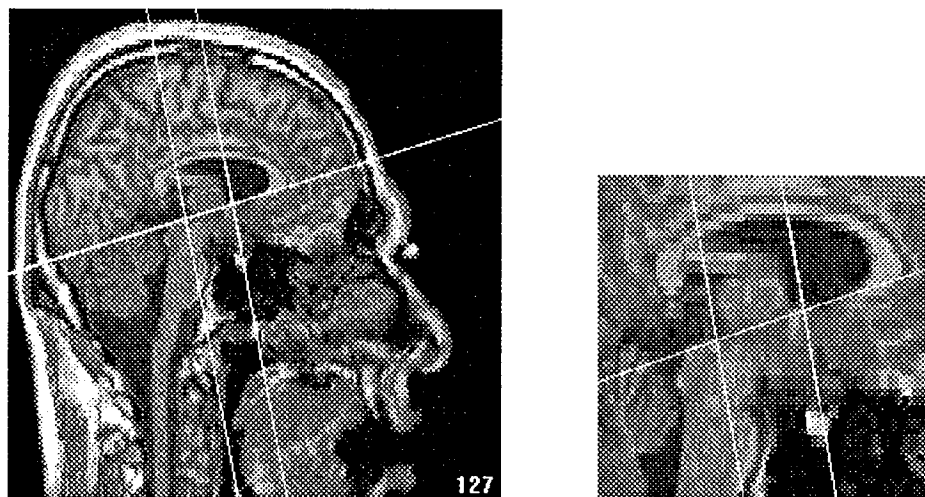
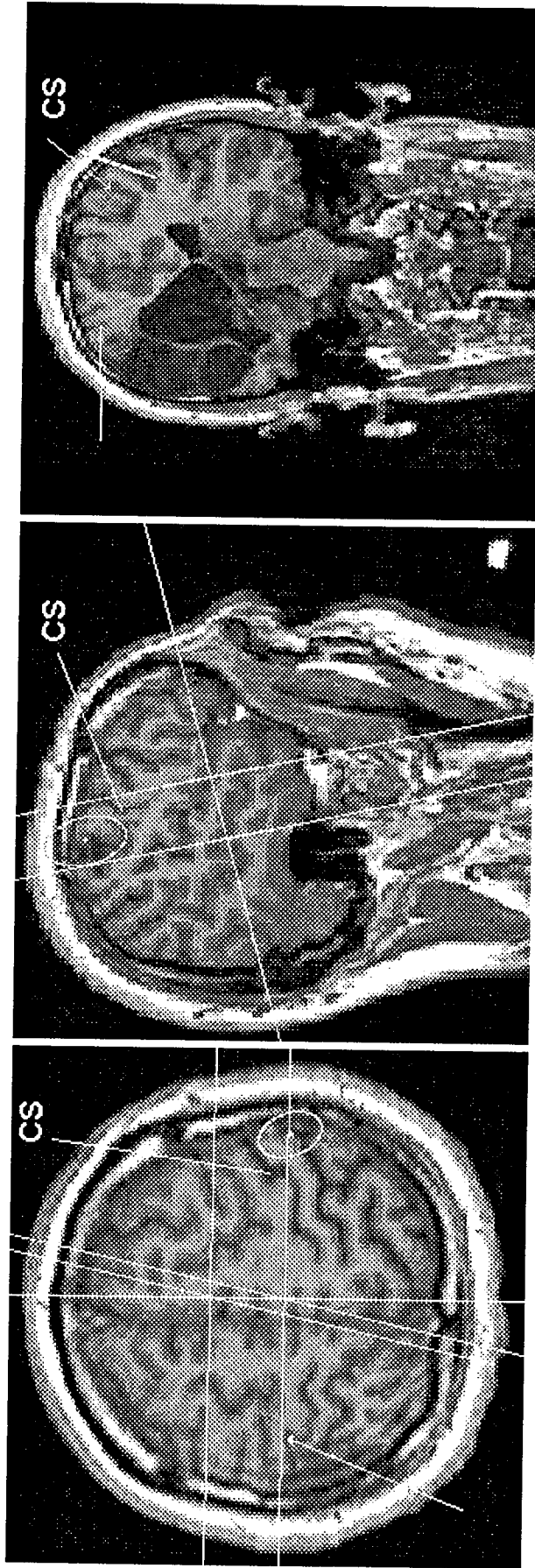


Figure 5.23 Plates show the baselines for the Talairach co-ordinate system superimposed onto the mid-line MRI slice.



a)

b)

c)

Figure 5.24 MEG dipole localisations for patient JC. Plate a) shows the smallest confidence volume at 29.0 milliseconds co-registered with the appropriate MRI slice. The bilateral positions of the predicted line of the central sulcus are indicated. This data is shown in the respective saggital (plate b) and coronal planes (plate c).

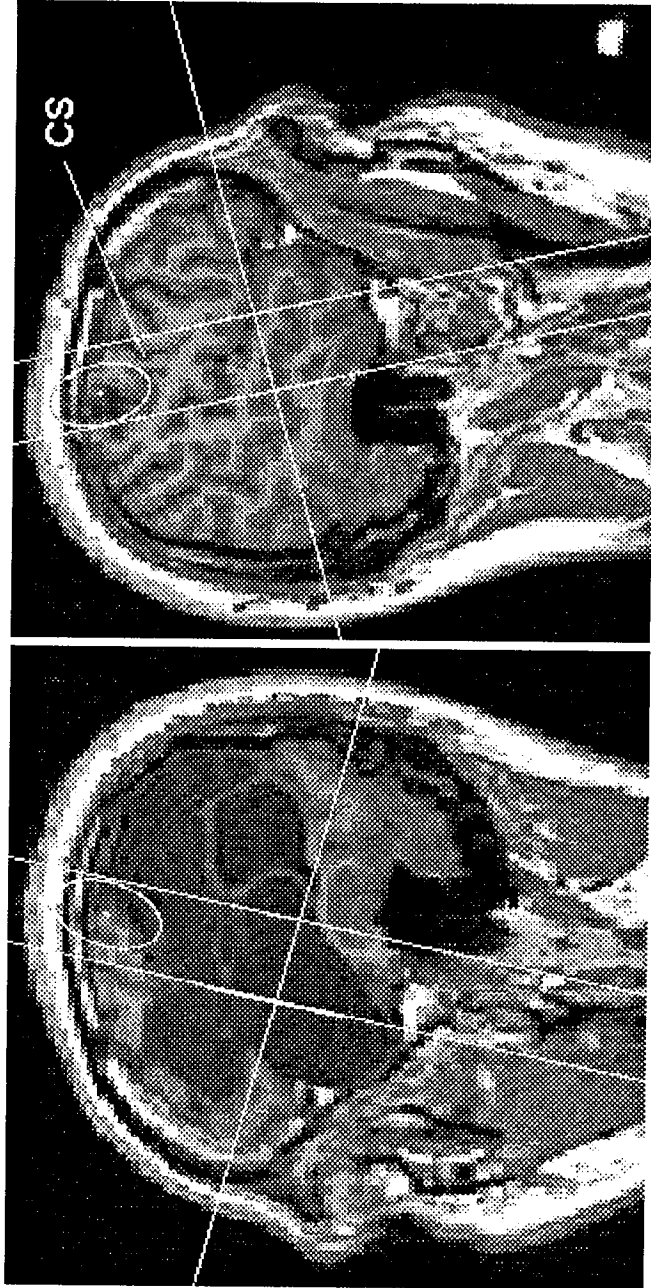


Figure 5.25 Since no dipole localizations could be made directly following right median nerve stimulation, an approximation of location of function in the left hemisphere was made based on symmetry of response in the opposite hemisphere.

## 5.4.4.5 Predicted line of the central sulcus

Localisations for two separate trials of median nerve stimulation (at latencies of 24.0 and 23.5ms) yielded a mean Talairach co-ordinate of:

CA-CP axis: -7.0 mm      Lateral axis: -54.4 mm      VCA-VCP axis: 46.6 mm.

Neuroanatomical inspection of the MRI together with Talairach co-ordinate data suggested that the dipole for trial 1 (smallest volume at 24.0 ms) was localised to the post-central gyrus in this patient. The central point for the larger volume of trial 2 was placed anterior to the first and possibly therefore within the pre-central gyrus. However, the confidence volume for trial 2 was slightly more than the required confidence limit ( $>2 \text{ cm}^3$ ) and so was not regarded as robust. The data is depicted graphically below (Fig 5.26).

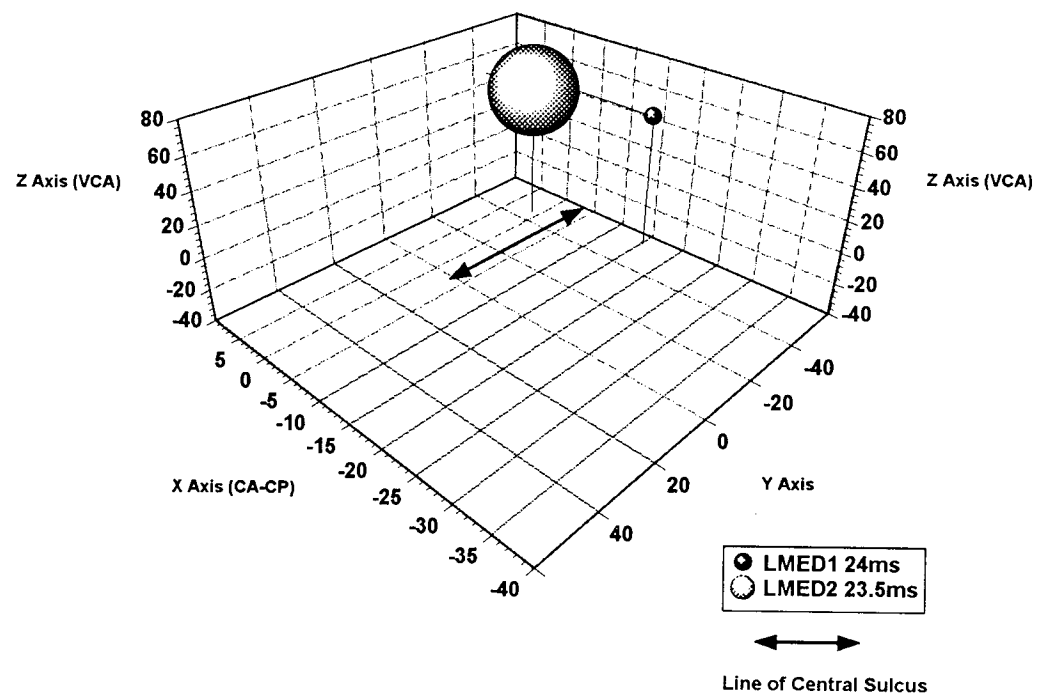


Figure 5.26 Left median nerve localisations in patient JC. Relative sizes of the localisation icons reflect the proportional sizes of the corresponding confidence volumes. The double arrow indicates the predicted position (in the x-y axis only) of the line of the central sulcus.

### 5.4.4.6 Surgical Validation

In this particular case, MEG localisation was based on symmetry of response between hemispheres.

At the time of writing, the patient had still to undergo surgery and so validation in this case was not possible. However, Neuro-Radiological assessment was in agreement with MEG determination as to the location of the hand area of the sensory cortex.

### 5.4.5 Case study 5: Patient TH

#### 5.4.5.1 Clinical History

This patient suffered a stroke in 1985 which left him with weakness on the Left side of body with involuntary movement of Left arm. Presented with chronic head pain as well as pain in Left arm and Left upper body. Medication includes Carbamazepine, Epilim and Valium. Previously prescribed Morphine which was apparently ineffective against the pain.

Considered for cortical surgery to explore implant for pain relief.

#### 5.4.5.2 Investigations

Magnetometry was performed on January 16th 1996 but clear signals from the affected side could not be recorded. A repeat recording was attempted on February 26th 1996. The results of the second visit are detailed overleaf.

### 5.4.5.3 Magnetometry Results - Patient TH

Patient presented for Magnetometry with head pain and constant involuntary movement of LT hand and arm.

LT median nerve was stimulated but despite numerous attempts, clear signals could not be elicited. Despite the body movement the patient was able to maintain a reasonably stable position on the bite bar apparatus. RT median nerve stimulation was also measured to attempt to predict, through symmetry, the functional localisation of the left hand. Clear reproducible signals were obtained from this side (Figure 5.27).

Inverse solution algorithms were applied to the data to obtain source localisation coordinates. Goodness of fit analysis indicated statistically significant correlation coefficients ( $p > 0.95$ ) at 24.0 milliseconds and 40.5 milliseconds for Right median nerve stimulation.

Monte Carlo analysis was performed on the data to assess 95% confidence boundaries for the source localisation's. Confidence ellipses with volumes of less than  $2 \text{ cm}^3$  were then superimposed onto the MR images. The smallest confidence volumes for Right median nerve data was obtained at 24.0ms ( $423 \text{ mm}^3$ ).

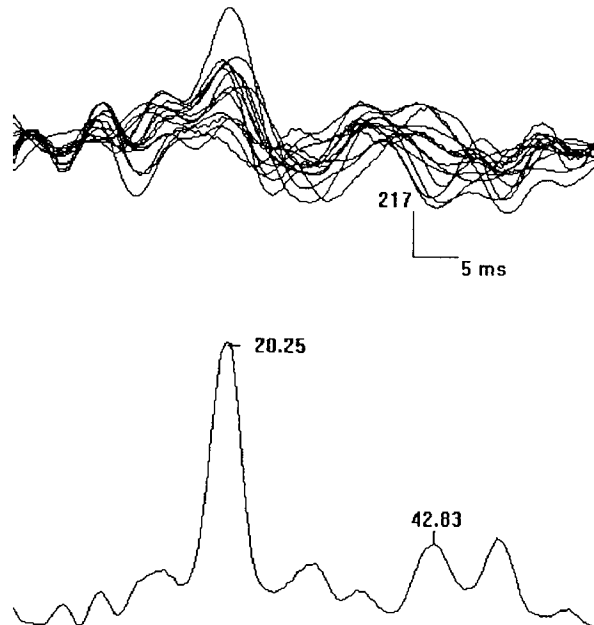


Figure 5.27 Upper figure shows the magnetic field waveforms following Right median nerve stimulation in patient TH. The lower figure shows the corresponding Global Field Power plot. The latencies indicated are those from which single equivalent dipole models were calculated.

#### MEG-MRI co-registration

MRI's were acquired with the bite bar in situ. Slice thickness of the MRI was 1.25mm. Bite bar markers were located from the MRI and a matching matrix derived. This match was checked by plotting a digitised head shape onto the MRI. Talairach co-ordinates were derived. A mid-line sagittal slice was selected to identify the anterior and posterior commissures. CA-CP and VCA lines were constructed (Figure 5.28).

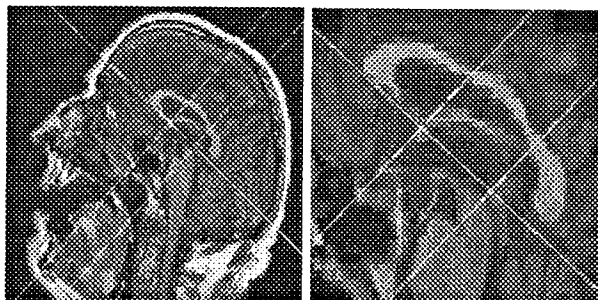
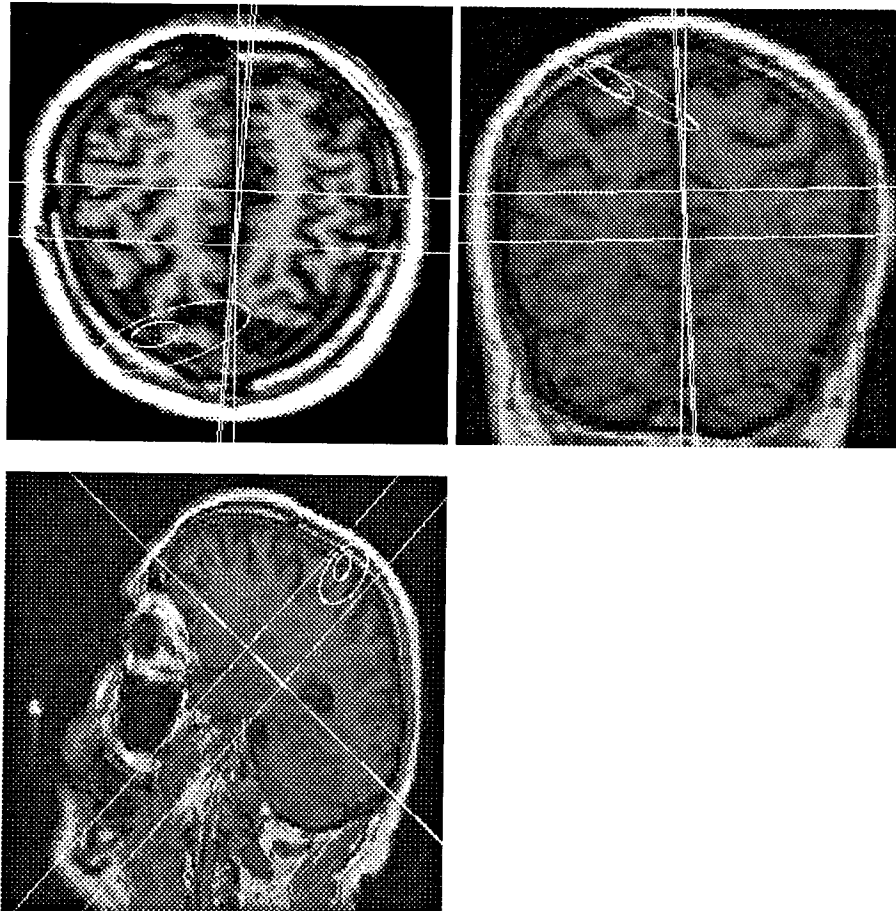


Figure 5.28 Talairach co-ordinate lines were constructed from the location of the anterior and posterior commissures in a midline sagittal slice.

## 5.4.5.4 MEG-MRI Source localisations

95% confidence volumes were co-registered with the MRI.



*Figure 5.29 Right median nerve source localisations for patient TH. Ellipses were obtained at 24.0 ms (smallest volume) and 40.0 ms.*

Although Left median nerve data was not obtained from this patient, prediction through symmetry of cortical function was attempted. This data is shown in Figure 5.30 overleaf.



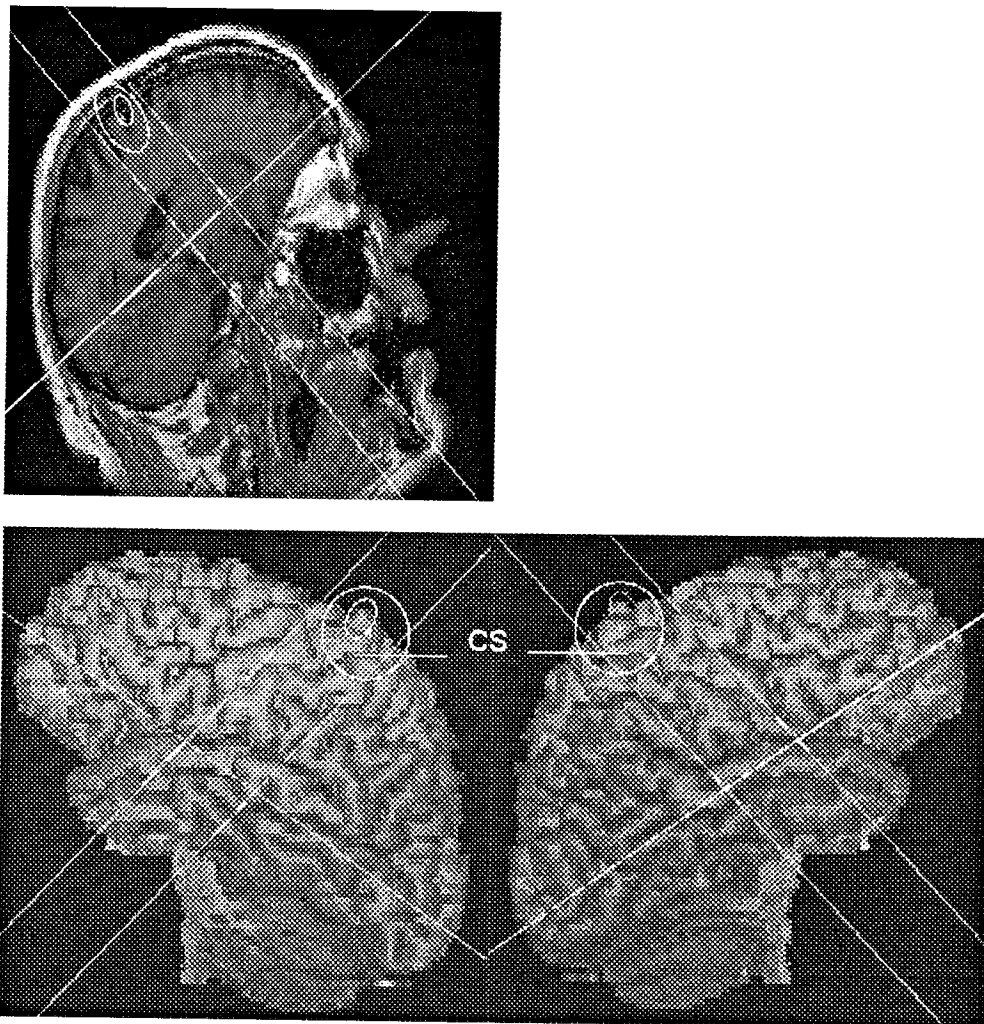


*Figure 5.30 Neuro-Radiological prediction of the line of the central sulcus in the right hemisphere from symmetry of functional localisation computed for the left hemisphere.*

#### 5.4.5.5 Prediction of the central sulcus

Mean Talairach co-ordinates for the two confidence volumes for right median nerve stimulation co-registered with the MRI were:

CA-CP axis: -11.4 mm      Lateral axis: 19.6 mm      VCA-VCP axis: 61.6mm.

Neuro-Radiological inspection of the MRI together with Talairach co-ordinate data suggested that the confidence volumes were centred on the anterior wall of the pre-central gyrus in this patient. The predicted relationship with the central sulcus therefore is depicted graphically overleaf (Fig 5.31).

### 5.4.6 Case Study 6: Patient AS

#### 5.4.6.1 Clinical history

At the age of 4 years this patient had a history of myoclonic jerks of the Right leg, though there was a possibility of earlier seizures at age 18 months. No apparent aetiology.

Normal birth though developmental milestones slightly delayed.

Mother has epilepsy.

At the time of the MEG investigation, aged 16, this young man presented with frequent sensations of electric shocks and pain in Rt leg with no warning. Least severe symptoms included Rt leg extension and stiffness. Most severe symptoms involved stiffness of the whole body and abduction of the arms and crossing of the legs. On these occasions the patient could fall and injure himself. There were some movement in these fits which lasted up to 2 minutes though not associated with any impairment of consciousness. Speech was never affected.

The patient could have runs of jerking affecting the whole body repeatedly over a 2 hour period which could occur from one to seven days per week.

#### 5.4.6.2 Investigations

Routine EEG's had shown a persistent Lt hemisphere focus localised to the centroparietal area. Additionally, abundant sharp waves and spike discharges had been observed multifocally but especially in the Lt parietal region.

MRI's in 1991 and 1995 revealed no abnormalities.

SPECT in 1993 similarly revealed no abnormalities.

Magnetometry was performed at the Clinical Neurophysiology Unit at Aston University on 11th March 1996 to localise Right hand and foot function using Somatosensory Evoked Response techniques.

## 5.4.6.3 Magnetometry Results - Patient AS

Stimulation of the Right and Left Median nerves at the wrist produced reproducible magnetic field waveforms (Figure 5.32). Inverse solution algorithms were applied to the data to obtain source localisation co-ordinates. Goodness of fit analysis indicated statistically significant correlation coefficients ( $r > 0.95$ ) at 18.0 milliseconds and 30.5 milliseconds for Right median nerve stimulation and 18.5ms, 26.5ms and 32.5ms following Left median nerve stimulation.

Stimulation of the Posterior tibial nerves at the ankles did not yield data of sufficient quality to produce significant correlations.

Monte Carlo analysis was performed on the Median nerve data to assess 95% confidence boundaries for the source localisations. Lowest volumes for both Right and Left median nerve data were obtained from data between 30.5 - 32.0ms.

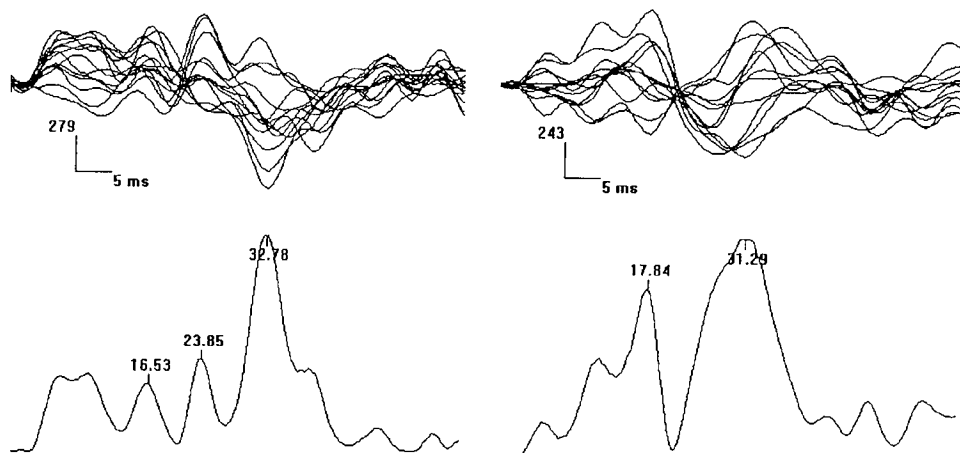


Figure 5.32 Upper traces show magnetic field waveforms following Right (right side traces) and Left Median nerve stimulation. Below these are the corresponding Global Field Power analysis of the data. The latencies indicated are those from which single equivalent dipole models were calculated.

## 5.4.6.4 MEG - MRI Co-Registration

Due to the frequency of jerking in this patient, MRI's were acquired under general anaesthesia. MEG bite bar was taped in position in the patients mouth during MRI acquisition. This methodology will have increased the possibility of displacement error for subsequent MEG / MRI matching. Slice thickness of the MRI was 1mm. MRI quality was poor. Bite bar markers were located from the MRI with some difficulty and a matching matrix derived. This match was checked by plotting a digitised head shape onto the MRI.



Figure 5.33 MEG-MRI matching matrix confirmation by superimposition of digitised headshape file acquired during MEG measurements.

A mid-line sagittal slice was selected to indentify the anterior and posterior commissures. CA-CP and VCA lines were constructed (Figure 5.34).

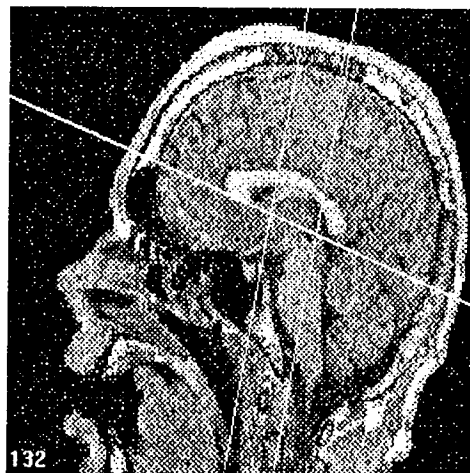


Figure 5.34 Talairach co-ordinate lines were constructed from the location of the anterior and posterior commissures in a midline sagittal slice.

#### 5.4.6.5 MEG-MRI Source localisation

Confidence ellipses of volumes less than  $2 \text{ cm}^3$  were superimposed onto the MR images (Figures 5.35 & 5.36).

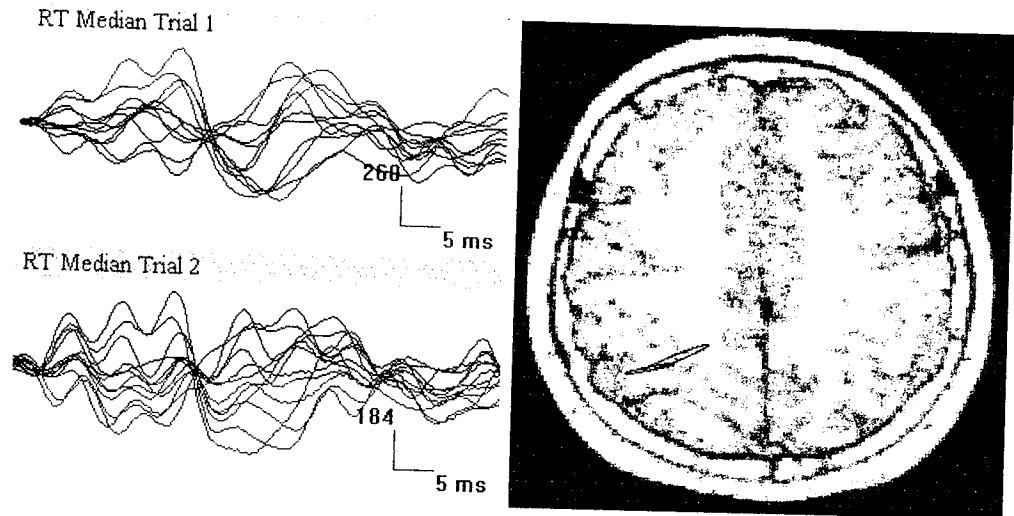


Figure 5.35 Several trials of each stimuli were performed to assess reliability of response. Latencies from the two trials shown above were at 31.0ms (Trial 1, green ellipse) and 30.5ms (trial 2, blue ellipse).

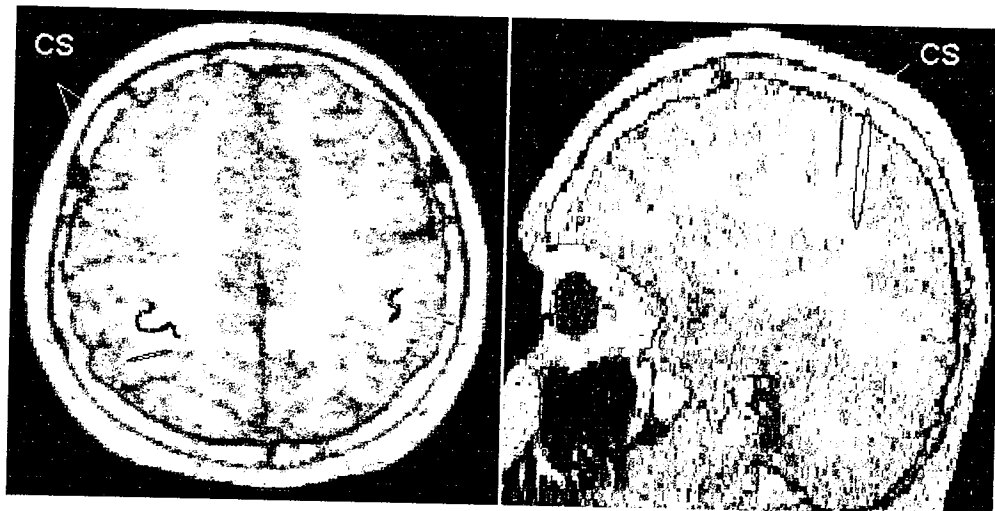


Figure 5.36 Smallest confidence volumes from both right (green ellipse) and left median nerve stimulation were co-registered with the MRI and the predicted line of the central sulcus indicated. Latencies of the right and left hemisphere confidence volumes were 30.0 and 32.0 milliseconds respectively.

## 5.4.6.6 Predicted location of the central sulcus

Mean Talairach co-ordinates for the confidence volumes for median nerve stimulation co-registered with the MRI were:

## Right Median

CA-CP axis: -39.5 mm      Lateral axis: 27.5 mm      VCA-VCP axis: 37.6 mm.

## Left Median

CA-CP axis: -27.6 mm      Lateral axis: -51.7 mm      VCA-VCP axis: 46.5 mm.

Neuroanatomical inspection of the MRI together with Talairach co-ordinate data suggested that the dipoles were localised to the post-central gyrus in this patient.

This is depicted graphically below (Fig 5.37).

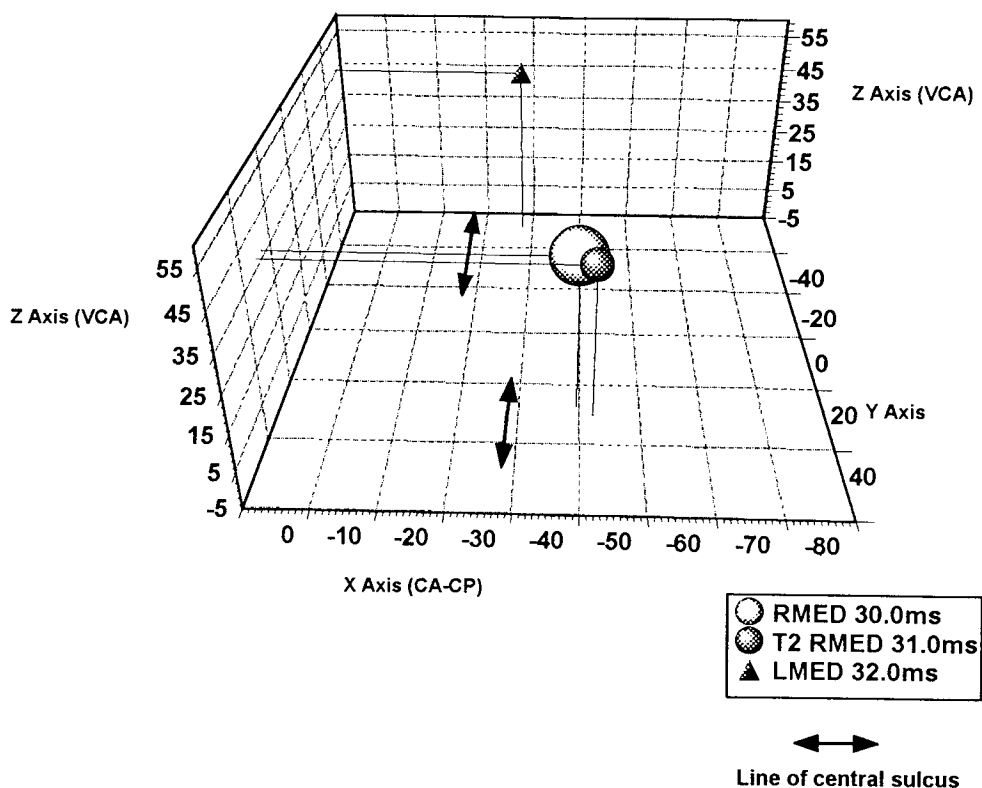


Figure 5.37 Smallest confidence volumes from two trials of Right Median nerve localisations and one Left median trial in patient AS. Relative sizes of the localisation icons reflect the proportional sizes of the corresponding confidence volumes. The double arrow indicates the predicted position in the x-y axis of the line of the central sulcus.

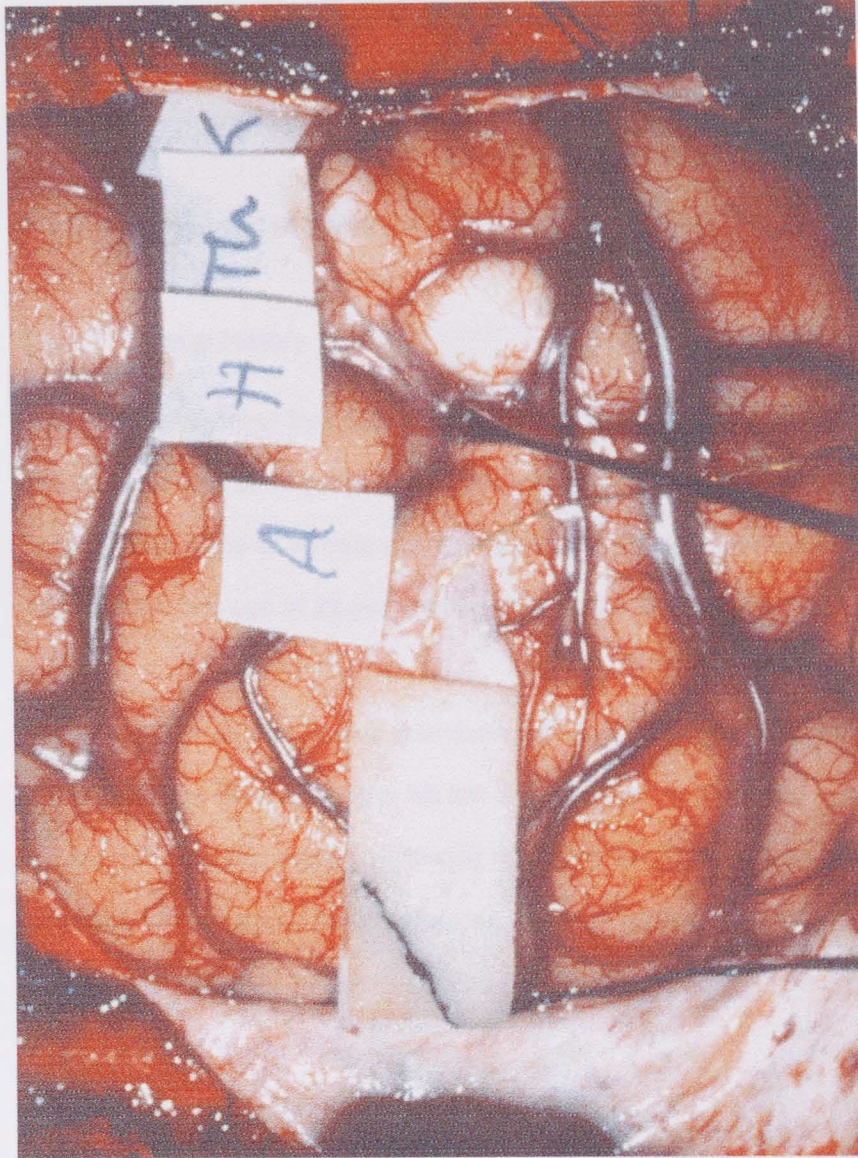


Figure 5.38 Patient AS. Labelling following electrical stimulation of the surface of the cortex to monitor motor function.

A = arm, H = hand, Th = thumb.

### 5.4.6.7 Surgical validation - Patient AS

Intra-operative somatosensory evoked response techniques together with cortical stimulation (Figure 5.38) confirmed the predicted line of the central sulcus in this patient. MEG localisations were therefore towards the posterior wall of the post-central gyrus.

### 5.4.7 Case study 7: Patient AD

#### 5.4.7.1 Clinical History

Patient AD presented for MEG investigation at the age of 49 years with a history of onset of seizures at 14 years of age. Attacks consisted of shaking of left leg.

Surgery took place at 16 years of age to remove fibrillary astrocytoma. Seizures stopped until the age of 22 years when they recurred and had gradually become worse.

At presentation he was having 3 seizures per day. Only rarely did he get a warning in the form of a funny feeling in his left leg from the waist down. He would then black out and fall over backwards. Following this there would be a period of acute confusion accompanied by lip smacking although without twitching of limbs. During this episode he would be totally unaware of events.

#### 5.4.7.2 Investigations

MRI showed the expected evidence of previous surgery in the high right fronto-parietal area. There was no evidence of recurrent or residual tumour.

Planned investigations: Video EEG monitoring; SPECT; Neuropsychological assessment

**Magnetometry** was performed at the Clinical Neurophysiology Unit at Aston University on March 19th 1996 to localise Left hand and foot function using Somatosensory Evoked Response techniques.



5.4.7.3 Magnetometry Results - Patient AD

Reproducible signals were obtained following both Left and Right median nerve stimulation at the wrist although the return fields were indistinct in each case. Poor signal to noise ratio's were obtained following stimulation of the Left Posterior Tibial nerve at the ankle.

Inverse solution algorithms were applied to the data to obtain source localisation coordinates. Goodness of fit analysis indicated statistically significant correlation coefficients ( $r > 0.95$ ) at 36.5 milliseconds and 50.5 milliseconds for Left median nerve stimulation and at 58 milliseconds for Right Median nerve stimulation.

Left Posterior Tibial nerve data was contaminated by high noise levels and no latency reached significance.

Monte Carlo analysis was performed on the data to assess 95% confidence boundaries for the source localisation's. Confidence ellipses with volumes of less than  $2\text{cm}^3$  were chosen for superimposition onto the MR images.

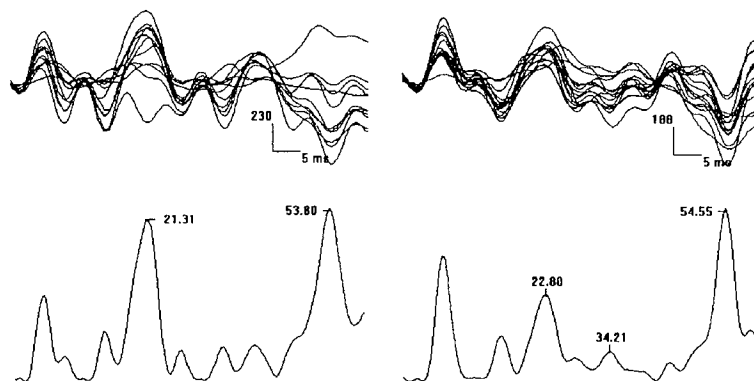


Figure 5.39 Magnetic field waveforms for Left (upper left) and right (upper right) median nerve stimulation. Beneath are the corresponding Global Field Power plots.

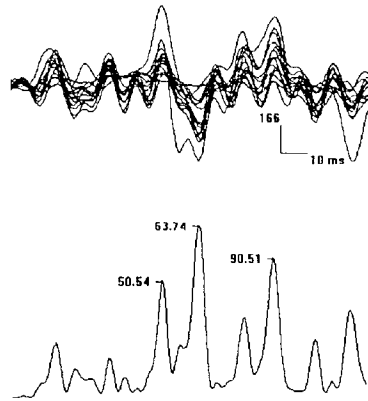
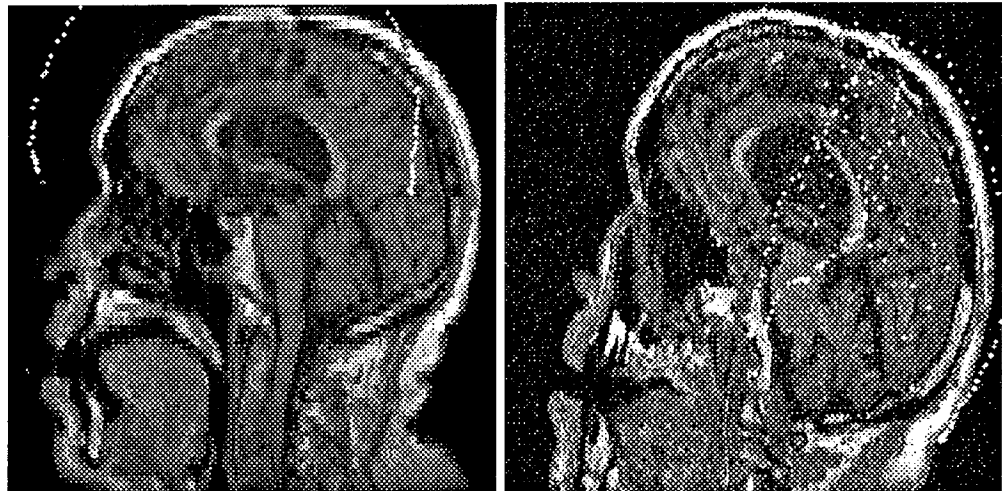


Figure 5.40 Left Posterior Tibial nerve data in patient AD.

The latencies indicated in the Global Field Power plot are those from which single equivalent dipole models were calculated. Unfortunately, at no latency were dipole fits at significance levels ( $r < 0.95$ ).

#### 5.4.7.4 MEG-MRI Co-registration

MRI's were acquired with the bite bar in situ allowing a co-registration matrix to be calculated. Matching an MRI of 3mm slice thickness, it became clear that a significant error had been introduced at some stage as the matching digitised head shape revealed (Figure 5.41a).



a)

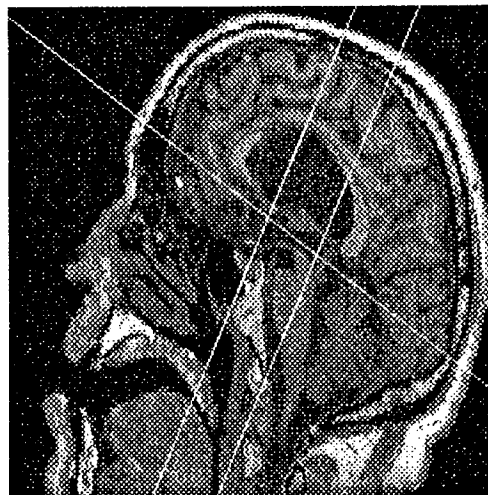
b)

Figure 5.41 Headshape files co-registered with the MRI of patient AD. Clearly, a positional error had been introduced in the first MRI (left plate a)). It later became clear that a mobile dental plate had been responsible for the misalignment of the bite bar in the mouth. The second MRI at 1.5mm slice thickness (b) shows the correct alignment.

## Chapter 5

It was ascertained that a mobile dental plate had been responsible for the misalignment of the bite bar in the MRI and so a second volume was arranged. Care was taken to ensure correct alignment and this proved successful as can be seen in Figure 5.41 b).

A mid-line sagittal slice was selected to identify the anterior and posterior commissures. CA-CP and VCA lines of the Talairach co-ordinate system were constructed (Figure 5.42).



*Figure 5.42 Talairach co-ordinate lines were constructed from the location of the anterior and posterior commissures in a midline sagittal slice.*

### 5.4.7.5 MEG-MRI Source localisations

95% confidence volumes for right and left median nerve data were co-registered with the MRI. Smallest volumes were at 36.0ms for Left median nerve stimulation and at 58.0ms for Right Median nerve stimulation

The appropriate MRI slices are illustrated overleaf.

## Chapter 5

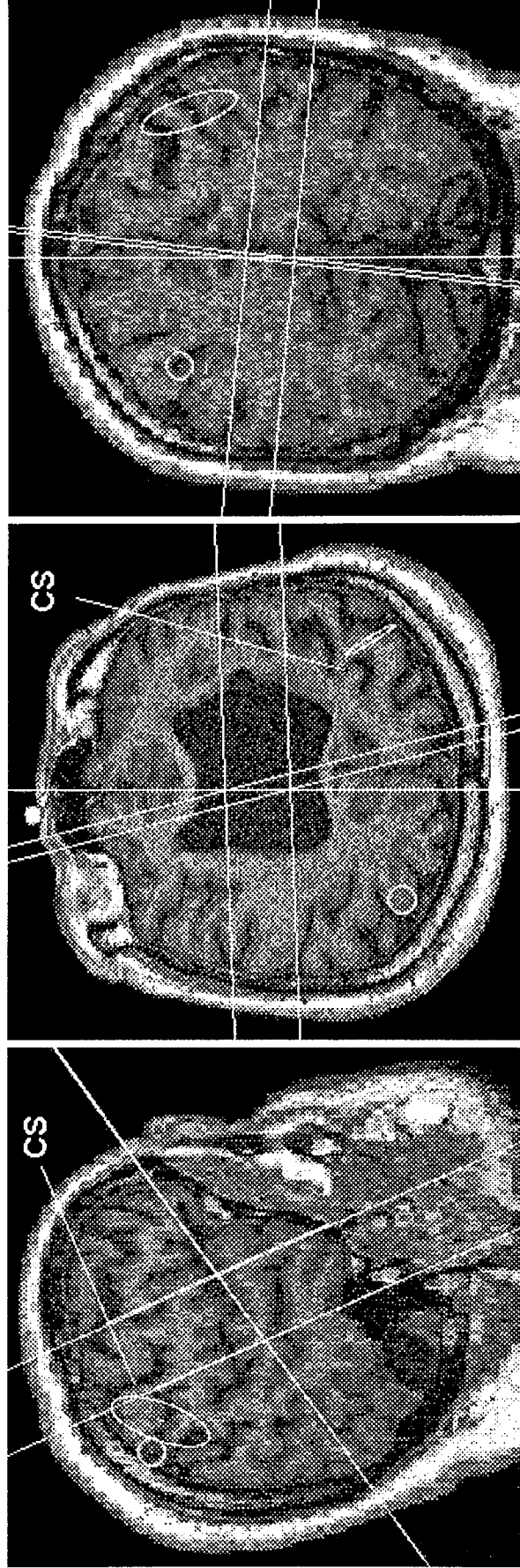


Figure 5.43 Source localisations for patient AD for right and left median nerve stimulation superimposed upon single slices for ease of comparison. The predicted line of the central sulcus (CS) is indicated.

5.4.7.6 Prediction of the central sulcus

Talairach co-ordinates for the confidence volumes for right and left median nerve stimulation co-registered with the MRI were:

Right Median:

CA-CP axis: -46.7 mm      Lateral axis: 47.8 mm      VCA-VCP axis: 55.3 mm.

Left Median:

CA-CP axis: -38.8 mm      Lateral axis: -37.7 mm      VCA-VCP axis: 48.1 mm.

Neuro-Radiological inspection of the MRI together with Talairach co-ordinate data suggested that the confidence volumes were located within the of the post-central gyrus in this patient. The relationship with the central sulcus is depicted graphically below (Fig 5.44).

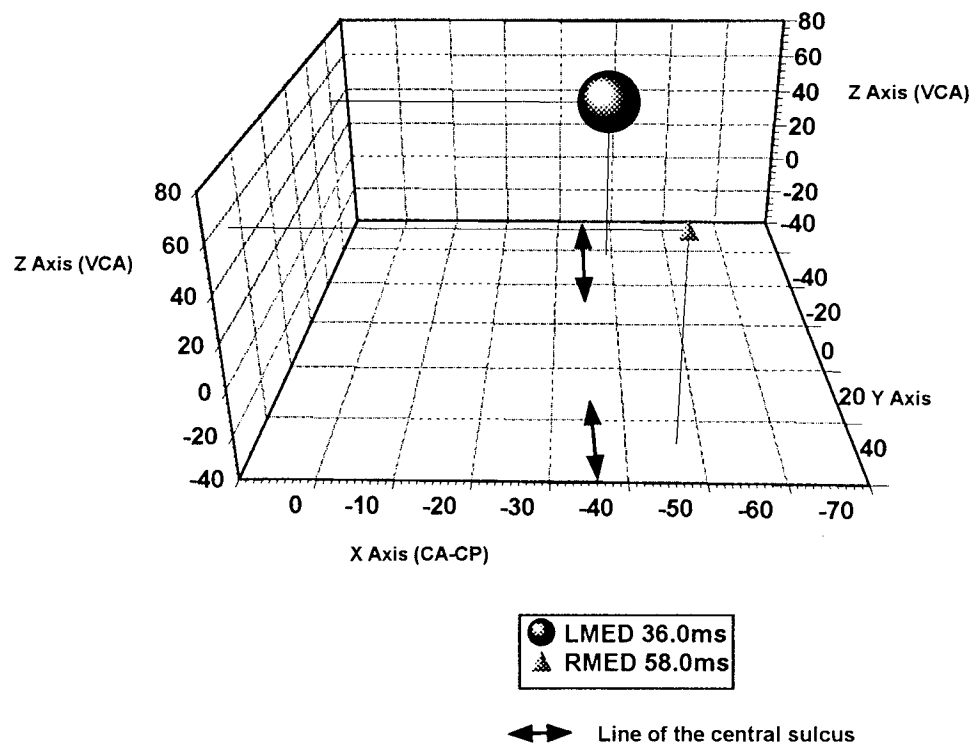


Figure 5.44      Smallest confidence volumes from trials of Right and Left Median nerve localisations in patient AD. Relative sizes of the localisation icons reflect the proportional sizes of the corresponding confidence volumes. The double arrow indicates the predicted position in the x-y axis of the line of the central sulcus.

#### 5.4.7.7 Surgical validation in patient AD

Intra-operative somatosensory and cortex stimulation techniques confirmed the predicted line of the central sulcus from both MEG and Neuro-Radiological assessments.

### **5.4.8 Case study 8: Patient DB**

#### 5.4.8.1 Clinical history

This 52 year old lady had a Right frontal glioma removed in 1985. She presented for re-investigation in 1996 following a recurrence of tonic-clonic seizures. These seizures were occurring without warning affecting Left lower then Left upper limb. There was no loss of consciousness.

#### 5.4.8.2 Investigations

Magnetometry was performed at the Clinical Neurophysiology Unit at Aston University on 12th June 1996 to localise Left hand and foot function using Somatosensory Evoked Response techniques.

#### 5.4.8.3 Magnetometry Results - Patient DB

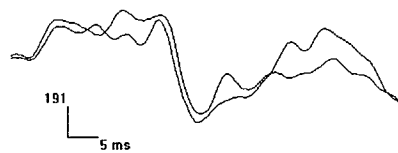
Stimulation of the Right Median nerve at the wrist produced reproducible magnetic field waveforms (Figure 5.45) despite a significant amount of electromagnetic interference.

Attempts to record data from the Right hemisphere to Left median or Posterior Tibial nerve stimulation had to be aborted due to the extreme electromagnetic interference which arose from the patient herself. It had to be concluded that this interference was likely to arise from metallic ties left from the previous craniotomy. This was to be confirmed.

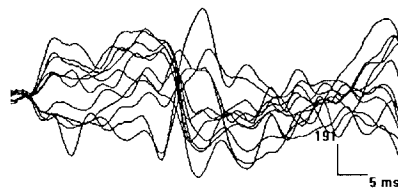
Left hemisphere data was as follows:

Inverse solution algorithms were applied to the data to obtain source localisation coordinates. Goodness of fit analysis indicated statistically significant correlation coefficients ( $p > 0.95$ ) between 21 and 29.5 milliseconds.

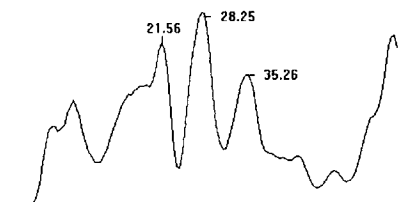
Monte Carlo analysis was performed on the Median nerve data to assess 95% confidence boundaries for the source localisation's.



a) Two separate Right Median nerve trials



b) 19 MEG channels superimposed



c) Global Field Power

*Figure 5.45 Magnetic Field waveforms following Right median nerve stimulation in patient DB. a) shows two separate trials superimposed to show repeatability. b) 19 channels of MEG data superimposed following a single trial of right median nerve stimulation and c) shows the corresponding Global Field Power plot for trial b).*

#### 5.4.8.4 MEG-MRI co-registration

MRI's were acquired with the bite bar in situ. Slice thickness was 1.5mm. Bite bar markers were located from the MRI and a matching matrix derived. This match was checked by plotting a digitised head shape onto the MRI (Figure 5.46 a).

Using a midline slice (131), co-ordinate matching as defined by Talairach was attempted (Figure 5.46 b).

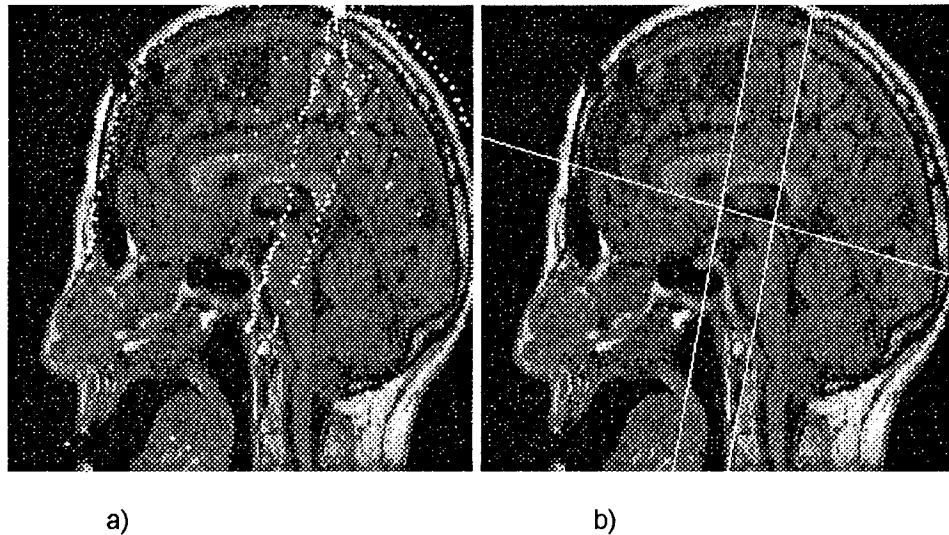


*Figure 5.46 Patient DB. Plate a) shows digitised head shape file, acquired at the time of the MEG acquisition, co-registered with the MRI. Plate b) shows the CA-CP and VCA-VCP lines of the Talairach co-ordinate system positioned on a mid-line slice.*

#### 5.4.8.5 MEG-MRI source localisation

Confidence ellipses of volumes less than  $2 \text{ cm}^3$  were superimposed onto the MR images. Lowest volumes were obtained from data at 29.5 milliseconds ( $180 \text{ mm}^3$ ) and 21.0 milliseconds ( $420 \text{ mm}^3$ ).

MRI slices following co-registration are shown overleaf (Figure 5.47).



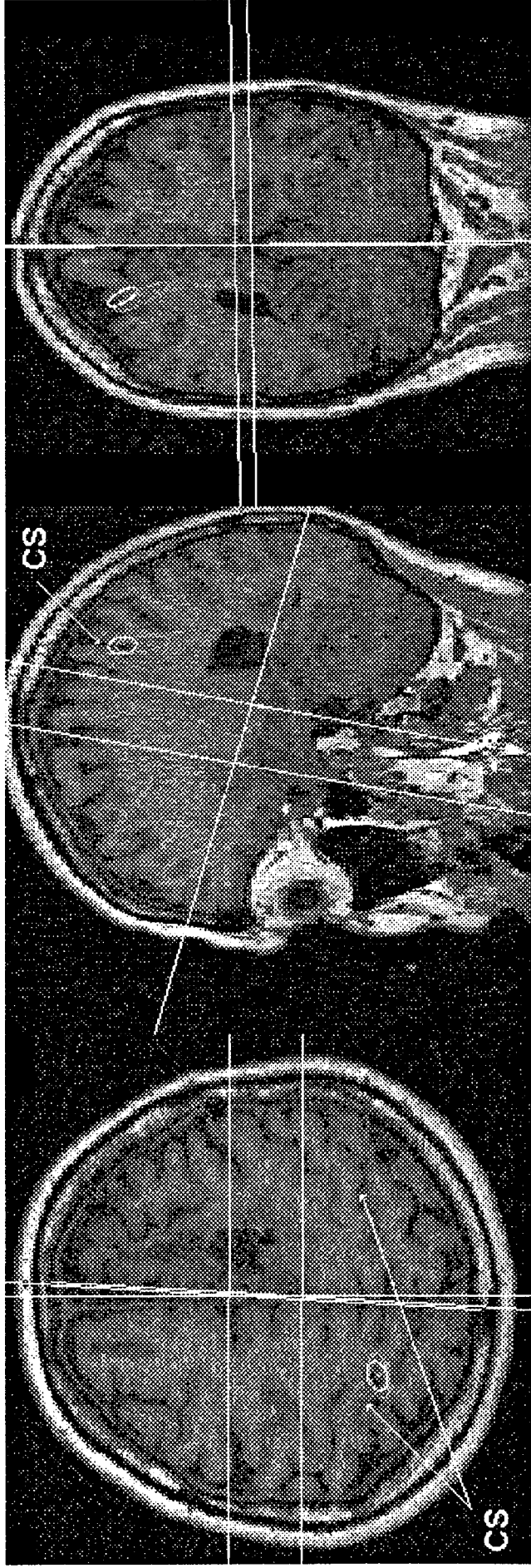


Figure 5.47 Two separate trials of Right median nerve source localisations for patient DB co-registered with the MRI. Smaller confidence ellipse was achieved at a latency of 29.0 ms and the other at 21.0ms. Predicted location of the Central Sulcus is indicated (CS).

### 5.4.8.6 Predicted location of the Central Sulcus

Mean Talairach co-ordinates for the confidence volumes for right median nerve stimulation co-registered with the MRI were:

Right Median:

CA-CP axis: -41.8 mm    Lateral axis: 22.7 mm    VCA-VCP axis: 48.5 mm.

Neuroanatomical inspection of the MRI together with Talairach co-ordinate data suggested that the confidence volumes were located within the of the post-central gyrus in this patient. The prediction of the position of the central sulcus for the right hemisphere was made therefore on the basis of symmetry as is shown in Figure 5.48.

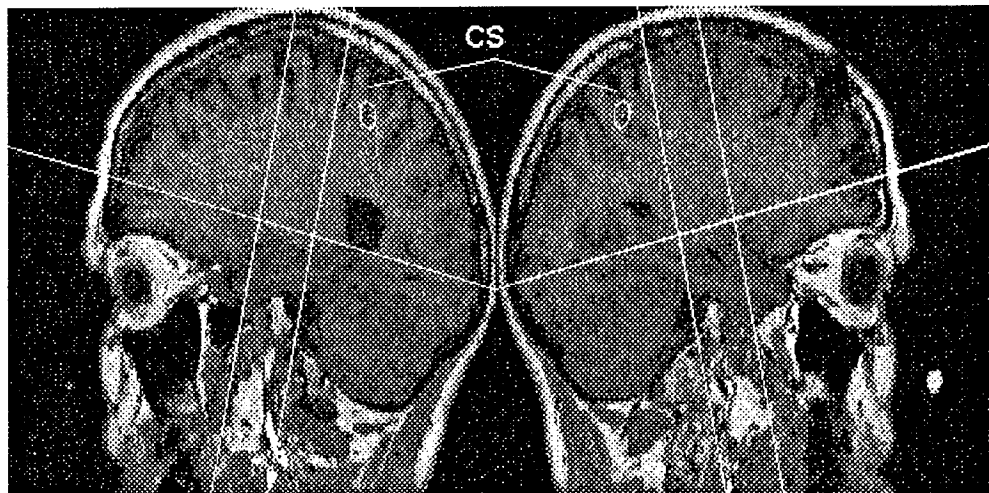


*Figure 5.48 Prediction of the location of the Central Sulcus in patient DB was made on the basis of assumed symmetry between hemispheres. The predicted location for the left median nerve is shown in the sagittal plate on the right.*

The relationship of the source localisations with the central sulcus is depicted graphically below (Fig 5.49).

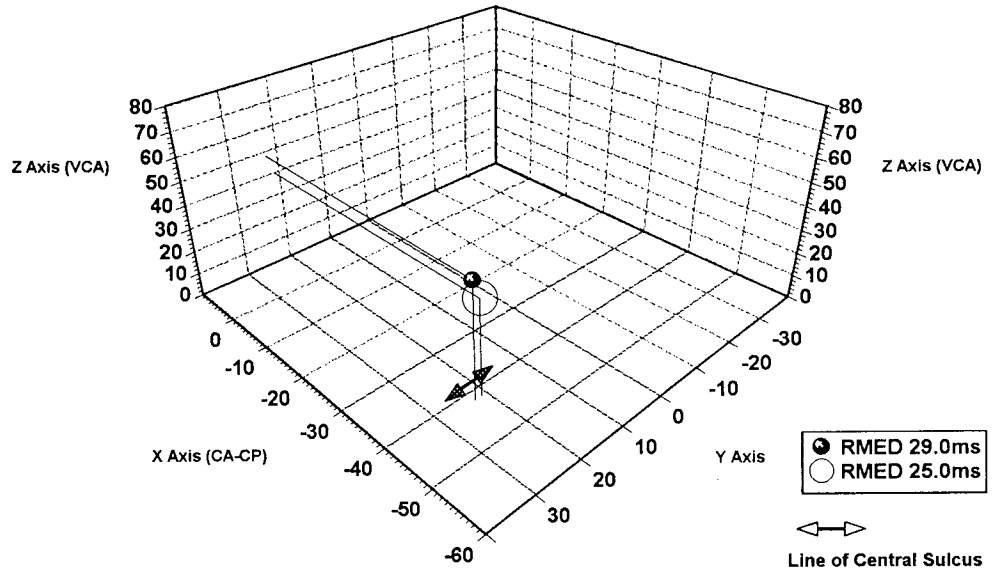


Figure 5.49 Smallest confidence volumes from trials of Right Median nerve localisations in patient DB. Relative sizes of the localisation icons reflect the proportional sizes of the corresponding confidence volumes. The double arrow indicates the predicted position in the x-y axis of the line of the central sulcus.

#### 5.4.8.7 Surgical validation - Patient DB

Intra-cranial localisations during surgery confirmed that the predicted location of the central sulcus in the right hemisphere had been entirely accurate.

The electromagnetic interference in the right hemisphere during the MEG recordings was found to be due metal clips inserted at the time of the previous surgical intervention.

### 5.4.9 Case study 9: Patient CJ

#### 5.4.9.1 Clinical History:

This 35 year old man presented with a previous history of a Left parietal cystic astrocytoma which was removed at the age of 5 years. This had resulted in a right-sided weakness since that time.

Developed epilepsy at the age of 16 and was being evaluated for surgical intervention.

#### 5.4.9.2 Investigations

**Magnetometry** was performed at the Clinical Neurophysiology Unit at Aston University on August 6th 1996 to localise sensory function of the right hand and foot.

#### 5.4.9.3 Magnetometry Results - Patient CJ

Clear reproducible cortical signals were obtained following electrical stimulation of both Left and Right median nerves at the wrist as well as from the Left Posterior Tibial nerve. Right Posterior Tibial nerve stimulation yielded poor data which was insufficient to yield localisations.

Inverse solution algorithms were applied to the data to obtain source localisation coordinates. Goodness of fit analysis indicated statistically significant correlation coefficients ( $r > 0.95$ ) at 25 milliseconds for Left median nerve stimulation and between 19.5 and 43.5 milliseconds for Right Median nerve stimulation.

For Left Posterior Tibial nerve stimulation latencies between 41.5 and 58.0 milliseconds produced significant dipole fit correlations.

## Chapter 5

Monte Carlo analysis was performed on the data to assess 95% confidence boundaries for the source localisation's. Confidence ellipse volumes of less than  $2\text{cm}^3$  were found in each modality.

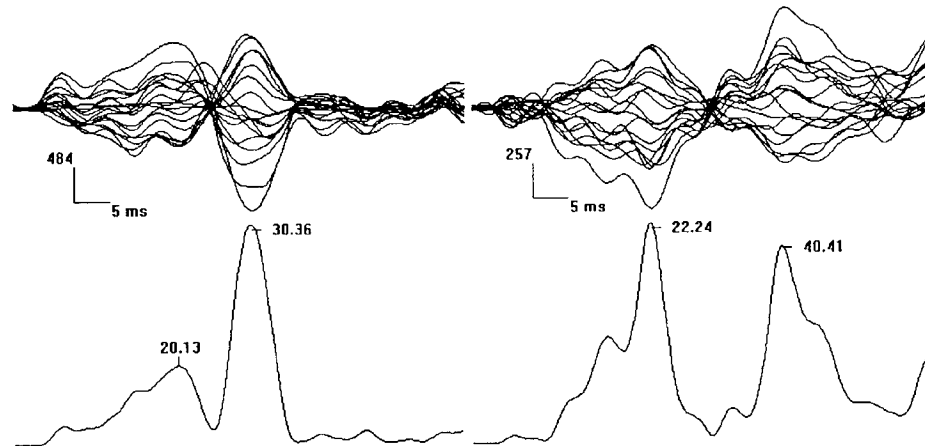


Figure 5.50 19 channels of magnetic field data following single trials of **Left Median nerve** (upper left) stimulation and **Right Median nerve** stimulation (upper right). The figures beneath these waveforms (lower left and right) show the corresponding Global Field Power plots of the data.

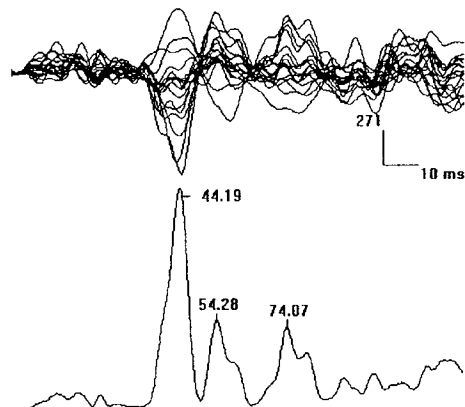
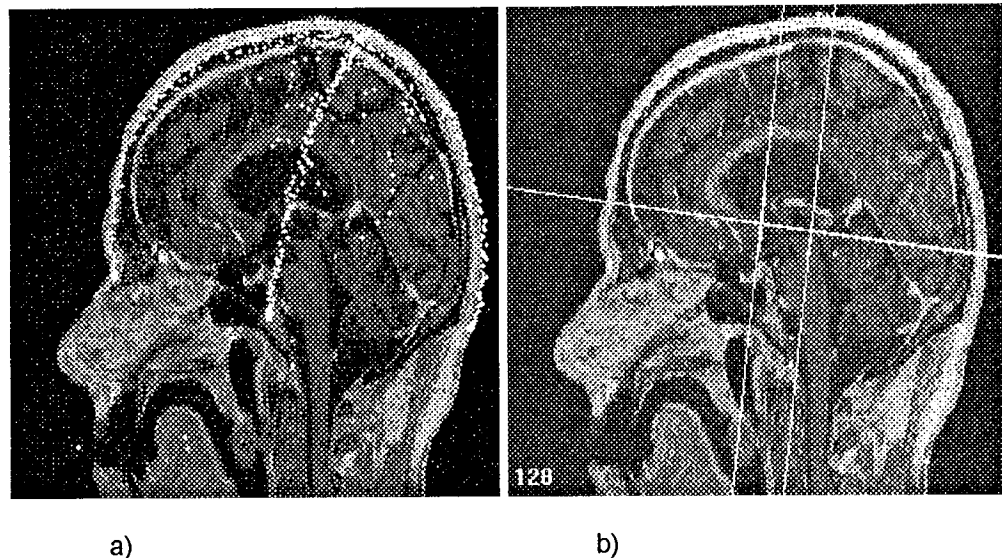


Figure 5.51 **Left Posterior Tibial nerve** data from patient CJ. 19 MEG channels from a single trial are superimposed (upper) with the corresponding Global Field Power plot below.

### 5.4.9.4 MEG-MRI co-registration

MRI's were acquired with the bite bar in situ. Slice thickness was 1.5mm. Bite bar markers were located from the MRI and a matching matrix derived. This match was checked by plotting a digitised head shape onto the MRI (Figure 5.52 a).

Using a midline slice (128), co-ordinate matching as defined by Talairach was attempted (Figure 5.52 b).



*Figure 5.52 Patient CJ. Plate a) shows digitised head shape file, acquired at the time of the MEG acquisition, co-registered with the MRI. Plate b) shows the CA-CP and VCA-VCP lines of the Talairach co-ordinate system positioned on a mid-line slice.*

### 5.4.9.5 MEG-MRI source localisations

95% confidence volumes ( $< 2\text{cm}^3$  total volume) were coregistered with the MRI.

Appropriate MRI slices are illustrated overleaf.

## Chapter 5

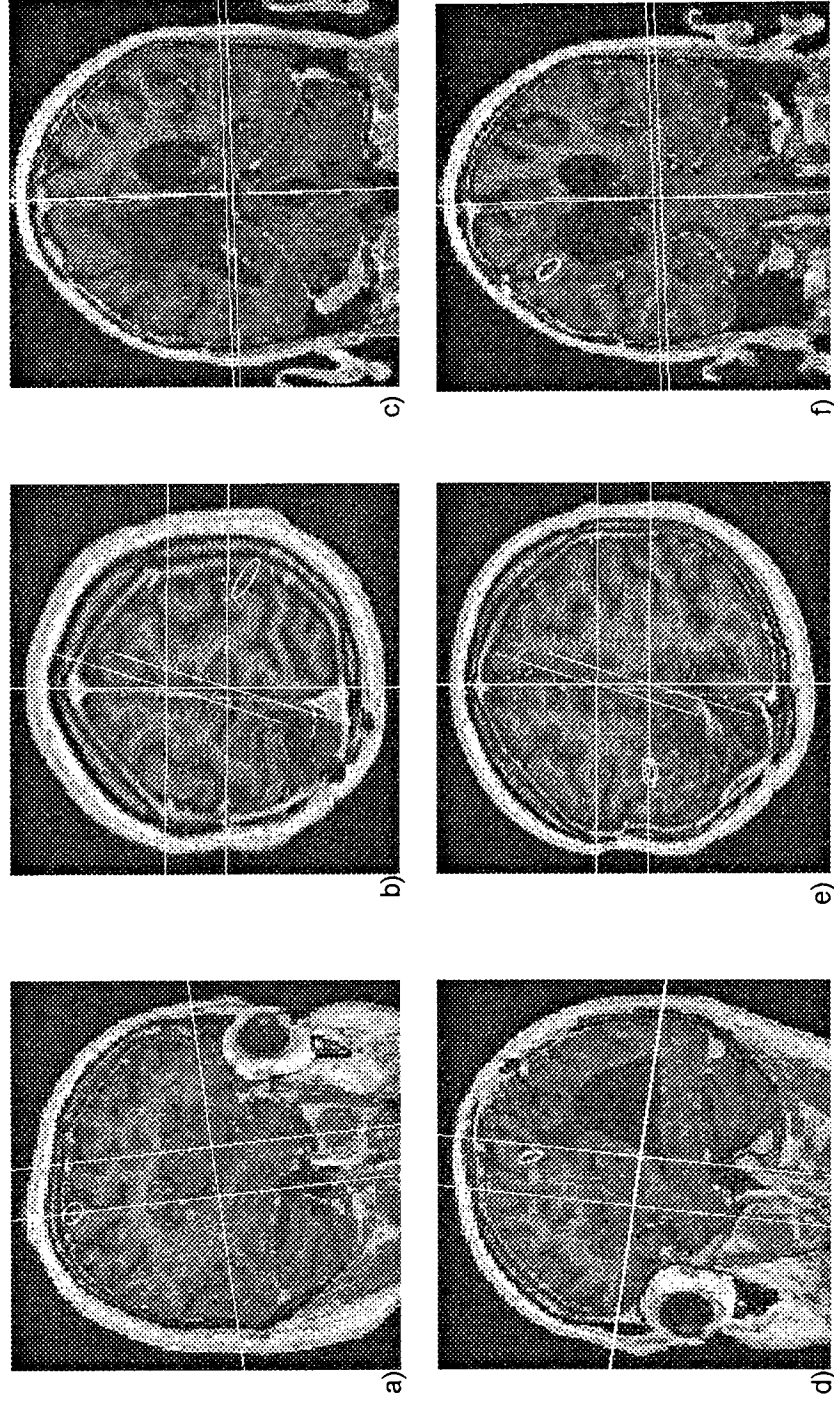


Figure 5.53 Patient C.J. Plates a-c, co-registration of smallest volume at 25.0ms following Left median nerve stimulation. Plates d-f show localisations following separate trials of right median nerve stimulation (20.0ms and 19.5ms).

Chapter 5

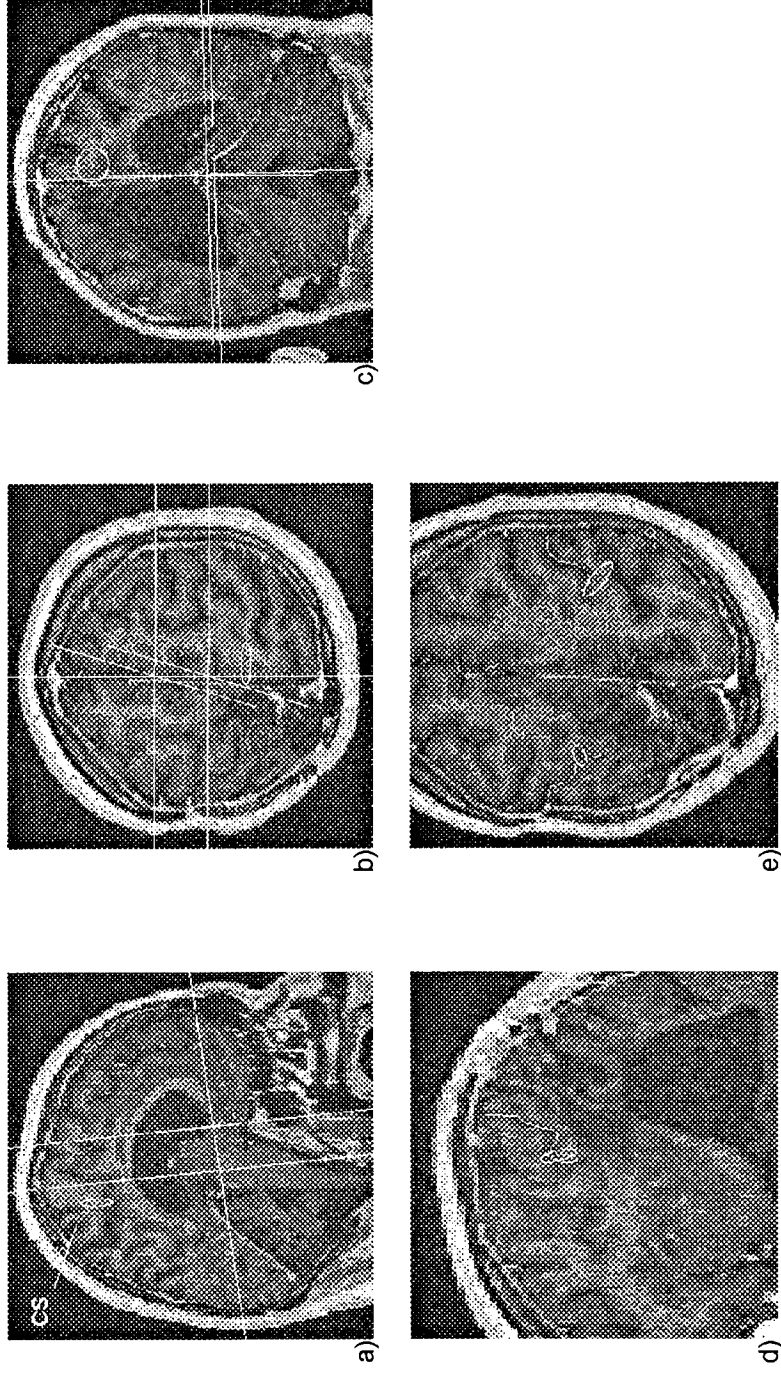


Figure 5.54 Upper plates a-c show co-registration of **Left Posterior Tibial** nerve data at 41.5ms. Lower plates d and e show predicted line of the central sulcus with right median nerve confidence ellipse shown on the sagittal slice and both right and left median nerve data co-registered to a single axial slice for ease of comparison.



## Chapter 5

### 5.4.9.6 Patient CJ - Predicted location of the central sulcus

Mean Talairach co-ordinates for the confidence volumes co-registered with the MRI were:

#### Right Median

CA-CP axis: -18.8 mm      Lateral axis: 33.2 mm      VCA-VCP axis: 49.5 mm.

#### Left Median

CA-CP axis: -24.8 mm      Lateral axis: -37.7 mm      VCA-VCP axis: 65.2 mm.

#### Left Posterior Tibial

CA-CP axis: -36.9 mm      Lateral axis: -5.9 mm      VCA-VCP axis: 59.8 mm.

Neuroanatomical inspection of the MRI together with Talairach co-ordinate data suggested that the median nerve dipoles were localised to the post-central gyrus and the posterior tibial nerve data to the pre-central gyrus in this patient. This is depicted graphically below Fig 5.55

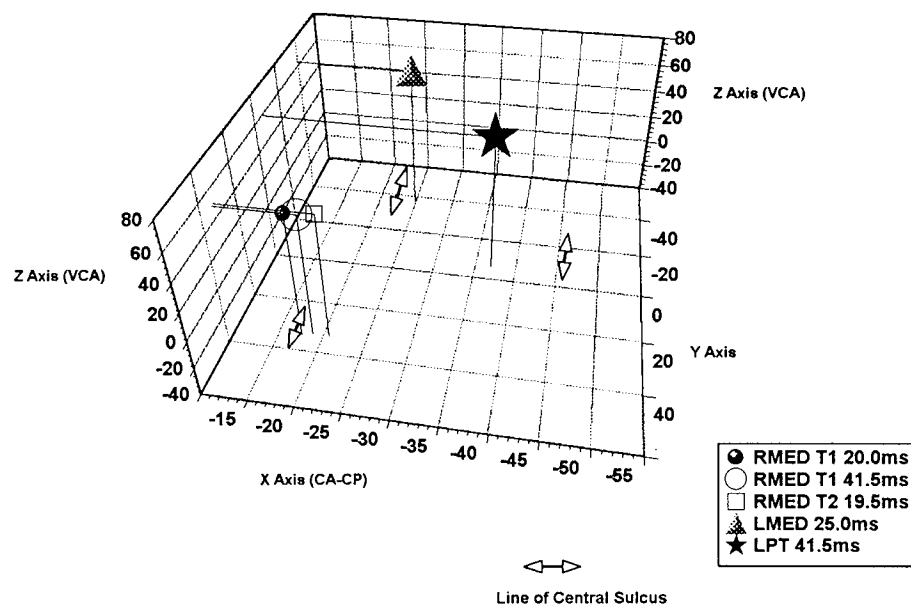


Figure 5.55 Right and Left median nerve with Left Posterior Tibial nerve localisations in patient CJ. Relative sizes of the localisation icons reflect the proportional sizes of the corresponding confidence volumes. The double arrow indicates the predicted position (in the x-y axis only) of the line of the central sulcus.

### 5.4.9.7 Surgical validation - Patient CJ

Intra-cranial localisations during surgery confirmed that the predicted location of the central sulcus in the right hemisphere had been entirely accurate.

### 5.4.10 Case study 10: Patient PP

#### 5.4.10.1 Clinical History:

This 64 year old man presented with a history of a CVA 2.5 years ago which resulted in a right hemiparesis. During the following six months he developed left sided chronic pain which was diagnosed as thalamic pain syndrome. Pain had been partly controlled by Diazepam but he was now being considered for a motor cortex stimulator.

#### 5.4.10.2 Investigations

**Magnetometry** was performed at the Clinical Neurophysiology Unit at Aston University on April 9th 1997 to localise sensory function of the left hand.

#### 5.4.10.3 Magnetometry Results - Patient PP

Clear reproducible cortical signals were obtained following electrical stimulation of the Left median nerve at the wrist (Figure 5.56)

Inverse solution algorithms were applied to the data to obtain source localisation co-ordinates. Goodness of fit analysis indicated statistically significant correlation coefficients ( $p > 0.95$ ) between 18 and 40 milliseconds for Left median nerve stimulation.

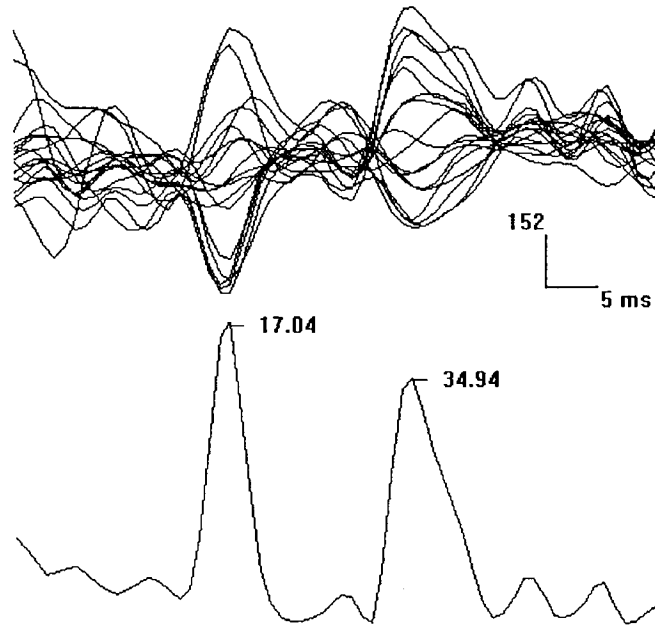


Figure 5.56 19 channels of superimposed MEG data (upper) following Left median nerve stimulation in patient PP. Below is the corresponding Global Field Power plot.

Monte Carlo analysis was performed on the data to assess 95% confidence boundaries for the source localisation's. Confidence ellipse volumes of less than  $2\text{cm}^3$  were obtained in two independent trials of Left median nerve stimulation.

#### 5.4.10.4 MEG-MRI co-registration

MRI's were acquired with the bite bar in situ. Slice thickness was 1.5mm. Bite bar markers were located from the MRI and a matching matrix derived. This match was checked by plotting a digitised head shape onto the MRI (Figure 5.57 a).

Using a midline slice (126), co-ordinate matching as defined by Talairach was attempted (Figure 5.57 b).

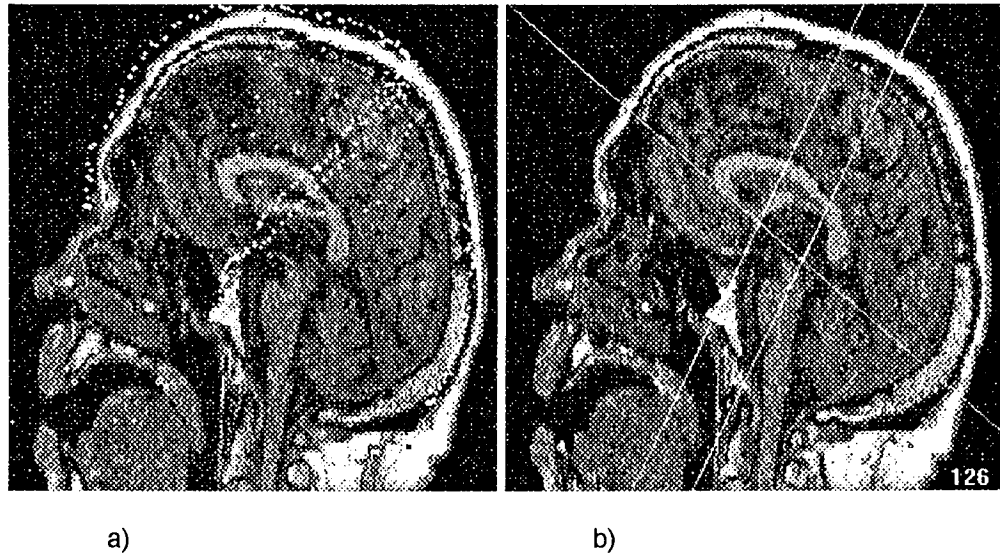


Figure 5.57 Patient PP. Plate a) shows digitised head shape file, acquired at the time of the MEG acquisition, co-registered with the MRI. Plate b) shows the CA-CP and VCA-VCP lines of the Talairach co-ordinate system positioned on a mid-line slice.

#### 5.4.10.5 MEG-MRI source localisation - Patient PP

95% confidence volumes for left median nerve stimulation were co-registered with the MRI. Smallest volumes from two separate trials were both achieved at 18.0ms (160 mm<sup>3</sup> and 180 mm<sup>3</sup>). Appropriate MRI slices are illustrated overleaf (Figure 5.58).

## Chapter 5

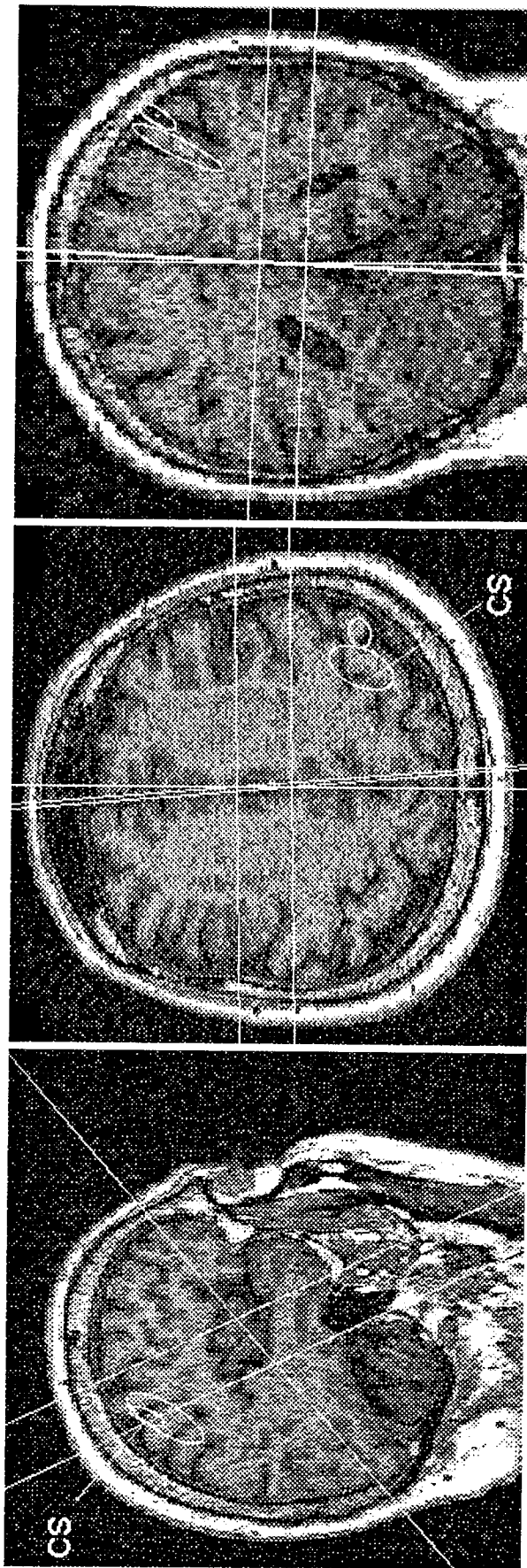


Figure 5.58 Patient PP. Localisations following two trials of Left Median nerve stimulation. Sources computed at a latency of 18.0ms. The predicted line of the central sulcus is indicated (CS).

5.4.10.6 Patient PP- Predicted location of the central sulcus

Localisations for two separate trials of median nerve stimulation (at a latency of 18.0ms) yielded a mean Talairach co-ordinate of:

CA-CP axis: -26.5 mm      Lateral axis: -41.4mm      VCA-VCP axis: 52.6 mm.

Neuroanatomical inspection of the MRI together with Talairach co-ordinate data suggested that the dipoles were localised to the post-central gyrus in this patient. The data is depicted graphically below (Fig 5.59).

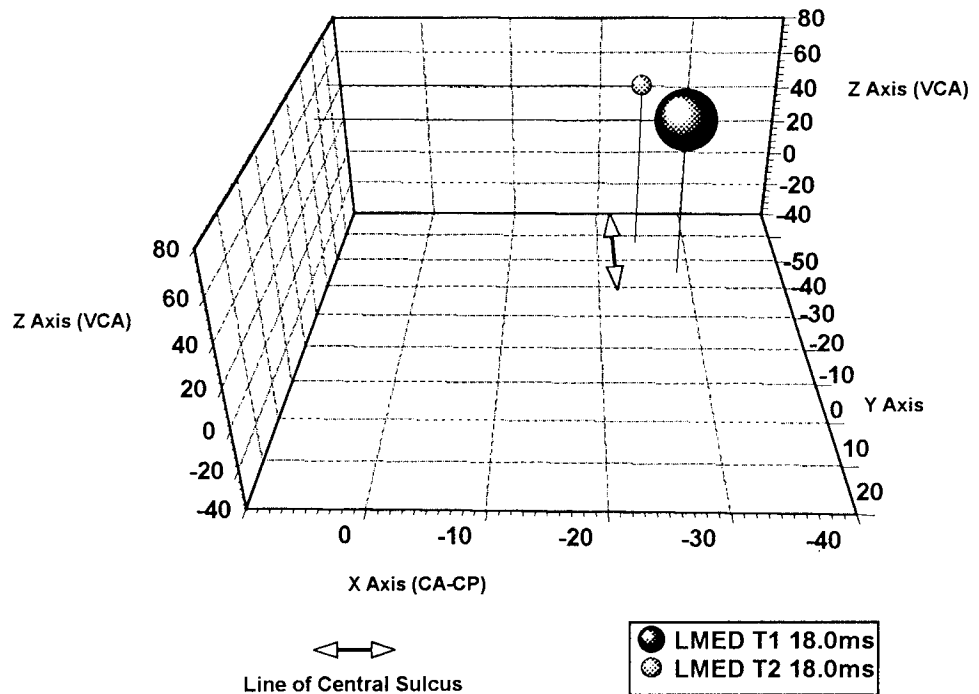


Figure 5.59 Left median nerve localisations in patient PP. Relative sizes of the localisation icons reflect the proportional sizes of the corresponding confidence volumes. The double arrow indicates the predicted position (in the x-y axis only) of the line of the central sulcus. Legend indicates separate trials of Left Median nerve stimulation (T1 and T2).

### 5.4.10.7 Surgical validation - Patient PP

This patient is currently awaiting a surgical date.

### 5.4.11 Case study 11: Patient RL

#### 5.4.11.1 Clinical History

This 37 year old man presented with a history of Jacksonian seizures commencing in Left index finger and thumb.

#### 5.4.11.2 Investigations

MRI confirmed the presence of a Right parietal lesion. Biopsy confirmed a Grade 3 astrocytoma.

**Magnetometry** was performed at the Clinical Neurophysiology Unit at Aston University on March 11th 1997 to localise Left hand motor and sensory function.

#### 5.4.11.3 Magnetometry Results - Patient RL

Clear reproducible cortical signals were obtained following electrical stimulation of both Left and Right median nerves at the wrist. In addition, a self paced index finger movement paradigm was used in both hands which also produced clear magnetic fields from the cortex.

## Chapter 5

Inverse solution algorithms were applied to the data to obtain source localisation coordinates. Goodness of fit analysis indicated statistically significant correlation coefficients ( $p > 0.95$ ) between 18 and 36 milliseconds for Left median nerve stimulation and at 23 milliseconds for Right Median nerve stimulation.

Following index finger movement, statistically significant data ( $r > 0.95$ ) was found at 32, 91 and 228 milliseconds following finger movement initiation in the left hand and at 25, 150 and 209 milliseconds for the right hand.

Monte Carlo analysis was performed on the data to assess 95% confidence boundaries for the source localisation's. Where confidence ellipse volumes were less than  $2\text{cm}^3$ , these were superimposed onto the MR images. All latencies listed above produced ellipses within this criterion.

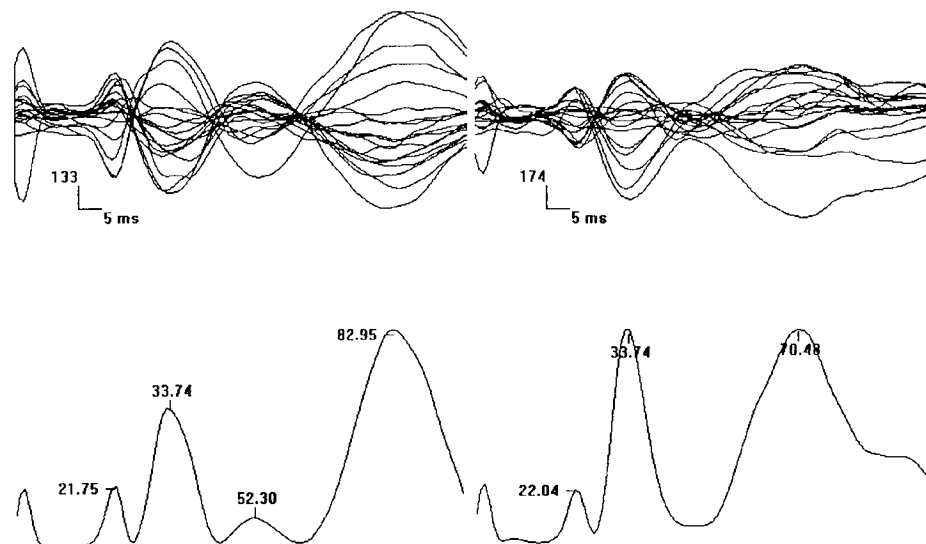


*Figure 5.60 Magnetic field waveforms following Left Median nerve (upper left) and Right Median nerve stimulation (upper right). Below are the corresponding Global Field Power plots.*



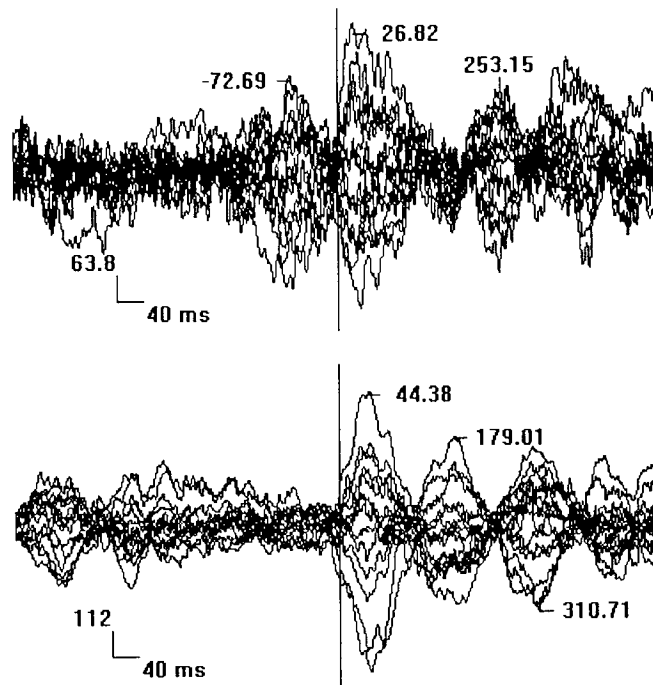


Figure 5.61 Figures show the magnetic field waveforms following self paced movement of the Left (upper figure) and Right (lower figure) index finger. The vertical line indicates the point at which an electrical contact was made as part of the movement and was defined as time zero. Latencies were calculated with respect to this point.

#### 5.4.11.4 MEG-MRI co-registration

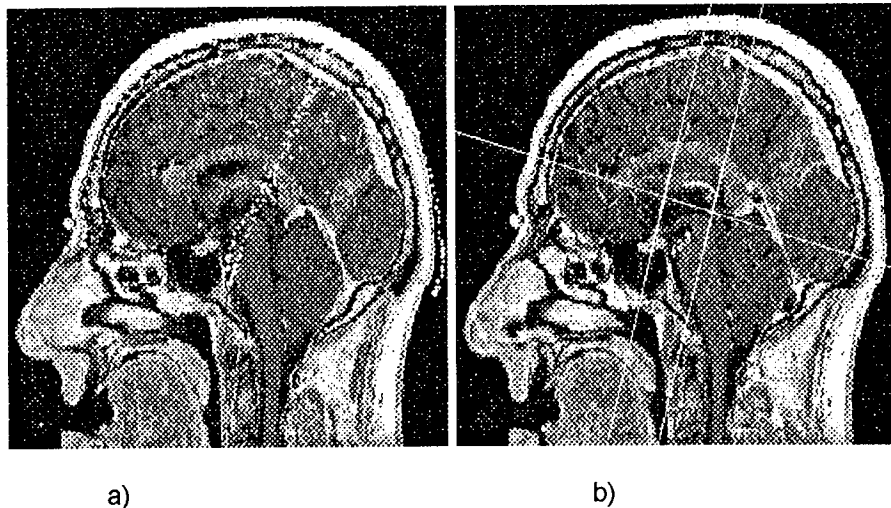


Figure 5.62 Patient RL. Plate a) shows digitised head shape file, acquired at the time of the MEG acquisition, co-registered with the MRI. Plate b) shows the CA-CP and VCA-VCP lines of the Talairach co-ordinate system positioned on a mid-line slice.

MRI's were acquired with the bite bar in situ. Slice thickness was 1.5mm. Bite bar markers were located from the MRI and a matching matrix derived. This match was checked by plotting a digitised head shape onto the MRI (Figure 5.62 a).

Using a midline slice, co-ordinate matching as defined by Talairach was attempted (Figure 5.62 b).

### 5.4.11.5 MEG-MRI source localisation

95% confidence volumes for Right and Left median nerve stimulation together with Right and Left self paced finger movement are illustrated overleaf (Figures 5.63 and 5.64).

### 5.4.11.6 Patient RL - Predicted location of the Central Sulcus

Localisations for three separate trials of **left median nerve** stimulation (at latencies of 18.0ms, 30.0ms and 35.0ms) yielded a mean Talairach co-ordinate of:

CA-CP axis: -33.3 mm      Lateral axis: -44.1 mm      VCA-VCP axis: 40.0 mm.

Localisations for two separate trials of **right median nerve** stimulation (at a latency of 23.0ms) yielded a mean Talairach co-ordinate of:

CA-CP axis: -30.9 mm      Lateral axis: 50.7 mm      VCA-VCP axis: 40.2 mm.

Localisations for two separate trials of **left index finger movement** (at latencies of 32.0ms, 91.0ms) yielded a mean Talairach co-ordinate of:

CA-CP axis: -33.8 mm      Lateral axis: -36.5 mm      VCA-VCP axis: 52.0 mm.

Localisations for two separate trials of **right index finger movement** (at latencies of 25.0ms, 150.0ms) yielded a mean Talairach co-ordinate of:

CA-CP axis: -28.1 mm      Lateral axis: 29.1 mm      VCA-VCP axis: 48.1 mm.

Neuroanatomical inspection of the MRI together with Talairach co-ordinate data suggested that the median nerve dipoles were localised to the post-central gyrus in this patient with the self paced finger movement dipoles consistently anterior and predominantly pre-central. The data is depicted graphically in Figure 5.65.

## Chapter 5

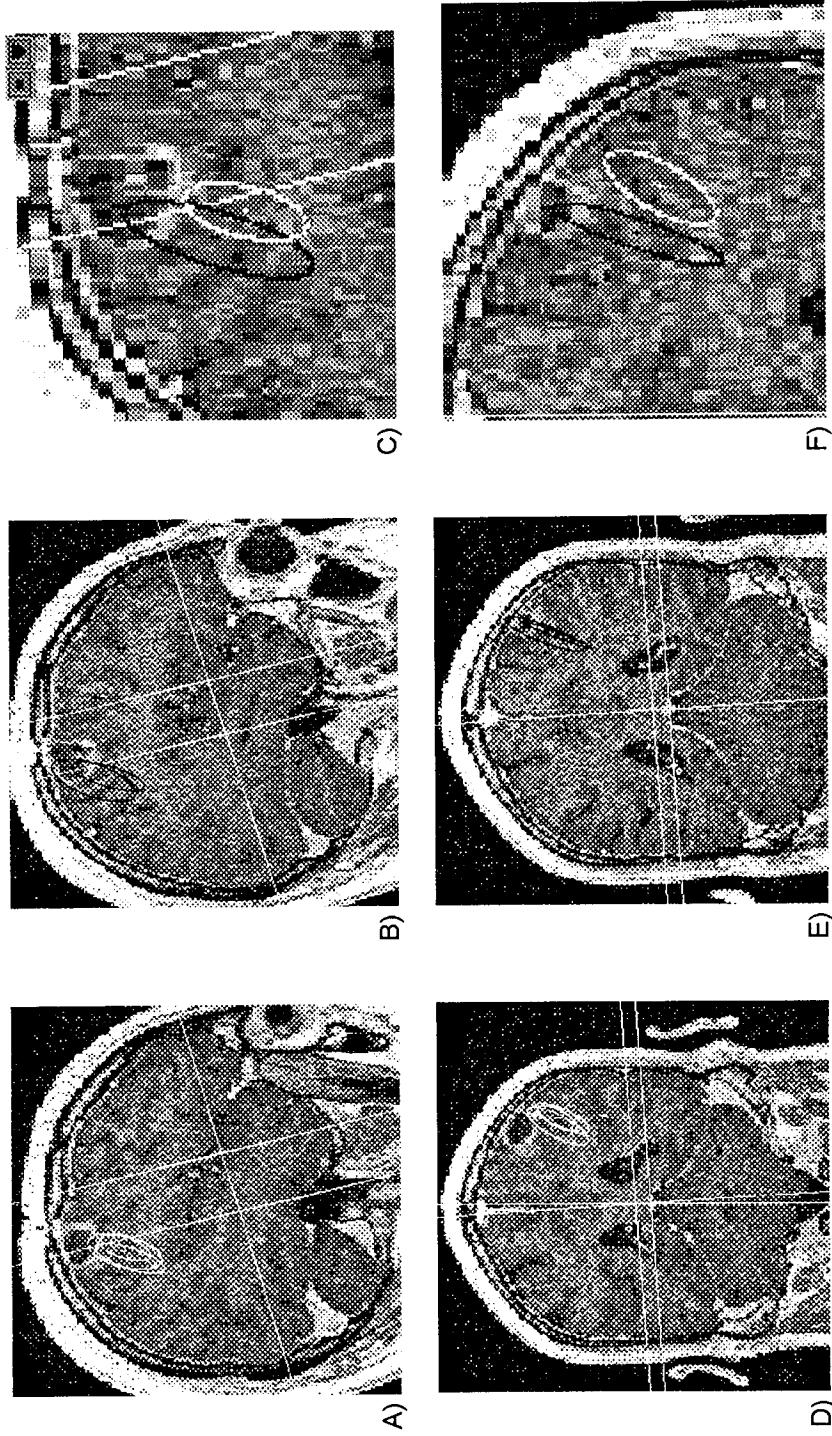


Figure 5.63 Plates A and D show the location of three separate trials of Left Median nerve stimulation (white ellipses) with plates B and E showing the location of two separate trials of Left index finger movement confidence volumes. Plates C and F show the juxtaposition of sensory and movement evoked confidence volumes.

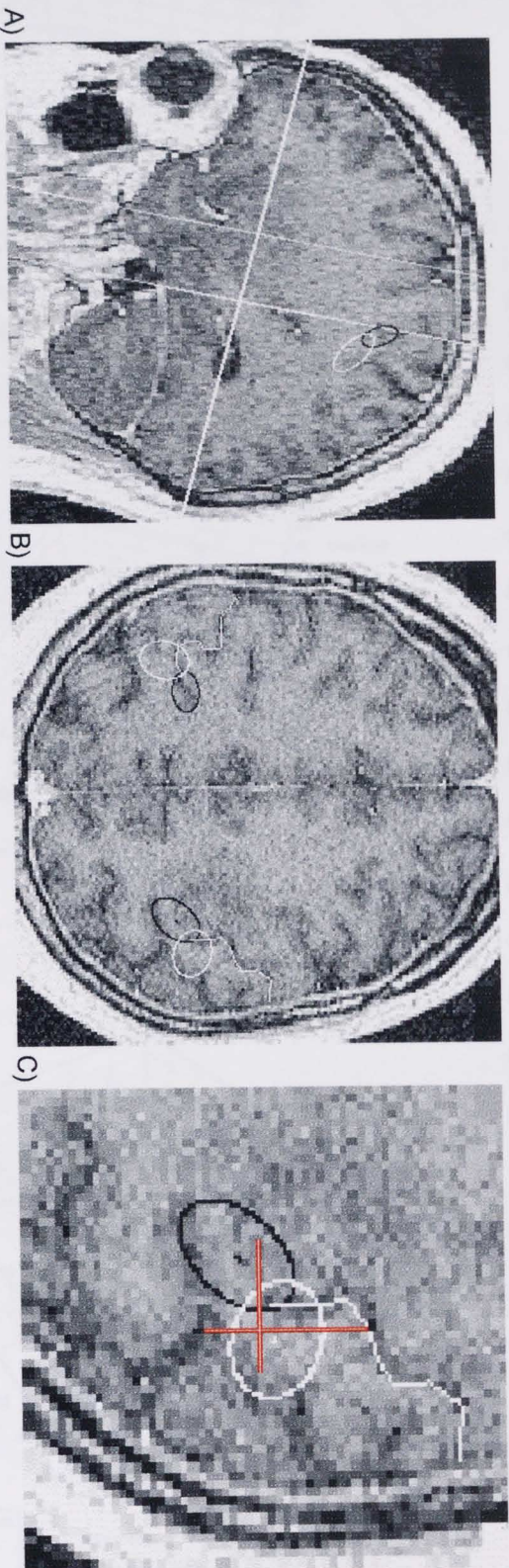


Figure 5.64 Right Median nerve and Right index finger movement confidence volumes (white and black respectively) are shown in plate A. Plate B shows right and left sensory and motor localisations with respect to the predicted line of the central sulcus. Plate C shows the extent of outline of the astrocytoma (cross in centre of plate) 6-7 millimetres superior to the indicated slice.

4.4.11.6 (Continued) Predicted location of the Central Sulcus

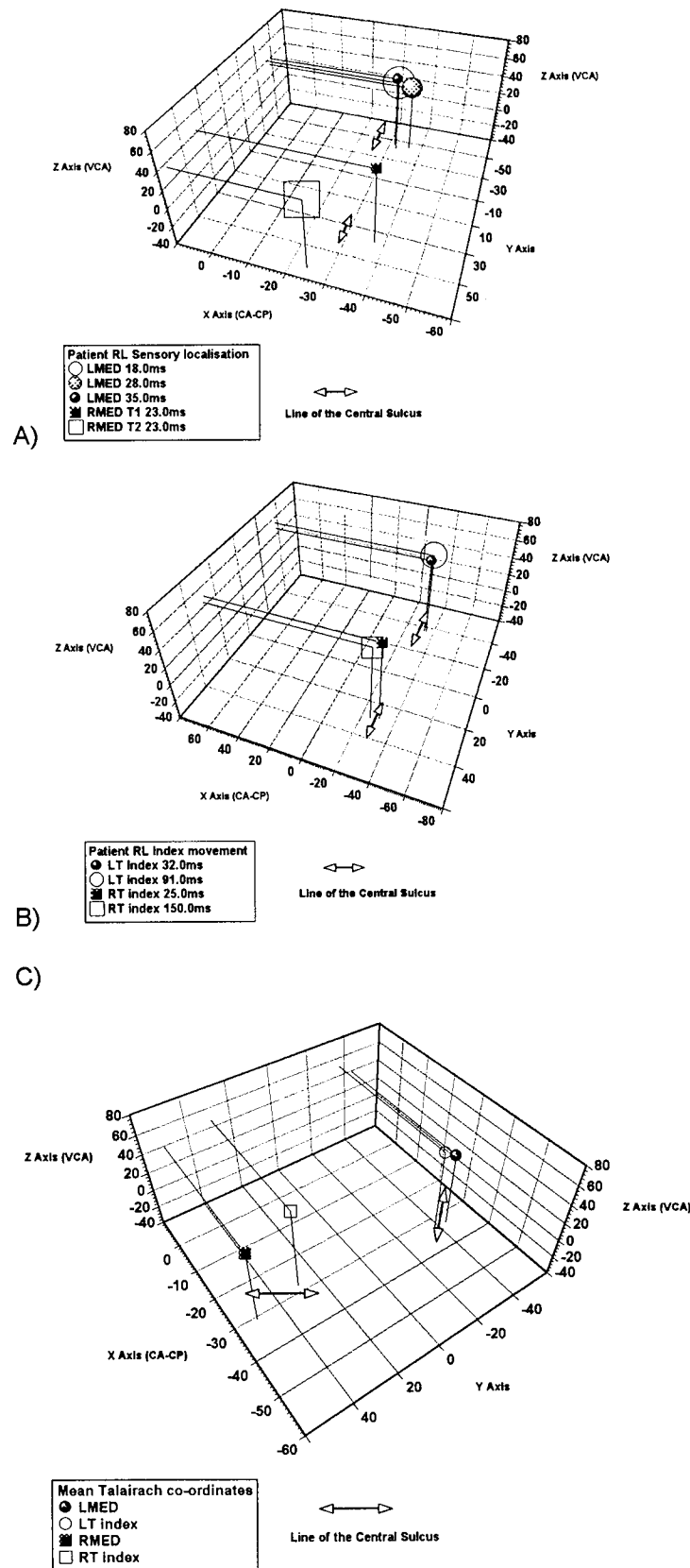


Figure 5.65 Graph A) shows the relative size and positions of separate trials of median nerve data over a range of latencies with Graph B) showing the corresponding index finger movement data. Graph C gives the mean positions of the previous data for ease of comparison. Icon size represents the proportional confidence volumes with the double arrows indicating the predicted lines of the Central Sulcus.

Both Left Median nerve and Left index finger movement localisations appeared to be located in the postcentral gyrus in this patient although the motor data was consistently superior and anterior in position compared with sensory stimulation. From the localisations it appeared that the lesion involved the superior aspect of the motor cortex but may not have involved the hand area.



*Figure 5.66 Sagittal section showing*

*Left index finger localisation with respect  
to the lesion in patient RL.*

#### 5.4.11.7 Surgical validation - Patient RL

Intra-operative somatosensory and cortical stimulation techniques were employed in this case together with arousal of the patient during the procedure to confirm hand motor function. MEG localisation of the central sulcus was entirely accurate in this case. Not all of the lesion could be excised from this patient because of the intrusion into motor cortex.

#### 5.4.12 Case Study 12: Patient JS

##### Clinical History

Eight years ago, this 37 year old lady had five fits while in the early stages of pregnancy. Investigations at the time, including cerebral angiography, yielded no specific diagnosis. She then remained well until May 1996 when she developed pins and needles and then clumsiness and numbness of her right hand. This was followed by focal fits involving the right hand at least one of which was secondary generalised.

##### 5.4.12.1 Investigations

MRI scanning revealed an abnormality in the left parietal region which had the characteristics of a cavernous angioma.

**Magnetometry** was performed at the Clinical Neurophysiology Unit at Aston University on February 19th 1997 to localise motor and sensory function of the Right hand.

##### 5.4.12.2 Magnetometry Results - Patient JS

Reproducible cortical signals were obtained following electrical stimulation of Right median nerves at the wrist. In addition, a self paced index finger movement paradigm was used in both hands which also produced consistent magnetic fields from the cortex.

Inverse solution algorithms were applied to the data to obtain source localisation coordinates. Goodness of fit analysis indicated statistically significant correlation coefficients ( $r > 0.95$ ) for the computed sources at latencies between 23 and 50 milliseconds for Right Median nerve stimulation.

Following **index finger movement**, statistically significant data was found at 38, 52 and 81 milliseconds following finger movement initiation in the Right hand and at 118 milliseconds for the Left hand.

Monte Carlo analysis was performed to assess 95% confidence boundaries for the source localisation's. Where confidence ellipse volumes were less than  $2\text{cm}^3$ , these were superimposed onto the MR images. All latencies listed above produced ellipses within this criterion.

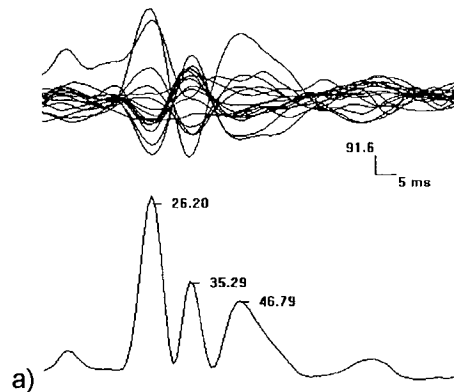
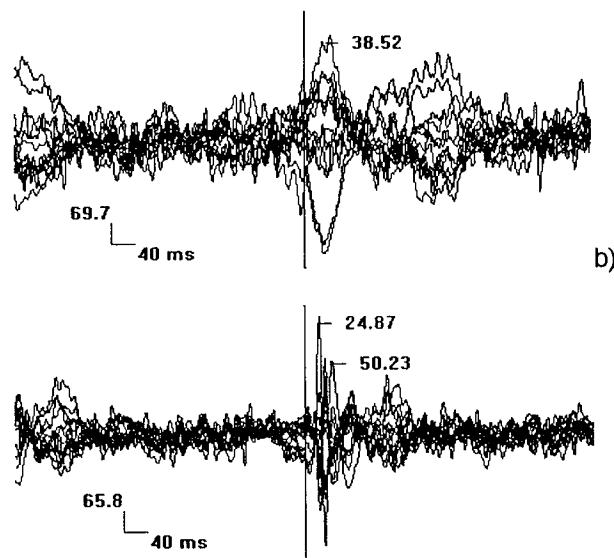


Figure 5.67 Magnetic field waveforms following **Left Median nerve stimulation** (upper a). The corresponding Global Field Power analysis of the data is shown beneath the MEG plots. The latencies indicated are those from which single equivalent dipole models were calculated.

**Below (b)**, the MEG waveforms following **Right** (upper traces) and **Left self paced index finger movement**. The vertical line indicates the moment of contact formed by depression of a contact switch and corresponds to time zero for the purposes of latency presentation.





#### 5.4.12.3 MEG-MRI co-registration

MRI's were acquired with the bite bar in situ. Slice thickness was 2.0 mm. Bite bar markers were located from the MRI and a matching matrix derived. This match was checked by plotting a digitised head shape onto the MRI (Figure 5.68 a).

Using a midline slice, co-ordinate matching as defined by Talairach was attempted (Figure 5.68 b).

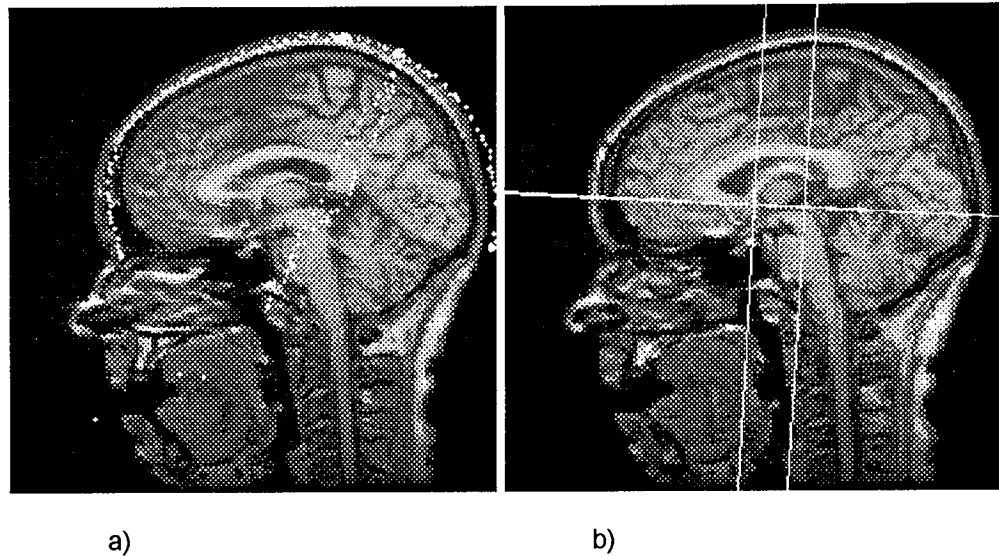


*Figure 5.68 Patient JS. Plate a) shows digitised head shape file, acquired at the time of the MEG acquisition, co-registered with the MRI. Plate b) shows the CA-CP and VCA-VCP lines of the Talairach co-ordinate system positioned on a mid-line slice.*

#### 5.4.12.4 MEG-MRI source localisation

95% confidence volumes for Right median nerve stimulation together with Right and Left self paced finger movement are illustrated overleaf (Figures 5.70 and 5.71).

## Chapter 5



Figure 5.69 Patient JS: Two trials of right median nerve stimulation both locate to what is predicted to be the post-central gyrus in this patient.

## Chapter 5

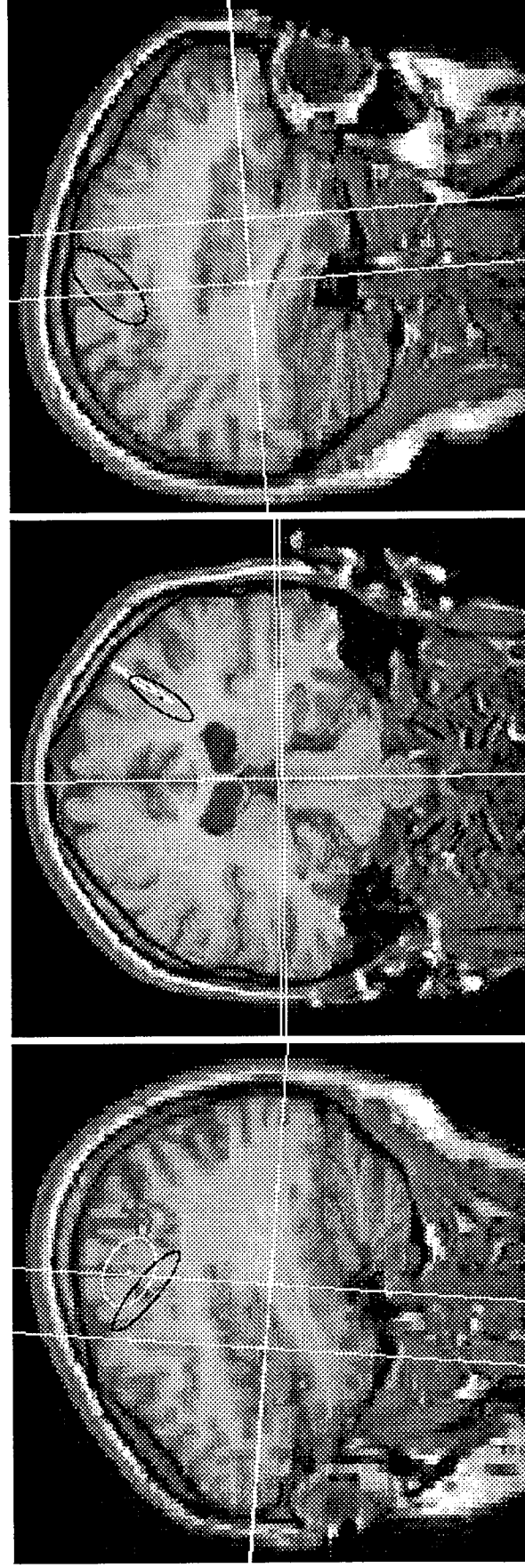


*Figure 5.70 The juxtaposition of right median (white ellipse) with right index finger movement (black ellipse) confidence volumes are shown in the left and middle plates. Left index finger localisation is shown in the right sagittal plate.*

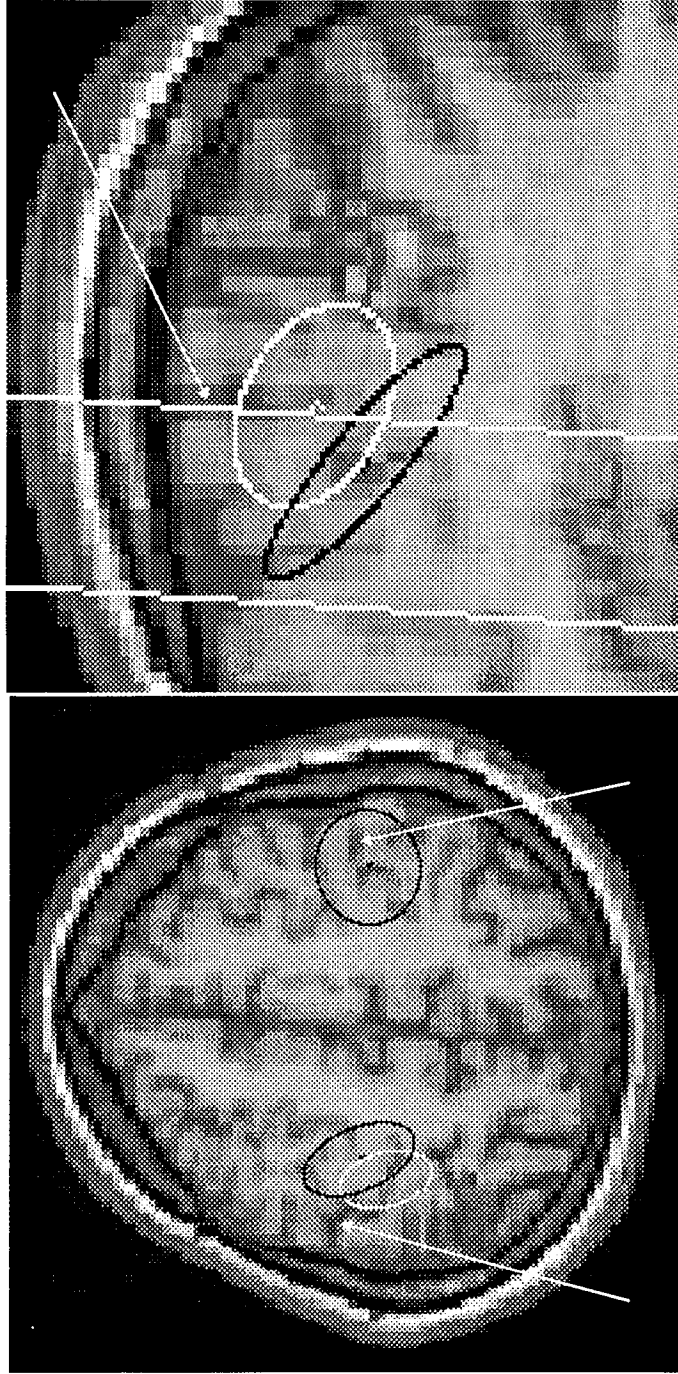


Figure 5.71 Smallest median nerve confidence volume (white ellipse) together with index finger movement confidence volumes (black) are shown on this axial and sagittal slice. The predicted positions of the central sulci are indicated by the arrows. The lesion is clearly visible in the enlarged sagittal slice (right) and appears to lie in the gyrus posterior to the sensory cortex.

#### 5.4.12.5 Patient JS - Predicted location of the Central Sulcus

Localisations for two separate trials of **right median nerve** stimulation (at latencies of 23.0ms and 50.0 ms) yielded a mean Talairach co-ordinate of:

CA-CP axis: -31.3 mm      Lateral axis: 35.2 mm      VCA-VCP axis: 53.2 mm.

Localisations for two separate trials of **right index finger movement** (at latencies of 32.0ms, 91.0ms) yielded a mean Talairach co-ordinate of:

CA-CP axis: -19.8 mm      Lateral axis: 28.6 mm      VCA-VCP axis: 44.9 mm.

Localisations for two separate trials of **left index finger movement** (at latencies of 118.0ms and 131.0ms) yielded a mean Talairach co-ordinate of:

CA-CP axis: -21.2 mm      Lateral axis: -37.7mm      VCA-VCP axis: 54.7 mm.

Neuroanatomical inspection of the MRI together with Talairach co-ordinate data suggested that the median nerve dipoles were localised to the post-central gyrus in this patient with the self paced finger movement dipoles consistently anterior and predominantly pre-central. The data is depicted graphically in Figure 5.72 overleaf.

5.4.12.5 (continued)

Predicted location of the Central Sulcus - Patient JS

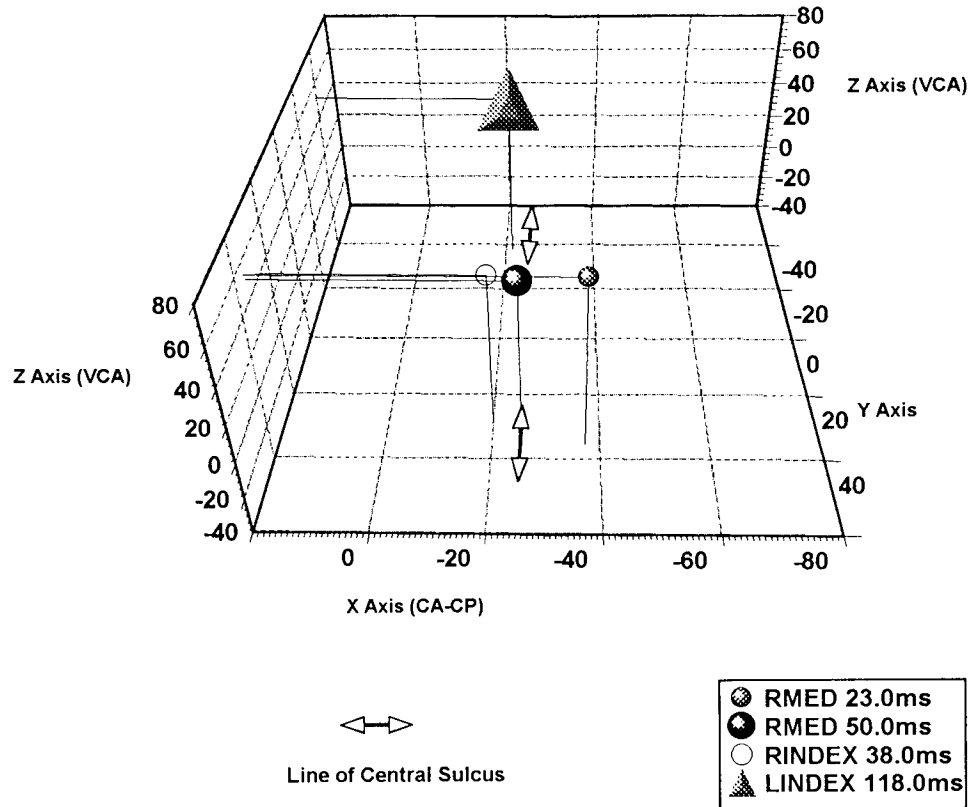


Figure 5.72 Right median nerve (RMED) and right and left index finger movement localisations (RINDEX and LINDEX) in patient JS. Relative sizes of the localisation icons reflect the proportional sizes of the corresponding confidence volumes. The double arrow indicates the predicted position (in the x-y axis only) of the line of the central sulcus.

5.4.12.6 Surgical validation - Patient JS.

In view of the close relationship of the sensory motor cortex to the cavernous angioma, craniotomy under local anaesthesia was performed so that the sensory motor cortex could be mapped by electrical stimulation of the cortex and the exact relationship confirmed.

The angioma was resected and at the surface was found to be one gyrus behind the primary sensory cortex so that in addition to the removal of the cavernous angioma the haemosiderin stained cortex could also be removed.

Postoperatively, the patient made an uncomplicated recovery with no neurological deficit.

Prediction of the central sulcus through MEG localisation had therefore proved entirely accurate.

### **5.4.13 Case study 13: Patient DO**

#### **5.4.13.1 Clinical History**

This 40 year old man presented with a two year history of epileptic seizures and a CT scan 2 years ago had showed some right frontal calcification. Initially his fits were well controlled on Carbamazepine but over the months they returned and increased in frequency. Most commonly these were left focal seizures starting with a flickering around the left eye and then spreading to involve the whole of the left arm and at their worst would spread down the legs.

#### **5.4.13.2 Investigations**

A recent MRI showed evidence of an intrinsic lesion in the right frontal region which could represent an intrinsic tumour.

Magnetometry was performed at the Clinical Neurophysiology Unit at Aston University on Thursday June 5th 1997 to localise motor and sensory function of the left hand.

#### **5.4.13.3 Magnetometry Results - Patient DO**

Clear reproducible cortical signals were obtained following electrical stimulation of both Left and Right median nerves at the wrist (Figures 5.73 and 5.74). In addition, a self paced index finger movement paradigm was used in the left hand which also produced clear magnetic field from the cortex (Figure 5.75).

Inverse solution algorithms were applied to the data to obtain source localisation coordinates. Goodness of fit analysis indicated statistically significant correlation coefficients ( $r > 0.95$ ) between 29 and 59 milliseconds for Left median nerve stimulation and between 29 and 53 milliseconds for Right median nerve stimulation.

Following left **index finger movement**, statistically significant data was found between 241 and 255 milliseconds following finger movement initiation in the left hand.

Monte Carlo analysis was performed on the data to assess 95% confidence boundaries for the source localisations. Where confidence volumes were less than  $2 \text{ cm}^3$ , these were co-registered with the MR images.

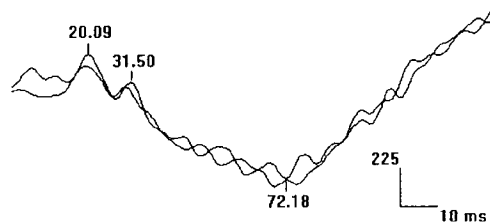


Figure 5.73 Patient DO. Two trials of Left median nerve stimulation (top) are superimposed to allow comparison.

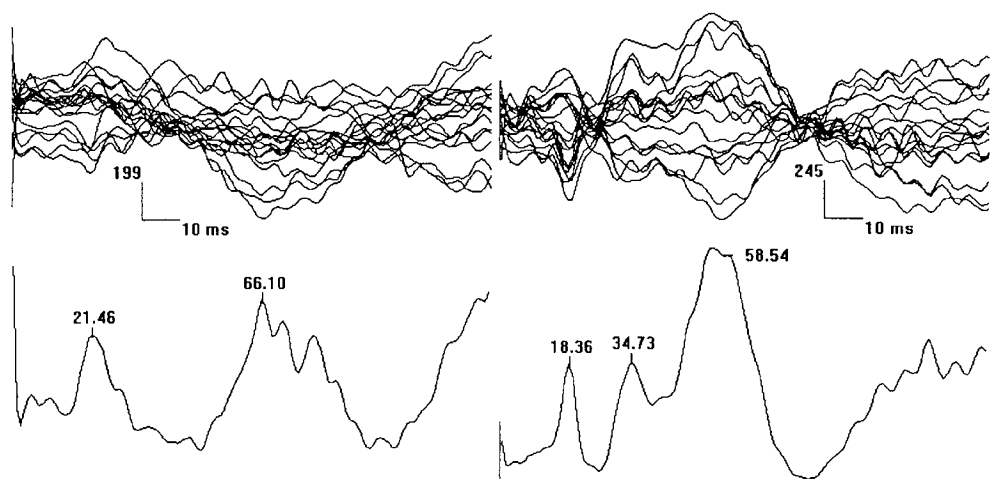


Figure 5.74 19 MEG channels superimposed following a single trial of Left median nerve stimulation with the corresponding Global Field Power plot with the Right median nerve data alongside to the right.



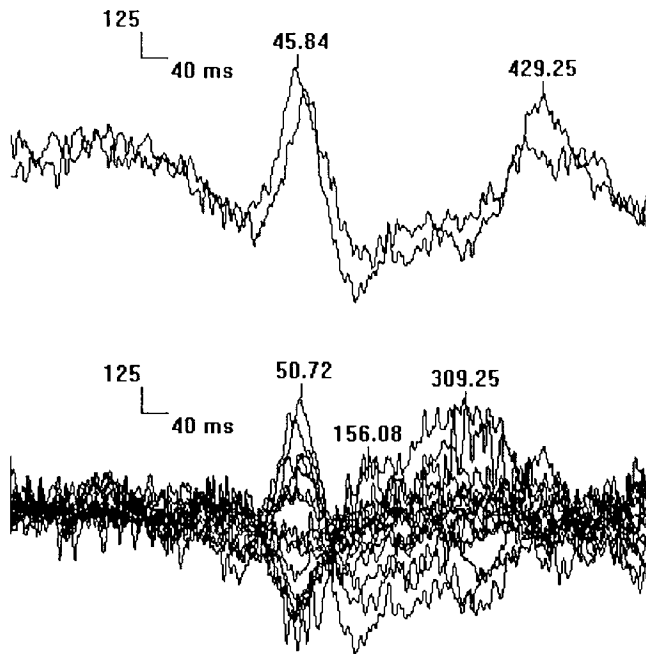


Figure 5.75 Top traces show two separate trials of Left index finger movement data superimposed for comparison. Beneath are 19 MEG channels from a single trial superimposed. Latencies are calculated from the moment that a button switch was depressed as part of the finger movement and represents time zero. Vertical axis is in femtotesla ( $10^{-15}$  T).

#### 5.4.13.4 MEG-MRI co-registration

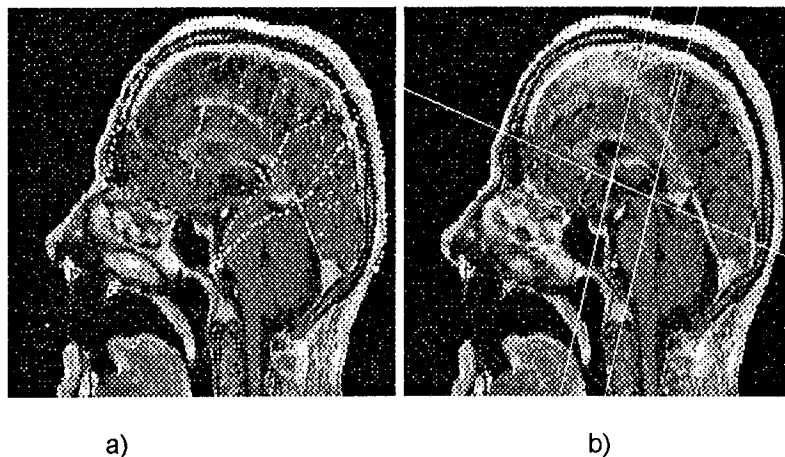


Figure 5.76 Patient DO Plate a) shows digitised head shape file, acquired at the time of the MEG acquisition, co-registered with the MRI. Plate b) shows the CA-CP and VCA-VCP lines of the Talairach co-ordinate system positioned on a mid-line slice.

#### 5.4.13.5 MEG-MRI source localisation

95% confidence volumes for Right and Left median nerve stimulation together with Left self paced finger movement are illustrated overleaf (Figures 5.78 and 5.79).

#### 5.4.13.6 Patient DO - Predicted location of the Central Sulcus

Localisations for two separate trials of **left median nerve** stimulation (at latencies of 29.0 and 59.0ms) yielded a mean Talairach co-ordinate of:

CA-CP axis: -19.6 mm      Lateral axis: -48.1 mm      VCA-VCP axis: 40.8 mm.

Localisations for two separate trials of **right median nerve** stimulation (at latencies of 41.0ms and 53.0ms) yielded a mean Talairach co-ordinate of:

CA-CP axis: -46.9 mm      Lateral axis: 36.3 mm      VCA-VCP axis: 39.5 mm.

Localisations for two separate trials of **left index finger movement** (at latencies of 241.0 and 255.0ms) yielded a mean Talairach co-ordinate of:

CA-CP axis: -22.9 mm      Lateral axis: -56.2 mm      VCA-VCP axis: 39.5 mm.

Neuroanatomical inspection of the MRI together with Talairach co-ordinate data suggested that the left median nerve dipoles were centred predominantly over the pre-central gyrus in this patient with the self paced finger movement dipoles located post-centrally. Right median nerve data was consistently located in what appeared to be the post-central gyrus. The data is depicted graphically in Figure 5.77

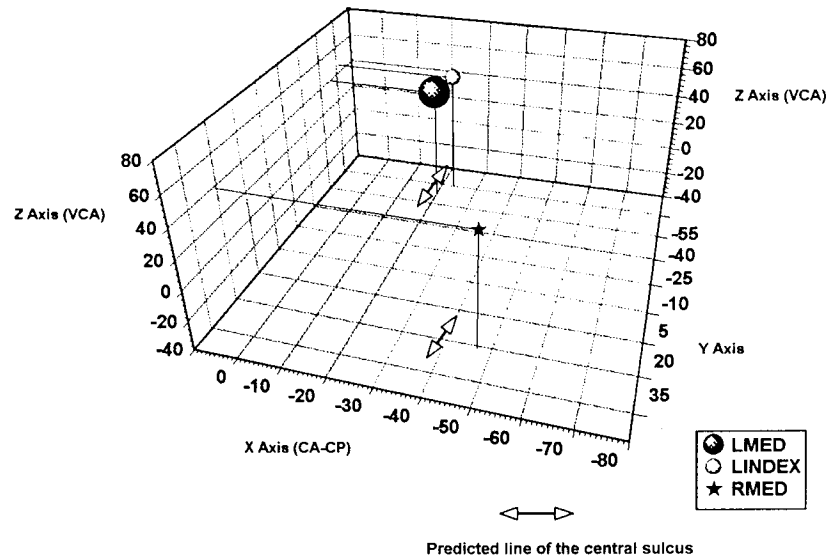


Figure 5.77 Mean Talairach co-ordinates for dipole localisation in patient DO.

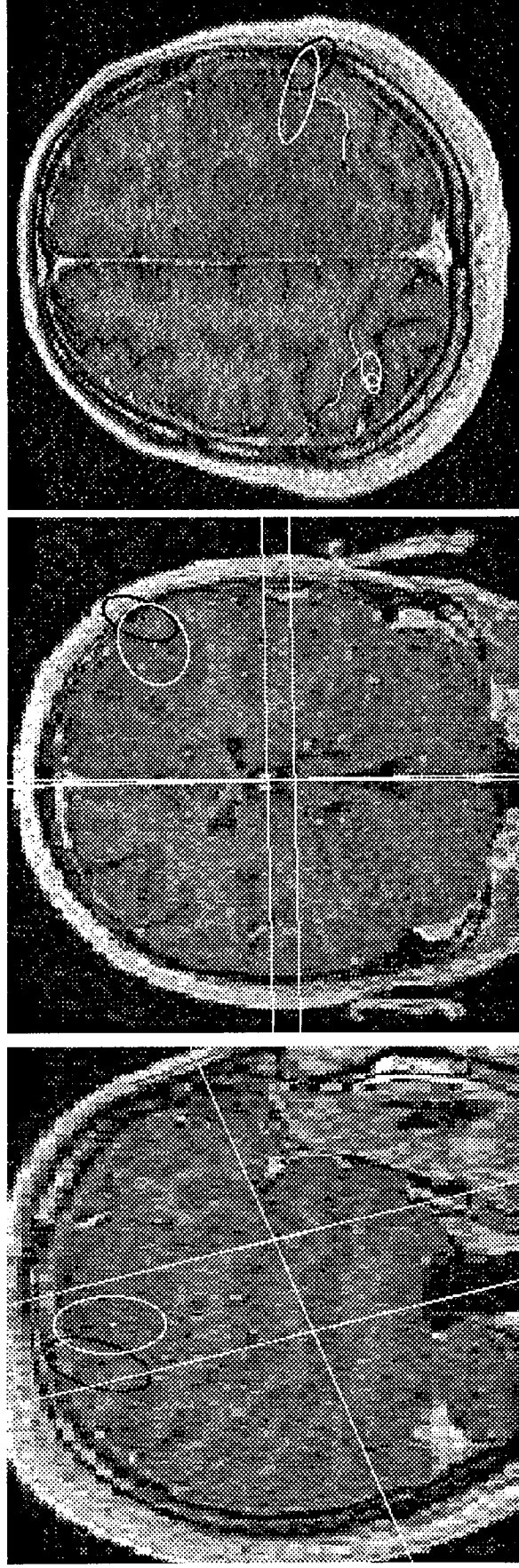
#### 5.4.13.7 Surgical validation - patient DO

Cortical measurements of somatosensory evoked potentials were used to localise hand function for the sensory motor strip. When compared with MEG localisations, these were found to be entirely accurate.

#### 5.4.13.8 Summary - Patient DO

The confidence volume following left median nerve stimulation lay over both pre- and post central gyri whilst that of the self paced finger movement lay post-centrally. The latency of the finger movement data was consistent with an MEFII component which would support the underlying generator for this component as lying in the postcentral gyrus. The combination of the two data sets allowed central sulcus prediction to be more readily made.

## Chapter 5



a)

b)

c)

Figure 5.78 Patient DO. Plates a) and b) show 95% confidence volumes for localisations of Left Median nerve stimulation (white ellipses) and Left index finger movement (black ellipses). Plate c) shows Left and Right median somatosensory confidence volume localisations with white ellipses and that of the Left index finger movement with the black confidence ellipse. The white lines superimposed on the axial slice indicate the predicted line of the central sulcus.

## 5.5 Summary and discussion

Table 5-1 Summary of pre-surgical evaluation data

Patient	Age	Diagnosis	Modalities Tested	Distance from Central Sulcus (mm)	Latency of closest localisation (ms)	Accurate localisation of Central Sulcus?
PR	44	Left parietal low grade astrocytoma	1. Rt Median 2. Rt Post Tib	1. +8.0mm 2. +10.0mm	1. 44.0ms 2. 42.0ms	No. Localisations pre-central
DT		Tonic clonic seizures. Left Jacksonian onset	1. Lt Median 2. Lt Post Tib	1. -8.0mm 2. -3.0mm	1. 21.5ms 2. 75.5ms	Yes Differs from Neuro-Radiology
SM	38	Left hemisphere lesion. Tonic-clonic seizures	1. Rt Median 2. Rt Post Tib	1. -3.0mm 2. $r < 0.95$	1. 47.5ms	Yes
JC	28	Right hemiplegia. Right sided seizures	1. Rt Median 2. Lt Median	1. No signal 2. -11.0mm	2. 24.0ms	Based on hemisphere symmetry. Awaiting surgery
TH		CVA . Left sided intractable pain	1. Rt Median 2. Lt Median	1. +7.0mm 2. No signal	1. 40.0ms	Yes Differs from Neuro-Radiology
AS	17	Right sided myoclonic seizures	1. Rt Median 2. Lt Median 3. Rt Post Tib	1. -9.0mm 2. -8.0mm 3. $r < 0.95$	1. 30.0ms 2. 32.0ms	Yes
AD	50	Fibrillary astrocytoma. Complex partial seizures	1. Rt Median 2. Lt Median 3. Lt Post Tib	1. -12.0mm 2. -3.0mm 3. $r < 0.95$	1. 58.0ms 2. 36.0ms	Yes
DB	52	Right frontal glioma with tonic clonic seizures	1. Rt Median 2. Lt Median 3. Lt Post Tib	1. -2.0mm 2. No signal 3. No signal	1. 29.0ms	Yes - Based on hemisphere symmetry

Continued overleaf

Table 5-2 Summary of pre-surgical evaluation data

Patient	Age	Diagnosis	Modalities Tested	Distance from Central Sulcus (mm)	Latency of closest localisation (ms)	Accurate localisation of Central Sulcus?
CJ	35	Left parietal cystic astrocytoma	1. Rt Median	1. -1.0mm	1. 20.0ms	Yes
			2. Lt Median	2. -3.0mm	2. 25.0ms	
			3. Rt Post Tib	3. +10.0mm	3. 41.5ms	
			4. Lt Post Tib	4. $r < 0.95$		
PP	64	Rt hemiparesis from CVA.	1. Lt Median	1. -2.0mm	1. 18.0ms	Awaiting surgery
RL	37	Jacksonian seizures from Rt Grade 3 astrocytoma	1. Rt Median	1. -8.0mm	1. 23.0ms	Yes
			2. Lt Median	2. -6.0mm	2. 35.0ms	
			3. Lt index motor	3. -1.0mm	3. 32.0ms	
			4. Rt index motor	4. -1.0mm	4. 25.0ms	
JS	37	Left cavernous angioma	1. Rt Median	1. 0.0mm	1. 50.0ms	Yes
			2. Rt index motor	2. +4.0mm	2. 38.0ms	
			3. Lt index motor	3. +3.0mm	3. 118.0ms	
DO	40	Right frontal tumour	1. Rt Median	1. -7.0mm	1. 41.0ms	Yes
			2. Lt Median	2. -2.0mm	2. 29.0ms	
			3. Lt index motor	3. -5.0mm	3. 241.0ms	

Tables 5-1 and 5-2 provide a summary of the pre-surgical evaluation data in thirteen patients. Distance from central sulcus was assessed from the mean localisation of the best fitting confidence volume. Minus sign indicates a localisation posterior to the central sulcus and a positive sign indicates an anterior location. The column assessing the accurate localisation of the central sulcus is based on the premise that using MEG alone the position of the central sulcus could be reliably discerned.

### Summary and discussion (continued)

#### 5.5.1 MEG, Neuro-Radiology and surgical validation

Of the 13 patients studied, 11 had surgery and in 10 of these cases, MEG accurately determined the location of the hand area of the sensory-motor cortex (91%). Over the same patient sample, Neuro-Radiology was successful in identifying the somatosensory cortex in 9 cases (82%). Across the entire patient group, MEG and Neuro-Radiological localisations of the position of the central sulcus agreed in 10 of the 13 cases (77%). We will now review these important differences case by case:

In patient PR (number 1), the MEG localisations lay entirely within the pre-central gyrus for both median and posterior tibial nerve data and therefore wrongly implicated the anterior sulcus. Neuro-radiology successfully identified the line of the central sulcus.

There are a number of important points to consider from the data in this patient. The consistent localisations of both median and posterior tibial nerve data in this patient implies a systematic displacement, if indeed this data represents an error of source localisation. One explanation in this case would be that the astrocytoma represented a large conductivity perturbation and so the true conductivity profile may not have been represented by the homogeneous sphere model used in the source localisation algorithm.

A further consideration may be that the cortical displacement caused by the astrocytoma made the correlation of the MEG data, located in the depths of the sulcus, extremely difficult to compare in relation to surface landmarks. Since no intrasurgical cortical imaging co-registration was available, the findings could represent a failure to accurately match the MRI with the cortical stimulation data obtained at surgery.

Finally, the error could result as a failure due to a scaling error in the translation matrix for the MRI co-registration technique.

fMRI was extremely useful in this case since the juxtaposition of the two sources gave a more reliable estimate of the true picture.

Neuro-Radiology disagreed with the MEG localisations in two cases.

In patient DT (number 2), Neuro-Radiology suggested that MEG localisations were lying in the pre-central gyrus. Surgical measures revealed that they accurately implicated the sensory post-central gyrus. This case particularly highlighted the potential value of MEG in assisting localisations where the neuroanatomy may be indistinct.

In patient TH (number 5), no reliable MEG signals could be discerned from the affected hemisphere and so localisations were based on hemisphere symmetry. Here again though, the confidence volumes lay within the pre-central gyrus as determined by Neuro-Radiology. Surgical outcome identified the MEG data as accurately implicating the sensory cortex.

It is interesting to compare this data with that achieved by Sobel et al., 1993. In this study, the authors compared MR anatomic and MEG functional methods in locating the central sulcus. Eleven healthy subjects and five patients with focal cerebral lesions were studied. The central sulcus was located anatomically with MR by two independent observers and locations via MEG were achieved by measuring somatosensory evoked magnetic fields. They reported that MR localisations were most reliable in the axial slice with inter-rater agreement in 76% of sections for both control subjects and patients. The concordance of MR and MEG methods ranged from 55% to 84% in control subjects and 65% to 67% in patients.

It is interesting to note from this study that the inter-rater agreement on central sulcus localisation was only marginally superior to the MRI / MEG concordance. These authors concluded that whilst MR anatomic techniques can usually identify the central sulcus, in the presence of anatomic distortion the MEG functional method made a significant contribution.



### 5.5.2 Median and Posterior Tibial nerve localisations

Median nerve stimulation proved a highly effective way to localise the post central gyrus and in 10 patients would have been adequate if used in isolation to other measures. The combination of multiple nerve trunk stimulation provided additional confidence for the use of the technique, particularly when comparing right and left median nerve localisations.

Localisation of data from the hand was considerably more robust than that achieved from stimulation of posterior tibial nerve. Posterior tibial nerve data was achieved from six patients and measures were made from seven hemispheres. In one patient (DT) a localisation within 3 mm of the central sulcus and within the post-central gyrus was achieved and in two others (PR and CJ) a pre-central localisation some 10mm from the central sulcus was observed. In the remaining four subjects, dipole fits from the data failed to yield correlation co-efficients of 0.95 or greater and so were rejected.

The explanation for this poor outcome may in part be due to the lower signal to noise ratio's in this data set which was also observed in the control group (Chapter 3)

### 5.5.3 Self paced finger movement

The high signal to noise ratio of the movement paradigm consistently yielded small confidence volumes which may well be improved upon by more sophisticated triggering protocols such as using the rectified EMG instead of the crude button depression.

Overlying confidence volumes achieved from independent paradigms (sensory and movement) gave a high measure of confidence to the data which could not be achieved simply by repetition of the sensory paradigm nor indeed by measurements from other nerve trunks

Localisations from movement data were achieved from two patients (RL and JS) at latencies consistent with the MF component described for control subjects in Chapter

4 and with an wave II component in one patient (DO). One must be necessarily guarded in implying location with function in these patients due to the close proximity of space occupying lesions to sensory motor cortex.

In patient RL, the MF components were located in both the affected and unaffected hemispheres predominantly post-centrally, although in each case, the finger movement localisations were between 5 and 7 mm anterior to their median nerve counterparts.

In patient JS, both right and left MF components were located in the pre-central gyrus in contrast to the right median nerve data which was located post-centrally.

Finger movement data in patient DO was consistent with a so called MEFII component (Cheyne and Weinberg 1989) and was located in the post-central gyrus posteriorly to the median nerve counterpart.

This thesis suggests that MF data is generated at least in part by a different neuronal population than that achieved through median nerve stimulation, although there is a small overlap in the 95% confidence volumes achieved by each modality. MEFII may well reflect a predominantly sensory response.

There is some consistencies with a study by Kristeva-Feige et al., 1996 who reported an anterior and deeper source for their MEFI component (peaking 100ms post movement onset) than the SEF and concluded that this reflected a contribution from Brodmann area 3a which is known to receive proprioceptive afferents from joints.

Other workers (Kassubek et al 1996) have attributed MF component activity to the pre-central gyrus (equivalent in latency to the MEFI component of Kristeva-Feige et al., 1996).

### 5.5.4 fMRI

Data was only obtained from one patient in the study and so does not represent any reasonable sample. It proved of particular interest in this patient (PR) because of the juxtaposition with the MEG data which was located in the pre-central gyrus. The fMRI data was located on the gyral surface of the pre-central gyrus in contrast to that seen

in the control subject reported in Chapter 2. Here, the fMRI localisation was seen over the post central gyrus given the exact same stimulus conditions.

Jack et al., (1994; 1996) described their experiences in applying fMRI to study pre-operative mapping of the sensorimotor area in 20 patients with epilepsy.

Identification of the central sulcus was accomplished unequivocally in 9 of 20 patients. The reasons for failure in the other 11 patients was due to patient head motion (9 cases), artefacts caused by previous craniotomy (1 case) and no clear activational area detected above noise (1 case).

These authors made a number of pertinent comments related to their data:

'Although the ability of fMRI to identify the functional sensorimotor area may appear to be a problem that has been entirely resolved, several key issues remain before the technique can be considered a clinically reliable test. First, we often find, in patients and volunteers, fMRI activation that meets statistical criteria for significance in more than one cortical sulcus. Furthermore, the method of processing the fMRI time series, which currently appears to be a fairly arbitrary choice made by individual investigators, can markedly influence the interpretation of the fMRI study. However, neurosurgeons need to know unequivocally which sulcus is the central sulcus.....In performing functional studies, the central sulcus region will routinely activate with a finger tapping task but so will other "surgically insignificant" areas'.

### 5.5.5 Conclusion

The very high success rate of MEG in accurately locating sensory motor cortex in the studies in this thesis suggests a promising future for the technique in both clinical and research applications. An important element in the success of the technique lies not only in robust instrumentation and inverse solution computation, but equally in co-registration strategy.

It may be concluded that the use of MEG measures of median nerve stimulation together with self paced finger movement paradigms provide a robust method of assessing the location of the central sulcus and the functional organisation of the sensory-motor cortex. Data from this thesis is in agreement with those authors who

suggest that the motor field (MF) achieved through self paced finger movements is generated by the motor cortex. Thus the combination of sensory and motor data achieved independently provides a confidence to the localising power of the technique which would be impossible to achieve by either method used independently.

The 'gold standard' for cortical location of function is intra-operative measurement. Whilst the absolute resolution of MEG compares favourably with ECoG (Gharib et al 1995), it cannot be envisaged that MEG or any other functional imaging technique could or should attempt to replace intra-operative measures. However, the pre-operative decision as to the extent of excision and the prognosis of surgical outcome could all be strongly influenced by such techniques. Since awake craniotomy is unachievable in children, developments in the application of the technique to paediatric surgery, together with intrasurgical cortical imaging, may significantly advance the use of surgical intervention in this field.

Current pre-surgical evaluation is achieved in part through Neuro-Radiological examination of topographical landmarks as seen in MRI acquisition. The approach to the lesion can be planned on the basis of the topographical relationship between the coronal suture and the pre-central or central fissure. Due to the variability of this relationship and the distortions caused by space-occupying lesions, such landmarks can only be used as guides. In agreement with Sobel and co-workers (1993) data from this thesis would support the view that whilst MR anatomic techniques can usually identify the central sulcus, in the presence of anatomic distortion, the co-registration of MEG or other functional data considerably improves an understanding of the functional cortical organisation.

It will be important to develop protocols to allow the data to be displayed in an interactive form intraoperatively, thus allowing co-registrations to be more readily and accurately.

The combination of MEG with fMRI is clearly a development which would bring added confidence to such non-invasive assessments. The failure of fMRI to be able

to reliably distinguish between sensory and motor cortex places significant limitations on its effectiveness for clinical evaluation if used in isolation.

### **6. Cortical localisation of magnetic fields evoked by Oesophageal distension.**

#### **6.1 Introduction**

Despite much study of the brain-gut axis in man in recent years, little is still known of the nature and location of the cortical representation of visceral sensation.

A number of studies have described cortical evoked potentials elicited from stimulation of the viscera, including the bladder (Badr et al., 1982), the rectum (Collet et al., 1988) and the oesophagus (Castell et al. 1990; Frieling et al. 1989; Smout et al. 1990; Tougas et al. 1993).

The oesophagus is a unique organ to examine; with the proximal one third comprising striated muscle and the distal two-thirds smooth muscle, this presents an opportunity to compare cortical sensory mechanisms for both somatic and visceral afferents.

A previous study by our group (Aziz et al. 1995, Appendix II) described the spatial and temporal features of potentials elicited following balloon distension of the proximal and distal oesophagus. Although some assumptions about cortical generators could be postulated from this work, specific source localisation techniques were necessary for precise identification.

Recent studies of oesophageal evoked cortical potentials suggested multiple cortical sources process oesophageal sensation (Weusten et al., 1994)

Magnetoencephalography, since its early application in the recording of transient evoked magnetic events from the cortex (Brenner et al. 1978), has established itself as an important non-invasive tool for accurate and sensitive localisation of functionally eloquent cortex.

## Chapter 6

### 6.2 Aims

The aim of this study was to apply MEG source localisation techniques to the measurement of oesophageal evoked magnetic fields from the cerebral cortex in man, and to compare and contrast proximal versus distal oesophageal cortical representations following a balloon distension stimulus. A preliminary report has described these experiments (Furlong et al. 1995).

### 6.3 Method

#### 6.3.1 Subjects

Three male volunteers (ages 23, 37 and 48 years) were recruited from personnel affiliated with the research units. Each subject was free of oesophageal symptoms and each received oesophageal manometry to accurately localise the positions of the upper and lower oesophageal sphincters (Aziz et al. 1995). All subjects showed normal oesophageal manometric function. All subjects gave informed consent to the study.

#### 6.3.2 Oesophageal Stimulation

Oesophageal distension was selected as a stimulus because it provided a physiological and localised change within the walls of the organ.

Oesophageal distension was achieved by inflating a 2cm long silicone balloon in the oesophagus. The balloon was mounted 15cm from the tip of a 4mm diameter multilumen polyvinyl catheter (Wilson Cook, Letchworth, Herts., U.K.) For proximal stimulation, the centre of the balloon was placed 3cm distal to the upper oesophageal sphincter, while for distal stimulation it was located 5cm proximal to the

## Chapter 6

lower oesophageal sphincter.

The balloon was repeatedly inflated with air using a purpose built pump (described in detail previously; Aziz et al 1995), operated at a flow rate of 20 litres per minute. Inflation time was a constant for a given volume (80msec for 12ml for example) and the inflation duration was 0.1 -0.5 seconds. Inter stimulus interval was maintained at 5 seconds.

The inflation volume used in each individual was that which yielded a clearly perceptible but not painful sensation through the study.

### 6.3.3 Magnetometer system

Subjects were seated beneath the Aston Magnetometer system (refer to Chapter 2). Nineteen channels of MEG signal, acquired in 512 msec epochs and sampled at 1KHz, were stored for off line analysis with bandpass filters of 0.5 - 106Hz (-3db down point, 12db/octave). Epoch sampling was initiated by the onset of balloon inflation.

Environmental noise was sampled by three vector magnetometers housed on a separate probe in the same dewar and software enabled a proportion of this sampled noise to be removed off line from the data acquisition.

### 6.3.4 Recording protocol

To ensure comfort and reliability of recording position, as well as ensuring adequate co-registration with Magnetic Resonance Images (MRI), an acrylic bite bar was manufactured for each subject. This comprised a mouth piece covered with a dental thermoplastic material (Stents™) with two acrylic arms, one on each side of the mouthpiece, projecting backwards along the angle of the jaw. This assembly was mounted in a free standing wooden gantry.

Once the subject was seated comfortably in the appropriate recording position, the bite bar was presented to the subject and locked firmly in position.



## Chapter 6

The precise positional relationship between the magnetometer and subject was achieved using a Polhemus 3D space tracker™ which measured the spatial coordinates of 6 markers on the bite bar assembly (Singh et al. 1997).

At the beginning of each study, the oesophageal catheter was inserted perorally and the balloon was positioned in either the proximal or the distal oesophageal segment. The subject was then seated with the Magnetometer centred over one of seven head positions. With reference to the International 10-20 system of electrode placement (Jasper 1958), these positions would include as centre points either T3, T4, C3, C4, Cz, Pz or Fz.

Three trials consisting of 50 balloon inflations each were used for each head position and recordings were performed on at least two separate occasions for each head position.

The subjects were requested to attend to the stimuli throughout each trial. The procedure was then repeated for stimulation of the other oesophageal site.

Non stimulus runs consisting of 50 sham balloon inflations were interspersed throughout the procedure to use as control comparisons.

Each recording session was limited to 2 hours to prevent subject fatigue and each subject sat for between 8 and 12 recording sessions over a period of 18 months to establish repeatability of the data.

### 6.3.5 Magnetic Resonance Images (MRI)

Each subject received a high resolution anatomical T1 MRI scan ( 256 x 256 x128 voxels, 200mm field of view, 1.5 mm slice separation) acquired with the bite bar in situ. The six markers on the acrylic bite bar were filled with cod liver oil to enable them to be clearly visualised on the images and thus enable co-registration with the MEG dataset (Singh et al. 1997).

## Chapter 6

### 6.3.6 Data analysis

MEG data were averaged off line employing adaptive filtering which incorporated the environmental noise measures acquired by the vector magnetometers.

Global Field Power estimations (Lehmann and Skrandies 1984) were calculated for the nineteen averaged epochs in each run to ascertain latencies likely to yield good source localisation estimations. Field distributions were plotted for the appropriate latencies. Only those data which showed consistent waveforms when recordings were performed on separate occasions were used in the analysis.

Magnetic field waveforms were compared with their electrical potential counterparts (described in detail in Aziz et al., 1995) to establish equivalent identification of components. The N1, P1, N2 and P2 nomenclature was adopted for labelling of the MEG waveforms to allow comparisons to be made.

### 6.3.7 Source localisation

A single equivalent dipole in a homogeneous conducting sphere was used as the source model for localising the cortical generators of the evoked response. 20 discrete scalp points, centred around the measurement area, were digitised using the Polhemus device, and these were used calculate the radius of the sphere.

Estimation of the dipole parameters was by minimisation of the least squares measure (Chi squared), using the Powell algorithm (Press et al. 1989). A weighting function, based on the signal-to-noise ratio in each channel, was used in the minimisation.

Dipole estimations were made for each trial and all latencies indicating a dipolar field pattern, strong Global Field Power and signal-to-noise ratio's greater than 2:1. After minimisation, the acceptability of the fitted dipole was assessed using the Chi-

## Chapter 6

squared probability and the correlation coefficient,  $r$ , between the measured and estimated magnetic field. Datasets and latencies yielding significant correlations ( $r > 0.95$ ) were taken forward for secondary analysis.

### 6.3.8 Estimation of confidence for the localisation

Once source localisation was completed, an estimate of the confidence region for the localisation was computed using the method of Monte-Carlo estimation (Medvick et al. 1990). Firstly, the magnitude of the noise in each channel was estimated using the anti-average (Regan 1989). Then, trial datasets were created by adding random gaussian noise of this magnitude to the field from the calculated dipole. These trial datasets were then re-analysed using the same source localisation procedure to yield a spread of dipole positions. Finally, the 95% confidence ellipsoid was calculated such that 95% of this spread of dipoles was contained within the ellipsoid volume.

Following 50 iterations of Monte Carlo analysis, mean dipole estimations and 95% confidence ellipsoids were then superimposed onto the matching slice of the subjects MRI for localisation purposes.

### 6.3.9 Inter-subject comparisons

For comparison of dipole source localisations between subjects, spatial co-ordinates of the sources were obtained using the co-ordinate system of Talairach and Tournoux (1988).

### 6.4 Results

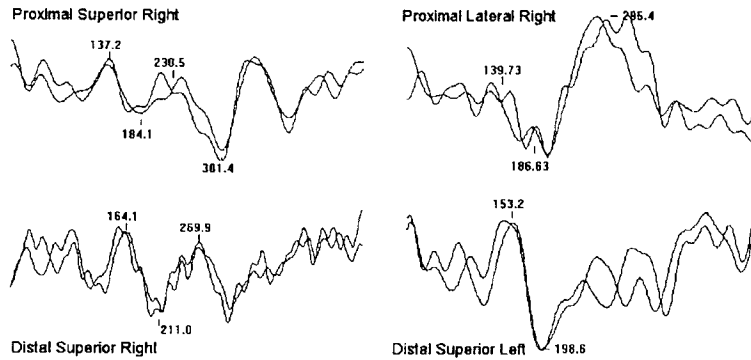
#### 6.4.1 Proximal Oesophageal Stimulation

In each of the three subjects, robust and reproducible waveforms could be discerned following balloon distension in the proximal oesophagus. These waveforms were similar in morphology to the electrically recorded evoked potentials reported previously (Aziz et al 1995). See Figure 6.1.

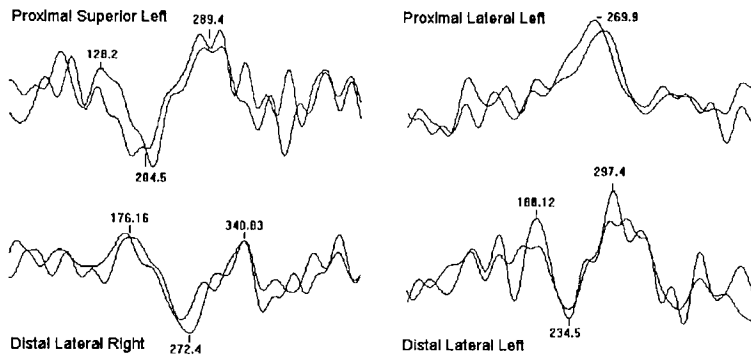
Systematic placement of the magnetometer around the skull yielded consistent locations where signals could be readily discerned when the magnetometer was centred over them. Using the nomenclature of the International 10-20 system for electrode placement (Jasper 1958), these sites were between the vertex and C3 and/or C4 and over T3 and/or T4 for all three subjects. For future reference in this text, we will refer to these sites as Superior Right or Superior Left for the former and Right or Left Lateral for the latter positions.

In all subjects the responses were clearly lateralised. Reproducible signals were obtained from the right hemisphere only in subjects 1 and 3, and from the left hemisphere only in subject 2.

Subject 1



Subject 2



Subject 3

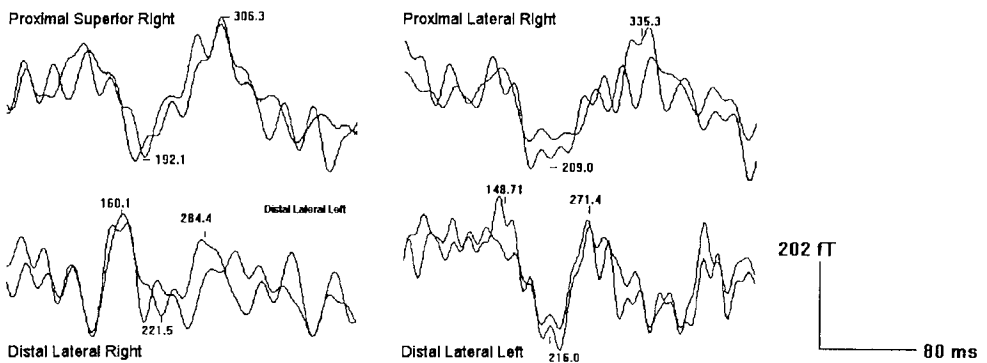


Figure 6.1 Evoked magnetic field waveforms from subject 2 for proximal and distal oesophageal stimulation. Separate trials of each evoked response are superimposed for comparison. The nomenclature adopted by Aziz et al (1985) for evoked potential data is used. The units on the vertical amplitude (x) axis on the scale bar are in femtoTesla ( $10^{-15}$  Tesla).

## Chapter 6

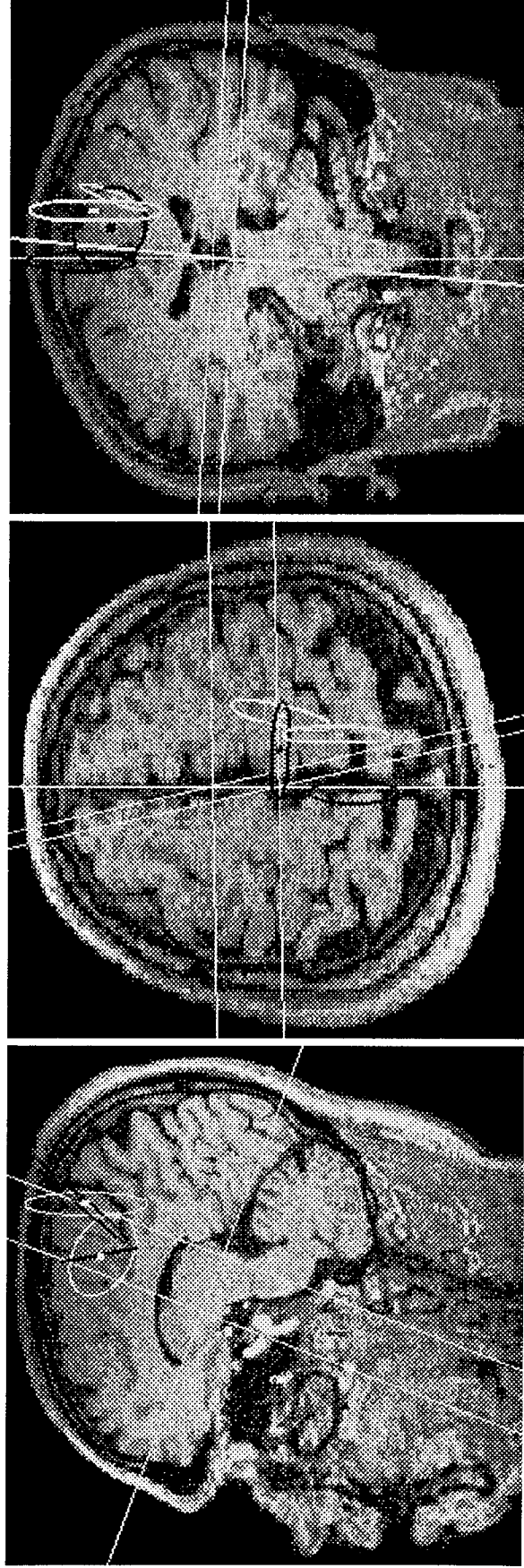
Examination of the Global Field Power plots revealed no consistent pattern in the temporal sequence of activation between the superior and lateral positions; the earliest field powers peaking between 171 and 190 milliseconds after the onset of balloon inflation. The exception to this was the left lateral response in subject 2 whose earliest peak was 267 milliseconds. If these latencies were corrected to allow for balloon inflation rise time, then the former latencies were consistent with the N1 or P1 components described by Aziz et al (1985) with the later lateral response in subject 2 corresponding to the N2 component.

### 6.4.2 Source locations for superior cortical aspects (proximal segment)

95% confidence ellipses of the dipole source localisations were co-registered with the individuals MRI (Figures 6.2-6.4). Only dipole fits which could be reproduced from at least two separate trials were used. In a given general location, where 95% confidence ellipsoids did not significantly overlap, these were plotted separately. In each case, the earliest component which yielded a strong dipolar field pattern was analysed.

In all subjects, source localisations from the superior aspect implicated the superior portion of the primary somatosensory cortex (SI). Latencies and morphology of the components from which these data were derived was consistent with the P1 component seen in electrical recordings.

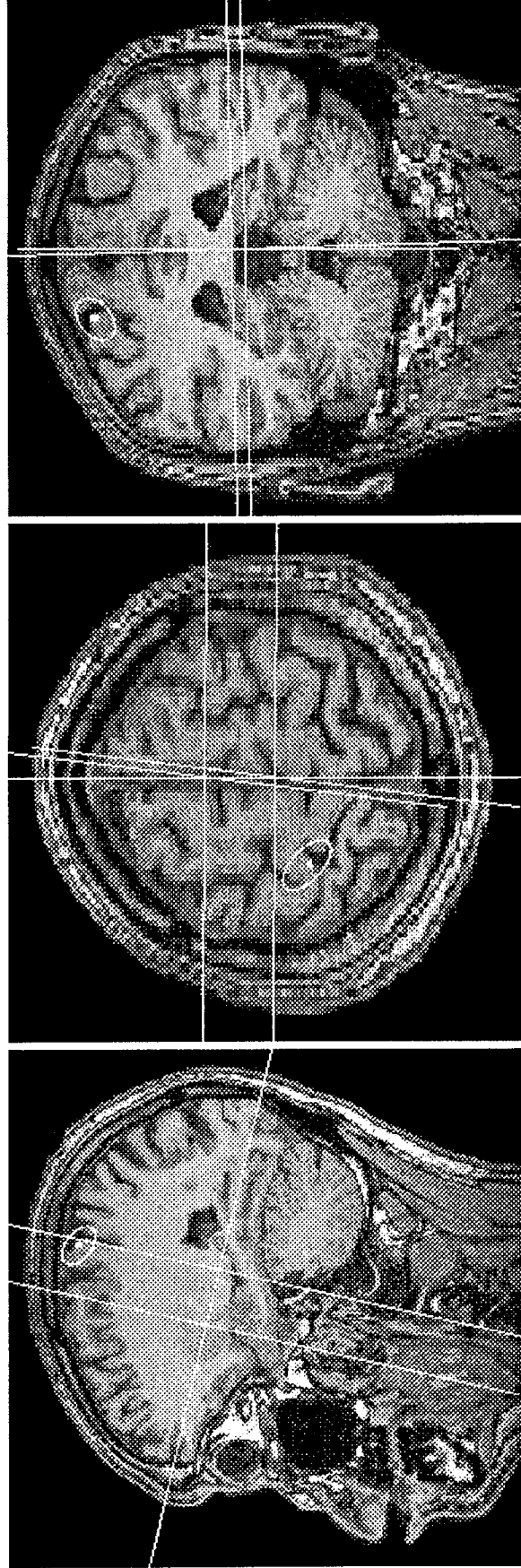
In subject 1, a second source which was deeper and more anteriorly placed was also derived from a P1 equivalent component. This source location was in the region of the cingulate gyrus at its junction with Brodmann area 6.



Subject 1

Source localisations acquired from the superior aspect of the cortex.

Figure 6.2 95% confidence ellipses were co-registered with the MRI of that individual. For ease of comparison, ellipses were plotted on a single slice of the sagittal, axial and coronal planes. White ellipses show proximal oesophageal data and black ellipses show the distal segment data. The mid-point of the ellipse represents the mean dipole source location following 50 iterations of Monte-Carlo analysis.

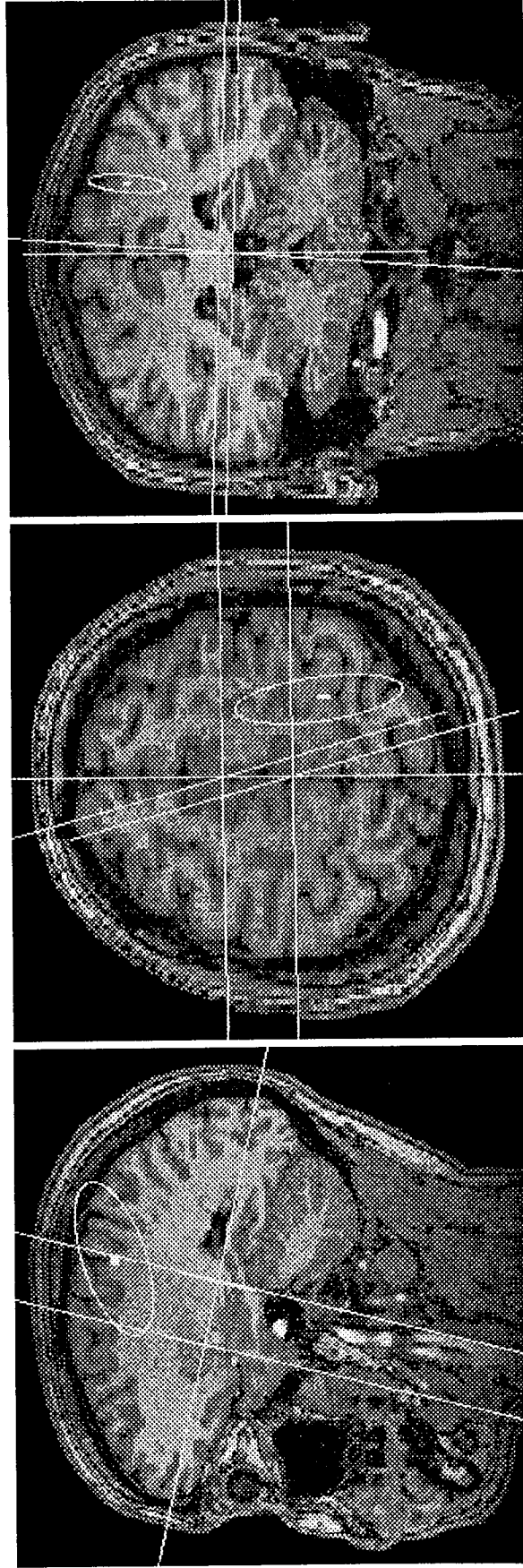


Subject 2

**Source localisations acquired from the superior aspect of the cortex.**

*Figure 6.3 95% confidence ellipses were co-registered with the MRI of that individual. For ease of comparison, ellipses were plotted on a single slice of the sagittal, axial and coronal planes. White ellipses show proximal oesophageal data and black ellipses show the distal segment data. The mid-point of the ellipse represents the mean dipole source location following 50 iterations of Monte-Carlo analysis.*





Subject 3

**Source localisations acquired from the superior aspect of the cortex.**

*Figure 6.4 95% confidence ellipses were co-registered with the MRI of that individual. For ease of comparison, ellipses were plotted on a single slice of the sagittal, axial and coronal planes. White ellipses show proximal oesophageal data and black ellipses show the distal segment data. The mid-point of the ellipse represents the mean dipole source location following 50 iterations of Monte-Carlo analysis.*

## Chapter 6

### 6.4.3 Source locations for lateral cortical aspects (proximal oesophagus)

In data acquired from the lateral aspects, the N2 component provided the dominant signal in subjects 1 and 2. In subject 3 the waveforms were equivocal, although the signal to noise ratios from this subject were generally poorer.

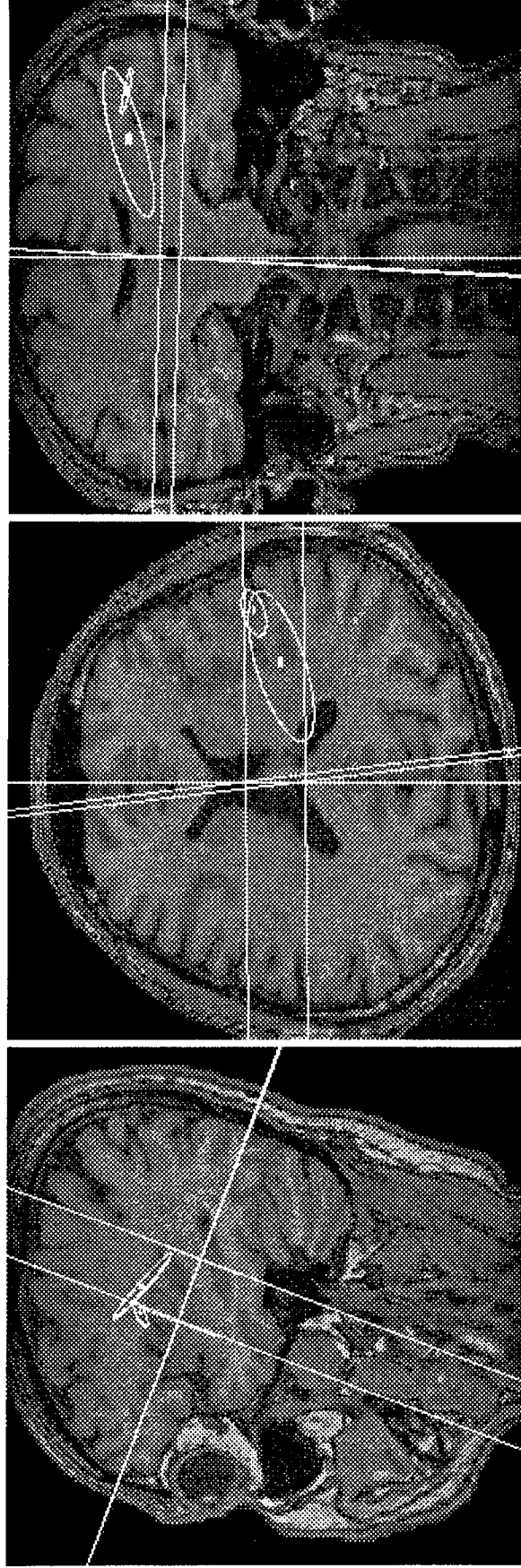
In subject 1, sufficient signal strength in several trials allowed the comparison of source localisation across a temporal sequence (Figure 6.1). No significant difference was determined between the right hemisphere source localisations of the N1 and P1 components whose volumes encompassed the posterior insular cortex together with the inferior portion of SI. The N2 component showed a consistent position on the the inferior aspect of SI which was more anterior and superficial than the earlier components. Confidence ellipsoids of this data is plotted in Figure 6.5 (N2 component shown as the smaller confidence ellipse).

In subject 2, confidence volumes in the left hemisphere were obtained at latencies consistent with the N2 component in this subject. Two distinct volumes were observed; the first was centred on the inferior portion of SI and bordered the insular cortex, the second encompassed the posterior insular cortex and the secondary somatosensory cortex (SII).

In subject 3, the right hemisphere data consistent with the P1 component encompassed the insular cortex and inferior portion of SI.

Talairach co-ordinates (Talairach and Tournoux 1988) were calculated for the mean source localisations of the 95% confidence volumes and plotted graphically for comparison (Figure 6.8). There was a close relationship between the source localisations in all three subjects.

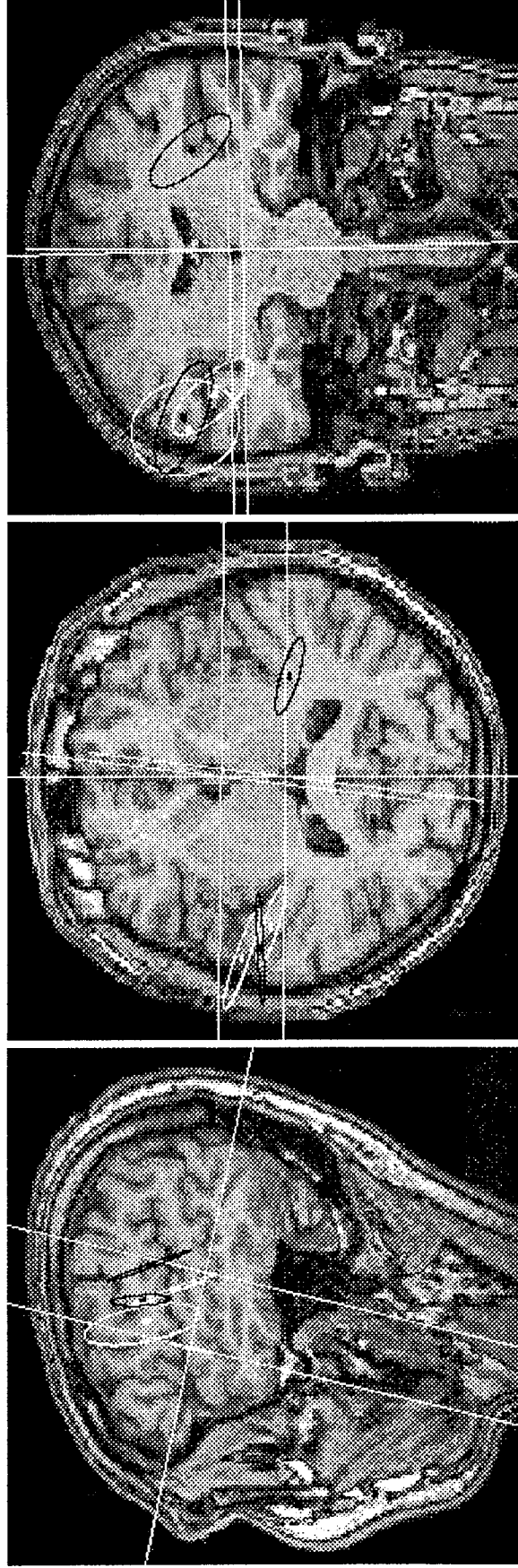
## Chapter 6



**Subject 1 - Source localisations acquired from the lateral aspect of the cortex.**

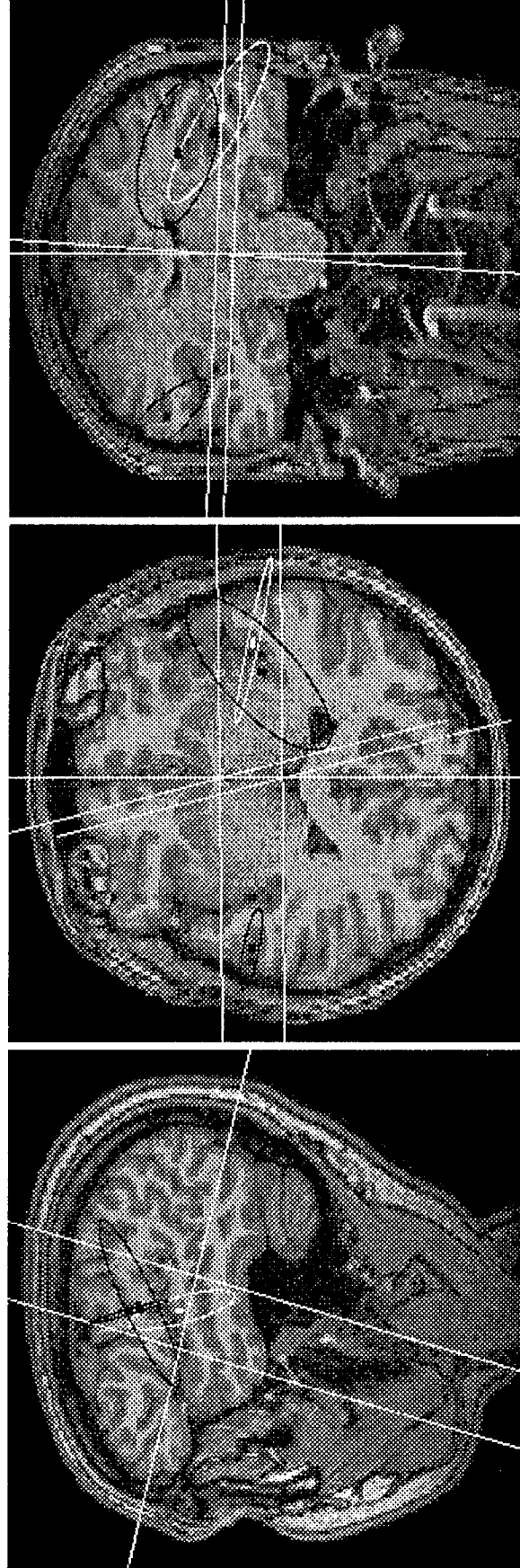
*Figure 6.5 95% confidence ellipses were co-registered with the MRI of that individual. For ease of comparison, ellipses were plotted on a single slice of the sagittal, axial and coronal planes. White ellipses show proximal oesophageal data and black ellipses show the distal segment data. The mid-point of the ellipse represents the mean dipole source location following 50 iterations of Monte-Carlo analysis.*

## Chapter 6



**Subject 2 - Source localisations acquired from the lateral aspect of the cortex.**

*Figure 6.6 95% confidence ellipses were co-registered with the MRI of that individual. For ease of comparison, ellipses were plotted on a single slice of the sagittal, axial and coronal planes. White ellipses show proximal oesophageal data and black ellipses show the distal segment data. The mid-point of the ellipse represents the mean dipole source location following 50 iterations of Monte-Carlo analysis.*



**Subject 3 - Source localisations acquired from the lateral aspect of the cortex.**

*Figure 6.7 95% confidence ellipses were co-registered with the MRI of that individual. For ease of comparison, ellipses were plotted on a single slice of the sagittal, axial and coronal planes. White ellipses show proximal oesophageal data and black ellipses show the distal segment data. The mid-point of the ellipse represents the mean dipole source location following 50 iterations of Monte-Carlo analysis.*

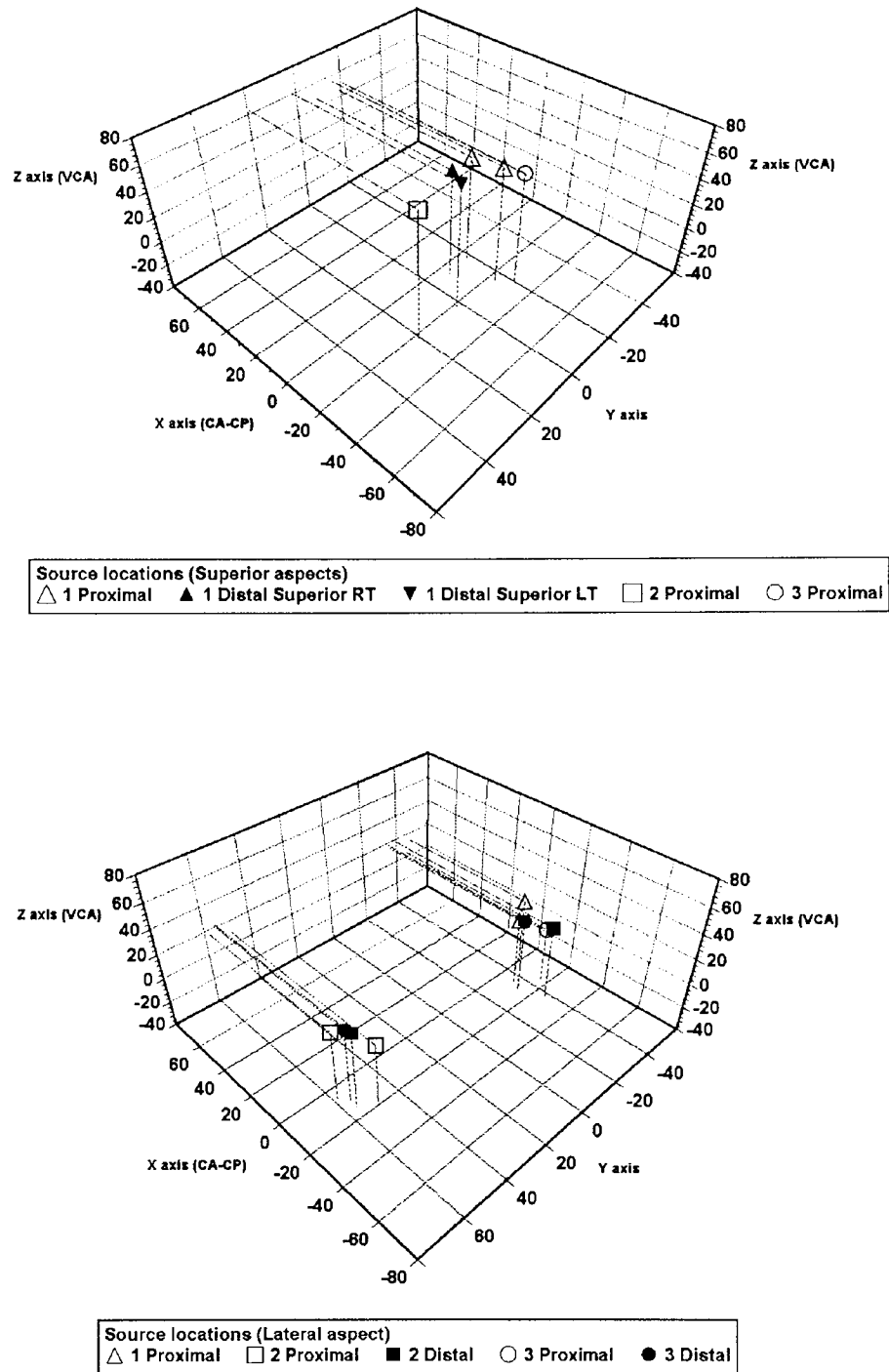


Figure 6.8 To more readily compare the source localisations between subjects, the three dimensional proportional grid system of Talairach and Tournoux (1988) was employed. Upper graph shows the relative localisations of superiorly placed sources with the lower graph depicting laterally located sources.

### 6.4.4 Distal Oesophageal Stimulation

Robust and reproducible waveforms could be discerned in each of the three subjects following distension of the distal oesophagus, with closely similar latencies and morphologies to those acquired from the proximal oesophagus (Figure 6.1).

In contrast to proximal stimulation, responses to distal stimulation were detected bilaterally.

Subject 1 produced signals from both right and left superior aspects. The determination of the existence of two independent sources close to the mid-line, as opposed to a single mid-line source, was obtained by making repeatable measures from separate dewar positions over each hemisphere. The resultant non-overlapping confidence volumes obtained by Monte-Carlo analysis were consistently located either side of the interhemispheric fissure. However, no discernable signals were detected from the lateral aspects in Subject 1. The converse was observed in subjects 2 and 3, with strong lateral right and left hemisphere signals being detected with no discernable signals recorded from the superior aspects.

Earliest maximum field power was between 168 milliseconds and 233 milliseconds after the onset of balloon inflation. In common with the data obtained by proximal stimulation, the left lateral response in subject 2 was significantly later at 298 milliseconds. When latencies were corrected to allow for balloon inflation rise time, latencies were consistent with the N1 or P1 components, with the later lateral response in subject 2 corresponding to the N2 component.

### 6.4.5 Source locations for superior cortical aspects (distal oesophagus)

Sources from the superior aspect were only obtained in subject 1, where signals acquired from the left superior aspect localised to the mid-line at a latency consistent with the N1 component. The confidence ellipse of this data implicated the superior portion of SI as the source for this signal. A second signal, acquired from a right

## Chapter 6

superior aspect at a latency consistent with P1, localised to an area consistent with the junction of Brodmann area 6 with the Cingulate gyrus (Figure 6.2 and 6.9).

### 6.4.6 Source locations for lateral cortical aspects (distal oesophagus)

In subject 2, right hemisphere data yielded confidence volumes which centred on and encompassed the posterior insular cortex at a latency consistent with a P1 component.

Left hemisphere volumes also bordered the insular cortex but centred on a junction consistent with the border of SI with SII (Figure 6.6 and 6.9). These data were derived from latencies consistent with N2 components.

In subject 3, N1 component confidence ellipses were centred on the posterior insular cortex in the right hemisphere and extended to encompass the inferior portion of SI. P1 component data in the left hemisphere was centred on the inferior portion of SI (Figures 6.7 and 6.9)

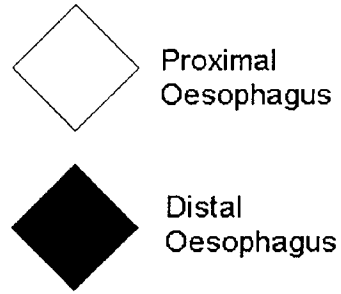
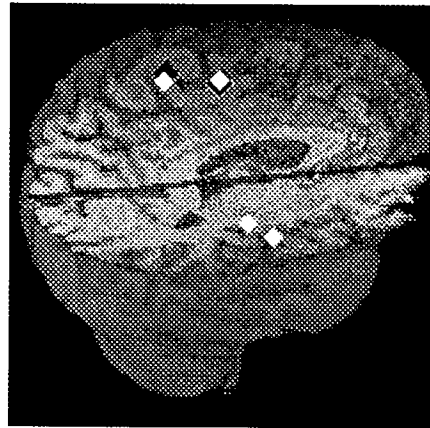
Comparison of Talairach co-ordinates (Figure 6.8) confirmed the close relationship of source localisations between subjects.

### 6.4.7 Comparison of Proximal and Distal Oesophageal data

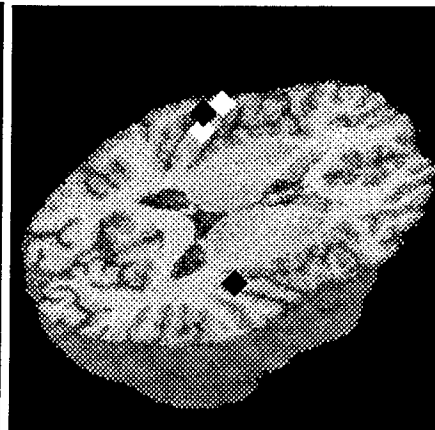
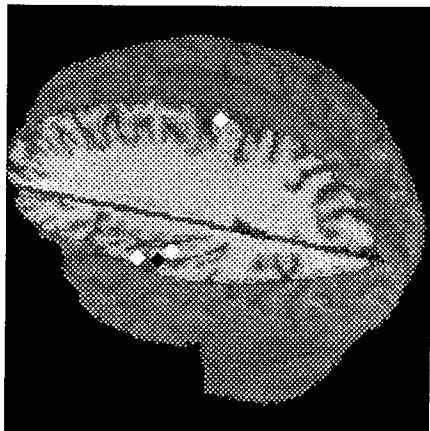
As can be seen from Figure 6.1, the morphology of waveforms was similar between Proximal and Distal data. No significant difference in temporal activation was noted either between stimulation sites or between cortical sites.

Cortical localisations confirm that a proportion of the N1 and P1 components are generated in superior SI following proximal stimulation.

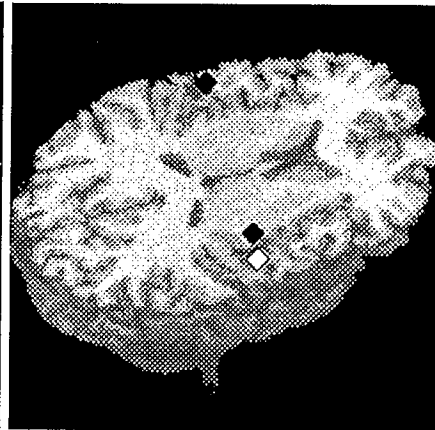
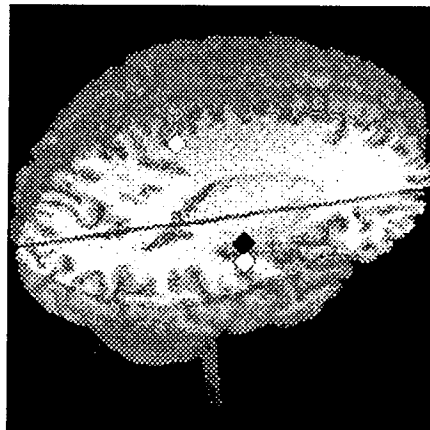




SUBJECT 1



SUBJECT 2



SUBJECT 3

Figure 6.9 Segmentation of surface rendered 3- dimensional MRI images illustrate the juxtaposition of dipole sources. White diamonds represent the mean dipole location following proximal oesophageal stimulation and the black diamonds represent the distal oesophageal data.

## Chapter 6

In the superior aspect, only subject 1 produced data suggesting cortical representation of both proximal and distal segments of the oesophagus in SI. Whilst there was a minor overlap in some boundaries of the confidence volumes in this subject, this data suggests that there is topographic organisation of visceral sensation here. Data in subject 1 further suggests that a proportion of the P1 component is generated in the Cingulate gyrus for both proximal and distal stimulation.

There was close association of localisations in the lateral cortex for both proximal and distal stimulation. The size and overlap of the 95% confidence volumes was such that no statement about a possible topographical organisation could be made.

Data recorded from the lateral cortex suggests the following generator sites of components for both proximal and distal stimulation:

N1 and P1: Insular cortex and inferior SI; N2: Insular cortex, inferior SI and SII.

### 6.5 Discussion

Since the work by Frieling et al., 1989, in first describing oesophageal stimulated cortical evoked potentials, several authors have reported that evoked potentials can be elicited by stimulation of the oesophagus and suggested that their data may be used as a measure of the integrity of oesophageal afferent pathway to the cortex. Conduction velocity estimates have been made (Smout et al. 1990), models for nociceptive mechanisms proposed (Frøbert et al., 1995) and studies of pathology made (Smout et al., 1992). However, all this work was performed against the background of uncertainty as to the number and location of underlying cortical generators.

More recent studies, which include the technique of evoked potential source modelling (Franssen et al., 1996) and Positron Emission Tomography (PET) (Aziz et al., 1997), confirm that multiple cortical generators contribute to the scalp recorded oesophageal evoked potential often described as a maxima at the vertex.

## Chapter 6

We have applied the technique of magnetoencephalography to identify cortical loci which process oesophageal sensation because it offers clear advantages over evoked potential dipole modelling and PET imaging.

Firstly, magnetic fields are unattenuated in their passage through tissue and bone and therefore simple algorithms may be applied to the recorded magnetic fields to calculate the Inverse solution and predict an equivalent current dipole source. This is a major advantage over electrical source modelling where incorrect estimation of conductivity and shape of the shell models for brain, meninges, skull and scalp may lead to errors (Roth et al. 1993)

Secondly, MEG is reference free and the characteristics of the gradiometer array are such that there is a relative insensitivity to far-field sources.

Unlike PET imaging, MEG is entirely non-invasive and many repeat studies may be performed in an individual without compromise. Most importantly, MEG provides high temporal resolution which enables imaging of the millisecond by millisecond sequencing of events, which is not possible with PET (Williamson et al., 1991, Hämäläinen et al., 1993, Harding 1993).

Data from our present study suggests that there may be as many as four discrete cortical hemispheric sites activated following stimulation of the oesophagus; the superior primary somatosensory cortex (SI), the insular cortex, the inferior portion of SI and the second somatosensory cortex (SII).

The location and overlapping temporal activation of these areas would yield the characteristic vertex potentials described in previous electrophysiological studies utilising balloon distension ( Castell et al., 1990; Smout et al., 1990; Weusten et al., 1994; Aziz et al., 1995).

## Chapter 6

The overlapping temporal sequencing of cortical activation between superior and lateral cortical sites for both the proximal and the distal oesophagus may be due to parallel processing of cortical events relayed via separate afferent pathways.

Recent animal studies support this view since oesophageal balloon distension has been shown to activate spinal as well as vagal afferents (Goyal et al. 1992; Sengupta et al. 1989; Sengupta et al. 1990).

Two important differences were noted in the pattern of cortical activation seen following proximal and distal oesophageal stimulation. First, activation of the superior aspect of SI was seen in all subjects following proximal stimulation but only in one subject following distal stimulation. The superior aspect of SI activated in our studies is consistent with the area known to receive afferent projections from the trunk (Penfield and Rasmussen 1950). SI is known to process the sensory discriminative aspects of sensation which allows the individual to localise the stimulus precisely. It is our observation that sensation arising following proximal oesophageal distension is localised quite precisely to the trunk while that arising from the distal distal oesophagus is more diffuse. This pattern of referral of oesophageal sensation could be explained by the results of our study which suggest that there is a stronger convergence of oesophageal and trunk afferents for the striated than the smooth muscle oesophagus. Second, the cortical representation of the proximal oesophagus appeared to be lateralised to either the left or right hemisphere, whereas, the distal oesophagus was seen to be represented bilaterally. Importantly though, with such a small sample size one must be necessarily guarded in the interpretation of the data at this stage. It is interesting, however, that recent studies of the cortical motor representation of human swallowing musculature also suggest that the pharynx and striated muscle oesophagus are asymmetrically represented on the motor and the premotor cortices irrespective of subject handedness (Aziz et al. 1996; Hamdy et al. 1996). This raises the possibility that there is a fundamental difference in the sensory and motor cortical representation of the two oesophageal regions and may explain the higher incidence of pharyngeal and proximal oesophageal abnormalities

## Chapter 6

(Robbins et al. 1993; Veis and Logemann 1985; Weber et al. 1991) seen after unilateral cortical lesions in comparison to the distal oesophagus.

Evidence for the excitation of both spinal and vagal afferents in our study is provided by the pattern of cortical activation seen. For instance, activation of the primary somatosensory cortex following both proximal and distal oesophageal stimulation implicates excitation of spinal afferents since animal studies do not provide evidence for a vagal afferent projection to SI (Cechetto and Saper 1990). In contrast, activation of the insular cortex is indicative of vagal afferent excitation as the insula is a major visceral sensory-motor area known to receive vagal afferent projections. Furthermore, recent studies in humans have shown that direct vagal stimulation evokes cortical potentials which are similar to those evoked by oesophageal stimulation (Tougas et al. 1993). However, it is known that the insular cortex also receives a projection from spinal afferents and therefore the relative contributions of spinal versus vagal afferents cannot be evaluated at this stage. Direct vagal stimulation in primates has produced evoked potentials in the cingulate cortex (Bachman et al. 1977) which may explain activation of this area observed in our subject 1.

Projections to and from the second somatosensory area (SII), located in the superior lip of the posterior limb of the lateral fissure, are poorly understood. Somatotopically organised, the area is associated with tactile and vibration sensation. Electrical stimulation of SII usually elicits bilateral responses, whereas only contralateral sensation is produced by stimulation of SI (Penfield and Jasper 1954). Furthermore, SII evoked fields have previously been reported following stimulation of both ipsilateral and contralateral somatic afferents (Hari et al. 1984), while activation of SI is strictly via excitation of contralateral somatic afferents.

Schnitzler et al., (1996) reported activation of SII following electrical stimulation of the oesophagus using whole head MEG recordings. These authors proposed that visceral afferents from the oesophagus project to SII bypassing SI. However, since

## Chapter 6

these authors did not employ confidence volume assessment, exclusion of SI activation should be considered with caution.

In our study, the contribution of SII to the oesophageal evoked response was uncertain since it was only clearly implicated in the N2 response in subject 2.

Our findings are consistent with those described by Franssen et al (1996) in which a signal similar to our distally evoked N2 component was measured. They proposed the cingulate gyrus and insular cortex as sources for evoked potentials following balloon distension. It is likely that due to the slower balloon inflation in this study, they failed to activate the N1 and P1 potentials which localise to SI.

In a recent PET experiment by Aziz et al (1997), using the same stimuli employed in our study, three clusters with increased blood flow were detected. These were the insular cortex, the caudal pre/post central gyrus and the operculum. The former two locations are clearly consistent with the data in our study. The responses from the operculum may reflect summation of later cortical events or were not recorded in our study because of their poor magnetic signature. Magnetic field measurements cannot detect radially oriented signals or those from deep sources.

In conclusion, the N1 / P1 / N2 complex described by Aziz et al (1995) have multiple generators and the vertex potential described by these, and previous authors who have also utilised balloon distension (Castell et al. 1990; Smout et al. 1992; Smout et al. 1990; Weusten et al. 1994), are likely to arise from summation of these sources.

### 7. Summary

The development of robust low noise SQUID devices brought magnetometers out of the physics laboratories and into physiology labs. In the 1970's, magnetic field measurements made from the human cortex began to appear in the scientific literature (Brenner et al., 1978). The increasing interest in source localisation and dipole modelling techniques, which had been applied with modest success to electrophysiological measurements, brought MEG methodologies into the limelight. However, the fact that in 1997, the multichannel MEG facility at Aston is still the only one of its kind in the U.K., is testimony to that fact that MEG has yet to prove its place in the minds of many scientists in this country. This should be contrasted with the fact that in 1997 there were 20 whole of head systems (> 100 channels) in Japan alone.

There are a number of factors which have kept MEG in the scientific backwater in the U.K.. Claims and counter claims relating to the relative efficiencies of source localisations of electrophysiological versus magnetoencephalographic techniques have done little to promote either technique. Furthermore, MEG is currently a high cost, high technology based technique requiring significant resource and a multidisciplinary infrastructure to maintain. This places the facility out of reach of many academic and most clinical environments. The well established centres promoting and evaluating PET and functional MRI methodologies has ensured that the relatively small pot of funding devoted to functional imaging in the United Kingdom has yet to find its way to MEG technology.

The 19 channel neuromagnetometer system at Aston University is a unique example of a multi-channel system in the United Kingdom located in a Clinical Sciences facility.

We have developed a bite bar head localisation and MRI co-registration strategy which enables accurate and reproducible localisation of MEG data into cortical space (Singh et al., 1997). In addition, we have developed a range of software tools for

## Chapter 7

acquisition and analysis which provides enormous capacity for variation of experimental design. This has afforded us the opportunity to study magnetic fields of the human cortex generated by stimulation of peripheral nerve (Furlong et al., 1995b), visceral sensory receptors (Furlong et al., 1995a; 1995d), as well as those evoked through voluntary finger movement (Furlong et al., 1997).

Following the study of such data in a healthy control population, the technique was applied to patients who were to undergo neurosurgical intervention for the treatment of epilepsy and / or space occupying lesions. This enabled both validation of the effective accuracy of source localisation using MEG as well as to determine the clinical value of MEG in pre-surgical assessment of functional localisation in human cortex.

The studies in this thesis have demonstrated that MEG can repeatedly and reliably locate sources contained within a single gyrus and thus potentially differentiate between disparate gyral activation. This ability is critical in the clinical application of any functional imaging technique; an ability which is yet to be fully validated by any other 'non-invasive' functional imaging methodology.

A major advantage of MEG and EEG techniques is that of very high temporal resolution (< 1ms). This has allowed the experimenter to examine the relative source localisation across a temporal window and therefore to have this vital additional input to disseminate primary cortical sources from secondary cortical processing. This essential ability is unachievable by other functional imaging techniques such as PET or fMRI.

Our application of MEG to pre-surgical assessment was highly successful. Of the 13 patients studied, 11 had surgery and in 10 of these cases, MEG accurately determined the location of the hand area of the sensory-motor cortex (91%). Over the same patient sample, Neuro-Radiology was successful in identifying the



## Chapter 7

somatosensory cortex in 9 cases (82%). Across the entire patient group, MEG and Neuro-Radiological localisations of the position of the central sulcus agreed in 10 of the 13 cases (77%).

It is interesting to note from the study by Sobel et al., (1993), that the inter-rater Neuro-radiological agreement on central sulcus localisation was only marginally superior to the MRI / MEG concordance. These authors concluded that whilst MR anatomic techniques can usually identify the central sulcus, in the presence of anatomic distortion the MEG functional method made a significant contribution.

In 1995, our group studied the electrophysiology and topographical distribution of oesophageal evoked potentials. This study is shown in Appendix II. However, source localisation techniques were not applied at this time and thus the precise nature of the cortical generators were undetermined.

Data from the study in this thesis suggests that there may be as many as four discrete cortical hemispheric sites activated following stimulation of the oesophagus; the superior primary somatosensory cortex (SI), the insular cortex, the inferior portion of SI and the second somatosensory cortex (SII).

The location and overlapping temporal activation of these areas would yield the characteristic vertex potentials described in our previous electrophysiological studies utilising balloon distension (Aziz et al 1995).

It is now proposed that MEG techniques will be applied to the study of evoked responses achieved from stimulation of other visceral sites (ano-rectum, stomach etc) to determine the extent and nature of viscerotopic organisation of the human cortex.

## References

Al-Chaer, E. D., Lawand, N. B., Westlund, K. N., and Willis, W. D. Visceral nociceptive input into the ventral posterolateral nucleus of the thalamus: A new function for the dorsal column pathway. *J. Neurophysiol.*, 1996, 76: 2661-2674.

Allison, T. Recovery functions of somatosensory evoked responses in man. *Electroenceph. clin. Neurophysiol.*, 1962, 14.

Allison, T., Goff, W. R., Williamson, P. D., and Van Gilder, J. C. On the neural origin of early components of the human somatosensory evoked potential. In: J. E. Desmedt, ed., *Clinical Uses of Cerebral, Brainstem and Spinal Somatosensory Evoked Potentials*, Karger, Basel, *Progr. Clin. Neurophysiol.*, 1980: 51-68.

Allison, T., McCarthy, G., Wood, C. C., Darcey, T. M., Spencer, D. D., and Williamson, P. D. Human cortical potentials evoked by stimulation of the median nerve. I. Cytoarchitectonic areas generating short-latency activity. *J. Neurophysiol.*, 1989, 62: 694-710.

Arezzo, J. C., Vaughan, H. G., and Legatt, A. D. Topography and intracranial sources of somatosensory evoked potentials in the monkey. II. Cortical components. *Electroenceph. clin. Neurophysiol.*, 1981, 51: 1-18.

Aziz, Q., Andersson, J., Valind, S., Sundin, A., Hamdy, S., Jones, A. K. P., Foster, E. R., Långström, B., and Thompson, D. G. Identification of human brain loci processing oesophageal sensation using Positron Emission Tomography. *Gastroenterol.*, 1997, (In Press).

Aziz, Q., Furlong, P., Barlow, J., Hobson, A., Whittle, D., Alani, S., Bancewicz, J., and Thompson, D. G. Topographic mapping and conduction velocity of cortical responses evoked by oesophageal distension. *Gut*, 1992a, 33: S55.

Aziz, Q., Furlong, P., Barlow, J., Hobson, A., Whittle, D., Alani, S., Bancewicz, J., and Thompson, D. G. Topographic mapping and conduction velocity of cortical responses evoked by oesophageal distension. *Gut*, 1992b, 33: F215.

Aziz, Q., Furlong, P., Rothwell, J., Singh, K., Barnes, G., Holliday, I., Barlow, J., Hughes, D. G., Robinson, L., Harding, G., and Thompson, D. G. Localisation of cortical centres for human oesophageal function by coregistration of magnetometry and magnetic stimulation data on magnetic resonance scans. *Neurogastroenterology and Motility*, 1994a, 6: 137.

Aziz, Q., Furlong, P., Rothwell, J. C., Barlow, J., Hobson, A., Whittle, D., Alani, S., Bancewicz, J., and Thompson, D. G. Topographic representation of oesophageal sensory and motor pathways on the human cortex. *Journal of Gastrointestinal Motility*, 1992c, 4: 206.

Aziz, Q., Furlong, P. L., Barlow, J., Hobson, A., Alani, S., Bancewicz, J., Ribbands, M., Harding, G. F. A., and Thompson, D. G. Topographic mapping of cortical potentials evoked by distension of the human proximal and distal oesophagus. *Electroenceph.clin. Neurophysiol.*, 1995, 96: 219-228.

Aziz, Q., Rothwell, J. C., Furlong, P., Barlow, J., Hobson, A., Alani, S., Harding, G., and Thompson, D. G. Sensory and motor representation of the human oesophagus on the cerebral cortex. *Gut*, 1994b, 35: S21.

Aziz, Q., Rothwell, J. C., Furlong, P., Barlow, J., Hobson, A., Harding, G., and Thompson, D. G. A study of oesophageal extrinsic neural pathways. *J.Auton.Nerv.Syst.*, 1993, 43: 59.

Aziz, Q., Rothwell, J. C., Hamdy, S., Barlow, J., and Thompson, D. G. The topographic representation of oesophageal motor function on the human cerebral cortex. *Gastroenterol.*, 1996, 111: 855-862.

Bachman, D. S., Hallowitz, R. A., and MacLean, P. D. Effects of vagal volleys and serotonin units of cingulate cortex in monkeys. *Brain Res.*, 1977, 130: 253-269.

Badr, G., Carlsson, C. A., Friberg, S., Lindstrom, L., and Ohlsson, B. Cortical evoked responses following stimulation of the urinary bladder in man. *Electroenceph. Clin. Neurophysiol.*, 1982, 54: 494-498.

Bailey, P., and Bremer, P. A sensory cortical representation of the vagus nerve. *J. Neurophysiol.*, 1938, 1: 405-412.

Baumgartner, C. *Clinical Electrophysiology of the Somatosensory Cortex*, Springer, New York, 1993.

Baumgartner, C., Barth, D. S., Levesque, M. F., and Sutherling, W. W. Human hand and lip sensorimotor cortex as studied on electrocorticography. *Electroenceph.clin.Neurophysiol.*, 1992, 82: 115-126.

Baumgartner, C., Doppelbauer, A., Deecke, L., Barth, D. S., Zeitlhofer, J., Lindinger, G., and Sutherling, W. W. Neuromagnetic investigation of somatotopy of human hand somatosensory cortex. *Exp.Brain.Res.*, 1991b, 87: 641-648.

Baumgartner, C., Doppelbauer, A., Sutherling, W. W., Zeitlhofer, J., Lindinger, G., Lindl, C., and Deecke, L. Human somatosensory cortical finger representation as studied by combined neuromagnetic and neuroelectric measurements. *Neuroscience Letters*, 1991a, 134: 103-108.

Baumgartner, C., Sutherling, W. W., Di, S., and Barth, D. S. Spatiotemporal modeling of cerebral evoked magnetic fields to median nerve stimulation. *Electroenceph.Clin.Neurophysiol.*, 1991c, 79: 27-35.

Berkley, K. J., and Hubscher, C. H. Are there separate central nervous system pathways for touch and pain? *Nature Medicine*, 1995, 1: 767-773.

Binder, J. R., Rao, S. M., Hammeke, T. A., and et al. Functional magnetic resonance imaging of human auditory cortex. *Ann.Neurol.*, 1994, 35: 662-72.

Bookheimer, S. Y., Zeffiro, T. A., Theodore, W., and et al. Multi-modal functional imaging for language localisation in epilepsy (abstract). *Neurology*, 1993, 43 Suppl: A193.

Brenner, D., Lipton, J., Kaufman, L., and Williamson, S. J. Somatically evoked fields of the human brain. *Science*, 1978, 199: 81-83.

Buchner, H., Adams, L., Knepper, A., Ruger, R., Laborde, G., Gilsbach, J. M., Ludwig, I., Reul, J., and Scherg, M. Preoperative localization of the central sulcus by dipole source analysis of early somatosensory evoked potentials and three-dimensional magnetic resonance imaging. *J.Neurosurg*, 1994, 80: 849-856.

Burgess, P. R., and Clark, F. J. Characteristics of knee joint receptors in the cat. *J.Physiol. (Lond.)*, 1969, 203: 317-335.

Cao, Y., Towle, V. L., Levin, D. N., and et al. Functional mapping of human motor cortical activation with conventional MR imaging at 1.5T. *J.Magn.Reson.Imaging*, 1993, 3: 869-75.

Castell, D. O., Wood, J. D., Frieling, T., Wright, F. S., and Vieth, R. F. Cerebral Electrical Potentials evoked by balloon distention of the human esophagus. *Gastroenterology*, 1990, 98: 662-666.

- Cechetto, D. F., and Saper, C. B. Evidence for a viscerotopic sensory representation in the cortex and thalamus in the rat. *J. Comp. Neurol.*, 1987, 262: 27-45.
- Cechetto, D. F., and Saper, C. B. Role of the cerebral cortex in autonomic function. In: A. D. Loewy and K. M. Spyer, eds., *Central regulation of autonomic function*, Oxford University Press, New York, 1990: 208-223.
- Cheyne, D., Kristeva, R., and Deecke, L. Homuncular organization of human motor cortex as indicated by neuromagnetic recordings. *Neurosci.Lett.*, 1991, 122: 17-20.
- Cheyne, D., and Weinberg, H. Neuromagnetic fields associated with unilateral finger flexions: premovement and movement-evoked fields. *Exp.Brain Res.*, 1989, 78: 604-612.
- Chiarenza, G. A., Hari, R. K., Karhu, J. J., and Tessore, S. Brain activity associated with skilled finger movements: multichannel magnetic recordings. *Brain Topogr.*, 1991, 3: 433-439.
- Cohen, D., and Cuffin, B. N. EEG versus MEG localization accuracy: theory and experiment. *Brain Topogr.*, 1991, 4: 95-103.
- Cohen, D., Cuffin, B. N., Yunokuchi, K., Maniewski, R., Purcell, C., Cosgrove, G. R., Ives, J., Kennedy, J. G., and Schomer, D. L. MEG versus EEG localization test using implanted sources in the human brain. *Ann.Neurol.*, 1990, 28: 811-817.
- Collet, L., Meunier, P., Duclaux, R., Chery-Croze, S., and Falipou, P. Cerebral evoked potentials after endorectal mechanical stimulations in humans. *Am.J. Physiol.*, 1988, 254: G477-G482.
- Dann, R., Hoford, J., Kovacic, S., and et al. Evaluation of elastic matching system for anatomic (CT, MR) and functional (PET) cerebral images. *J. Comput. Assist. Tomogr.*, 1989, 13: 603-11.
- Dawson, G. D. Cerebral responses to electrical stimulation of peripheral nerve in man. *J. Neurol. Neurosurg. Psych.*, 1947, 10: 134.
- Dawson, G. D. Cerebral responses to nerve stimulation in man. *Br. Med. Bull.*, 1950, 6: 326.
- Dawson, G. D. A summation technique for the detection of small evoked potentials. *Electroenceph.clin.Neurophysiol.*, 1954, 6: 65.

- Dawson, G. D. The relative excitability and conduction velocity of sensory and motor nerve fibres in man. *J.Physiol.*, 1956, 131: 146.
- Debecker, J., and Desmedt, J. E. Les potentiels évoqués cérébraux et les potentiels de nerf sensible chez l'homme. *Acta. Neurol. Belg.*, 1964, 64: 1212.
- Deecke, L., Weinberg, H., and Brickett, P. Magnetic fields of the human brain accompanying voluntary movements: Bereitschafts-magnetfeld. *Exp.Brain Res.*, 1982, 48: 144-148.
- Dell, P., and Olson, R. Projections thalamiques corticales et cerebelleuses des afferences viscerales vagales. *C.R.Soc.Biol. (Paris)*, 1951, 145: 1084-1088.
- Desmedt, J. E., Debecker, J., and Manil, J. Mise en évidence d'une signe électrique cérébral associé à la détection par la sujet d'un stimulus sensoriel tactile. *Bull. Acad. Roy.Med. Belg.*, 1965, 5: 887.
- Drasdo, N., and Furlong, P. Coordinate systems for evoked potential topography. *Electroenceph.clin.Neurophysiol.*, 1988a, 71: 469-473.
- Drasdo, N., and Furlong, P. A simple co-ordinate system providing exact notation of scalp position and quasi-cylindrical projections for evoked potential topography. *Electroenceph.clin.Neurophysiol.*, 1988b, 69: 43P.
- Dusser de Barenne, J. G. Corticalisation of function and functional localisation in cerebral cortex. *Archs. Neurol.Psychiat.*, 1933, 30: 884-901.
- Ebeling, U., Schmid, U. D., and Reulen, H. J. Tumor-surgery within the central motor strip: surgical results with the aid of electrical motor cortex stimulation. *Acta Neurochir*, 1989, 101: 100-107.
- Engel, S. A., Rumelhart, D. E., Wandell, B. A., and et al. fMRI of human visual cortex (letter). *Nature*, 1994, 369: 525.
- Erné, S. N., Curio, G., Trahms, L., Trontelj, Z., and Aust, P. Magnetic activity of a single peripheral nerve in man. In: K. Atsumi, M. Kotani, S. Ueno, T. Katila, and S. J. Williamson, eds., *Biomagnetism '87*, Tokyo Denki University, Tokyo, 1988: 166-169.
- Foerster, O., and Penfield, W. The structural basis of traumatic epilepsy and results of radical operations. *Brain*, 1930, 53: 99-119.

- Fox, P. T., Burton, H., and Raichle, M. E. Mapping human somatosensory cortex with positron emission tomography. *J. Neurosurg*, 1987, 67: 34-43.
- Fox, P. T., Perlmutter, J. S., and Raichle, M. E. A stereotactic method of anatomical localisation for positron emission tomography. *J. Comput. Assist. Tomogr.*, 1985, 9: 141-53.
- Franssen, H., Weusten, B. L. A. M., Wieneke, G. H., and Smout, A. J. P. M. Source modeling of esophageal evoked potentials. *Electroenceph.clin.Neurophysiol.*, 1996, 100: 85-95.
- Frieling, T., Enck, P., and Wienbeck, M. Cerebral responses evoked by electrical stimulation of the esophagus in normal subjects. *Gastroenterology*, 1989, 97: 475-8.
- Frøbert, O., Arendt-Nielsen, L., Bak, P., Funch-Jensen, P., and Bagger, J. P. Oesophageal sensation assessed by electrical stimuli and brain evoked potentials - a new model for visceral nociception. *Gut*, 1995, 37: 603-609.
- Fukuyama, T., Umezaki, T., and Shin, T. Origin of laryngeal sensory-evoked potentials (LSEP's) in the cat. *Brain Res. Bull.*, 1993, 31: 381-392.
- Furlong, P., Aziz, Q., Barlow, J., Harding, G., Thompson, D., Alani, S., and Bancewicz, J. Morphology and Topography of Cortical Responses Evoked by Oesophageal Distension. *Electroenceph.Clin.Neurophysiol.*, 1993a, 87: S89.
- Furlong, P. L. Cerebral evoked responses and Magnetoencephalography. *Neurogastroenterol. Mot.*, 1995a, 7: 119.
- Furlong, P. L., Aziz, Q., Singh, K. D., Holliday, I., Barnes, G., and Harding, G. F. A. Localisation of the cortical centres for human esophageal sensation using magnetoencephalography. *Gastroenterol.*, 1995b, Supplement: A726.
- Furlong, P. L., Aziz, Q., Singh, K. D., Holliday, I., Barnes, G., Harding, G. F. A., and Thompson, D. G. Spatiotemporal distribution of the cortical magnetic field evoked by human oesophageal stimulation using Magnetoencephalography. *Neurogastroenterol. Mot.*, 1995c, 7: 136.
- Furlong, P. L., Harding, G. F. A., Singh, K., D, Barnes, G. R., Walton, N. H., Sandeman, D., and Renowden, S. MEG for pre-surgical localisation of sensori-motor cortex. *Electroenceph.clin.Neurophysiol.*, 1997, 103: 200.

Furlong, P. L., Weale, P., Singh, K. D., Harding, G. F. A., and Chavda, S. Magnetoencephalography and Functional Magnetic Resonance Imaging for pre-surgical evaluation. *Human Brain Mapping*, 1995d, Suppl 1: 345.

Furlong, P. L., Wimalaratna, S., and Harding, G. F. A. Augmented P22-N31 SEP component in a patient with a unilateral space occupying lesion. *Electroenceph.clin.Neurophysiol.*, 1993b, 88: 72-76.

Gallen, C. C., Schwartz, B., Rieke, K., Pantev, C., Sobel, D., Hirschkoff, E., and Bloom, F. E. Intrasubject reliability and validity of somatosensory source localization using a large array biomagnetometer. *Electroenceph.clin.Neurophysiol.*, 1994, 90: 145-156.

Gallen, C. C., Sobel, D. F., Lewine, J. D., Sanders, J. A., Hart, B. L., Davis, L. E., and Orrison, W. W. Neuromagnetic Mapping of Brain function. *Radiology*, 1993a, 187: 863-7.

Gallen, C. C., Sobel, D. F., Waltz, T., Aung, M., Copeland, B., Schwartz, B. J., Hirschkoff, E. C., and Bloom, F. E. Non-invasive presurgical neuromagnetic mapping of somatosensory cortex. *Neurosurg.*, 1993b, 33.

Gharib, S., Sutherling, W. W., Nakasato, N., Barth, D. S., Baumgartner, C., Alexopoulos, N., Taylor, S., and Rogers, R. L. MEG and ECoG localisation accuracy test. *Electroenceph.clin.Neurophysiol.*, 1995, 94: 109-114.

Giblin, D. R. Somatosensory evoked potentials in healthy subjects and in patients with lesions of the nervous system. *Ann. N.Y. Acad. Sci.*, 1964, 112.

Gilman, S., and Newman, S. W. *Essentials of Clinical Neuroanatomy and Neurophysiology*, F.A. Davis Company, Philadelphia, 1987.

Goff, W. R., Rosner, B. S., and Allison, T. Distribution of cerebral somatosensory evoked responses in normal man. *Electroenceph.clin.Neurophysiol.*, 1962, 14: 697.

Goyal, R. K., Sengupta, J. N., and Saha, J. K. Properties of esophageal mechanosensitive receptors. In: G. E. Holle et al, ed., *Advances in the Innervation of the Gastrointestinal tract*, Elsevier Science Publishers B.V., , 1992: 523-546.

Gregorie, E. M., and Goldring, S. Localization of function in the excision of lesions from the sensorimotor region. *J.Neurosurg*, 1984, 61: 1047-1054.



Grigg, P., and Greenspan, B. J. Response of primate joint afferent neurons to mechanical stimulation of knee joint. *J. Neurophysiol.*, 1977, 40.

Hämäläinen, M., Hari, R., Ilmoniemi, R., Knuutila, J., and Lounasmaa, O. V. Magnetoencephalography - theory, instrumentation, and applications to noninvasive studies of the working brain. *Rev.Mod.Phys.*, 1993, 65: 414-496.

Hamdy, S., Aziz, Q., Rothwell, J. C., Singh, K. D., Barlow, J., Hughes, D. G., Tallis, R. C., and Thompson, D. G. The cortical topography of human swallowing musculature in health and disease. *Nature Medicine*, 1996, 2: 1217-1224.

Harding, G. F. A. How surgeons could navigate the brain. *New Sci.*, 1993, 140: 28-31.

Hari, R., Reinikainen, K., Kaukoranta, E., Hämäläinen, M., Ilmoniemi, R., Penttinen, A., Salminen, J., and Teszner, D. Somatosensory evoked cerebral magnetic fields from SI and SII in man. *Electroenceph.clin.Neurophysiol.*, 1984, 57: 245-263.

Huttenen, J., Hari, R., and Leinonen, L. Cerebral magnetic responses to stimulation of the ulnar and median nerves. *Electroenceph.clin.Neurophysiol.*, 1987, 66: 391-400.

Hyvärinen, J. *The Parietal Cortex of Monkey and Man*, Springer-Verlag, 1982.

Jack, C. R., Lee, C. C., and Riederer, S. J. Functional Magnetic Resonance Imaging. In: G. D. Cascino and C. R. Jack, eds., *Neuroimaging in Epilepsy: Principles and Practice*, Butterworth-Heinemann, Boston, 1996: 151-164.

Jack, C. R., Thompson, R. M., Butts, R. K., Sharbrough, F. W., Kelly, P. J., Hanson, D. P., Riederer, S. J., Ehman, R. L., Hangiandreou, N. J., and Cascino, G. D. Sensory motor cortex: correlation of presurgical mapping with Functional MR imaging and invasive cortical mapping. *Radiology*, 1994, 190: 85-92.

Jasper, H. H. Report of Committee on Methods of Clinical Examination in Electroencephalography. *Electroenceph.clin.Neurophysiol.*, 1958, 10: 370-375.

Jones, E. G., and Porter, R. What is area 3a ? *Brain Res.*, 1980, 198: 307-321.

Jones, E. G., and Powell, T. P. S. Connections of the Somatic Sensory Cortex of the Rhesus Monkey. I. - Ipsilateral Cortical Connections. *Brain*, 1969a, 92: 477-502.

Jones, E. G., and Powell, T. P. S. Connections of the Somatic Sensory Cortex of the Rhesus Monkey. II. - Contralateral Cortical Connections. *Brain*, 1969b, 92: 717-730.

Kaas, J. H., Sur, M., Nelson, R. J., and Merzenich, M. M. The postcentral somatosensory cortex. In: C. N. Woolsey, ed., *Cortical sensory organisation*, Vol. 1, Humana Press, Clifton, N.J., *Multiple Somatic Areas*, 1981: 29-45.

Kassubek, J., Stippich, C., Sörös, P., Hopfengärtner, R., Kober, H., and Vieth, J. B. Precentral motor cortex localisation using magnetoencephalography. *Proceedings 2nd International Conference on Functional Mapping of the Human Brain*, 1996.

Kaufman, L., and S.J, W. The evoked magnetic field of the human brain. *Ann. N.Y. Acad. Sci.*, 1980, 340: 45-65.

Kawamura, T., Nakasato, N., Seki, K., Kanno, A., Fujita, S., Fujiwara, S., and Yoshimoto, T. Neuromagnetic evidence of pre- and post-central cortical sources of somatosensory evoked responses. *Electroenceph.clin.Neurophysiol.*, 1996, 100: 44-50.

Kober, H., Grummich, P., and Vieth, J. Precise fusion of MEG and MRI tomography using a surface fit. *Biomed.Eng. (Berlin)*, 1993, 38 (Suppl): 355-356.

Kristeva, R., Cheyne, D., and Deecke, L. Neuromagnetic fields accompanying unilateral and bilateral voluntary movements: topography and analysis of cortical sources. *Electroenceph.clin.Neurophysiol.*, 1991, 81: 284-298.

Kristeva-Feige, R., Rossi, S., Pizzella, V., Tecchio, F., Romani, G. L., Edrich, J., and Rossini, P. M. Functional organisation of the primary sensory cortex in humans: a neuromagnetic study. In: C. Barber, G. Celesia, G. C. Comi, and F. Mauguière, eds., *Functional Neuroscience, EEG Suppl. 46*, Elsevier, , 1996: 215-220.

Lehmann, D., and Skrandies, W. Spatial analysis of evoked potentials in man - a review. *Prog. Neurobiol.*, 1984, 23: 227-250.

Levin, P. M., and Bradford, F. K. The exact origin of the cortico-spinal tract in the monkey. *J. Comp. Neurol.*, 1938, 68: 411-22.

Matlashov, A., Slobodchikov, V., Bakharev, A., Zhuravlev, Y., and Bondarenko, N. Biomagnetic Multichannel System Built with 19 Cryogenic Probes. In: *Recent Advances in Biomagnetism, 9th International Conference on Biomagnetism*, Vienna:1993 285.

- Matthews, P. B. Proprioceptors and their contribution to somatosensory mapping: complex messages require complex processing. *Can.J.Physiol.Pharmacol.*, 1988, 66: 431-438.
- McIntyre, A. K., Holman, M. E., and Veale, J. L. *Expl.Brain Res.*, 1967, 4.
- McNaught, A. B., and Callander, R. *Illustrated Physiology*, Churchill Livingstone, 1983.
- Medvick, P., Lewis, P. S., Aine, C. J., and Flynn, E. R. Monte Carlo analysis of localization errors in magnetoencephalography. In: S. J. Williamson, ed., *Advances in Biomagnetism*, Plenum Press, New York, 1990: 543-546.
- Meltzer, C. C., Bryan, R. N., Holcomb, H. H., and et al. Anatomical localisation for PET using MR imaging. *J. Comput. Assist. Tomogr.*, 1990, 14: 418-26.
- Menon, R. S., Ogawa, S., Kim, S. G., and et al. Functional mapping usinh magnetic resonance imaging. Signal cahnges accompanying visual stimulation. *Invest. Radiol.*, 1992, 27 Suppl: S47-S53.
- Moberg, E. The role of cutaneous afferents in position sense, kinaesthesia, and motor function of the hand. *Brain*, 1983, 106: 1-19.
- Mogilner, A., Grossman, J. A. I., Ribary, U., Joliot, M., Volkman, J., Rapaport, D., Beasley, R. W., and Llinas, R. R. Somatosensory cortical plasticity in adult humans revealed by magnetoencephalography. *Proc.Natl.Acad.Sci.USA.*, 1993, 90: 3593-3597.
- Nakasato, N., Seki, K., Kawamura, T., Fujita, S., Kanno, A., Fujiwara, S., and Yoshimoto, T. Functional brain mapping using an MRI-linked whole head magnetoencephalography (MEG) system. In: C. Barber, G. Celesia, G. C. Comi, and F. Mauguière, eds., *Functional Neuroscience*, Elsevier, Amsterdam, *Electroenceph.clin.Neurophysiol.*, Suppl. 46, 1996: 119-126.
- Narici, L., Modena, I., Opsomer, R. J., Pizzella, V., Romani, G. L., Torrioli, G., Traversa, R., and Rossini, P. M. Neuromagnetic somatosensory homunculus: a non-invasive approach in humans. *Neuroscience Letters*, 1991, 121: 51-54.
- Ogawa, S., Lee, T. M., and Nayak, A. S. Oxygenation-sensitive contrast in magnetic resonance image of rodent brain at high magnetic fields. *Magn.Reson.Med.*, 1990, 14: 68-78.

Ogawa, S., Tank, D. W., Menon, R., and et al. Intrinsic signal changes accompanying sensory stimulation: functional brain mapping with magnetic resonance imaging. *Proc. Natl. Acad. Sci. USA*, 1992, 89: 5951-5.

Okada, Y. C., Kaufman, L., Brenner, D., and Williamson, S. J. Application of a SQUID to measurement of somatically evoked fields: transient responses to electrical stimulation of the median nerve. In: S. N. Ern, H. D. Hohlbohm, and H. Lubbig, eds., *Biomagnetism*, Walter de Gruyter, Berlin, 1981.

Okada, Y. C., Tananbaum, R., Williamson, S. J., and Kaufman, L. Somatotopic organization of the human somatosensory cortex revealed by neuromagnetic measurements. *Exp. Brain Res.*, 1984, 56: 197-205.

Orrison, W. W., Davis, L. E., Sullivan, G. W., Mettler, F. A., and Flynn, E. R. Anatomic localization of cerebral cortical function by magnetoencephalography combined with MR imaging and CT. *Am.J.Radiol.*, 1990, 11: 713-716.

Orrison, W. W., Rose, D. F., Hart, B. L., Maclin, E. L., Sanders, J. A., Willis, B. K., Marchand, E. P., Wood, C. C., and Davis, L. E. Noninvasive preoperative cortical localization by magnetic source imaging. *Am. J. Neuroradiol.*, 1992, 13: 1124-1128.

Pandya, D. N., and Vignolo, L. A. Interhemispheric projections of the parietal lobe in the rhesus monkey. *Brain Research*, 1968, 15: 49-65.

Penfield, W., and Boldrey, E. Somatic and sensory representation in the cerebral cortex of man as studied by electrical stimulation. *Brain*, 1937, 60: 389-443.

Penfield, W., and Jasper, J. *Epilepsy and the functional anatomy of the human brain*, Little Brown & Co., Boston, 1954.

Penfield, W., and Rasmussen, T. *The Cerebral Cortex of Man*, Macmillan, New York, 1950.

Phillips, C. G., Powell, T. P. S., and Wiesendanger, M. Projection from low threshold muscle afferents of hand and forearm to area 3a of babboons cortex. *J.Physiol.* (London), 1971, 217: 419-446.

Powell, T. P., and Mountcastle, V. B. The cytoarchitecture of the postcentral gyrus of the monkey *Macaca mulatta*. *Bull. John Hopkins Hosp.*, 1959, 105: 108-120.

Press, W. H., Flannery, B. P., Teukolsky, S. A., and W.T., V. *Numerical Recipes In C*, Cambridge University Press., Cambridge., 1989.

Rademacher, J., Caviness Jr, V. S., Steinmetz, H., and Galaburda, A. M. Topographical variation of the human primary cortices: Implications for Neuroimaging, Brain Mapping and Neurobiology. *Cerebral Cortex*, 1993, 3: 313-29.

Randich, A., and Gebhart, G. F. Vagal afferent modulation of nociception. *Brain.Res.Rev.*, 1992, 17: 77-99.

Regan, D. Human brain electrophysiology. Evoked potentials and evoked magnetic fields in science and medicine, Elsevier, New York., 1989.

Rezai, A. R., Hund, M., Kronberg, E., Zonenshayn, M., Cappell, J., Ribary, U., Kall, B., Llinás, R., and Kelly, P. J. The interactive use of Magnetoencephalography in stereotactic image-guided neurosurgery. *Neurosurgery*, 1996, 39: 92-102.

Robbins, J. A., Levine, R. L., Maser, A., Rosenbek, J. C., and Kempster, G. B. Swallowing after unilateral stroke of the cerebral cortex. *Arch.Phys.Med.Rehab.*, 1993, 74: 1295-1300.

Roth, B. J., Balish, M., Gorbach, A., and Sato, S. How well does a three-sphere model predict positions of dipoles in a realistically shaped head? *Electroenceph.clin.Neurophysiol.*, 1993, 87: 175-184.

Rumeau, C., Tzourio, N., Murayama, N., Peretti-Viton, P., Levrier, O., Joliot, M., Mazoyer, B., and Salamon, G. Location of hand function in the sensorimotor cortex: MR and functional correlation. *Am.J.Neuroradiol.*, 1994, 15: 567-572.

Sarvas, J. Basic mathematical and electromagnetic concepts of the biomagnetic inverse problem. *Phys.Med.Biol.*, 1987, 31: 11-22.

Schneider, W., Noll, D. C., and Cohen, J. D. Functional topographic mapping of the cortical ribbon in human vision with conventional MRI scanners. *Nature*, 1993, 365: 150-3.

Sengupta, J. N., Coauvar, D., and Goyal, R. K. Characteristics of vagal esophageal tension-sensitive afferent fibres in the opossum. *J. Neurophysiol.*, 1989, 61: 1001-1010.

Sengupta, J. N., Saha, J. K., and Goyal, R. K. Stimulus-response function studies of esophageal mechanosensitive nociceptors in sympathetic afferents of opossum. *J. Neurophysiol.*, 1990, 64: 796-812.

- Shagass, C., and Schwartz, M. Recovery functions of somatosensory peripheral nerve and cerebral evoked responses in man. *Electroenceph.clin.Neurophysiol.*, 1964, 17: 126.
- Singh, K. D., Holliday, I. E., Furlong, P. L., and Harding, G. F. A. Evaluation of MRI-MEG/EEG co-registration strategies using Monte Carlo simulation. *Electroenceph.clin.Neurophysiol.*, 1997, 102: 81-85.
- Smout, A. J. P. M., DeVore, M. S., Dalton, C. B., and Castell, D. O. Cerebral potentials evoked by oesophageal distension in patients with non-cardiac chest pain. *Gut*, 1992, 33: 298-302.
- Smout, A. P. M., DeVore, M. S., and Castell, D. O. Cerebral potentials evoked by esophageal distension in humans. *Am. J. Physiol.*, 1990, 259: G955-G959.
- Sobel, D. F., Gallen, C. C., Schwartz, B. J., Waltz, T. A., Copeland, B., Yamada, S., Hirschkoff, E. C., and Bloom, F. E. Locating the central sulcus: Comparison of MR anatomic and Magnetoencephalographic functional methods. *Am.J.Neuroradiol.*, 1993, 14: 915-925.
- Stippich, C., Kassubek, J., Sörös, P., Freitag, P., Kamada, K., Kober, H., Hopfengärtner, R., Scheffler, K., Radü, E. W., and Vieth, J. B. Functional imaging of human somatosensory cortex: a comparative study using magnetoencephalography (MEG) and functional magnetic resonance imaging (fMRI). *Electroenceph.clin.Neurophysiol.*, 1996, 99: 335. P276.
- Sutherling, W. W., Crandall, P. H., Darcey, T. M., Becker, D. P., Levesque, M. F., and Barth, D. S. The magnetic and electric fields agree with intracranial localizations of somatosensory cortex. *Neurology*, 1988, 38: 1705-1714.
- Sutherling, W. W., Levesque, M. F., and Baumgartner, C. Cortical sensory representation of the human hand: Size of finger regions and nonoverlapping digit somatotopy. *Neurology*, 1992, 42: 1020-1028.
- Talairach, J., and Tournoux, P. *Co-Planar Stereotaxic Atlas of the Human Brain*, Georg Thieme, Germany, 1988.
- Tiihonen, J., Hari, R., and Hämäläinen, M. Early deflections of cerebral magnetic responses to median nerve stimulation. *Electroenceph.clin.Neurophysiol.*, 1989, 74: 290-296.

Tougas, G., Hudoba, P., Fitzpatrick, D., Hunt, R. H., and Upton, A. R. Cerebral-evoked potential responses following direct vagal and esophageal stimulation in humans. *Am.J.Physiol.*, 1993, 264: G486-491.

Uddenberg, N. Functional organisation of long, second order afferents in the dorsal funiculus. *Expl. Brain Res.*, 1968, 4: 377-82.

Vallbo, Å. B., K.-E, H., H.E, T., and B.G, W. Somatosensory, Proprioceptive and Sympathetic Activity in Human Peripheral Nerves. *Physiological Reviews*, 1979, 59.

Van den Elsen, P. A., Viergever, M. A., Van Huffelen, A. C., Van der Meij, W., and Wieneke, G. H. Accurate matching of electromagnetic dipole data with CT and MR images. *Brain Topogr.*, 1991, 3: 425-432.

Veis, S. L., and Logemann, J. A. Swallowing disorders in persons with cerebrovascular accident. *Arch.Phys.Med.Rehab.*, 1985, 66: 372-5.

Weber, J., Roman, C., Hannequin, D., Onnient, Y., Beuret-Blanquart, Mihout, F., and Denis, P. Esophageal manometry in patients with unilateral hemispheric cerebrovascular accidents or idiopathic parkinsonism. *J.Gastrointest.Motil.*, 1991, 3: 98-106.

Weusten, B. L. A. M., Franssen, H., Wieneke, G. H., and Smout, A. J. P. M. Multichannel recording of cerebral potentials evoked by esophageal balloon distension in humans. *Dig.Dis.Sci*, 1994a, 39: 2074-2083.

Weusten, B. L. A. M., Lam, H. G. T., Akkermans, L. M. A., Van., B.-H. G. P., and Smout, A. J. P. M. Influence of age on cerebral potentials evoked by oesophageal balloon distension in humans. *Euro.J.clin.Invest.*, 1994b, 24: 627-631.

Williamson, S. J., and Kaufman, L. Analysis of neuromagnetic signals. In: A. Gevins and A. Remond, eds., *Handbook of Electroencephalography and Clinical Neurophysiology*, Revised series, Elsevier, Amsterdam, 1987.

Williamson, S. J., Lü, Z.-L., Karron, D., and Kaufman, L. Advantages and limitations of magnetic source imaging. *Brain Topogr.*, 1991, 4: 169-180.

Wood, C. C., Cohen, D., Cuffin, B. N., Yarita, M., and Allison, T. Electrical sources in human somatosensory cortex: identification by combined magnetic and potential recordings. *Science*, 1985, 227: 1051-1053.

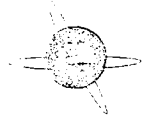
Wood, C. C., Spencer, D. D., Allison, T., McCarthy, G., Williamson, P. D., and Goff, W. R. Localization of human sensorimotor cortex during surgery by cortical surface recording of somatosensory evoked potentials. *J. Neurosurg.*, 1988, 68: 99-111.

Woods, R. P., Mazziotta, J. C., and Cherry, S. R. MRI-PET registration with automated algorithm. *J. Comput. Assist. Tomogr.*, 1993, 17: 536-46.

Yang, T. T., Gallen, C. C., Schwartz, B. J., and Bloom, F. E. Noninvasive somatosensory homunculus mapping in humans by a large-array biomagnetometer. *Proc.Natl.Acad.Sci.USA*, 1993, 90: 3098-3102.



# Appendix I



## Evaluation of MRI-MEG/EEG co-registration strategies using Monte Carlo simulation

K.D. Singh\*, I.E. Holliday, P.L. Furlong, G.F.A. Harding

*Clinical Neurophysiology Group, Department of Vision Sciences, Aston University, Aston Triangle, Birmingham, B4 7ET, UK*

Accepted for publication: 11 July 1996

---

### Abstract

We present a Monte Carlo analysis method for evaluating MRI-MEG/EEG co-registration techniques. The method estimates the error in co-registration as a function of position within the brain. Using this analysis technique, we demonstrate the limitations of conventional head-based fiducial point methods, and propose a new strategy utilising a dental bite-bar incorporating accurately machined fiducial markers. Results presented demonstrate the improved accuracy of MEG/EEG to MRI co-registration using the bite-bar. © 1997 Elsevier Science Ireland Ltd. All rights reserved.

*Keywords:* Magnetoencephalography; Electroencephalography; MRI; Co-registration; Bite-bar; Monte Carlo analysis

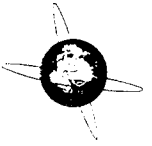
---



Aston University

**Content has been removed for copyright reasons**

## **Appendix II**



## Topographic mapping of cortical potentials evoked by distension of the human proximal and distal oesophagus

Q. Aziz <sup>a</sup>, P.L. Furlong <sup>d,\*</sup>, J. Barlow <sup>a</sup>, A. Hobson <sup>a</sup>, S. Alani <sup>b</sup>, J. Bancewicz <sup>a</sup>,  
M. Ribbands <sup>c</sup>, G.F.A. Harding <sup>d</sup>, D.G. Thompson <sup>a</sup>

<sup>a</sup> Department of Gastroenterology, Hope Hospital, University of Manchester, Manchester, UK

<sup>b</sup> Department of Neurophysiology, Hope Hospital, University of Manchester, Manchester, UK

<sup>c</sup> Department of Medical Physics, Hope Hospital, University of Manchester, Manchester, UK

<sup>d</sup> Department of Vision Sciences, Aston University, Aston Triangle, Birmingham B4 7ET, UK

Accepted for publication: 4 November 1994



Aston University

**Content has been removed for copyright reasons**